## *New tetracyanoquinodimethane chromophores, synthesis and physical properties*

Yasuyuki Kagawa

# New Tetracyanoquinodimethane Chromophores,

# Synthesis and Physical Properties



**Yasuyuki KAGAWA**

Submitted for the degree of Doctor of Philosophy

University of Durham

Department of Physics

1998

# Abstract

Synthesis and physical characterizations of a novel class of zwitterionic organic chromophores were carried out. A series of tetracyanoquinodimethane (TCNQ) derivatives was prepared from reactions with primary and secondary amines. By modifications of the structure it was hoped to optimize their nonlinear properties. The newly synthesized organic chromophores were highly polar, zwitterionic and transparent at wavelengths above 600nm, which is a requirement for waveguide devices at 650nm. The molecular dipole moments were determined experimentally and theoretically. The experimental dipole moments and the theoretical dipole moments were found to be in agreement. The nonlinear optical properties of the new compounds were studied using the Kurtz powder technique. Large second harmonic generation was observed from 7-(2,6, dimethylmorpholino)-7-(4-methylpiperidine)-8,8-dicyanoquinomethane (25 times urea) as a result of the noncentrosymmetric crystal lattice ($P2_12_12_1$). A large twist between the donor moieties and the benzene ring was found from the crystallographic data, and compared with a theoretical model using an *ab initio* calculation. Strong fluorescence was observed in the solid states and glass forming solvents at low temperatures. An increase of the quantum yields as a function of viscosity was observed due to the constraining effect of the environment. Variations in the quantum yields from chromophore doped polymeric matrices such as PMMA at room temperature and at low temperature are attributed to the different "free volume" of the polymeric matrices. Possible mechanisms for the emission process in either viscous or non-viscous media are proposed. Photodegradation in solution was observed for illumination by a white light source. In parallel studies photodegradation in PMMA films was observed both in air and under vacuum. A possible photodegradation mechanism via free radicals, compatible with these experimental observations is suggested.

# Acknowledgements

It has been my honour to be a member of the Optoelectronics group in Physics Department at Durham. Firstly and foremost, I would like to thank my supervisor David Bloor for his invaluable guidance, his supervision, and his advice. Through the course of discussions during the last three years, he has brought me to the highest level. Sometimes I asked very fundamental questions to him, but he answered them kindly and patiently. I appreciate his supervision and his effort to my Ph.D project.

I would like to thank for Graham Cross for his important advice and encouragement to my Ph.D, especially in the coffee time. His jokes were great.

I would like to thank Marek Szablewski for his daily discussion in the chemistry lab and showing how chemists should be. Also, he corrected my English writing from his generosity. I appreciate his kindness to help me. I still remember the goal he made in the cup semi final 97. It was a very nice goal.

I would like Stewart Clark for *ab initio* calculation. His excellent calculation supports my experimental data.

I would like to thank Andy Monkman and Ifor Samuel for letting me use their equipment. Especially, thank Ifor for the discussion and Andy for playing football with me. He is an excellent defender.

I would like to thank Andrew Beeby in Chemistry Department for his useful advice on my luminescence work and reading through my luminescence chapter. I also thank him for letting me use his equipment. Discussions with him were very useful.

I would like to thank Garry Rumbles in Imperial College, London for accommodating me in his lab and letting me use his facilities for several days. Discussions with him were interesting, and useful for the low temperature study.

I would like to thank Norman Thompson and Davey Pattinson for technical support. Their technical support was vital for running experiments.

I would like to thank Andrei Basanov for providing me with X-ray crystallographic data.

I would like to thank Martin Bryce for the discussions associated with the initial calixarene work.

I would like to thank Moniur Halim for measuring quantum yields of the solid samples, and helping me to spin polymeric films.

I would like to thank Chetan Parmar in Imperial college for helping me to do "steady state" measurements, and carried out time resolved spectroscopy.

I would like to thank Anna Thornton, Philip Thomas, and Maria Farsari for their kind advice and encouragement to me. They helped me to integrate into the group and made me feel at home. Especially, thank Anna for her Chemistry advice, disciplining me to tidy up in the chemistry lab, Phil for helping me to understand the Physics side of nonlinear optics, and Maria for introducing me to the Durham society.

I would like to thank Ravi Mosurkal for providing the crystals of MORPIP, and Paul Laughlin for his encouragement to me, while I was writing my thesis. He is the top scorer in 5-a-side games.

I would like to thank Y Tao Ren, Nancy-Ann Hackman, Akira Matsutani, and Christoph Renger for sharing office with me and keeping me sane. Especially, thank Tao for the degradation measurements, Nancy-Ann for powder SHG and cheering me up, Akira for computing, and Christoph for teaching me "bad" words. I would like them to keep the fantastic family group atmosphere to the future. Also "lodger" Stuart Dailey for his useful advice.

I would like to thank Josep Carles-Albert, Dan Harrison, Rick Coles, Dave Hoare, Des Ryan ($R^2D^2$), Dave Dugdale, Steve Pugh, Stewart Clark, and Gavin Craw for welcoming me to their group. The time with them was very nice and memorable.

I would like to thank Mark Chang, Steve Willis, and Phil Dent for our friendship. The party at Fisher house on my 25$^{th}$ birthday was great.

I would like to thank Andrew Caink and Julie King for helping me to integrate into English society.

Lastly, I would like to thank Robert Williams at Oxford and Hiroyuki Sasabe at RIKEN for introducing me to David Bloor.

# Declaration and Copyright

I hereby declare that the work presented in this thesis has not previously been submitted for any degree and is not being currently submitted in candidature for any other degree.

Signed.....
(Candidate)

The work reported in this thesis was carried out by the candidate. Any work not carried out by the candidate is acknowledged in the main text.

Signed.....
(Supervisor)

Signed.....
(Candidate)

# Dedication

To the memory of Dora Wolcheover

# Abbreviations and Chemical structures

EO Electro-Optic

nlo Nonlinear optical

SHG Second Harmonic Generation

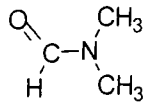

*N,N*-Dimethylforamide (DMF)

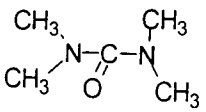

Tetramethylurea (TMU)

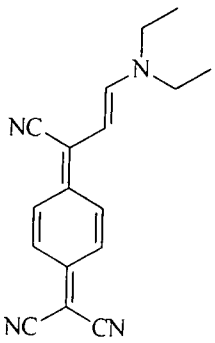

DEM1

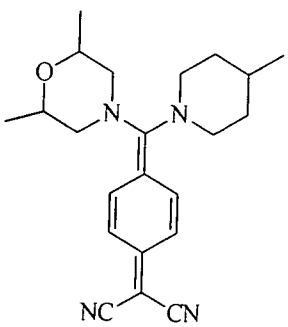

MORPIP

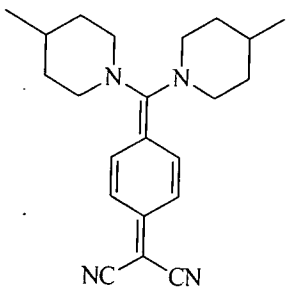

PIP2

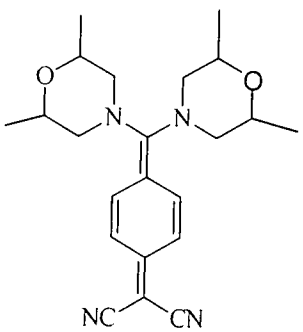

MOR2

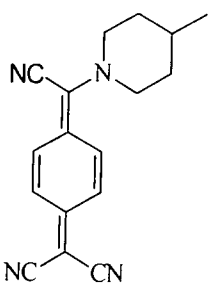

Mono PIP

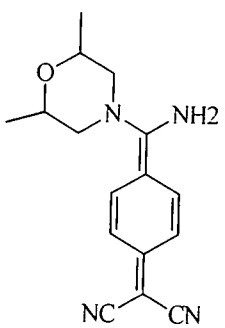

Si

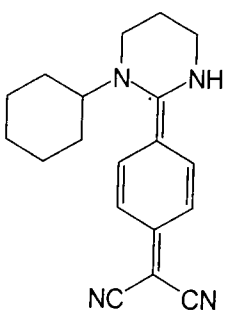

AMINO

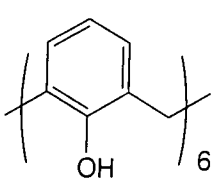

Calix[6]arene

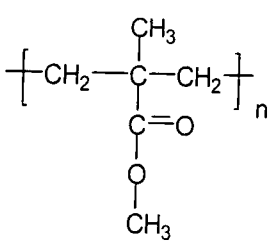

Poly(methyl methacrylate) (PMMA)

# Table of Contents

**It is a capital mistake to theorize before one has data.**

**Insensibly one begins to twist facts to**

**suit theories, instead of**

**theories to suit facts.**

*Sherlock Holmes*

# Chapter 1: Introduction

## 1.1 Introduction

Although the Pockels (EO) and Kerr effects [1,2] were known in the last century, it was only since lasers were invented [3], providing coherent, intense beams of light at particular wavelengths that nonlinear optical (nlo) effects were extensively studied [1,2,4-7]. Nonlinear optics is now established as a major area of research. Parallel developments in microelectronics, computing and data transmission have resulted in the emergence of communication networks based on optical fibres. The increasing demand of high speed computing in our daily life leads to the concept of the optical Information Highway. The development of the optical Information Highway requires the development of high speed optical modulators and switches. Nonlinear optics is of importance as the basis for devices to be used for the next generation of the optical network, since nonlinear optical devices are likely to be a key component for optical data transmission via optical fibres [2,4,6,8]. For long distance networks glass optical fibres are used with transmission wavelengths of 1.3 and 1.5μm. The primary focus on nonlinear optics has been the development of nonlinear optical materials with large nonlinearities at infra-red wavelengths [9]. However, relatively few devices are required to facilitate high speed data transmission over long distance fibre links. Currently, the data is generally converted into electrical signals and then distributed to the end users via local area networks (LANs) using copper wire. At the level of individual buildings, distribution can be either via copper wires or optical LANs utilizing polymer optical fibres (POFs). POFs have high attenuation in the infra-red but adequate transmission at shorter wavelengths

where cheap LEDs are available. Recently, high bandwidth, low loss, and multimode graded index POFs at visible and near infra-red wavelengths were reported [10-13]. Whilst step index optical fibres are commonly used, different modes travel at different velocities in step index fibres giving rise to dispersion [4], as shown in Fig1.1. Graded index optical fibres have a refractive index distribution that is parabolic to reduce this dispersion.

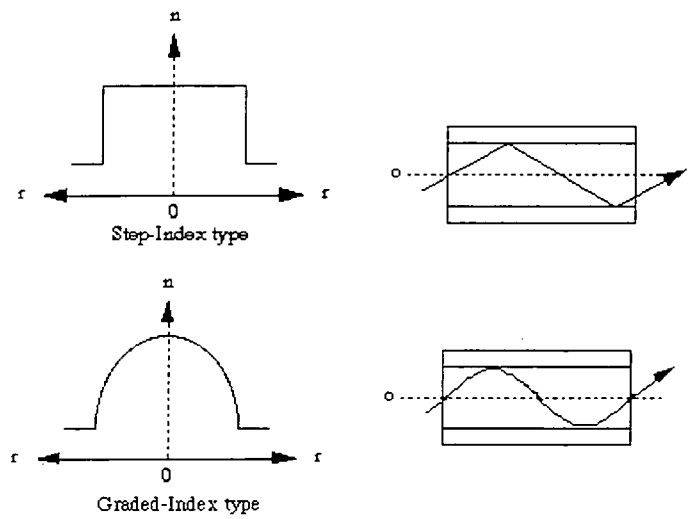


Figure.1.1 Step-Index and Graded-Index Optical Fibre

As the optical data network is extended closer to the end users, the need for inexpensive LANs based on POFs will increase. The LANs based on POFs are expected to become a much larger market since communication systems require low cost, mass produced fibres and devices.

The nlo chromophores and the nlo polymers developed so far have been designed for high nonlinearities at 1.3 and 1.5 μm, hence most of the materials are unsuitable for use of POF LANs due to strong absorption at visible wavelengths [5,14]. The focus of this research is the synthesis of chromophores that will have the low absorption profile in the range between 550 and 700nm with potential for

incorporation into nlo polymers. Physical properties of the nlo chromophores synthesized were also studied.

In the following sections the basis of the nonlinear optical properties of organic materials will be described.

## 1.2 Nonlinear optics

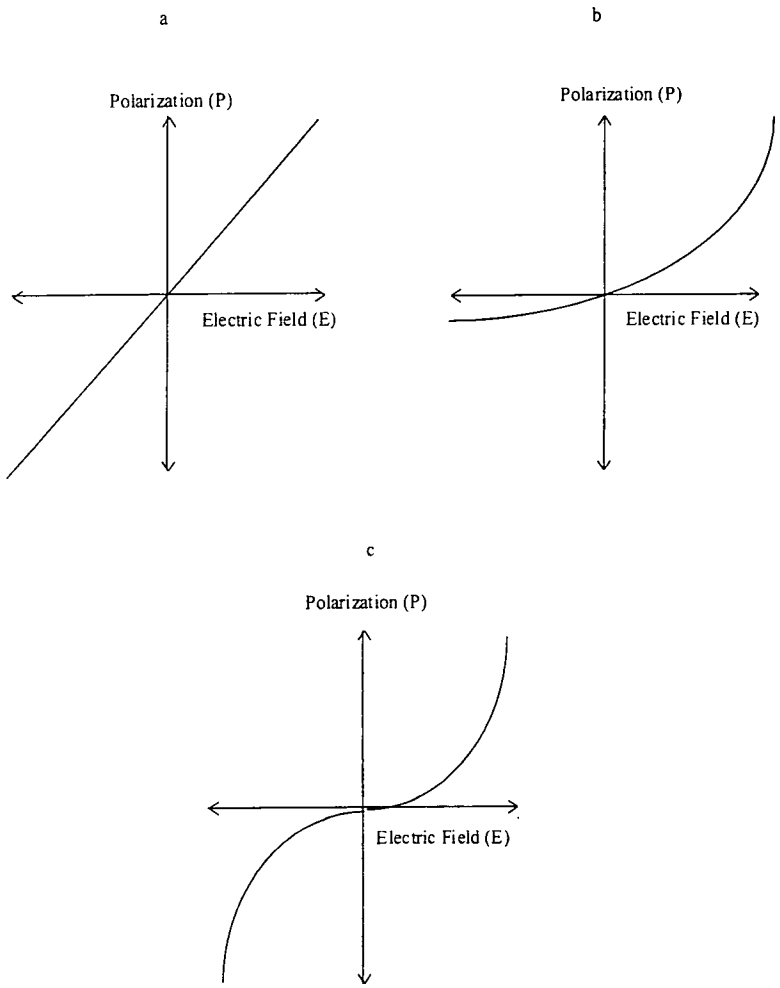


Figure 1.2 Schematic representation of the optical polarization in a) linear, b) noncentrosymmetric nonlinear media, c) centrosymmetric media

Nonlinear optical phenomena are a consequence of the interaction between light and matter. Light is an oscillating electric field. When light passes through a material, electrical interactions between the oscillating electrical field and the nuclei and electrons polarise the material. Usually, the polarization is proportional to the electrical field as shown in Fig.1.2.a. If a strong oscillating electrical field is applied with a laser then the polarization is no longer proportional to the applied electric field as shown for Fig.1.2.b and Fig.1.2.c. The nonlinear response of Fig.1.2.b is for a noncentrosymmetric medium. That of Fig.1.2.c is for a centrosymmetric medium [1,2,4-7] as discussed below.

### 1.2.1 Macroscopic nonlinearities

Nonlinear optics can be described in terms of the response of either a bulk media (macroscopic nonlinearities) or, in organic systems, of the individual molecules (microscopic nonlinearities). Although samples consist of many individual molecules, the measured values of the nonlinear optical properties correspond to the macroscopic nonlinearities, and hence these are described first.

The polarization per unit volume, P, is given by [1,2,4-7]

$$\tilde{P} = \varepsilon_o \bar{\chi} \tilde{E} \qquad (1.1)$$

where $\bar{\chi}$ is the linear susceptibility, which measures the ease of polarization, and $\tilde{E}$ is the applied electric field. $\tilde{P}$ and $\tilde{E}$ are vectors and $\bar{\chi}$ is a tensor.

The linear susceptibility is related to the relative permittivity, $\bar{\varepsilon}_r$, of the medium by:

$$\bar{\chi} = \bar{\varepsilon}_r - 1 \qquad (1.2)$$

The components of $\bar{\varepsilon}_r$ at optical frequencies are given by the squares of the components of the refractive index tensor.

$$\varepsilon_r(i,j,k) = n^2(i,j,k) \tag{1.3}$$

There are two circumstances under which the linear approximation described by eq.1.1 can break down; firstly, under the condition of high field strengths such as those generated by high power lasers, and secondly under an extreme condition, which may apply in case of specially designed materials of the material possessing a large high order susceptibility.

Then, the induced polarization is represented [1,2]

$$\begin{aligned}\tilde{P}(\omega) = \tilde{P}_i^o + \bar{\chi}_{ij}^{(1)}(-\omega)\tilde{E}_j(\omega) + \bar{\chi}_{ijk}^{(2)}(-\omega;\omega_1,\omega_2)\tilde{E}_j(\omega_1)\tilde{E}_k(\omega_2) \\ +\bar{\chi}_{ijkl}^{(3)}(-\omega;\omega_1,\omega_2,\omega_3)\tilde{E}_j(\omega_1)\tilde{E}_k(\omega_2)\tilde{E}_l(\omega_3)+.....\end{aligned} \tag{1.4}$$

Where $\chi^{(2)}$ and $\chi^{(3)}$ are the first and the second nonlinear susceptibilities, respectively, and the subscripts i, j, k, l refer to the bulk coordinate system of the medium.

Both e.q.1.4 and Fig.1.2.b show that the even numbered susceptibilities require a noncentrosymmetric medium. If the magnitude of the polarization, P(+E) is equal to P(-E), the material is a centrosymmetric medium as shown in Fig.1.2.c. However, if the polarization, P(+E) is not equal to P(-E) as shown in Fig.1.2.b, the medium must be noncentrosymmetric. It follows from eq.1.4 that the terms in even powers of $\tilde{E}$, hence the first nonlinear susceptibility, ($\chi^{(2)}$), are nonzero, only if the medium lacks inversion symmetry, i.e. P(+E)≠P(-E). If P(+E)=P(-E), the power series expansion of P can not contain even powers of E, hence the first nonlinear susceptibility, $\chi^{(2)}$, must be zero.

$\chi^{(2)}$ and $\chi^{(3)}$ provide the largest nonlinear effects and hence the most extensively studied [6,7,8].

The first nonlinear susceptibility, $\chi^{(2)}$, describes the frequency conversion of the incident radiation. The Sum frequency generation is expressed by $\chi^{(2)}_{ijk}(-\omega;\omega_1,\omega_2)$ ($\omega=\omega_1+\omega_2$) where the minus sign denotes that the energy of the radiation is conserved. $\omega$, $\omega_1$, and $\omega_2$ take values appropriate to this condition. Second harmonic generation (SHG) results when $\omega_1=\omega_2=\omega'$. The output frequency is twice as large as the input frequency ($\omega=2\omega'$). The linear electro-optic effect (or Pockels effect), $\chi^{(2)}_{ijk}(-\omega;\omega',0)$, is also a consequence of the first nonlinear susceptibility [1,2]. The Pockels effect is the dependence of the refractive index of the medium on a static electric field.

A well-known effect of the second nonlinear susceptibility, $\chi^{(3)}$, is the optical Kerr effect, i.e. the refractive index ($n$) of the medium is dependent on the intensity of light [1,2].

$$n = n_o + n_2 I \tag{1.5}$$

also the nonlinear refractive index ($n_2$) is defined by

$$n_2 = \frac{12\pi^2}{n_o^2 c}\chi^{(3)} \tag{1.6}$$

where c is the speed of the light.

Third harmonic generation is similar to the second harmonic generation, i.e., $\omega_1=\omega_2=\omega_3=\omega'$, $\omega=3\omega'$. The technique of field induced second harmonic generation (EFISH) uses the second nonlinear susceptibility described by $\chi^{(3)}_{ijkl}(-2\omega;\omega',\omega',0)$ [2,3,15,16,17]. In this technique a strong static electric field is applied to a solution causing a change of the average orientation of the molecules

with the permanent molecular dipoles. The applied electric field aligns molecules to give the noncentrosymmetry necessary for second harmonic generation.

### 1.2.2 Microscopic nonlinearities

A change in properties of the material induced by an electric field leads to nonlinear optical effects. The origin of the nonlinear effects are interactions between individual molecules and an applied electric field [1,2,4-7].

$$p_I = \mu_I + \alpha_{IJ}F_J + \beta_{IJK}F_JF_K + \gamma_{IJKL}F_IF_JF_K + .... \qquad (1.7)$$

where $\alpha$ is the polarizability, $\beta$ and $\gamma$ are the first and second hyperpolarizabilities, and I,J,K, are the principal molecular axes. These molecular susceptibilities are very similar to the macroscopic ones in eq.1.4, but the field F, applied in eq.1.7 is a local field. The local field is different from the external applied field since the internal field experienced by the molecules in a dielectric medium containing polarisable particles is influenced by the surrounding medium.

It is common to use the Lorentz-Lorenz local field factor for optical or high frequency fields [4,17,18]. The local field, $F_L$, is given by

$$F_L(\omega) = f_L(\omega)E(\omega) \qquad (1.8)$$

where $f_L$ is a local field factor, E is the external applied electric field, and then the Lorentz-Lorenz local field factor is given by

$$f_L(\omega) = \frac{(\varepsilon_h(\omega)+2)}{3} \qquad (1.9)$$

Where $\varepsilon_h(\omega)$ is the relative permittivity of the host medium at frequency $\omega$.

### 1.2.3 Models for nonlinear optics

Understanding the origin of nonlinearity is of importance for the optimization of the nonlinear optical properties of organic molecules. Model organic molecules with the second order response usually consist of three fundamental parts [2,4-7] as shown in Fig.1.3.

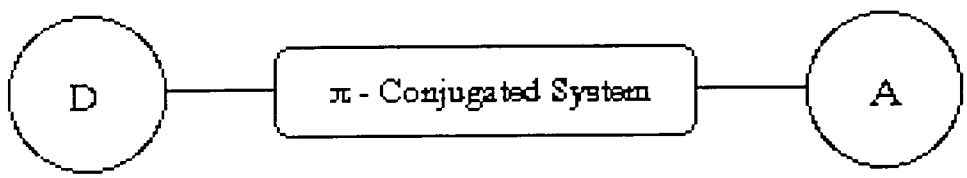


Figure 1.3 Basic model for the second order response in organic materials

Here A represents electron acceptors ($NO_2$, CN, etc), D represents electron donors ($NH_2$, $NR_2$, etc.) and the π conjugated system is an extented π conjugated sequence (one or more ethylenic, polyenic, aromatic unit, or conjugated heterocyclic units). Highly delocalized electrons in the π conjugated sequence allow electrons to move freely between the end of groups. The polarised charge distribution of such molecules between the electron donors and acceptors provides the required molecular noncentrosymmetry for finite first hyperpolarizability, β.

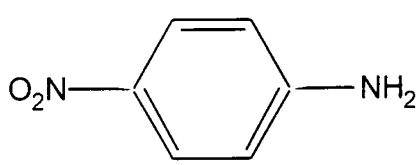


Figure 1.4 *p*-nitroaniline

*p*-nitroaniline, as shown in Fig.1.4, was well studied due to its structural simplicity [19,20,21]. Oudar proposed a two level model that considers only the

ground state and the first excited state, thus β of *p*-nitroaniline can be separated into two parts [15,22]:

$$\beta = \beta_{add} + \beta_{CT} \qquad (1.10)$$

Where $\beta_{add}$ is an additive term that comes from the distribution of the substituent - induced asymmetry of π cloud, and $\beta_{CT}$ is the charge transfer term that comes from the contributions of the configuration change from the ground state to the lowest energy polar resonance state, i.e., $n_{NH_2} \rightarrow \pi^*_{NO_2}$ in the case of *p*-nitroaniline where the charge transfer from the nitrogen nonbonding orbital of the amino group to the vacant orbital of the nitro group is the dominant contribution to the first excited state. The charge transfer term, $\beta_{CT}$, thus can be expressed by [15,22]:

$$\beta_{CT} = \frac{3e^2\hbar^2}{2m} \frac{W}{\left(W^2 - (2\hbar\omega)^2\right)\left(W^2 - (\hbar\omega)^2\right)} f\Delta\mu_{ge} \qquad (1.11)$$

where $\hbar\omega$ is the energy of a laser photon, $\Delta\mu_{ge}$ is the difference between the excited state dipole moment and the ground state dipole moment, W is the energy of the optical transition, and *f* is the optical transition strength. So $\beta_{CT}$ can be defined by the relations between the optical transition strength, the excited state energy, and the change of dipole moment between the excited state and the ground state [5,22].

## 1.2.4. Bond length alternation (BLA)

The permanent dipole moment, μ°, of an isolated molecule in the gas phase is located at the centre of a sphere with the radius, $a_o$, defined as the Onsager radius, as shown in Fig.1.5 [23,24]. The dipole moment in a medium such as a solution, μ, can

be expressed as the sum of the term of the permanent dipole, $\mu^{\circ}$, and the solvent induced part through an intrinsic internal field, or reaction field, R [23,24].

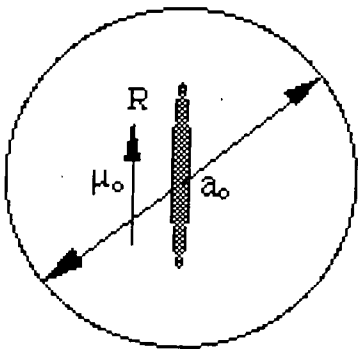


Figure 1.5. Onsager radius

$$\mu = \mu^{o} + \alpha R \qquad (1.12.)$$

$$R = \left( \frac{\mu}{4\pi\varepsilon_{o} a_{o}^{3}} \frac{2(\varepsilon - 1)}{2\varepsilon + 1} \right) \qquad (1.13)$$

where $\alpha$ is the polarizability of the solute. $\varepsilon_{o}$ and $\varepsilon$ are the permittivity of the vacuum and the relative permittivity of the corresponding solvent, respectively.

The electronic distribution of polar molecules is a function of the reaction field of the surrounding medium due to the charge transfer from donors to acceptors. Hence, it is important to know how the charges are separated at the accepting and donating substituents in the molecule. A convenient scale of the $\pi$ conjugation and charge structure for a model molecule with a polyenic bridge is given by the bond length alternation (BLA) [25-27]; the average difference between the lengths of alternating double and single carbon-carbon bonds.

In Fig.1.6.a, the neutral polyene structure is non-polar and the ground state dipole moment, $\mu$, is zero. With increasing reaction field the electronic distribution of the molecule changes from neutral to cyanine-like (Fig.1.6.b) and then to the zwitterionic

(Fig.1.6.c) form. The value of the dipole moment increases as value of the BLA increases from negative to positive as shown in Fig.1.6. The polarizability, $\alpha$, is the sum of the bond polarizabilities. The most polarizable molecule in Fig.1.6 is the cyanine model (Fig.1.6.b), where charges are equally distributed between atoms. Hence $\alpha$ becomes maximum, and at the same time BLA goes to zero because the average difference between the lengths of alternating carbon-carbon bonds is zero. Both polar and non-polar models in Fig.1.6 are less polarizable than the cyanine model due to the more localized charges between atoms in both models. $\alpha$ increases from negative BLA at zero reaction field and then, reaches maximum at the cyanine limit and then decreases.

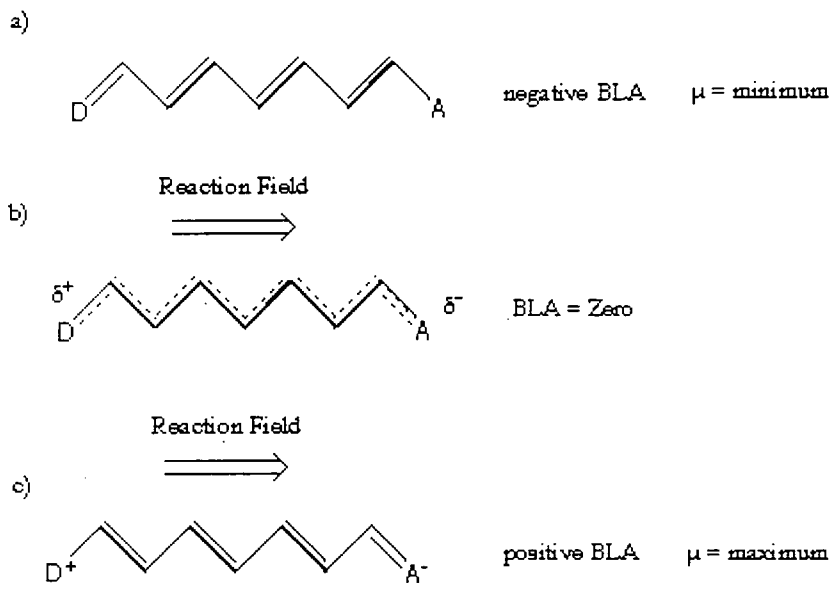


Figure 1.6 Schematic BLA representation in the polyenic models of a) non-polar, b) cyanine-like and c) polar molecules

In eq.1.14, the expression of bulk and molecular nonlinearlity can be expressed as a Taylor expansion. Hence β and γ are derived from the Taylor expansion series [1,2,4-7].

$$p = \mu + \alpha F + \beta FF + \gamma FFF + ..$$

$$= \mu + \alpha F + \frac{\partial \alpha}{\partial F} F + \frac{\partial \beta}{\partial F} FF + ... \qquad (1.14)$$

The hyperpolarizability, β, initially increases and reaches maximum, and then decreases through zero as does the slope of α in eq.1.14. Finally the value of β becomes negative when the BLA is positive as shown in Fig.1.7. The polar structure is the zwitterionic structure that tends towards the complete charge transfer model between the donor and the acceptor parts of molecules, and is also potentially highly nonlinear.

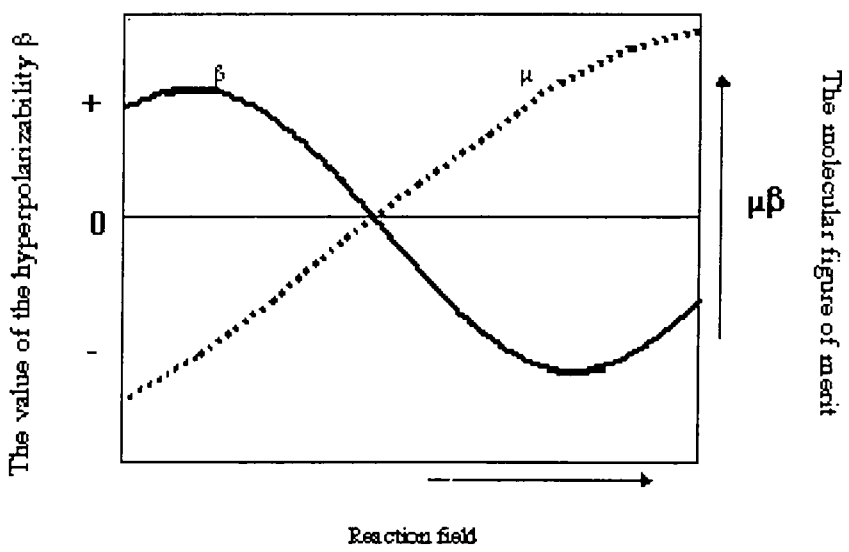


Figure 1.7 The molecular figure of merit

## 1.3 Organic Materials for nonlinear optics

### 1.3.1 Materials and Devices

Light modulators are an example of the application of nonlinear optical materials. Modulation of light is effected by a change of refractive index in a nonlinear optical medium [2,28]. An example of a light modulators is the Mach-Zender interferometer shown in Fig.1.7 [29,30]. The light in the Mach-Zender interferometer is split between the two arms of the interferometer, and then recombined where electrodes are set in one arm of the interferometer, and then recombined. Without a field on the electrodes maximum light output is achieved because the input light travels into the two arms equally and recombines in phase. When an electric field is applied in one arm, the refractive index of the arm changes due to the electro-optic effect. As a result of applying a field, the light travels in each arm at different speeds because the refractive indices of two arms are no longer the same.

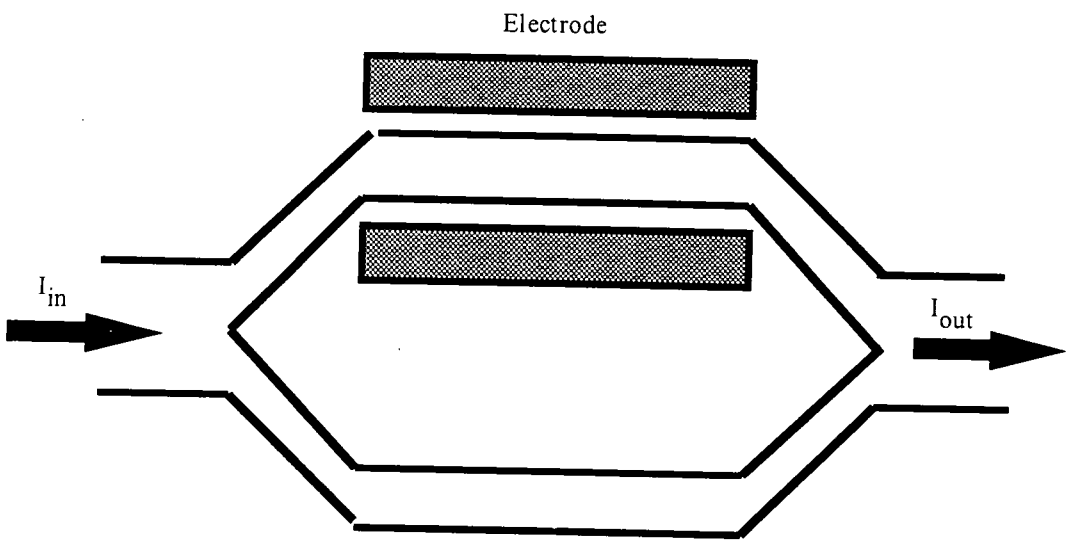


Figure 1.8 Mach-Zender interferometer

The refractive index change can be derived from either the second order electro-optic effect or the third order optical Kerr effect [1,2,4]. The principle of light modulation is the phase shift of light between two interfering light beams.

The phase shift for the electro-optic is given effect by

$$\phi = \frac{2\pi\Delta nL}{\lambda} = \frac{2\pi n_o^3 rEL}{\lambda} \qquad (1.15)$$

Where r is the electro-optic constant, E is the applied electric field, L is the propagation length of the nonlinear optical medium, $n_o$ is the linear refractive index, $\lambda$ is the wavelength of light, and $\Delta n$ is the change in refractive index.

For the optical Kerr effect

$$\phi = \frac{2\pi\Delta nL}{\lambda} = \frac{2\pi n_2 IL}{\lambda} \qquad (1.16)$$

Where $n_2$ is the intensity - dependent refractive index, I is the intensity, and L is the interaction length of the nonlinear medium.

The phase shift of the propagating light by either of these two nonlinear optical effects produces output optical signals that are different from the input optical signals. This can be used in optical switching devices. Inorganic materials such as $LiNbO_3$ are used in light modulators, but organic nonlinear materials could have the potential to replace them.

### 1.3.2 Comparison between inorganic and organic materials

Polymer light modulators offer several potential advantages over devices fabricated from inorganic materials. One difference between inorganic and organic materials is the speed of their polarization responses; polarization of inorganic materials generally comes from atomic displacements, but that of organic materials is

primarily due to electronic displacements, electronic displacements are much faster than the atomic displacements. It is very costly to grow large single inorganic crystals suitable for photonic devices [31]. Organic materials can be integrated into a polymeric medium. The advantages of polymeric systems are their potential low cost and ease of fabrication. The optical quality of polymers is high and their optical properties can be rationally modified. Polymeric modulators can be operated at lower voltages due to a higher non-linear coefficient, which means that smaller modulators can be fabricated. They can be operated at a much higher frequency up to gigahertz, because the change of dielectric constants in organics is small when going from the microwave region (gigahertz) to the optical signal region (terahertz). The low frequency dieletric constant in organics is well matched to the square of the refractive index in a polymeric medium ($n \approx 1.6$) so that the phase match between microwave signals and optical signals is very good in polymeric devices ($n^2 \approx \varepsilon$) [2,4]. For instance, the dielectric constant in inorganics such as $LiNbO_3$ ($\varepsilon \approx 34.7$) is higher than that of the dielectric constant in organics ($\varepsilon \approx 3$). Therefore polymeric devices can offer high bandwidth and high speed modulation.

### 1.3.3 Polymeric systems

The development of practical polymeric systems requires careful study to optimize their properties. Two assessment techniques have been used for the determination of the nonlinearities of chromophores that can be included in polymers. The Kurtz powder second harmonic generation (SHG) technique [32] allows SHG to be measured without the growth of large single crystals. However finite $\chi^{(2)}$ requires noncentrosymmetry in the bulk medium, i.e. a noncentrosymmetric crystal lattice.

After the synthesis of N-(4-nitrophenyl)-(L)-prolinol (NPP), the word, "molecular engineering" became common, because organic materials were carefully designed and prepared for nonlinear optics to achieve a noncentrosymmetric crystal lattice [33-35]. The technique of electric field induced second harmonic generation (EFISH) described in 1.2.1 provides a method of measuring the first hyperpolaribility of molecules in solution [15,16]. Not all molecules form noncentrosymmetric crystals that can be studied by the Kurtz method, but EFISH allows many potentially interesting molecules to be explored.

Polar molecules can be incorporated into glassy (amorphous) polymers to give high optical transmission. The required nonsymmetry of the bulk medium can be achieved by electric field poling. In electric field poling the polar organic molecules are aligned by an electric field applied above the glass transition temperature ($T_g$) of the host polymer as shown in Fig.1.9.

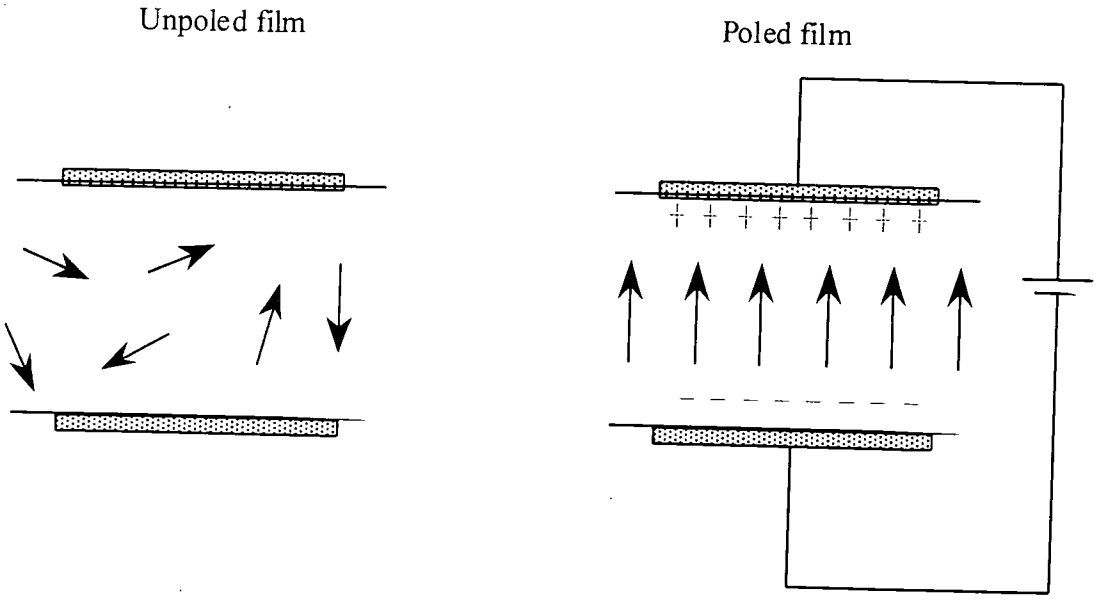


Figure 1.9 Introducing noncentrosymmetry in a polymeric medium by electric field poling

Above the glass transition temperatures the host polymers are like a viscous liquid so the dopants can be dissolved and aligned, and the alignment can be fixed below the glass temperature. These non-equilibrium alignments of the guest molecules are found to relax after poling [2,4,17]. This leads to decay of the second order nonlinearity. Hindering the relaxation of the alignments is possible by either the incorporation of the nlo active constituents as either part of the polymer main chain or the side chain, or the introduction of cross linking [8,36-39], or poling of high glass transition polymers at high temperature [2,4].

### 1.3.4. The molecular figure of merit

The macroscopic second order optical nonlinearity in a polymeric medium can be introduced with dipolar chromophores by the poling method. The relationship between macroscopic and microscopic nonlinearities in a polymeric medium is defined as [2,18];

$$\chi^{(2)}_{ijk}(-\omega;\omega_1,\omega_2) = Nf_i(\omega)f_j(\omega_1)f_k(\omega_2)\langle\beta_{IJK}(-\omega;\omega_1,\omega_2\rangle_{ijk} \qquad (1.17)$$

Where the term in brackets is a weighted sum of the averaged values of $\beta_{IJK}$ over all the orientations of chromophores in the polymeric medium. All *f*'s are local field factors.

After poling, the molecular dipole moment, $\mu_z$, and the vector component of the hyperpolarzability, $\beta_z$, of a particular molecule may be as shown in Fig.1.10.

The relationship between macroscopic and microscopic nonlinearilites can be written taking into account of effects of poling [2,17,18] as:

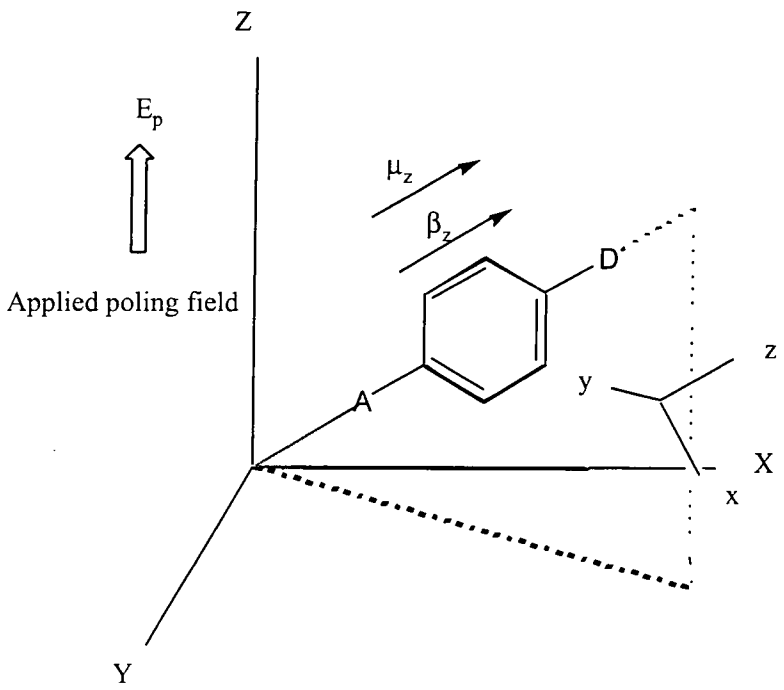


Figure 1.10 The molecular coordinates and the macroscopic frame in a poled polymeric medium

$$\chi^{(2)}_{ZZZ} = \frac{Nf_Z^2(\omega)f_Z(2\omega)\beta_z\mu E_P}{5kT} \qquad (1.16)$$

Where N is the number density of the chromophore, T is temperature, $\mu$ is the ground state dipole moment, and $E_p$ is the applied poling field. The number density of the chromophore, N, and molecular figure of merit, $\mu\beta$, have to be maximized for the optimization of the polymer nonlinearity. Careful synthesis can offer control of active substituents in the polymer to achieve the maximum density. However, the molecular figure of merit, $\mu\beta$, plays the dominant role in determining the values of $\chi^{(2)}$, because a large $\mu\beta$ gives a better material.

As disscussed earlier in 1.2.3, chromophores can have non-polar, and polar (zwitterionic) forms. The excited state dipole moment of chromophores with the zwitterionic character is larger than the ground state dipole moment. Therefore the

value of β is negative. Zwitterionic chromophores can have both large μ and a large negative β, hence achieving a large product, μβ, as shown in the right hand side of Fig.1.7.

As discussed earlier, $\beta_{CT}$ is the dominant factor of β. So $\beta_{CT}$ has to be considered for the optimization of the microscopic nonlinearities. In eq1.11, if the energies of photons ($\hbar\omega$ and $2\hbar\omega$) are equal to the energy of the optical transition (W), $\beta_{CT}$ goes to a maximum set by the natural line width, i.e. the damping factor, which was omitted from the e.q.1.11. $\beta_{CT}$ is frequency dependant due to this relation between the energy of optical transition and laser photons. So the β value at zero frequency (0 eV), which is termed as β(0) , and calculated with e.q.1.11 is used for the comparison of β values to avoid the effects of resonance [40].

## 1.4 Highly polar molecules

A class of organic molecules will be introduced of this section. These molecules have a zwitterionic nature, which gives a large molecular figure of merit.

### 1.4.1 7,7,8,8-tetracyanoquinodimethane (TCNQ) derivatives

#### 1.4.1.1 History of TCNQ

TCNQ was synthesized by Du Pont researchers in 1962 [41]. The molecule has four cyano groups. Since cyano qroups are very strong electron acceptors nucleophilic addition reactions are favourable [42-44]. The electron affinity ($E_A$=2.84 eV) of TCNQ is high due to not only to the presence of four electron acceptors but

also the conjugation system and planarity of the molecule. Therefore TCNQ can form stable charge transfer complexes with molecules like tetrathiofulvalene (TTF). These complexes show semiconducting properties, and the single TCNQ crystal is also an organic semiconductor [43]. Although the fact that TCNQ forms stable radical-ion salts through one electron transfer is of interest, these semiconducting complexes and stable radical salts are beyond the scope of thesis. Only the chemistry of TCNQ will be considered in this thesis.

### 1.4.1.2 Chemistry of TCNQ

Initially the synthetic chemistry to TCNQ derivatives was very restricted as a result of poor synthetic routes to TCNQ [41].

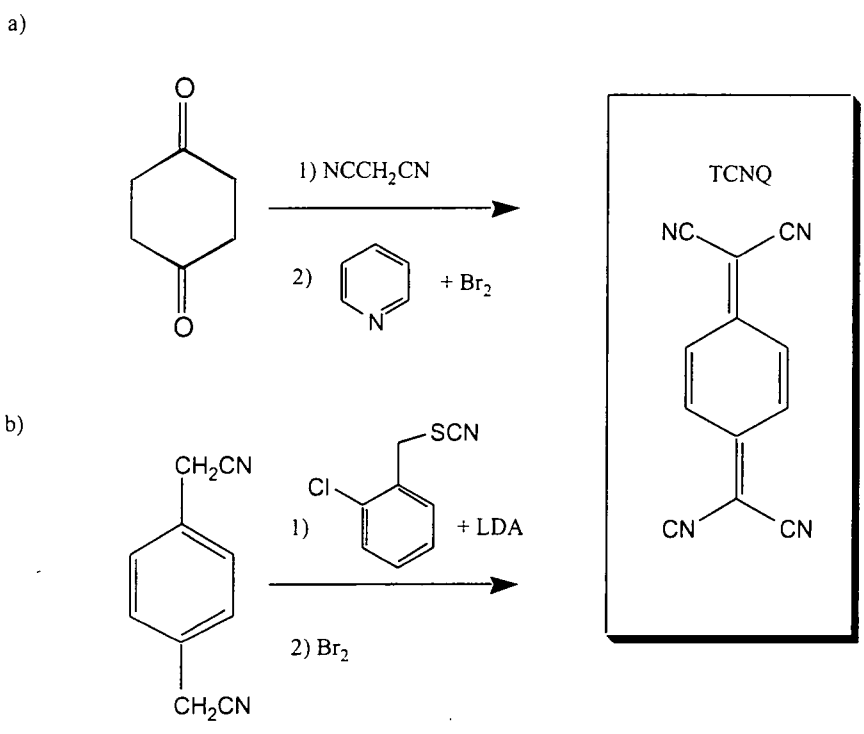


Figure 1.11 Synthetic routes to TCNQ

As shown in Fig.1.11.a, the earliest method found by the Du Pont group employed dicyanomethane, which was very difficult to work with due to its health hazard, and hence, there have been several attempts to achieve the preparation of TCNQ

derivatives more safely and easily [44-46]. The method using the non-toxic reagent, 2-chlorobenzyl thiocyanate was reported [47] and is shown in Fig.1.11.b.

The chemistry of 1,6 addition of TCNQ was then investigated [42,43,48,49]. The substitution of the cyano groups forms an intermediate product by 1,6 addition, which is shown in the middle structure of Fig.1.12. After the formation of the intermediate, one of the cyano groups is replaced by either a primary or secondary amine.

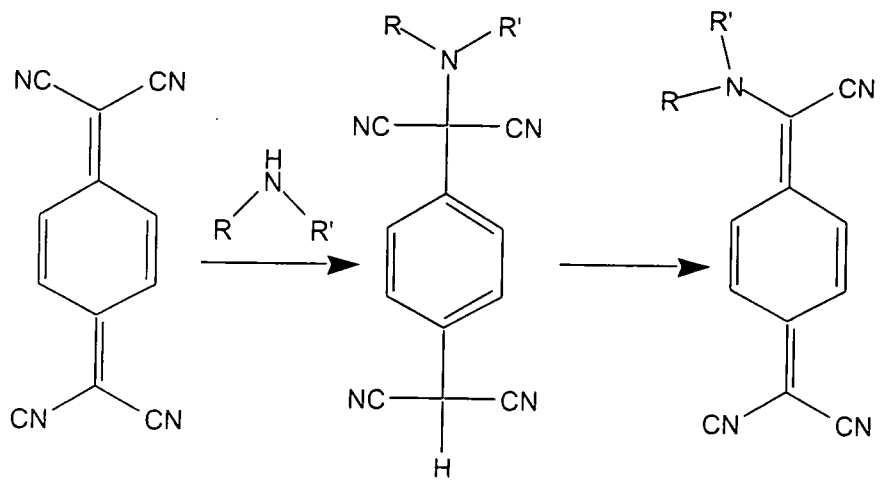


R=R'=H or R=H, R'=$C_nH_{2n-1}$

Figure 1.12 Substitution reaction of TCNQ with a primary or secondary amine via a 1,6 addition intermediate

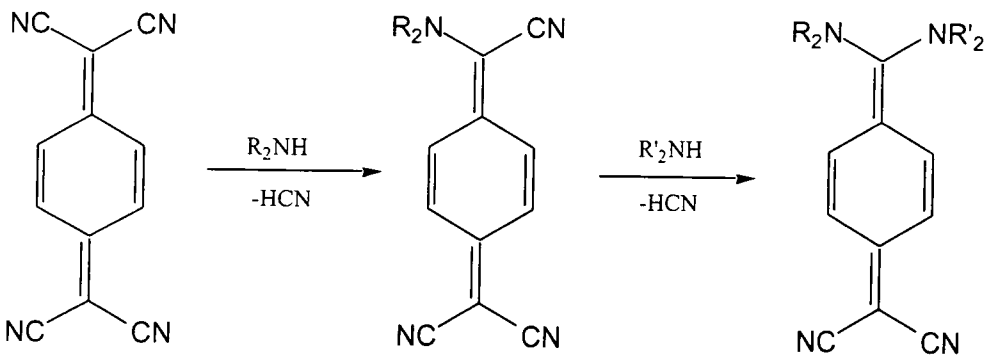


R and R' = H or Alkyl, R can = R'

Figure 1.13 Mono and di - substitutions of TCNQ with primary and secondary amines

As shown in Fig.1.12, one of the cyano groups of TCNQ can be replaced through the formation of the intermediate by 1,6 addition. The mono-substituted product can undergo further substitution in the same manner to give a di-substituted product shown in Fig.1.13. Bifunctional amines such as ethylenediamine can react with two cyano groups to give a cyclic product [42].

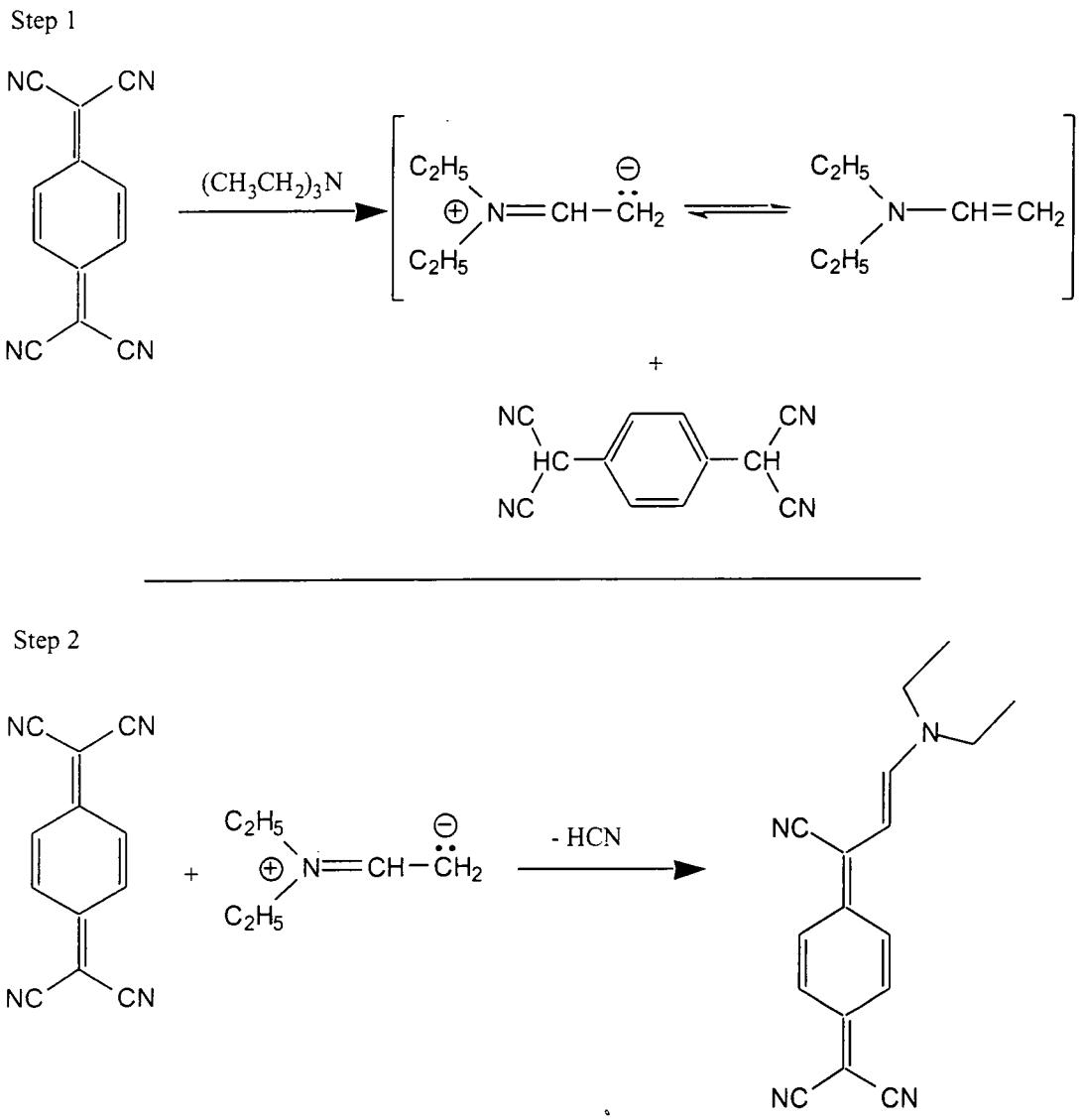


Figure 1.14 Reaction of TCNQ with a tertiary amine

Recently, the reaction of TCNQ with a tertiary amine leading to the formation of a zwitterionic adduct was found [50]. TCNQ, being an electron acceptor, extracts a proton from the tertiary amine to give an enamine and dihydro TCNQ ($TCNQH_2$) in

Fig.1.14, step1. The enamine reacts with TCNQ and eliminates HCN to give a new class of zwitterionic TCNQ derivatives in Fig.1.14, step2.

Two of these TCNQ derivatives that have been extensively studied are (4-[1-Cyano-3-(diethylamino)-2-propenylidene]-2,5-cyclohexadiene-1-ylidenepropnanedintrile) termed DEMI, and *N*-Acetaldehyde Diethyl Acetal-Piperidyl-(4-[1-Cyano-3-(diethylamino)-2-propenylidene]-2,5-cyclohexadiene-1-ylidenepropnanedintrile) termed Ultra[14], as shown in Fig1.15.

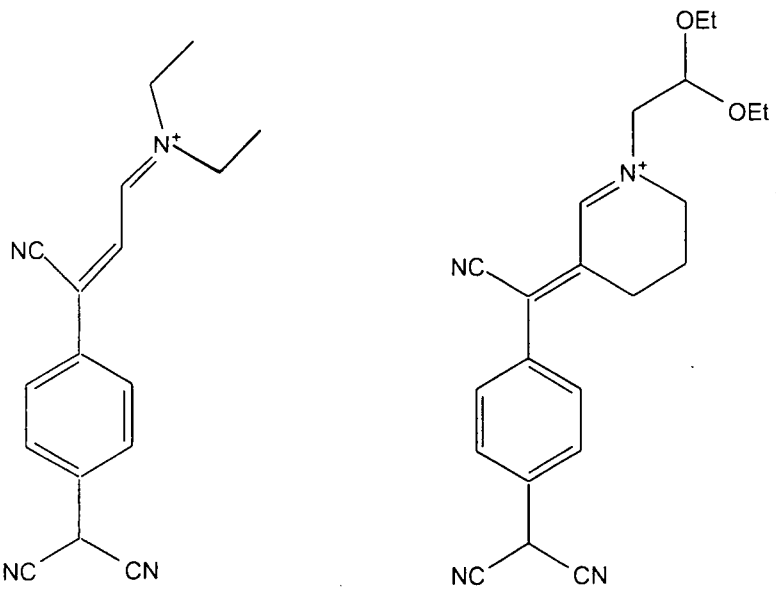


Figure 1.15 TCNQ derivatives, DEMI (left), and Ultra (right)

These two molecules are very polar. The dipole moment of DEMI was measured to be 27 D in chloroform with values up to 45 D with increasing solvent polarity. Also the molecular figure of merit at the zero frequency, $\mu\beta(0)$, was calculated to be $9450 \times 10^{-48}$ esu for DEMI in chloroform. This value belongs to the highest category ever reported for a molecular figure of merit [14].

DEMI is a very planar molecule as can be seen in the crystal structure and computational chemistry performed by 'Chem3D' (MM2 method) as shown below in

Fig.1.16. Electrons can easily flow within the molecule through the π conjugation between the donor $(NEt)_2$ and the acceptors (CN) without a barrier, this is essential to achieve a high value of the molecular figure of merit [14].

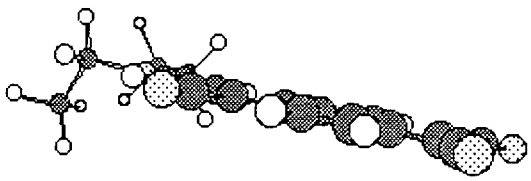

Figure 1.16 The side view of DEMI calculated by Chem3D.

The solubility of DEMI is very low in organic solvents, so it is very difficult to work with experimentally, e.g. in dielectric increment measurements to determine the dipole moment. Ultra is more soluble than DEMI. However, a twist in the conjugation system was found. As a result of the twisted conjugation system, μβ(0) for Ultra is lower than that for DEMI [14].

## 1.5 Photodegradation of organic materials for nonlinear optics

Targeted synthesis of nlo organic materials and their incorporation in polymeric systems for devices and waveguides is a very promising approach. Although organic materials for nonlinear optics offer many potential advantages over inorganic materials, they have a particular problem, the lack of photostability [51-59]. This is primarily due to their susceptibility to oxidation of their π conjugation system. DEMI suffers photodegradation [51,52,59,60]. If DEMI is exposed to light in the presence of oxygen, the π conjugation structure is fragmented. This can be seen in

the UV/visible spectrum where the value of absorption decreases, as a function of exposure time. Data for Ultra exposed to a white light source in acetonitrile is shown in Fig.1.17. After 45 minutes exposure Ultra was degraded.

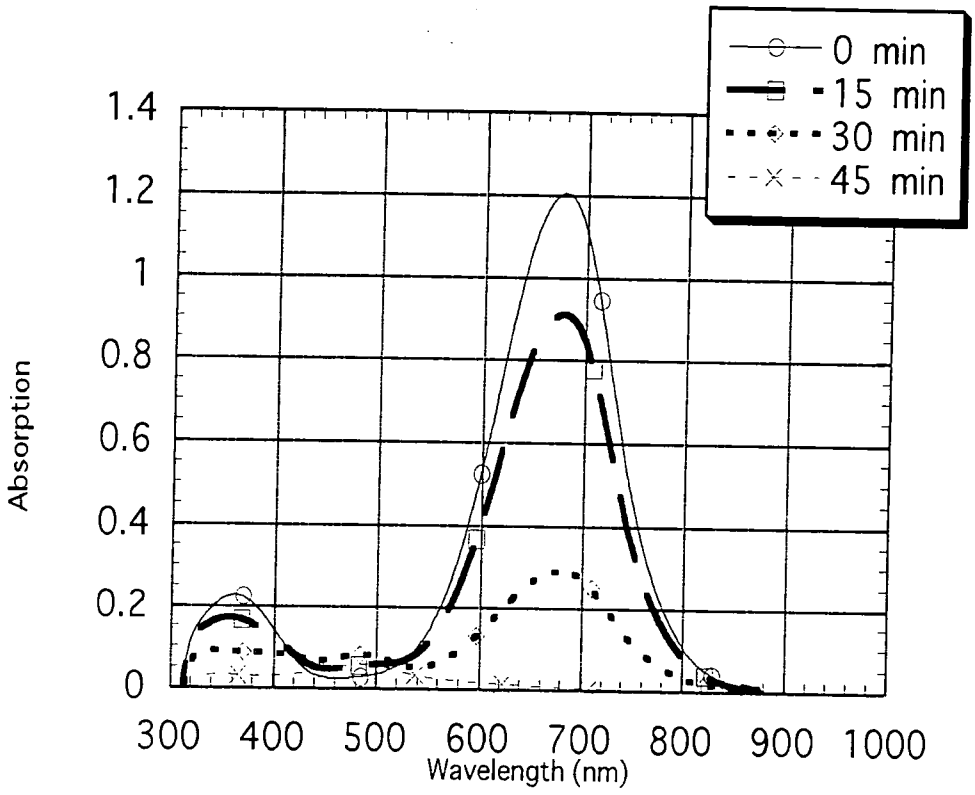


Figure 1.17 UV/Vis spectrum of Ultra under exposure of a white light source in acetonitrile solution

## 1.6 Light emitting organic materials

There are a large number of organic dyes that have been utilized in lasers [61]. Rhodamines are well known materials and amongst the most commonly used [61-68]. 4-(Dicyanomethylene)-methyl-6-(p-dimethylaminostyryl)-4H-pyran (DCM) is known as a laser dye [69,70], and *p*-Cyano-dialkyl anilines are known as twisted intramolecular charge transfer (TICT) molecules [71-77].

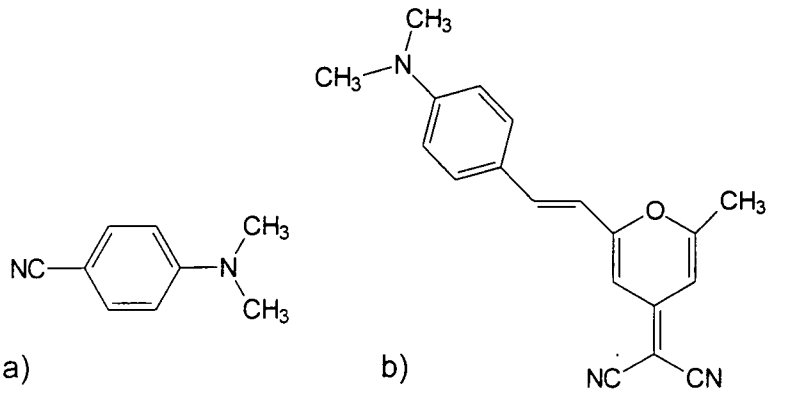


Figure 1.18 a) *p*-cyano dimethyl aniline, b) 4-(Dicyanomethylene)-methyl-6-(p-dimethylaminostyryl)-4H-pyran (DCM)

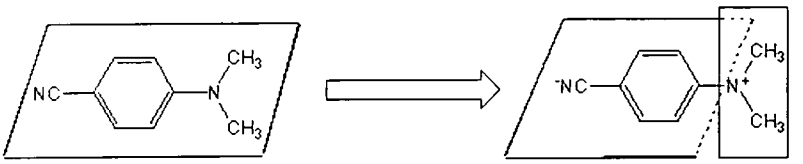


Figure 1.19 The TICT state of *p*-cyano dimethyl aniline

An example of a TICT molecule is *p*-cyano dimethyl aniline, as shown in Fig.1.18. *p*-Cyano dimethyl aniline has two competing fluorescence bands, depending on the polarity of the solvent in which it is dissolved. The emission band in non-polar solvents occurs in the visible region, whereas the emission band in the UV region is observed in polar solvents. The polar excited state of *p*-cyano dimethyl aniline is known as the TICT excited state [71-77] where the $-N(CH_3)_2$ group is twisted by 90° with respect to the aromatic ring as shown in Fig.1.19. A polar solvent stabilizes the TICT excited state. The formation of the TICT state is sensitive to the viscosity of solvent [72,77], the polarity of solvent [72,75,76,77], donor substiuent

ionization potential [72,77], acceptor substiuent electron withdrawing power [72,73,77], and the twist angle in the TICT state [72,77], because these five factors affect the stability of the TICT state. [71-77].

DCM and *p*-cyano dimethyl aniline have a structural similarity to TCNQ derivatives considered here in terms of the donor-acceptor molecular system.

An investigation of luminescence properties of some TCNQ derivatives considered in this project was carried out. It is noteworthy that this is the first time the luminescence properties of TCNQ derivatives have been investigated.

## 1.7 Research outline

My Ph.D. project involved the synthesis and characterization of a novel class of zwitterionic organic chromophores for nonlinear optics. By modifications of the structures and control of the molecular geometry of these chromophores it was hoped to optimize their nonlinear properties. The materials have a unique combination of physical and nonlinear optical properties making them potential candidates for use in waveguide devices at 650 nm, ideal for local area network applications, because the absorption of the chromophores around 650nm was low.

Physical properties such as nonlinearities and dipole moments of the target TCNQ derivatives were determined by computational methods. Computer packages such as MOPAC, Cerius2 and Chem3D were used for the prediction of physical properties. Chromophores were synthesized utilising theoretical predictions. The synthesized molecules were characterized chemically and physically. Nuclear Magnetic Resonance spectroscopy (NMR), Infrared spectroscopy (IR), UV/Vis absorption spectroscopy and dipole moment determinations were used as tools to study their behaviour and molecular properties. Second harmonic generation (SHG)

by the Kurtz powder technique was studied. One of the materials showed a strong powder SHG signal which was 25 times larger than that of urea. Crystal structures were well characterized and correlated with the results of powder SHG experiments.

Photoluminescence studies were carried out since some materials gave strong emission. Emission, photoluminescence excitation, time-resolved spectra were obtained. The chromophores considered here were very sensitive to the surrounding media. The materials were also doped into PMMA using various solvents and their luminescence properties examined. A PMMA film prepared from DMF gave better emission than a PMMA film prepared from cyclohexanone, so the choice of solvent has a marked effect on the their emission efficiency.

As mentioned in Section 1.5, photostability is the critical issue from the point of practical applications. Therefore the project also included efforts to prepare photostable organic molecules and determine the photostability of the prepared molecules. Intrinsically photostable materials were chosen as targets for synthesis.

Chapter 2 presents experimental methods used in synthesis and chemical characterization. Nonlinear optical properties and other related physical properties of TCNQ derivatives are presented in chapter 3. Dipole moments, solvatochromism were studied and the powder second harmonic generation is discussed in the context of the crystal structures of the TCNQ derivatives.

Luminescence studies of TCNQ derivatives will be described in chapter 4. Absorption, emission, photoluminescence excitation, and time resolved spectroscopy were carried out in various solvents and condensed phases. Measurement of quantum efficiency is presented here.

Photodegradation of TCNQ derivatives is presented in chapter 5. Degradation results will be compared for polar and non-polar media. The mechanism of

photodegradation will be also considered based on the proton NMR spectra of degraded chromophores.

Finally, chapter 6 contains closing remarks with an overview of this project and suggestions for further research.

## Chapter 1: References

[1] R.W.Boyd, Non-Linear Optics, Academic Press Inc., London (1992)

[2] P.N.Prasad, D.J.Williams, Introduction to Nonlinear Optical Effects in Molecules and Polymers, John Wiley&Sons, Inc., New York (1991)

[3] T.H.Maiman, Nature, **187**, 1960, 493

[4] L.A.Hornak,Polymer for lightwave and integrated optics., Marcel Dekker, inc., New York (1992)

[5] D.R.Kanis, M.A.Ratner, T.J.Marks, Chem.Rev., **94**, 1994, 195

[6] R.W.Munn, C.N.Ironside, Principles and Applications of Nonlinear Optical Materials, Blackie Academic&Professional, Glasgow (1993)

[7] A.J.Heeger, J.Orenstein, D.R.Ulrich, Nonlinear Optical Properties of Polymers, Materials Research Society, Pennsylvania (1987)

[8] G.A.Lindsay, K.D.Singer, Polymers for Second-Order Nonlinear optics, ACS Symposium Series 601, American Chemical Society (1995)

[9] L.R.Dalton, A.W.Harpar, B.Wu, R.Ghosn, J.Laquindanum, Z.Liang, A.Hubbel, C. Xu, Adv.Mater., **7**, 1995, 519

[10] A.Tagaya, S.Teramoto, T.Yamamoto, K.Fujii, E.Nihei, Y.Koike, K.Sasaki, IEEE J.Quantum Electronics,**31**,1995,2215

[11] R.T.Chen, D.Robinson, H.Lu, M.R.Wang, T.Jannson, R.Baumbick, Opt.Eng., **31**, 1992, 1098

[12] T.Ishigure, E.Nihei, Y.Koike, Appl.Opt., **35**, 1996, 2048

[13] Y.Koike, T.Ishigure, E.Nihei, J.Lightwave Tech., **13**, 1995, 1475

[14] M.Szablewski, P.R.Thomas, A.Thornton, D.Bloor, G.H.Cross, J.M.Cole, J.A.K.Howard, M.Malagoli, F.Meyers, J.Brédas, W.Wenseleers, E.Goovaerts, J.Am.Chem.Soc., **119**, 1997, 3144

[15] J.L.Oudar, J.Chem.Phys., **67**, 1977, 446

[16] B.F.Levine,C.G.Bethea, J.Chem.Phys.,**63**,1975,2666

[17] K.D.Singer,J.E.Sohn, S.J.Lalama, Appl.Phys.Lett., **49**, 1986, 248,

[18] D.M.Burland, R.D.Miller, C.A.Walsh; Chem.Rev., **94**, 1994, 31

[19] D.S.Chemla, J.L.Oudar, J.Jerphagnon, Phys.Rev B., **12**, 1975, 4534

[20] S.J.Lalama, A.F.Garito, Phys.Rev A.**20**, 1979, 1179

[21] M.Ståhelin, D.M.Burland, J.E.Rice, Chem.Phys.Lett., **191**, 1992, 245

[22] J.L.Oudar, D.S.Chemla, J.Chem.Phys., **66**, 1977, 2664

[23] J.Onsager, J.Am.Chem.Soc., **58**, 1936, 1486

[24] K.Nishiyama, T.Honda, H.Reis, U.Müller, K.Müllen, W.Baumann, T.Okada, J.Phys.Chem.A, **102**, 1998, 2934

[25] F.Meyers, S.R.Marder, B.M.Pierce, J.L.Brédas, J.Chem.Soc., **116**, 1994, 10703

[26] R.Ortiz, S.R.Marder, L.Cheng, B.G.Tiemann, S.Cavagnero, J.W.Ziller, J.Chem.Soc., Chem.Comm., 1994, 2263

[27] I.D.L.Albert, T.J.Marks, M.A.Ratner, J.Phys.Chem., **100**, 1996, 9714

[28] J.Wilson, J.F.B.Hawkes, Optoelectronics, Prentice Hall (1989)

[29] R.Lytel, A.J.Ticknor, G.F.Lipscomb, ACS Symposium Series 601., American Chemical Society (1995), 414

[30] Y.Shi, W.H.Steier, M.Chen, L.Yu,L.R.Dalton, Appl.Phys.Lett., **60**, 2577,

[31] R.Dagani, C&EN., March 4, 1996, 22

[32] S.K.Kurtz,T.T.Perry,J.Appl.Phys.,**39**,1968,3798

[33] J.Zyss, J.F.Nicoud, M.Coquillay, J.Chem.Phys., **81**, 1984, 4160

[34] M.Barzoukas, D.Josse, P.Fremaux, J.Zyss, J.F.Nicoud, J.O.Morely, J.Opt.Soc. Am.B, **4**, 1987, 977

[35] A.Fkyerat, A.Guelzim, F.Baert, J.Zyss, A.Perigaud, Phys.Rev B., **53**, 16236

[36] H.K.Hall, Jr.Thauming Kuo, T.M.Leslie, Macromolecules, **22**, 1989, 3525

[37] G.David Green, H.K.Hall, Jr.J.E.mulvaney, J.Noonan, D.J. Williams, Macromolecules, **20**, 1987, 717

[38] K.M.White, P.K.Kitipichai, C.V.Francis, Appl.Phys.Lett., **66**, 1995, 3099

[39] K.J.Drost, A.K-Y.Jen, V.P.Rao, Chemtech, **25**, 1995, 16

[40] S.J.Lalama, K.D.Singer, A.F.Garito, K.N.Desai, Appl.Phys.Lett., **39**, 1981, 940

[41] D.S.Acker, W.R.Hertler, J.Am.Chem.Soc., **84**, 1962, 3370

[42] W.R.Hertler, H.D.Hartzler, D.S.Acker, R.E.Benson, J.Am.Chem.Soc., **84**, 1962, 3387

[43] B.P.Bespalov, V.V.Titov, Russian.Chem.Rev., **44**, 1975, 1091

[44] R.C.Wheland, E.L.Martin, J.Org.Chem., **40**, 1975, 3101

[45] M.R.Bryce, S.R.Davies, A.M.Grainger, J.Hellberg, M.B.Hursthouse, M.Mazid, R.Bachmann, F.Gerson, J.Org.Chem., **57**, 1992, 1690

[46] R.J.Crawford, J.Org.Chem., **48**, 1983, 1366

[47] M.R.Bryce, A.M.Grainger, M.Hasan, G.J.Ashwell, P.A.Bates, M.B.Hursthouse, J.Chem.Soc.Perkin Trans.I., 1992, 611

[48] O.A.El.Seoud, F.P.Ribeiro, A.Martins, P.P.Brotero, J.Org.Chem., **50**, 1985, 5099

[49] M.Ravi, D.N.Rao, S.Cohen, I.Agranat, T.P.Radhakrishnan, Chem.Mater., **9**, 1997, 830

[50] M.Szablewski, J.Org.Chem., **59**, 1994, 954

[51] N.A.Weir, J.Arct, A.Ceccarelli, Eur.Polym.J., **32**, 1996, 805

[52] J.R.Sheats, J.Phys.Chem., 1990, 94, 7194

[53] S.Panlasem, J.Kuczynski, J.K.Thomas, Macromolecules, **27**, 1994, 3773

[54] R.D.Scurlock, B.Wang, P.R.Ogilby, J.R.Sheats, R.L.Clough, J.Am.Chem.Soc., **117**, 1995, 10194

[55] R.Gooden, M.Y.Hellman, R.S.Hutton, F.H.Winslow, Macromolecules, **17**, 1984, 2830

[56] K.K.Okudaira, S.Hasegawa, P.T.Sprunger, E.Morikawa, U.Saile, K.Seki, Y.Harada, N. Ueno, J.Appl.Phys., **83**, 1998, 4292

[57] S.Popov, Pure Appl.Opt., 1998, 1379

[58] M.Yan, L.J.Rothberg, F.Papadimitrakopoulos, M.E.Galvin, T.M.Miller, Phys.Rev.Lett., **73**, 1994, 744

[59] Y.T.Ren, G.H.Cross, Private communications (1995-1998)

[60] A.R.Frimer, Chem.Rev., **79**, 1979, 359

[61] F.P.Schåfer, Dye Lasers, Springer-Verlag Berlin, New York (1973)

[62] C.J.Tredwell, A.D.Osborne, J.C.S.Faraday II, **76**, 1980, 1638

[63] A.D.Osborne, J.C.S.Faraday II,**76**,1980,1627

[64] K.G.Casey, E.L.Quitevis, J.Phys.Chem., **92**, 1988, 6590

[65] J.E.Selwyn, J.I.Steinfeld, J.Phys.Chem., **76**, 1972, 762

[66] A.Costela, I.Garcia-Moreno, J.M.Figuera, F.Amat-Guerri, R.Mallavia, M.D.Santa-Maria, R.Sastre, J.Appl.Phys, **80**, 1996, 3167

[67] F.Amato-Guerri, A.Costela, J.M.Figuera, F.Florido, R.Sastre, Chem.Phys.Lett., **209**, 1993,352,

[68] A.Costela, I.Garcia-Moreno,J.M.Figuera, F.Amat-Guerri,R.Sastre, Appl.Phys.Lett.,**68**,1996,593

[69] S.Pommeret, T.Gustausson, R.Naskrecki, G.Baldacchino, J.C.Mialocq, J.Mol.Liq., **64**, 1995, 101

[70] L.Tanja, A.K.Sharma, R.D.Singh, Material Science Forum., **223-224**, 1996, 325

[71] Z.R.Grabowski, J.Dobkowski, Pure&Appl.Chem., **55**, 1983, 245

[72] W.Retting, J.Luminescence, **26**, 1980, 21

[73] K.A.Zachariasse, M.Grobys, Th.von der Haar, A.Hebecker, Y.U.II'ichev, Y.-B.Jiang,O.Morawski, W.Kühnle, J.Photochem.Photobiol., A, Chem., **102**, 1996, 59

[74] D.Braun, P.L.Nordio, A.Polimeno, G.Saielli, Chem.Phys., **208**, 1996, 127

[75] J.Hicks, M.Vndersall, Z.Babarogic, K.B.Eisenthal, Chem.Phys.Lett., **116**, 1985, 18

[76] Y.Wang, K.B.Eisenthal, J.Chem.Phys., **77**, 1982, 6076

[77] W.Retting, Angew.Chem.Int.Ed.Engl., **25**, 1986, 971

# Chapter 2: TCNQ derivatives

## 2.1 TCNQ amino derivatives

There are relatively few papers reporting studies of the nonlinear optical properties of TCNQ derivatives substituted with primary and secondary amines [1,2], although the chemistry of TCNQ has been known for the last thirty years [3-5]. The reaction of TCNQ with primary and secondary amines mechanism was illustrated in Fig.1.12 and 1.13. The range of primary and secondary amines, which were employed to react with TCNQ, is shown in Fig.2.1. 2,6, Dimethyl morpholine as shown in Fig.2.1 (a) has two stereoisomers both cis/trans mixtures and pure cis materials were used in the syntheses described below

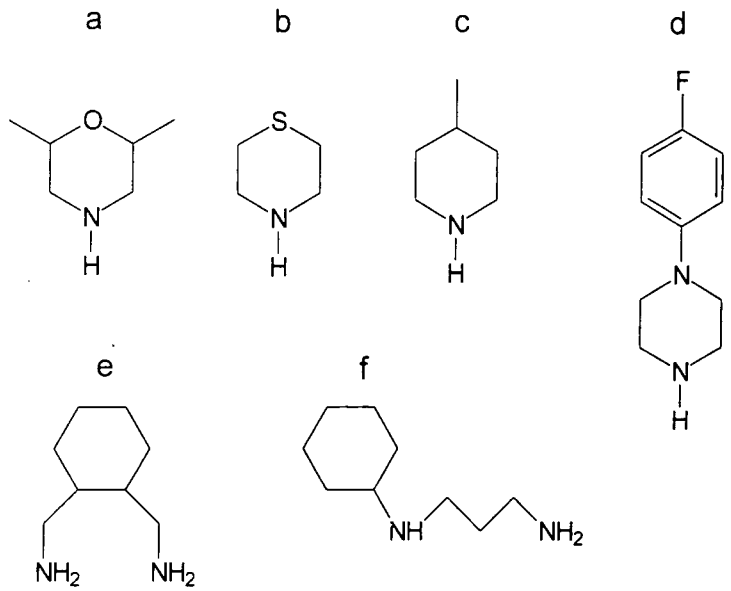


Figure 2.1 Amines reacted with TCNQ a) 2,6, dimethyl morpholine, b) thiomorpholine, c) 4-methyl morpholine, d) 1-(4-flourophenyl) piperazine, e) 1,2, diaminocyclohexane, f) (3-aminopropyl) cyclohexylamine

By substitution of either one or two nitrile groups, TCNQ adducts can be symmetric or asymmetric as shown in Fig.2.2. Asymmetric molecules may be able to form noncentrosymmetric crystals, because the asymmetry of the molecule favours formation of noncentrometric crystals such as *m*-nitroaniline.

Symmetric TCNQ adducts such as MOR2 were synthesized by a one step reaction as shown in Fig.2.2 (b). Hence, they are very easy to prepare. Asymmetric TCNQ adducts such as MORPIP were synthesized by two step reactions as shown in Fig.2.2 a. $TCNQ^-$ (normally $\lambda_{MAX}$=842,743,420 nm in acetonitrile) forms during the course of the reactions as an intermediate, and byproduct, and can be removed by recrystallization of the crude product in acetonitrile [3]. As the first step the purity of the product can be checked by the absence of the $TCNQ^-$ peaks in acetonitrile by UV/Vis spectroscopy.

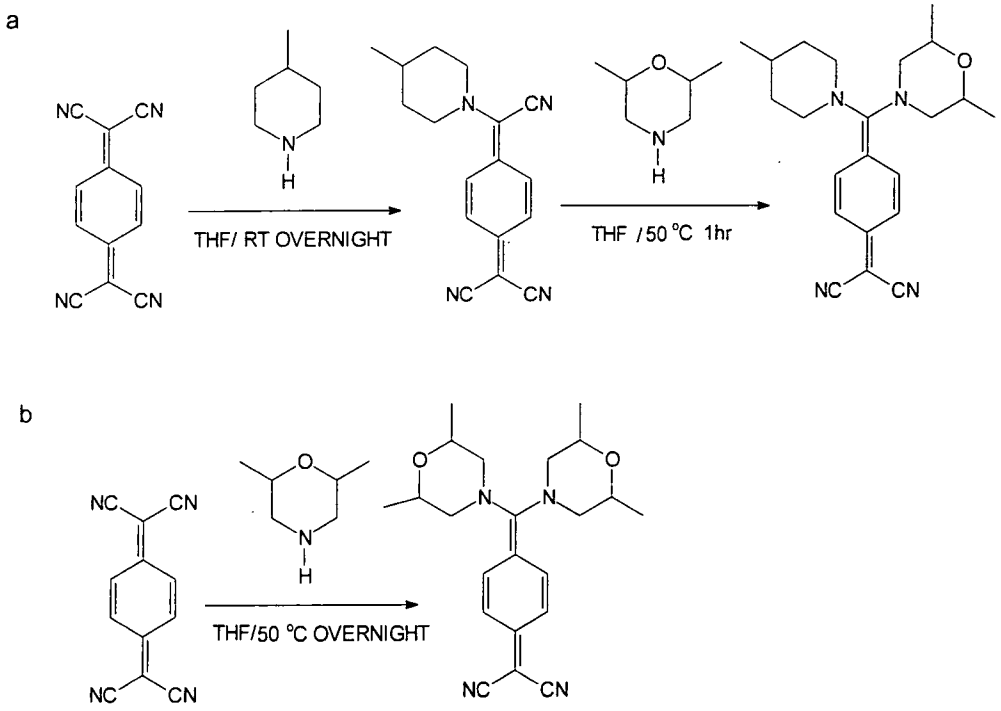


Figure 2.2 Synthesis of TCNQ derivatives

The amines, shown in Fig.2.3, were employed in the reaction, but the reaction did not proceed in the normal manner. Two amines, triphenyl amine (Fig.2.3 (a)) and t-butyl diethyl amine (Fig.2.3 (b)) were too bulky to form intermediates due to their steric hinderance. In the case of the triphenyl amine withdrawing electrons from the lone pair of the nitrogen atom affects the reactivity of the amine, since the three phenyl groups are electron withdrawing groups.

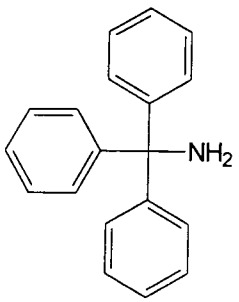


a

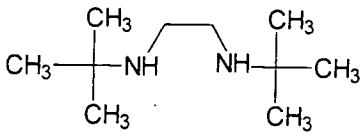


b

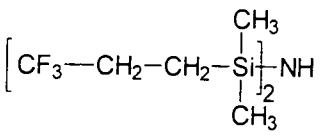


c

Figure 2.3 The range of amines considered

The final product of the reaction of 1,3-bis (3,3,3-trifluoropropyl) tetramethyl disilazane (Fig2.3.c) with 7-(2,6 dimethylmorpholino) -7,8,8-tricyanoquinodimethane was unexpected. The $H^1$ NMR spectrum of the final product was different from those of starting materials and the expected product.

The IR spectrum of the product was obtained. Peaks of the stretching nitrile at 2171 and 2126 $cm^{-1}$ were found. These peaks suggest that the product should be a bis substituted TCNQ derivative. Peaks due to the aliphatic primary amines at 3350,

3161 $cm^{-1}$, and the peak due to the C-N stretching of primary amines at 1326 $cm^{-1}$ were found. These peaks suggest the existence of the primary amines in the product. Tetramethyl silane (TMS) is used as a reference in $H^1$ NMR spectroscopy to define a chemical shift of 0 ppm. The starting amine has some methyl peaks located near zero shift (a) next to silane, as shown in Fig2.4 (left). But these peaks were not found in the spectrum of the final product, as shown in Fig2.4 (right). The only peak found in the final product between 0 and 2ppm was due to the six methyl protons (d) from 2,6,methyl morpholine, as shown in Fig.2.4.

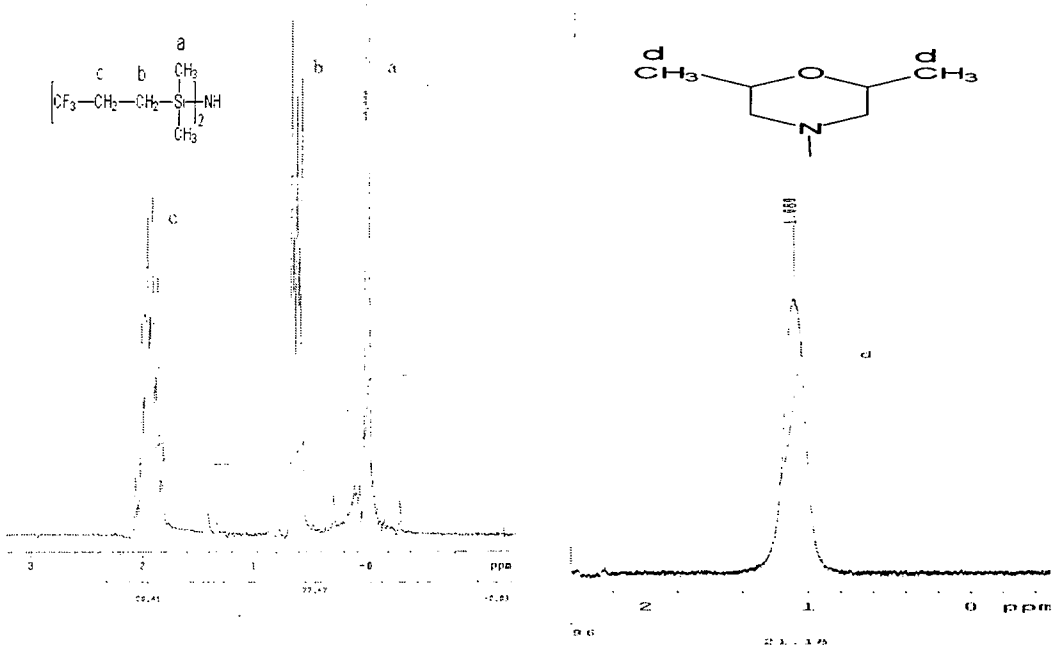


Figure 2.4 Parts of NMR spectra of the starting amine (left) and the product (right)

$Si^{29}$ NMR spectroscopy was carried out, but no silicon was detected in the compound. A proposed mechanism of this unexpected reaction is illustrated in Fig.2.5. Silicon can stabilize positive charges adjacent to it. In this molecular system the delocalised positive charge sits between the silicon and the nitrogen. Bonds between the silicon

and the nitrogen were broken as shown in Fig.2.5. The proposed product is consistent with the NMR, IR, mass spectra, and micro analysis data as described in 2.2.8.

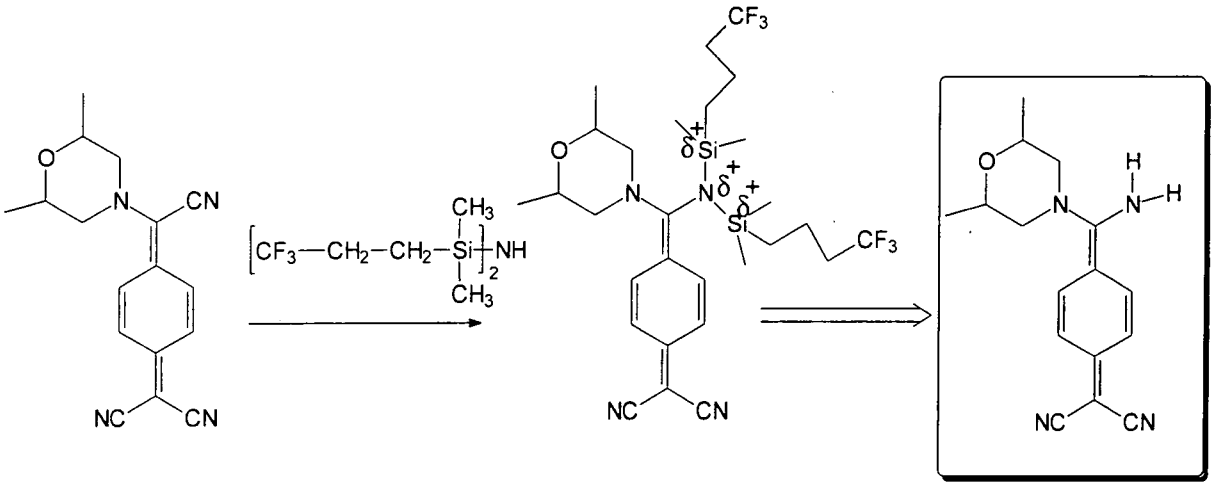

Figure 2.5 An unexpected reaction of the TCNQ derivative

## 2.2. Synthesis and chemical characterization

### 2.2.1 General procedure of chemical characterization

Varian VXR 200, Gemini 200 and VXR 400 spectrometers were used for proton NMR spectroscopy and carbon NMR spectroscopy. A Perkin Elmer Series FTIR 1600 was used for IR spectroscopy. A Micromass Automass was used for mass spectrometry, and a Perkin Elmer Lambda 19 spectrometer was used for UV/Vis spectroscopy.

### 2.2.2 Synthesis and Chemical characterizations

**1a 7-(2,6 dimethylmorpholino) -7,8,8-tricyanoquinodimethane (mixtures of cis and trans conformations) (Mono MOR)**

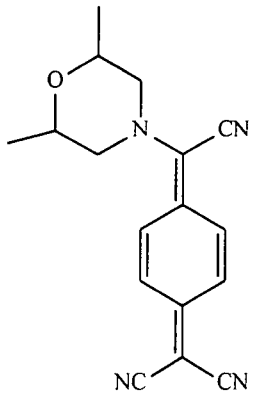


**1**

Figure 2.6 Chemical structure of Mono MOR

To a solution of TCNQ (1g,4.8mmol) in THF (100ml) heated at 50 °C was added (cis/trans) 2,6 dimethyl morpholine (0.527ml, 4.8mmol). The mixture was stirred at 50 °C for 3 hours, cooled to room temperature and then stirred overnight. The solvent was removed under vacuum. The residue was recrystallized in acetonitrile twice and dried under vacuum. Purple crystals (0.52g, yield 36%) were obtained.

IR: 2977, 2877 $cm^{-1}$ (aromatic C-H stretching)(M), 2175, 2138 $cm^{-1}$(nitrile stretching)(S). $\lambda_{max}$: 557 nm in acetonitrile, Microanalysis. Calcd for $C_{17}H_{16}N_4O$: % C, 69.84, H 5.51, N 19.16. Found: C, % 70.94, H, 5.71, N, 19.28. Mass spectrum: m/z 294 ($M^+$+2) (100%, molecular ion). Decomposition temperature: 220 °C.

**1b 7-(2,6-dimethylmorpholino)-7,8,8-tricyanoquinodimethane (cis conformation only)(Mono MOR)**

To a solution of TCNQ (2g,9.6mmol) in THF (200ml) heated at 50 °C was added cis 2,6 dimethyl morpholine (1ml, 9.1mmol). The mixture was stirred at 50 °C for 3 hours, and cooled to room temperature and stirred overnight. The solvent was removed under vacuum. The solid was recrystallized in acetonitrile twice and dried under vacuum. Purple crystals (1.09g, yield 40.7%) were obtained.
$H^1$-NMR IR: 2977, 2877 $cm^{-1}$ (aromatic stretching C-H)(M), 2175, 2138 $cm^{-1}$ (stretching nitrile)(S). Microanalysis. Calcd for $C_{17}H_{16}N_4O$:% C, 69.85, H, 5.52, N, 19.16. Found:% C, 69.75, H, 5.43, N, 19.35, Mass spectrum m/z 292 ($M^+$)(100%, molecular ion). Decomposition temperature: 220°C.

**2a 7,7-(2,6 dimethylmorpholino)-8,8-dicyanoquinodimethane (mixtures of cis and trans conformations) (MOR2)**

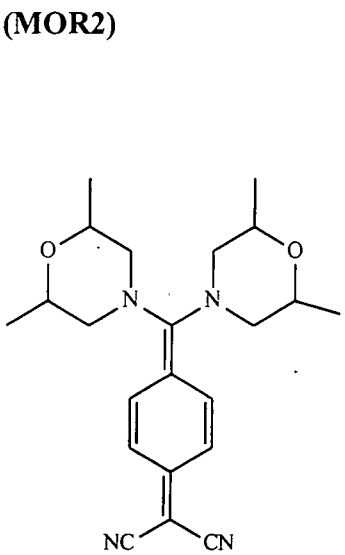


**2**

Figure 2.7 Chemical structure of MOR2

To a solution of TCNQ (2g,9.6mmol) in THF (200ml) heated at 50 °C was added (cis/trans) 2,6 dimethylmorpholine (5ml, 37.6mmol). The mixture was stirred at 50 °C overnight and cooled to room temperature. The product precipitated and was collected by filtration, recrystallized in acetonitrile twice and dried under vacuum. Yellow crystals (0.607g, yield 16.7%) were obtained.

$H^1$-NMR: ($CD_2Cl_2$, δ7.1ppm, singlet, bisubstituted qunoidal protons (4H), δ1.1,1.3ppm, doublet, methyl protons in morpholine (6H), δ3-4ppm, morpholine protons (12H) these peaks are consistent with the staring compound, IR: 2977, 2877 $cm^{-1}$ (aromatic stretching C-H)(M), 2175, 2138 $cm^{-1}$(stretching nitrile)(S), $\lambda_{max}$: 423.5 nm in acetonitrile, Microanalysis. Calcd for $C_{22}H_{30}N_4O_2$:% C, 69.08, H, 7.91, N, 14.65. Found:% C, 69.58, H, 7.45, N, 15.14. Decomposition temperature: 260 °C The molecular structure was confirmed by X-ray crystallography. The crystallographic data is shown in Appendix I.

**2b 7,7-(2,6 dimethylmorpholino)-8,8-dicyanoquinodimethane (MOR2) (cis conformation only)**

To a solution of TCNQ (1g,4.8mmol) in THF (100 ml) heated at 50 °C was added cis 2,6 dimethyl morpholine (1.32ml, 9.9mmol) The mixture was stirred at 50 °C for overnight and cooled to room temperature. The product precipitated was collected by filtration, recrystallized in acetonitrile twice and dried under vacuum. Yellow crystals (0.599 g, yield 16.5%) were obtained.

Microanalysis. Calcd.for $C_{22}H_{30}N_4O_2$:% C, 69.08, H, 7.91, N, 14.65. Found:% C, 69.00, H, 7.37, N, 14.64. Decomposition temperature: 260 °C. The molecular structure was confirmed by X-ray crystallography.

**3a 7-(2,6, dimethylmorpholino)-7-(4-methyl piperidino)-8,8,-dicyanoquinodimethane (mixtures of cis and trans conformations)(MORPIP)**

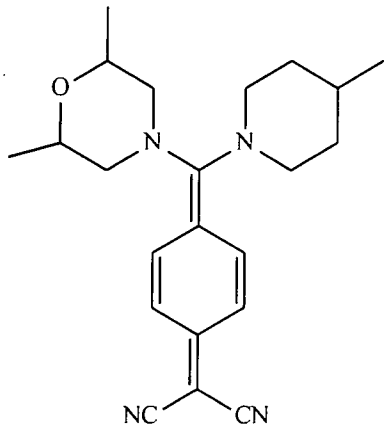


3

Figure 2.8 Chemical structure of MORPIP

To a solution of (cis/trans) 7-(2,6, dimethylmorpholino)-7,8,8,-tricyanoquinodimethane (0.4g, 1.36mmol) in THF (30ml) heated at 50 °C was added 4-methyl piperidine (0.2ml, 2mmol), and stirred for 30 min at 50 °C. The product was observed to precipitate. The solution was cooled to room temperature and stirred for 1 hour. The yellow prepicitate was collected by filtration and dried under vacuum. Recrystallization of the solid was carried out with acetoniltrile. Yellow crystals were obtained (0.24g, 46%).

$H^1$-NMR: ($CDCl_3$) δ7.0ppm, singlet, bi substituted qunoidal protons (4H), IR: 2863 $cm^{-1}$ (aromatic stretching C-H)(M), 2173, 2139 $cm^{-1}$(stretching nitrile)(S). $\lambda_{max}$: 417 nm in acetonitrile, Microanalysis. Calcd for $C_{22}H_{28}N_4O$ $0.1H_2O$:% C, 72.14, H, 7.75, N, 15.30. Found:% C, 72.13, H, 7.70, N, 15.18, Mass spectrum: 364($M^+$)(100%, molecular ion). Decomposition temperature: 260 °C.

**3b 7-(2,6, dimethylmorpholino)-7-(4-methylpiperidino)-8,8-dicyanoquinodimethane (cis conformation only)(MORPIP)**

To a solution of cis 7-(2,6, dimethylmorpholino)-7,8,8-tricyanoquinodimethane (0.4g, 1.36mmol) in THF (30ml) heated at 50 °C was added 4-methyl piperidine (0.2ml, 2mmol), and stirred for 30 min at 50 °C. The product was observed to precipitate. The solution was cooled to room temperature and stirred for 1 hour. The yellow precipitate was collected by filtration and dried under vacuum. Recrystallization of the solid was carried out with acetoniltrile. Yellow crystals were obtained (0.22g, 43%).

Microanalysis: Calcd for $C_{22}H_{28}N_4O$ $0.1H_2O$:% C, 72.14, H, 7.75, N, 15.30. Found:% C, 72.30, H, 7.82, N, 15.38. Mass spectrum 364 ($M^+$)(100%, molecular ion). Decomposition temperature: 260 °C. The molecular structure was confirmed by X-ray crystallography. The crystallographic data is shown in Appendix I.

**4 7,7-(4-methylpiperidino)-8,8-dicyanoquinomethane (PIP2)**

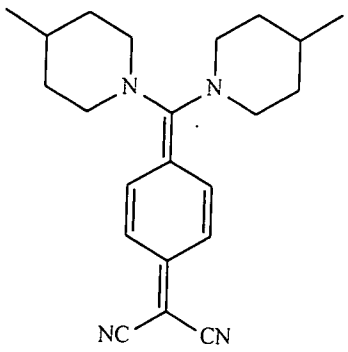


**4**

Figure 2.9 Chemical structure of PIP2

To a solution of TCNQ (0.5g, 2.4mmol) in THF (200ml) heated at 50 °C was added 2, 6 dimethylmorpholine (0.61ml, 7.2mmol). The mixture was stirred at 50 °C for overnight, and cooled to room temperature. The product precipitated and was collected by filtration, recrystallized in methanol and dried under vacuum. Green-yellow crystals were obtained.

$H^1$-NMR: (*d*-DMSO) δ6.9 ppm, 7.3 ppm, doublet bisubstituted qunoidal protons(4H), IR: 2977, 2877 $cm^{-1}$ (aromatic stretching C-H)(M), 2175, 2138 $cm^{-1}$(stretching nitrile)(S), $\lambda_{max}$: 413nm in acetonitrile, Microanalysis. Calcd for $C_{22}H_{28}N_4 0.1H_2O$:% C, 75,41, H, 8.11, N, 15.99. Found:% C, 75.41, H, 8.08, N, 16.02. Decomposition temperature: 260 °C. Mass spectrum: 348 ($M^+$)(100%, molecular ion)The molecular structure was confirmed by X-ray crystallography. The crystallographic data is shown in Appendix I.

**5 7,7-(thiomorpholino)-8,8-dicyanoquinodimethane (THIO2)**

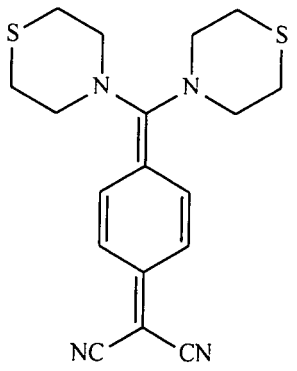


**5**

Figure 2.10 Chemical structure of THIO2

To a solution of TCNQ (1g,4.8mmol) in THF (200ml) heated at 50 °C was added thiomorpholine (3.53ml,19.2mmol), and stirred at 50 °C overnight. The mixture was cooled to room temperature. The product precipitated and was collected by filtration. The yellow solid was washed with a hot acetonitrile solution and dried under vacuum. A green powder (1.05g, yield 42.1%) was obtained.
MW 358.5, IR: 2915 $cm^{-1}$ (aromatic stretching C-H), 2170, 2128 $cm^{-1}$(stretching nitrile). $\lambda_{max}$: 434nm in acetonirtile, Microanalysis. Calcd for $C_{18}H_{22}N_4S_2$:% C, 60.30, H, 6.19, N, 15.53. Found:% C, 60.49, H, 5.70, N, 15.50. Mass spectrum 357 ($M^+$-1)(80%, molecular ion). Decomposition temperature: 260 °C.

**6 7,7-(*N*-(3-aminopropyl) cyclohexylamino)-8,8,-dicyanoquinodimethane (AMINO)**

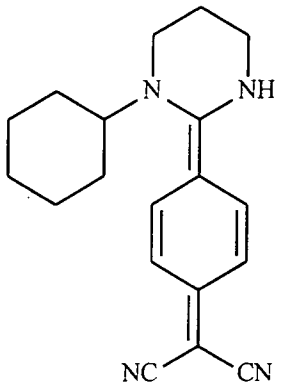


**6**

Figure 2.11 Chemical structure of AMINO

To TCNQ (0.5g,2.4mmol) in acetonitrile (30ml) heated at 50 °C was added *N*-(3-aminopropyl) cyclohexylamine (0.5ml, 2.8mmol), and stirred at 50 °C for 3 hours. The mixture was cooled to room temperature. The product precipitated and was collected by filtration. The precipitate was recrystallized in acetone and dried under vacuum. A brown powder (0.23g, yield 31.1%) was obtained.

A NMR spectrum of AMINO is shown in Fig.2.6. AMINO was dissolved into *d*-DMSO that is a polar solvent. Therefore aromatic protons of a and b are different electronic enviroments due to the charge separation between the donor (amino moieties) and the acceptors (cyano groups). The protons (2H, doublet) of a is at 7.1 ppm and protons (2H, doublet) of b is at 6.8ppm. These two peaks are commonly observed in such newly synthesized compounds.

NMR:(*d*-DMSO), δ 7.1 ppm, doublet (a) benzene protons (2H), δ 6,8 ppm, doublet, (b) benzene protons (2H), δ 3,6 ppm, quintet (c) amine proton (1H), δ 3.45 ppm,

triplet, (d) -($CH_2$)- next to NH (2H), δ3.35 ppm, triplet (f) -($CH_2$)- next to N (2H), δ1.95 ppm, triplet (g), cyclohexane proton next to N (1H), δ1,7 and 1.0 ppm, cyclohexane (h,i,j) and -(CH2)-protons (e), (12 H).

IR:2179, 2132 $cm^{-1}$(stretching nitrile)(S). $\lambda_{max}$: 368nm in acetonirile, Microanalysis: Calcd for $C_{19}H_{22}N_4$:% C,74.48 H, 7.24 N, 18.28. Found:% C74.46, H 7.35, N, 18.28. Mass spectrum: 306($M^+$)(100%, molecular ion). Decomposition temperature: 220 °C.

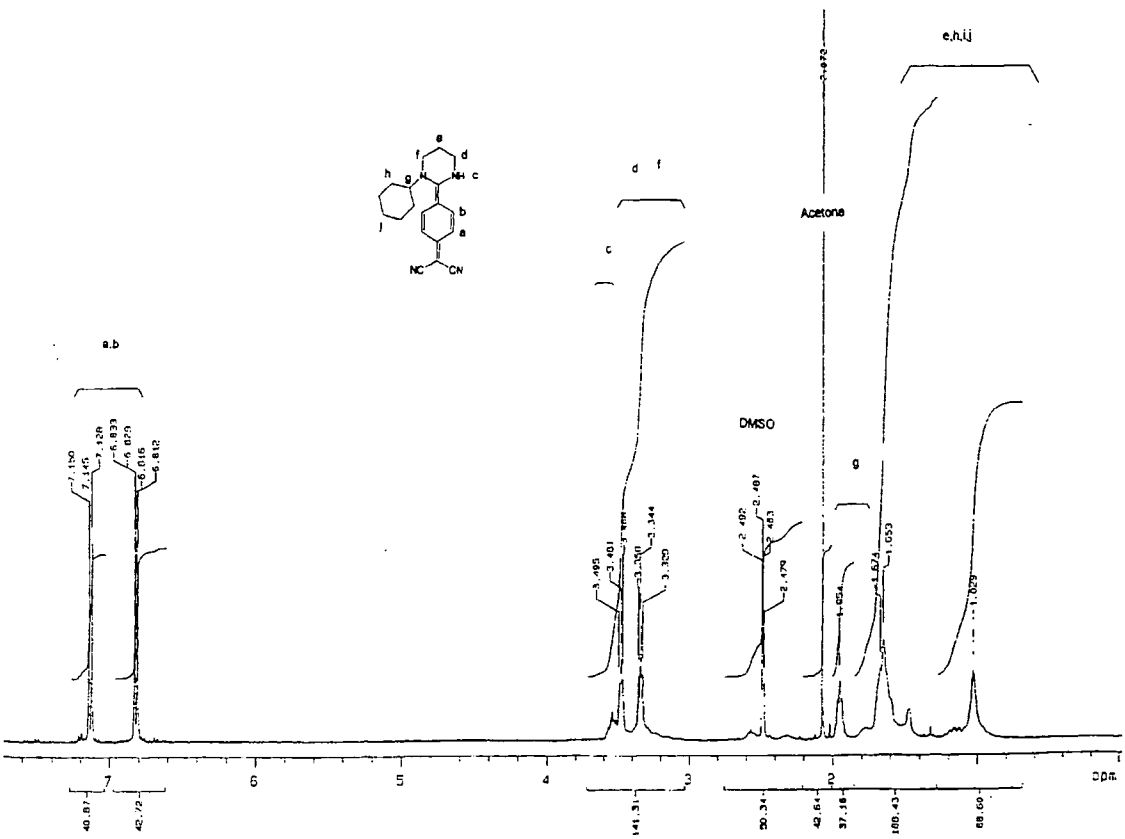


Figure 2.12 NMR spectrum of AMINO in d-DMSO

**7 7,7-(diamino cyclo hexano)-8,8-dicyanoquinodimethane (CYCLO)**

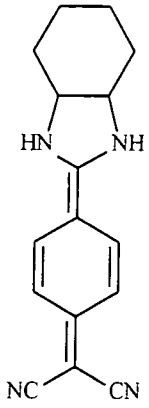


**7**

Figure 2.13. Chemical structure of CYCLO

To a solution of TCNQ (0.5g, 2.4mmol) in acetonitrile (30 ml) heated at 50 °C was added cis 1,2, diamino cyclo hexane (0.35 ml, 3.3mmol) and heated under reflux for 3 hours. A brown precipitate was found and collected by filtration. The solid was dried under vacuum and recrystallized from acetonitrile to give a brown powder (0.277g, 43.7%)

$H^1$-NMR: (*d*-DMSO), δ9.8ppm, singlet, N-H (2H), δ7.6ppm, doublet bisubsituted qunoidal protons, cyclohexane protons are consistent with the starting compound, $\lambda_{max}$: 415nm in acetonitrile, Microanalysis: Calcd for $C_{16}H_{16}N_4$ $0.1H_2O$:% C, 72.21, H, 6.13, N, 21.05. Found:% C, 72.12, H, 6.08, N, 20.76. Mass spectrum: 264($M^+$)(30%, molecular ion). Decomposition temperature: 300 °C.

**8 7-(2,6, dimethylmorpholino)-7-(amino)-8,8-dicyanoquinodimethane (Si)**

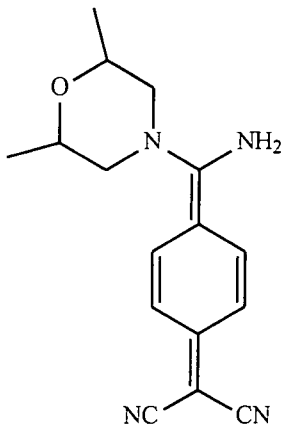


**8**

Figure 2.14 Chemical structure of Si

To a solution of 7-(2,6, dimethylmorpholino)-7,8,8-tricyanoquinodimethane (0.39g, 1.33mmol) in THF (30ml) heated at 50 °C was added 1,3-bis (3,3,3-trifluoropropyl) tetramethyl disilazane (0.47ml, 1.96mmol) and stirred for 4 hours at 50 °C. The product precipitated. The solution was cooled to room temperature and stirred overnight. The brown precipitate was collected by filtration and dried under vacuum. Recrystallization of the solid was carried out with methanol. A green powder was obtained (0.20g, 54%).

$H^1$-NMR: (*d*-DMSO), δ9.1, 8.7ppm, singlet N-H (2H), δ7.2ppm, 6.8ppm, doublet bisubstituted quinoidal protons (4H), IR: 3350,3161 $cm^{-1}$ (aliphatic primary amine), 2171, 2126 $cm^{-1}$ (stretching nitrile), 1595 $cm^{-1}$ (N-H bending vibration), 1326 $cm^{-1}$ (C-N stretching of the primary amine). $\lambda_{max}$: 394nm in acetonirtile, Microanalysis: Calcd for $C_{16}H_{18}N_4O$:% C,72.13, H,7.75, N,15.29. Found:% C, 72.30, H, 7.82, N, 15.38.

Mass spectrum: 283 ($M^+$-1)(50%, molecular ion). Decomposition temperature 260 °C.

**9 7,7-(4-flourophenyl piperazino)-8,8-dicyanoquinodimethane (FPHPIP)**

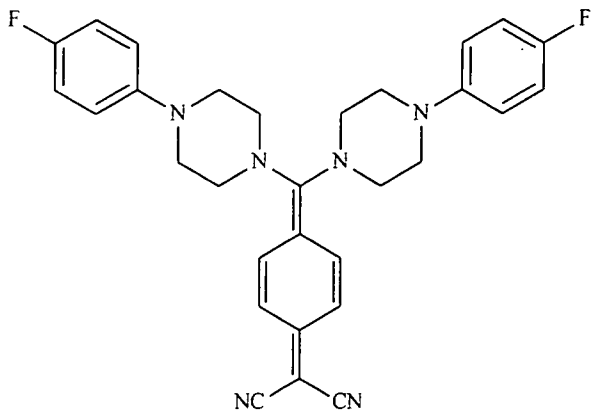


**9**

Figure 2.15 Chemical structure of FPHPIP

To a solution of TCNQ (1g,4.8mmol) in THF (200ml) heated at 50 °C was added 4 flouro piperidine (3.53ml, 19.2mmol) and stirred at 50 °C overnight. The mixture was cooled to room temperature. The product precipitated and was collected by filtration. The solid was washed with a hot acetonitrile solution and dried under vacuum. A green powder (1.05g, yield 42.1%) was obtained.

$\lambda_{max}$: 426nm in acetonitrile, MW 510, Microanalysis: Calcd for $C_{30}H_{28}F_2N_6$:% C, 70.57, H, 5.53, N, 16.46. Found:% C, 70.29, H, 5.59, N, 16.21. Mass spectrum: 510 ($M^+$)(100%, molecular ion). Decomposition temperature: 300 °C.

**10 7-(2,6,dimethyl morpholine)-7-(R-1-amino-2-propanol)-8,8,dicyanoquino dimethane (MORPROL)**

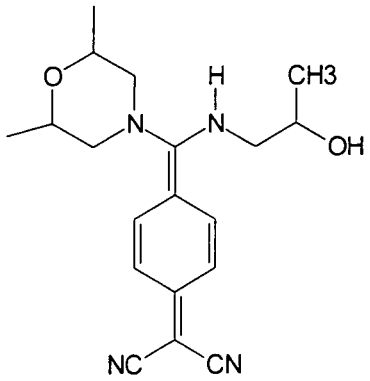


10

Figure 2.16 The chemical structure of MORPROL

To a solution of 7-(2,6, dimethylmorpholino)-7,8,8-tricyanoquinodimethane (0.43g, 1.46mmol) in THF (30ml) heated at 50 °C was added R-1-amino 2 propanol (0.14ml, 1.85mmol), and stirred for 4 hours at 50 °C. The product precipitated. The solution was cooled to room temperature and stirred overnight. The yellow precipitate was collected by filtration and dried under vacuum. Recrystallization of the crude product was attempted, but the pure form of the target compound could not be obtained due to the insolubility and a possible side reaction between amines (hydroxyl and amino groups) [6]. The crude products had two absorption maxima (360nm and 450nm in acetonitrile). The compound ($\lambda_{max}$=450nm) was the targeted compound [7] (MORPROL), and the other compound ($\lambda_{max}$=360nm) was a byproduct [7].

# Chapter 2: References

[1] S.J.Lalama, K.D.Singer, A.F.Garito, K.N.Desai, Appl.Phys.Lett., **39**, 1981, 940

[2] M.Ravi, D.N.Rao, S.Cohen, I.Agranat, T.P.Radhakrishnan, Chem.Mater., **9**, 1997, 830

[3] B.P.Bespalov, V.V.Titov, Russian.Chem.Rev., **44,** 1975, 1091

[4] W.R.Hertler, H.D.Hartzler, D.S.Acker, R.E.Benson, J.Am.Chem.Soc., **84**, 1962, 3387

[5] D.S.Acker, W.R.Hertler, J.Am.Chem.Soc., **84**, 1962, 3370

[6] J.Fuhrhop, G.Penzlin, Organic Synthesis, Weinhein, New York (1994)

[7] M.Szablewski, Private communication (1995-1998)

# Chapter 3: Nonlinear Optical and Related Physical Properties

## 3.1 Introduction

### 3.1.1 Kurtz powder method

The Kurtz powder technique is a very quick and a convenient method to determine the second order nonlinearity without growing large single crystals. There are two types of powders used in the Kurtz powder technique, non-phase matchable and phase matchable powders. The schematic representation of the intensity of second harmonic light as a function of $\langle r \rangle / \langle l_c \rangle$ for the non-phase matchable and phase matchable powders [1,2] is shown in Fig.3.1.

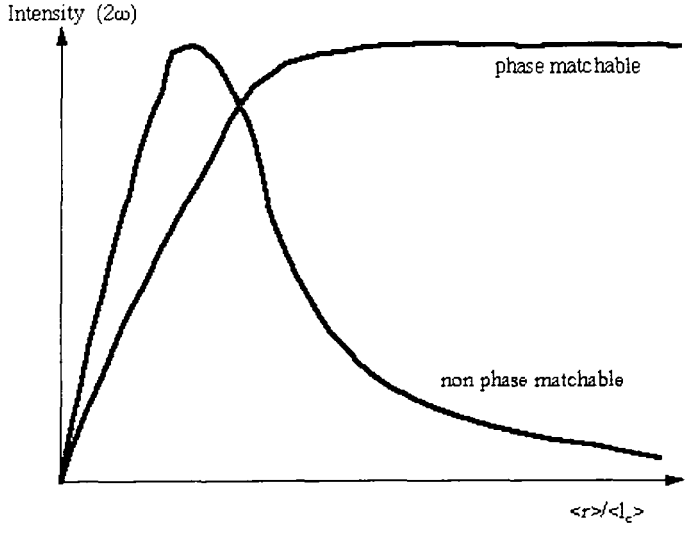


Figure 3.1 Schematic representation of the intensity of second harmonic light

$\langle r \rangle$ is the average particle size of the powder and $\langle l_c \rangle$ is the average coherence length. The coherence length, $l_c$, can be defined as

$$l_c = \frac{\lambda}{4(n_{2\omega} - n_{\omega})} \quad \text{for non-phase matchable powders} \tag{3.1}$$

$$l_c = \frac{\lambda}{4(n^{o}_{2\omega} - n^{e}_{2\omega})(\sin 2\theta_m)(\theta - \theta_m)} \quad \text{for phase matchable powders} \tag{3.2}$$

Where $\theta_m$ is the angle between the phase matching direction and an optic axis, $\theta$ is the angle between the direction of the fundamental wave and an optic axis, $n^{e}_{2\omega}$ is the extraordinary refractive index at the second harmonic wave, and $n^{o}_{2\omega}$ is the ordinary refractive index at the second harmonic wave.

For non-phase matchable powders, the effective refractive index of the second harmonic wave propagating is different from that of the fundamental wave, i.e. ($n_{2\omega} \neq n_{\omega}$). However, for phase matchable powders both the effective refractive indices of the second harmonic and the fundamental waves can be the same due to the birefringence of the crystals.

### 3.1.2 Chirality

If structures of the same constitution differ in spatial arrangement, these structures are stereoisomers that can be described by their topology, i.e. their configuration [3]. If two stereoisomers have a symmetry of mirror images, which are nonsuperimposable, they are enantiomeric as shown in Fig.3.2. Structures that have nonsuperimposable mirror images are chiral [3]. A chiral center is a carbon that has four different substituents as indicated as * in Fig.3.2.

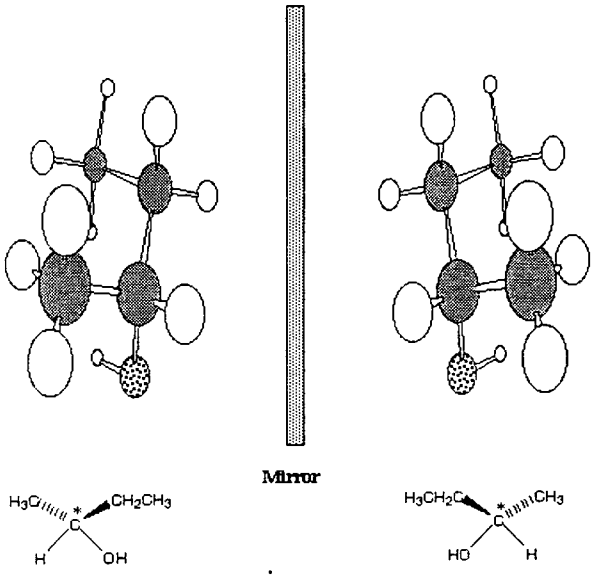


Figure 3.2 Mirror image of the chiral molecule

The characteristic property of chiral molecules is that one of the separated enantiomers can rotate the plane of polarized light. This is called optical activity [3,4]. The degree of optical rotation of the plane of polarization can be measured by the use of polarisers. If the plane of polarised light rotates clockwise, it is dextrorotary, and a positive sign (+) will be in conjunction with the degree of rotation. If the plane of polarised light rotates anticlockwise, this is levorotatory, and the minus sign (-) will be used in conjunction with the degree of rotation. This can be explained by the rotation of the plane of polarisation, and it is as the result of the recombination of the two circularly polarized waves that originate from the birefringence in the crystal, and have opposite directions of rotation [3,4].

The incorporation of chirality can produce a noncentrosymmetric crystal lattice. The formation of noncentrosymmetric crystals of nlo materials is essential to produce second harmonic generation from the crystalline state.

### 3.1.3 Crystal packing

Organic nonlinear optical molecules are polar and tend to form dimers or higher aggregates due to electrostatic forces, which result in the molecules being found in centrosymmetric structures in the solid state [5-8]. Preventing the formation of the centrosymmetric crystal lattice can be achieved by the use of chiral molecules. The introduction of molecular asymmetry and hydrogen bonding also helps the formation of noncentrosymmetric crystals [5-8].

The organic chiral crystal, methyl-(2,4,dinitrophenyl)-aminopropanoate (MAP) was investigated by Oudar et al. in 1977 [9]. The study of NPP followed by Zyss et al. [10-12] showed that the incorporation of chirality results in the expected noncentrosymmetry in the packing.

After the investigation of 3-methyl-4- nitropyridine-1-oxide (POM), a new idea of crystal packing to enhance the formation of a noncentrosymmetric lattice was reported [13]. The idea was that the packing force could be well controlled if the molecular dipole moment was reduced to zero. The classic organic model for a second order nlo is the donor - acceptor so called "push-pull" system. However if chromophores have a "push-pull-push" or a "pull-push-pull" system like POM, the total dipole moment that drives centrosymmetry would vanish. Therefore in the absence of the dipole-dipole interaction, van der Waals forces govern crystal packing, and help in the establishment of noncentrosymmetric packing. It is, however, noteworthy that the removal of the total dipole moment is not useful for either incorporation into polymeric media or for EFISH measurements in solution, because the molecular dipole moment is used to achieve alignment of the targeted molecules in the media [14-16].

Zyss et al. [10-12] suggested that the optimal angle (θ) between the charge transfer axis (a) and two fold axis (Z) for the powder SHG in the monoclinic $P_2$ symmetry is 54.74°, as shown in Fig.3.3.

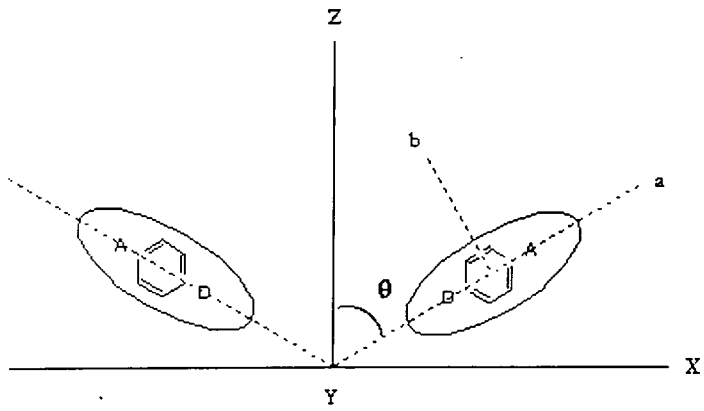


Figure 3.3 Two fold axis (Z) and the charge transfer axis (a) in the crystal lattice of the Monoclinic $P_2$ symmetry

The angle of NPP between the two fold symmetry axis and the transition dipole moments is 58.6°. Thus the angle of NPP is very close to the optimal angle. This explains why the intensity of the powder SHG of NPP is 160 times as large as that of urea [10-12].

## 3.1.4 Solvatochromism

The position, intensity, and shape of absorption spectra measured with UV/Vis spectrometers are often different in various solvents due to the different solvent polarities i.e. the different reaction fields as defined in Chapter 1. The influence of solvent polarity results from the physical intermolecular interactions between solute and solvent i.e. dipole-dipole interactions [17]. These intermolecular interactions will affect the electronic energy states (the ground state and the first excited state, for

example). The polarity of solvents will normally change the electronic distribution of the molecules. The electronic energy states and the electronic distribution of the molecule affect β as described in the previous chapter so the effect of solvent polarity must be considered carefully. The term, solvatochromism, describes the positional change of absorption bands in solvents of various polarities. A hypsochromic shift with increasing polarity of solvents is called negative solvatochromism. A bathochromic shift with increasing polarity of solvents is called positive solvatochromism.

A polarity scale (the solvent density, $\Delta f$) is defined as [18]

$$\Delta f = \left(\frac{\varepsilon - 1}{2\varepsilon + 1}\right) - \left(\frac{n^2 - 1}{2n^2 + 1}\right) \tag{3.3}$$

Where ε and $n$ are the dielectric constant and the refractive index of the solvent, respectively.

### 3.1.5 Benzenoid and quinoid structures

BLA was introduced in the first chapter by using the polyenic model, but BLA also can be applied to an aromatic model [19-21]. A molecular structure can be found to exist between two extreme states, the neutral state (the quinoid structure) and the zwitterionic state (the benzenoid structure) as shown in Fig.3.4 [19-21]. Molecules that have low dipole moments and positive β values are of the quinoidal structure, so they belong to the left hand side in Fig.3.4. Molecules that have large dipole moments and negative β values in nature are of the benzenoid structures, they belong to the right hand side of Fig.3.4. With increasing reaction field (polarity of solvents, for

instance) the charge separation of the molecules will be increased, although the degree of the charge separation depends also on the polarizability of the molecule.

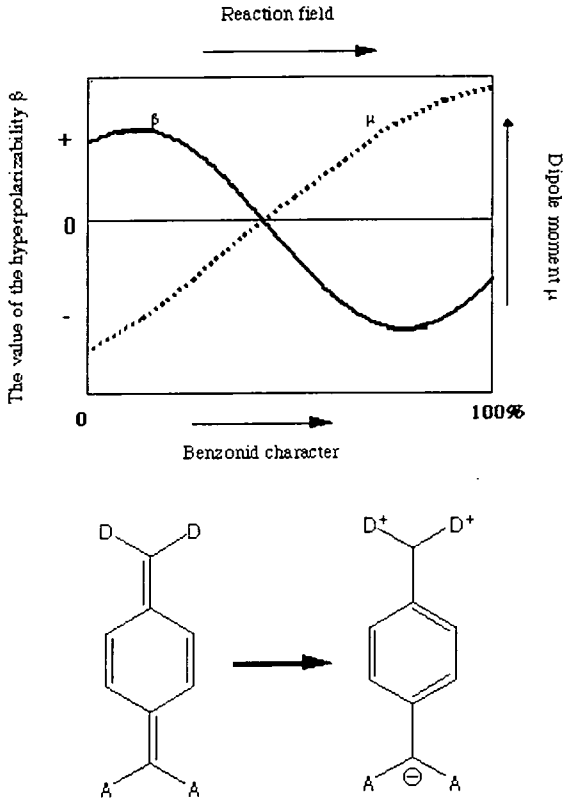


Figure 3.4 Molecular figure of merits with an aromatic model

## 3.2 Experimental

### 3.2.1 Powder second harmonic generation

After a powder sample was dried in the oven for several days, the sample was well ground with a mortar and pestle. The sample was placed between glass substrates. A urea sample was also prepared in the same manner. The set up of the powder SHG measurement is shown in Fig.3.5.

Before the measurement, the urea sample was placed in the beam of the Q-switched Nd:YAG laser. The photomultiplier tube (PMT) collected the second harmonic light, after a filter removed the incident light. The sample angle relative to the laser beam

and PMT was adjusted to maximize the second harmonic signal of urea, which was monitored with an oscilloscope. Neutral density filters were used if necessary. The value for urea was used as a reference. The sample was placed on the laser beam line and adjusted in the same manner as urea. The boxcar was used to average pulses from the laser. Finally, the particles were checked for uniformity of size under an optical microscope.

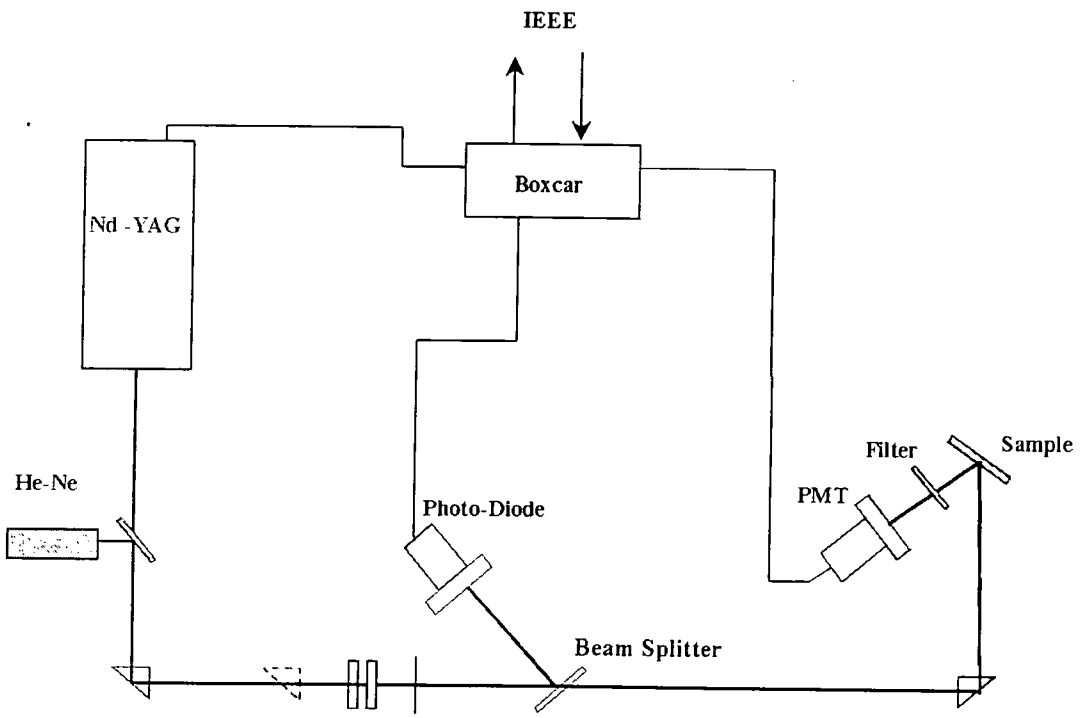


Figure 3.5 Set up for the powder SHG

### 3.2.2 Solvatochromism

Using a Perkin Elmer Lambda 19 spectrophotometer, a background scan was carried out with cells containing a solvent. Samples were then scanned and the absorption maximum was recorded. A typical value of the optical density of a solution was between 0.8 and 1.0. The measurements were started using acetonitrile,

which has the highest solvent density parameter,$\Delta f$, and repeated with lower parameter solutions such as chloroform. If an undissolved material was observed in the cuvette, the solution was filtered before the measurements were carried out.

### 3.2.3 Dipole moment measurement

The molecular dipole moment was determined from the measurement of the dielectric constant increment for solutions of the molecules under investigation. An experimental method of measurement of dielectric constants was developed at Durham [22]. Dielectric constants were obtained over a range of concentrations. The gradient at zero concentration was obtained from the measurements. Guggenheim's equation (eq.3.4.) was employed to extract the dipole moment [23].

$$\mu_m = \sqrt{\frac{10^{36}}{N_a}\frac{9k_BT}{4\pi}\frac{3}{(\varepsilon+2)(n+2)}\frac{\partial\varepsilon}{\partial C(0)}} \qquad (3.4)$$

Where N is Avogadro's constant, ε and $n$ are the dielectric constant and refractive index of the solvent, respectively, $k_B$ is the Boltzman constant and $\partial\varepsilon/\partial C(0)$ is the gradient of ε at zero concentration. The cell used for this measurement was designed by P.R.Thomas as a part of his Ph.D [22]. A 4278A Hewlett-Packard 1kHz/1MHz capacitance meter was used for the measurement of capacitance. A typical solution was prepared as described below.

MORPIP (26.6mg) was dissolved with chloroform in a 50ml volumetric flask. Successive dilutions were prepared from this stock solution. In the same manner five solutions were prepared. The HP capacitance meter was switched on 30 min before the measurement. The capacitance of air was measured at 1 MHz, which is very far from the molecular resonance. A typical value of the capacitance of the cell with air was 14.6±1 pF. The cell containing the lowest concentrated solution was attached to

the HP capacitance meter. The value of the capacitance of the lowest concentrated solution was recorded. All the capacitance values of the solutions were divided by that for air to obtain the dielectric constants of the solutions. The dielectric constants of the solutions were plotted as a function of concentration. A typical plot is shown in Fig. 3.6. The slope of the plot and the concentration gradients at zero were recorded. A program written by P.R.Thomas was used to extract the dipole moment [22]. Data from Fig.3.6 gives a dipole moment of 15.12 Debye for MORPIP.

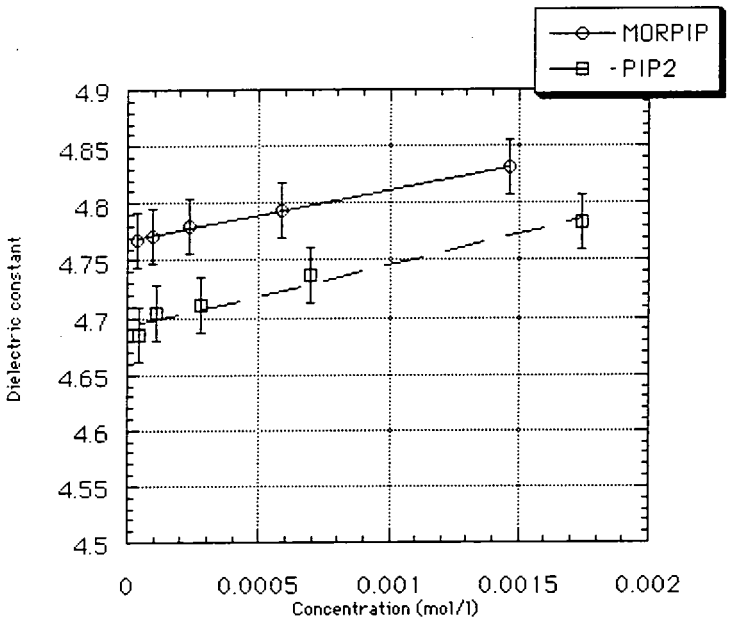


Figure 3.6 Typical plots for the dielectric increment measurement

### 3.2.4 X-ray crystallography

All data for each molecule were collected using a standard four-circle diffractometer. Graphite monochromatized MoKα X-radiation (λ=0.71073Å) and an Oxford cryosystems Cryostream (at 150K) were used.

### 3.2.5 Computational methods

**(a) Computationally minimized structure**

The targeted molecule was constructed using a commercial software package, Cerius2. The minimized molecule from Cerius2 was saved in a MOPAC format, and transferred to a PC networked terminal. The key words, AM1, POLAR, PRECISE, was added to the MOPAC file to complete minimization, and calculate the molecular dipole moment, and the molecular hyperpolarizability by MOPAC version 6 using an AM1 Hamiltonian.

**(b) Molecular structure deduced by x-ray crystallographic data**

The molecular structure was reconstructed by a software package, Ph4, by using the crystallographic data of the atomic coordinates of the targeted molecule. The reconstructed molecule was saved as a MOPAC format and transferred a networked PC. The key words, AM1, POLAR, 1SCF were added to the MOPAC file to calculate the molecular dipole moment, and the molecular hyperpolarizability without further minimization by MOPAC version 6 using AM1 Hamiltonian

## 3.3 Results and Discussion

### 3.3.1 Chemical structures

TCNQ was reacted with secondary amines to give either mono or di substituted dicyanoquinomethanes [6-8,21,24], of which five examples are illustrated in Fig.3.7. The five compounds were employed because of the availability of their X-ray crystallographic data and their structural similarities.

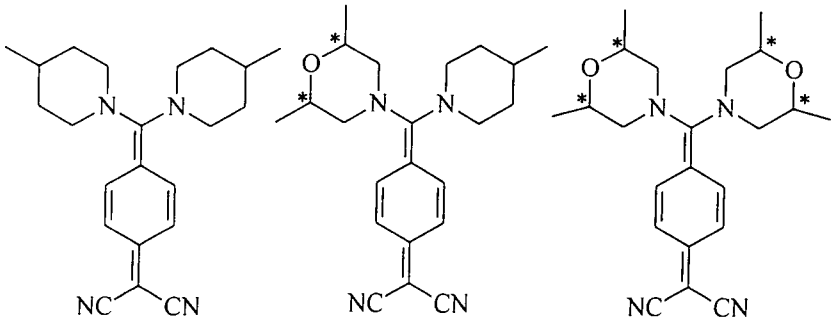

PIP2 MORPIP MOR2

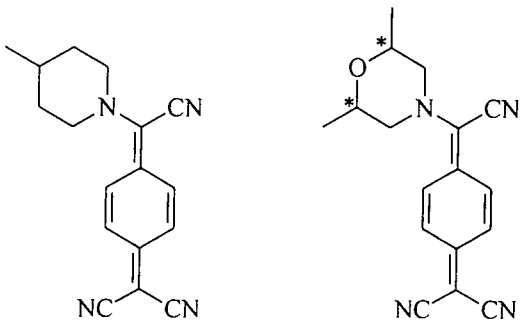

Mono PIP Mono MOR

Figure 3.7 Structures of TCNQ derivatives

### 3.3.2 Molecular structure

Molecular structures were deduced from X-ray crystallographic data of MOR2, MORPIP, and PIP2. Data for Mono PIP was added to this study due to its structural similarity. Full crystallographic data of the four compounds considered are shown in Appendix I

**(a) PIP2**

The molecular structure of PIP2 deduced from the x-ray crystallographic data is shown in Fig.3.8. The crystal packing diagrams of PIP2 are shown in Fig.3.9-3.11. The projection on the ac plane in Fig.3.11, gives a clear picture of the twist between the amino donors and the plane of the benzene ring and dicyano methylenes. The angle of the twist is 41.3°. Therefore PIP2 does not have a plane of molecular

symmetry due to the twist between C(1) and C(2). However both Fig.3.9, and Fig.3.10 show the presence of dimers in the crystal lattice, which leads to a centrosymmetric crystal packing with the space group ($C_2$/ c). The pair of dimers is pointing up and down along the b axis as shown in Fig.3.10. Molecules that have a highly polar nature tend to form centrosymmetric crystals due to the electrostatic force that leads to the formation of dimers [6-8]. The crystal packing of PIP2 is a good example of this.

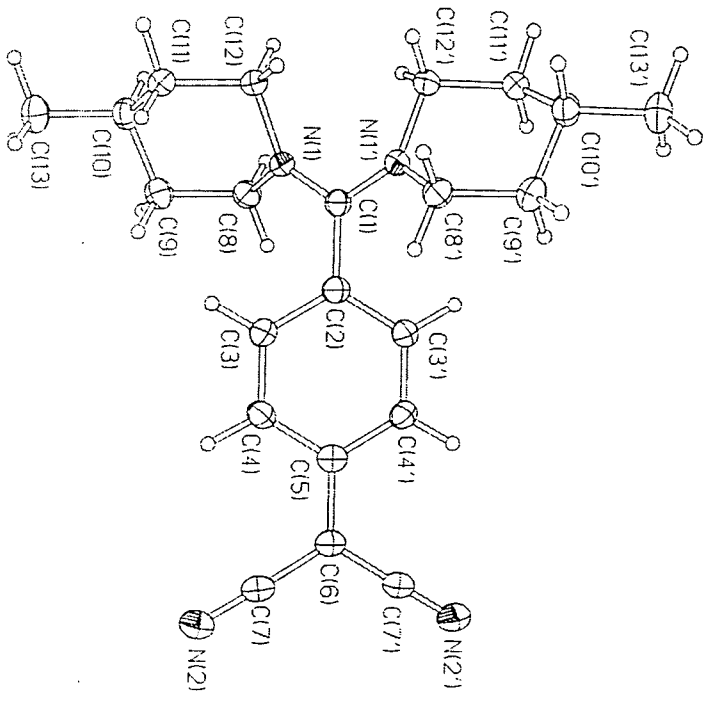


Figure 3.8 Molecular structure of PIP2

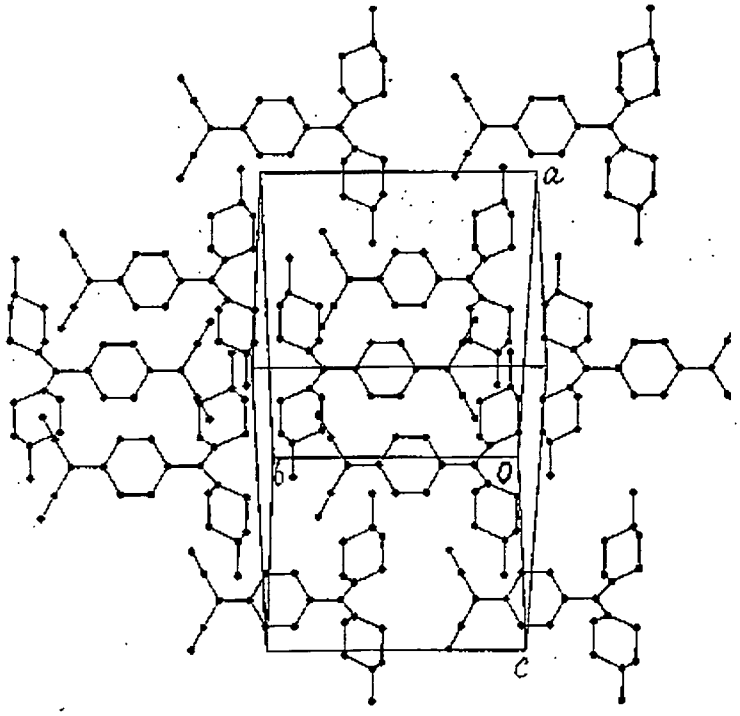


Figure 3.9 The cell packing diagram of PIP2

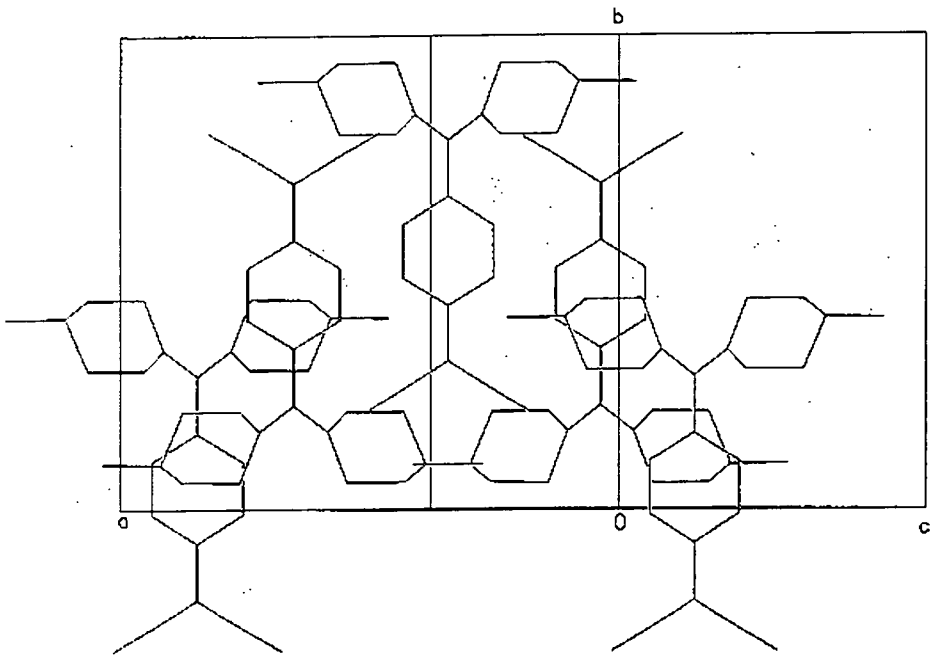


Figure 3.10 Side view of the cell packing diagram

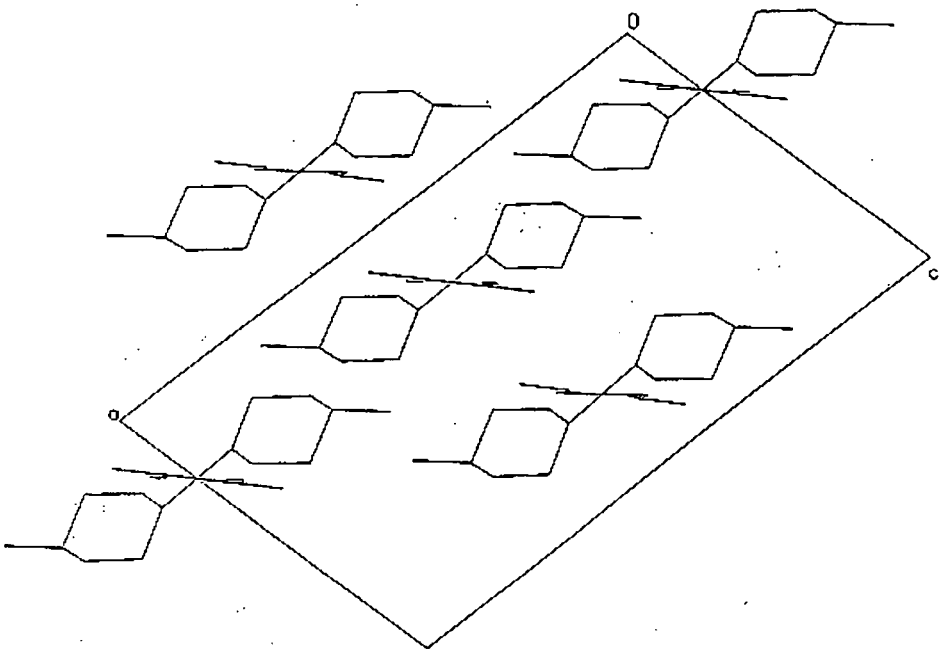


Figure.3.11 Top view of the cell packing diagram

**(b) MOR2**

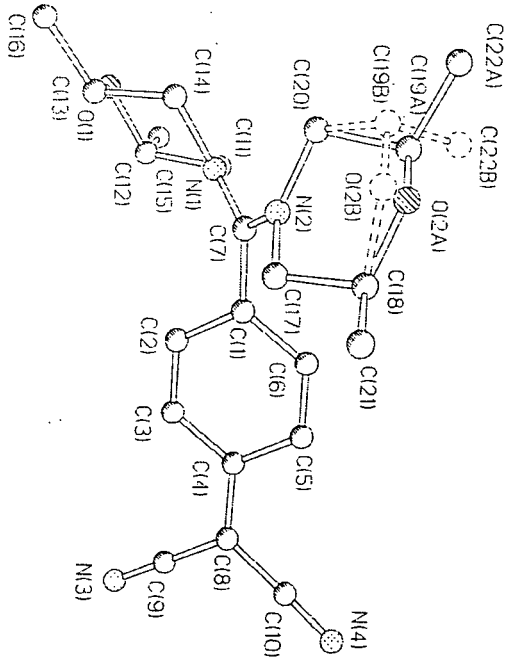


Figure 3.12 cis/trans Molecular structure of MOR2

MOR2 has chiral centres indicated * in Fig.3.7. The starting amine, 2,6-dimethyl morpholine was a racemic mixture. A pure enantiomeric form could not be obtained despite attempts at separation. Hence the final product prepared from a racemic mixtures was also a racemate. MOR2 has four chiral centres is assymetry due to the twist molecular structure. Hence there are 4 possible conformations (R,R-R,R, R,R-S,S, SS-RR, SS-SS). Moreover cis/trans mixtures of the starting amine were used to prepare for this compound. Therefore this structural complexity (cis/trans, racemate) leads to some disorder in the crystal structure. The presence of cis/tans conformations were confirmed by the x-ray crystallographic data as shown in Fig.3.12.

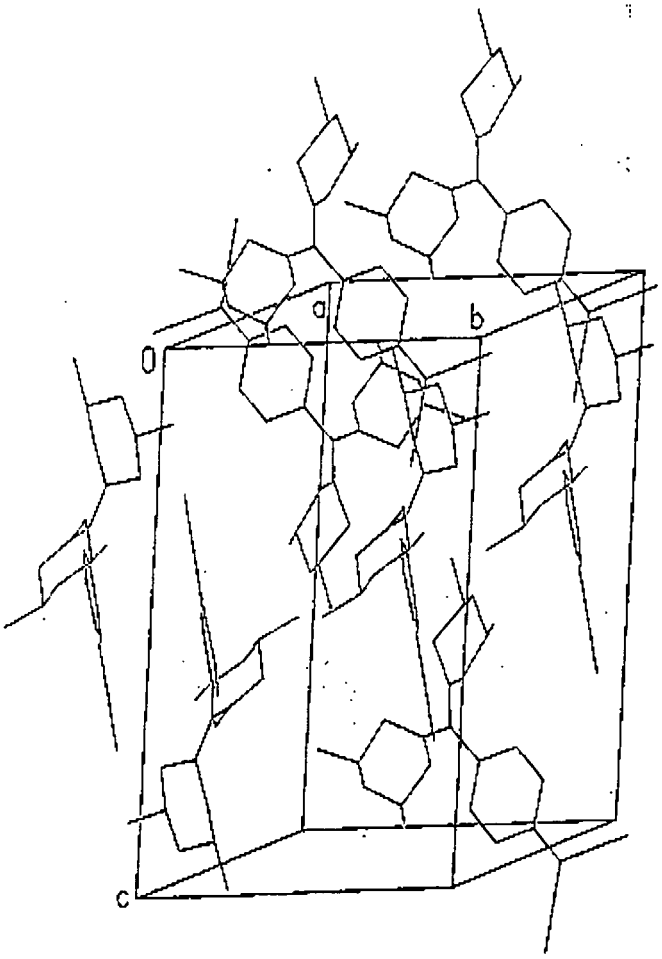


Figure 3.13 Cell packing diagram of MOR2

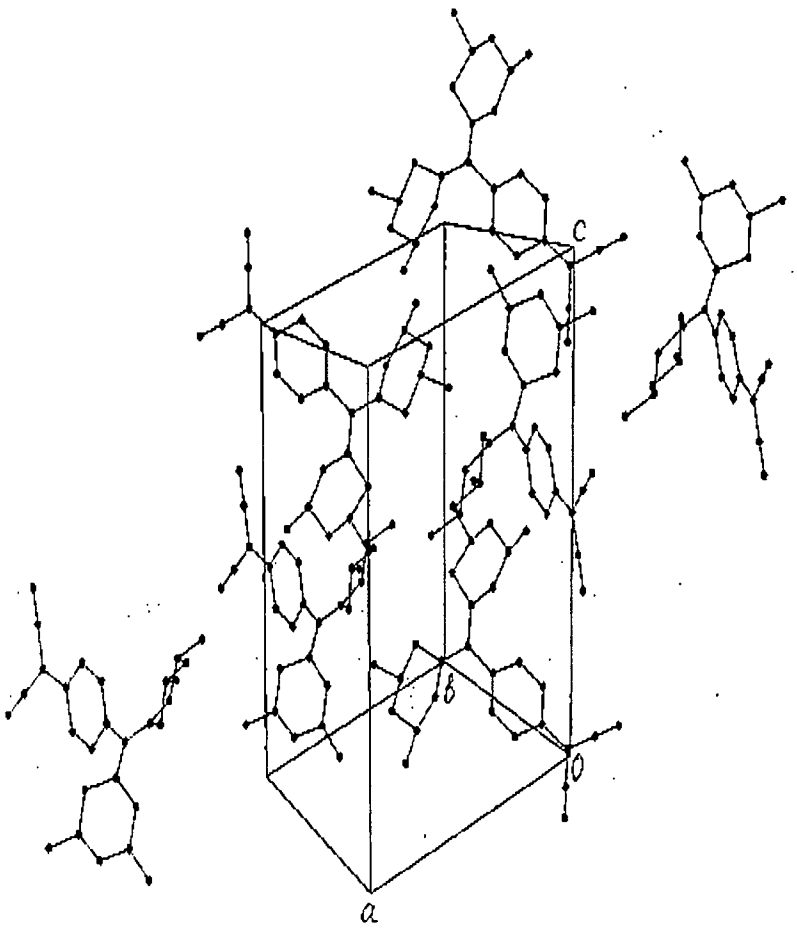


Figure 3.14 Cell packing diagram

The space group of MOR2 is $P2_1/c$, which is centrosymmetric as expected for a racemate. Two cell packing diagrams are shown in Fig.3.13-3.14. A different crystal orientation was obtained for crystals recrystallized from THF as shown in Fig.3.15-16. MOR2 molecules form a "molecular cage" and trap water inside the cavity of MOR2 molecules in the unit cell. The water molecules probably came from the solvent (THF), and held together the two MOR2 molecules to give pairs of dimers.

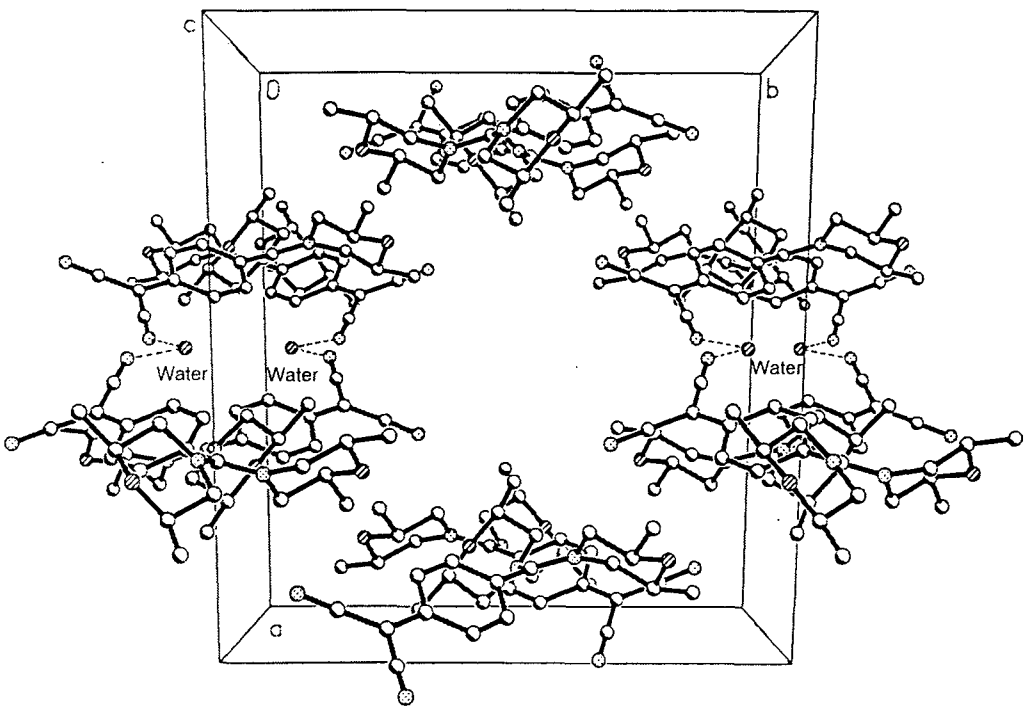


Figure 3.15 Cell packing diagram of MOR2 recrystallized from THF

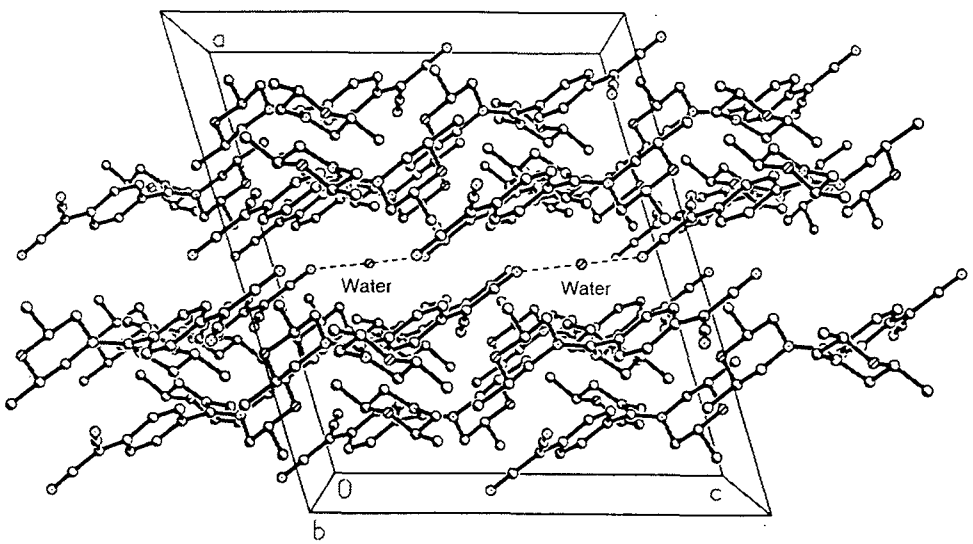


Figure 3.16 Cell packing diagram of MOR2 recrystallized from THF

**(c) MORPIP**

MORPIP has a molecular asymmetry due to the different substituent groups (piperidine and morpholine) even though the synthesised compound was a racemate. This compound produced noncentrosymmetric crystals. The molecular structure of MORPIP deduced from crystallographic data is shown in Fig.3.17. The sizes of C(15) and C16) are larger than other carbon atoms in the molecule. This implies that there is a disorder in the positions of atoms due to racemic mixtures.

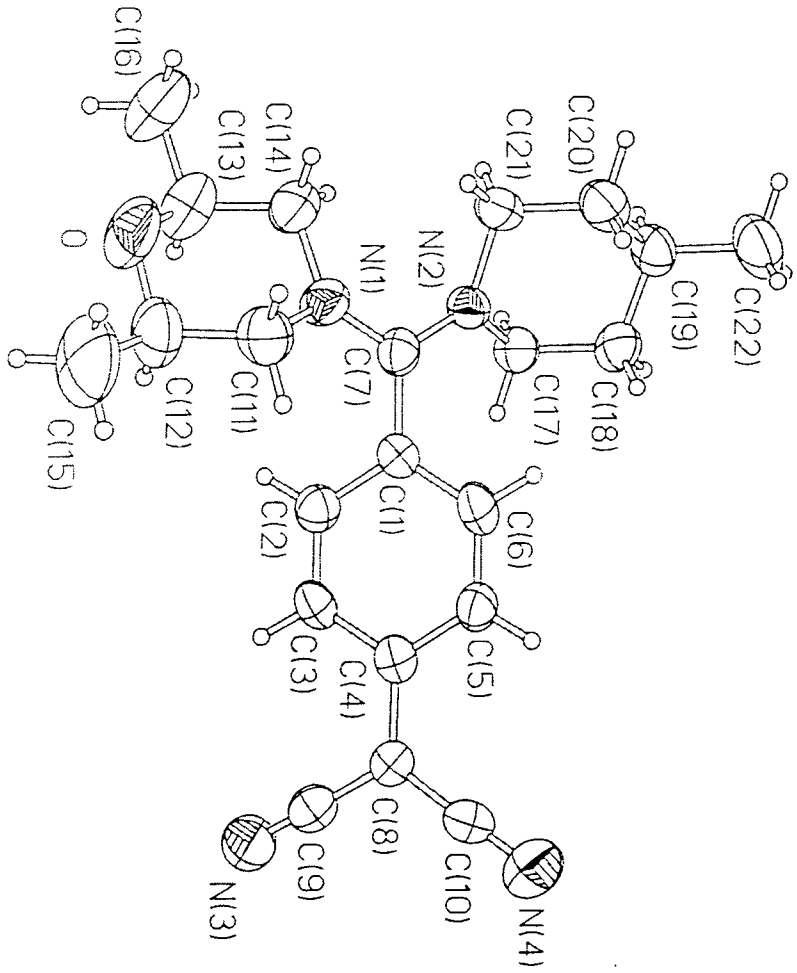


Figure 3.17 Molecular structures of MORPIP

The space group of MORPIP is $P2_12_12_1$. The cell packing diagram of MORPIP is shown in Fig.3.18.

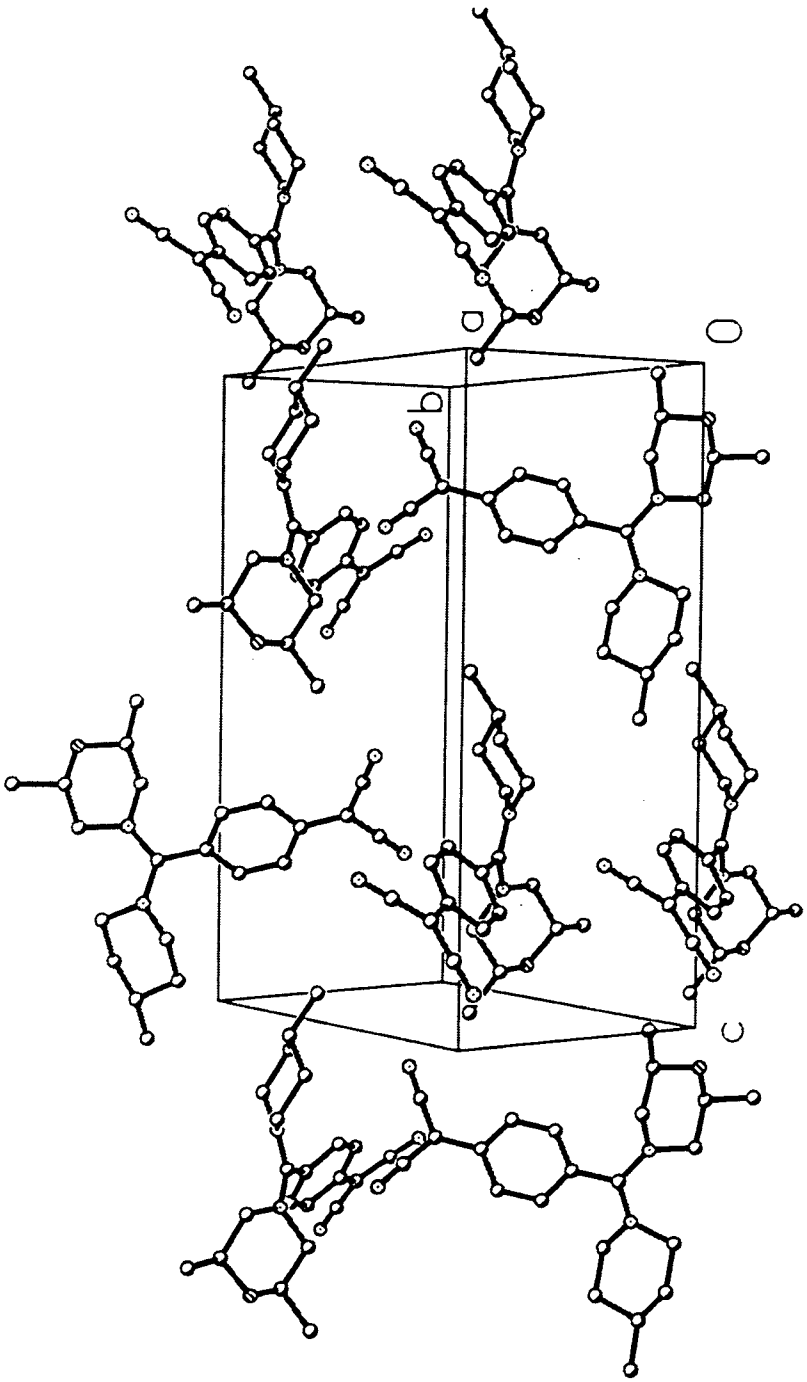


Figure 3.18 Cell packing diagram of MORPIP

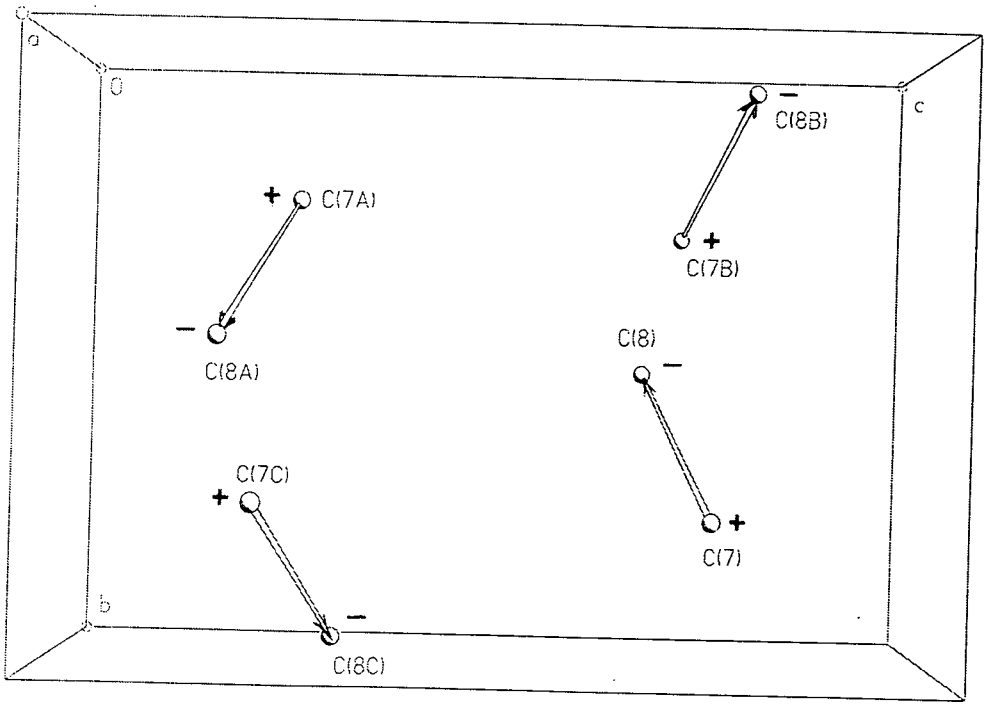


Figure 3.19 Simplified molecular orientations in the cell

Table 3.1 The orientation of MORPIP molecules in the unit cell

| | X (b axis) | Y (bc axis) | Z (a axis) |
|---|---|---|---|
| C7-C8 | 143.3° | 123.5° | 103.3° |
| C7A-C8A | 36.7° | 56.5° | 103.3° |
| C7B-C8B | 36.7° | 123.5° | 76.7° |
| C7C-C8C | 143.3° | 56.5° | 76.6° |

A diagram of simplified molecular orientations of MORPIP in the unit cell is shown in Fig.3.19. The orientations for four molecules with respect to the

crystallographic axis, X,Y,Z is shown in Table 3.1. These molecules in the unit cell have a screw type orientation as shown in Fig.3.19, and Table.3.1 [25].

Four molecules are very close to a tetrahedral arrangement in the orthorhombic crystal cell. This arrangement is the optimum for maximising SHG in the crystal symmetry [26].

**(d) Mono PIP**

Another example of noncentrosymmetric crystal packing is found in Mono PIP. The material was studied by J.C.Cole et al [27]. The symmetry of Mono PIP is monoclinic, spacing group P*n*. The crystal packing of the unit cell of Mono PIP is shown in Fig.3.21. There are two molecules in the unit cell and these two molecules are in head to tail in layers. The symmetry of P*n* has mirror planes between unit cells [25]. The angle ($\theta_2$) between the two fold axis and the molecular charge transfer axis is as shown in Fig.3.20, and is 22.4°, somewhat less than the optimal angle for maximising SHG [26].

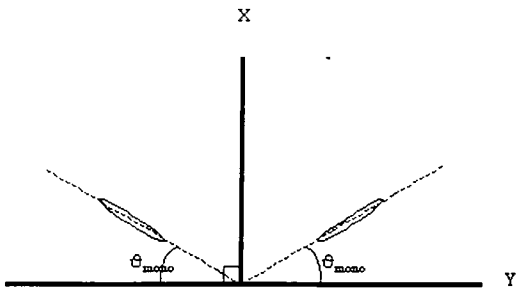


Figure 3.20 The angle between the charge transfer and two fold axis in the monoclinic crystal system

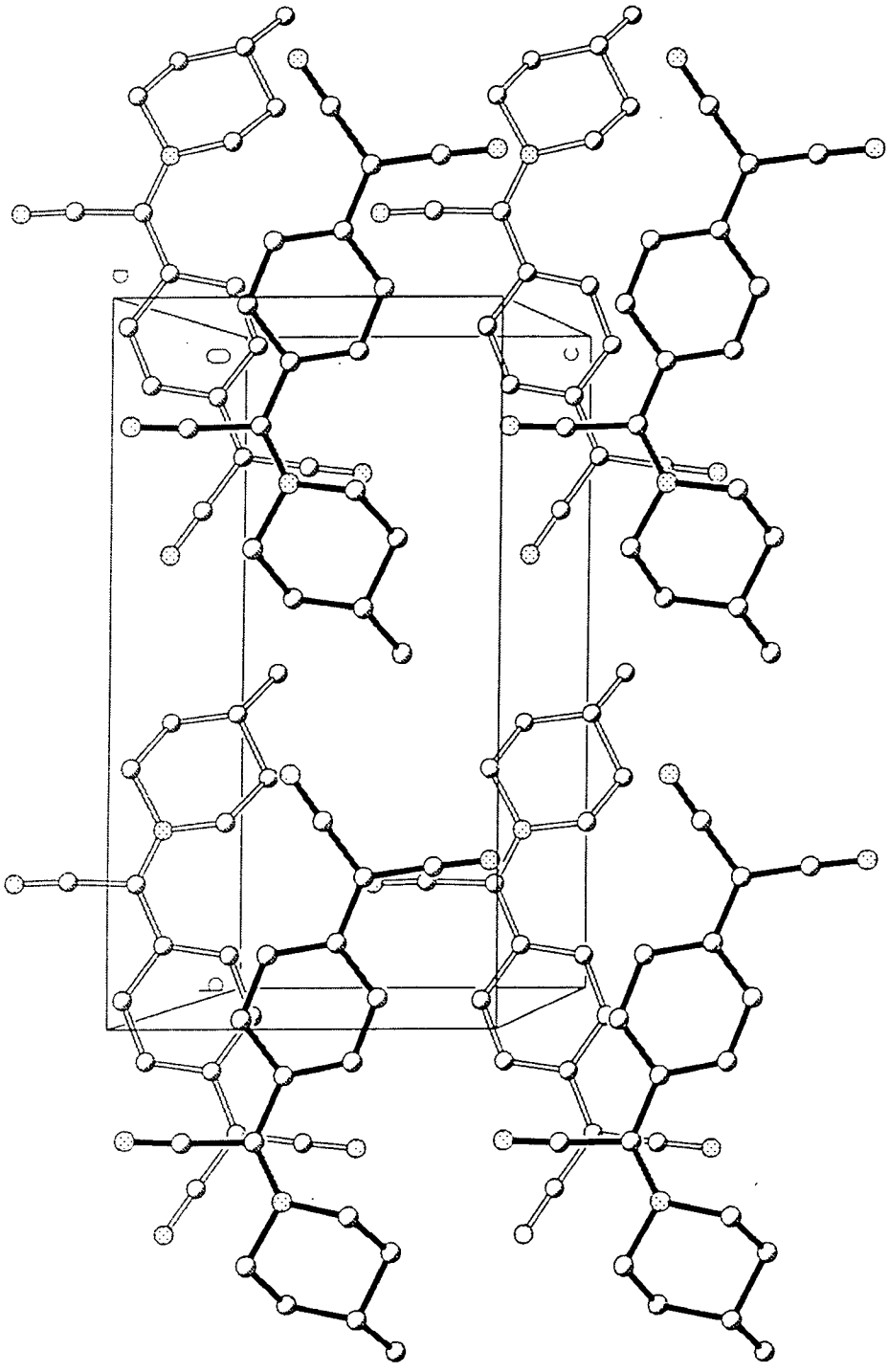

Figure 3.21 Crystal packing of Mono PIP

### 3.3.3 Powder second harmonic generation

The space group of PIP2 and MOR2 (cis and cis/trans mixtures) are $C_2/c$ and $P2_1/c$, respectively. Both crystals are centrosymmetric. The space group of MORPIP

is $P2_12_12_1$, and that of Mono PIP is P*n*. Both of them are noncentrosymmetric. Hence second harmonic generation is expected from powders of MORPIP and Mono PIP. The experiments on powder samples of Mono PIP and Mono MOR were carried out at 1907nm, because their powder samples absorb second harmonic light (532nm) for 1064nm excitation. All the experimental results are shown in Table 3.2.

Table 3.2 Intensity of powder SHG

| Compounds | Intensity of powder SHG (×Urea) |
|---|---|
| cis/trans MOR2 | 0.3 |
| cis MOR2 | 0.3 |
| cis/trans MORPIP | 26 ± 2 |
| cis MORPIP | 24 ± 2 |
| PIP2 | 0.03 |
| cis Mono MOR | No signal[a] |
| Mono PIP[b] | 13[a] |

a: at 1907 nm, b: J.C.Cole et al [27]

The intensities for cis/trans MORPIP (26±2 times urea), and that for cis MORPIP (24±2 times urea) are within experimental errors. Therefore there were no effects on the properties of noncentrosymmetric crystals of MORPIP due to either the cis/trans conformational change or the disorder present in the crystals of cis/trans mixtures.

The crystal system of MORPIP is orthorhombic, $P2_12_12_1$. The optimum crystal structure for powder SHG in this system is a tetrahedral arrangement of the molecular axis [26]. Thus as noted above the crystal arrangement of MORPIP is very

close to this arrangement. However, although the crystal structure of MORPIP is very close to the optimum arrangement (tetrahedral arrangement), two of the four molecules in the unit cell are inactive [26]. Therefore the estimated effective nonlinearity of MORPIP is about 50 % of the optimum in an equivalent monoclinic crystal. The optimum angle for maximum SHG for the symmetry of Mono PIP was reported as 35.26° [26]. The actual angle for Mono PIP is 22.4°. Therefore the estimated effective nonlinearity is about 85 % of that for the optimum monoclinic structure. The nonlinearlity estimated from the crystallographic data for MORPIP (50%) is lower than for Mono PIP (85%).

MOPAC calculations give values for $\beta_{zzz}$ (0) of MORPIP as -51 $\times 10^{-30}$ esu, and for that of Mono PIP as -25$\times 10^{-30}$ esu. Therefore the ratio of $\beta_{zzz}$ (0) for MORPIP and Mono PIP is about 2:1. The resonant enhancement for MORPIP and Mono PIP is 2.8, and 1.5, respectively using the two level model in e.q.1.11. Hence, the ratio of $\beta_{zzz}$ ($\omega$) becomes 3.7:1. Taking into account of the effective nonlinearities for the ratio of the two (1:1.7) deduced from the crystallographic data, the ratio of the effective $\beta_{zzz}(\omega)$ becomes (2.17:1). Hence the estimated ratio of the nonlinear coefficients for them becomes 4.7:1, because the nonlinear coefficient is proportional to $\beta^2(\omega)$ [2]. The experimentally observed SHG ratio (2:1) for MORPIP and Mono PIP is smaller than the estimated ratio from theoretical factors (4.7:1). Hence some enhancement of the nonlinearity of the molecules by the crystal field seems likely [28]. The enhancement by the induced crystal field for MORPIP is expected to be smaller than for Mono PIP because the molecular charge transfer axes of the MORPIP molecules are inclined at a larger angle to one another than for Mono PIP.

The Kurtz powder method to determine SHG is not a very accurate method to determine the nonlinearity of molecules because of its sensitivity to particle size [1,2] as shown in Fig.3.1. The effect of the phase matching was neglected in the case of MORPIP and Mono PIP because the particle size of the powder is small and comparable under an optical microscope.

The second harmonic light was observed from centrosymmetric crystals such as MOR2 and PIP2, although the intensity of the signal from PIP2 was very small. The SHG signal from PIP2 powders could be two photon induced fluorescence. The racemic mixture consists of R and S enantiomers as described earlier in 3.3.2. Each R and S enantiomer interacts with circularly polarised light, differently. This individual interaction between enantiomers (R,S) and circularly polarised light leads to second harmonic light generated by a racemic mixture [29,30]. Scattering in a birefringent powder will produce circularly polarised light, hence SHG is possible in a compound such as MOR2 which is a racemate.

### 3.3.4. Solvatochromism

The solvatochromic shifts for the four newly synthesised compounds (PIP, MOR, MORPIP, and Mono MOR) and the mono substituted compound (Mono PIP) are shown in Fig.3.22. The solvent density parameter ($\Delta f$) defined in 3.1.5. is used as a scale of solvent polarity [17,18].

All three di substitued amino dicyanoquinodimethane compounds show negative solvatochromism. This suggests that all three compounds should be zwitterionic in nature. However, there was very small solvatochromic shift for the mono amino substituted tricyanoquinodimethanes. The list of the absorption maxima in various solvents is presented in Appendix II.

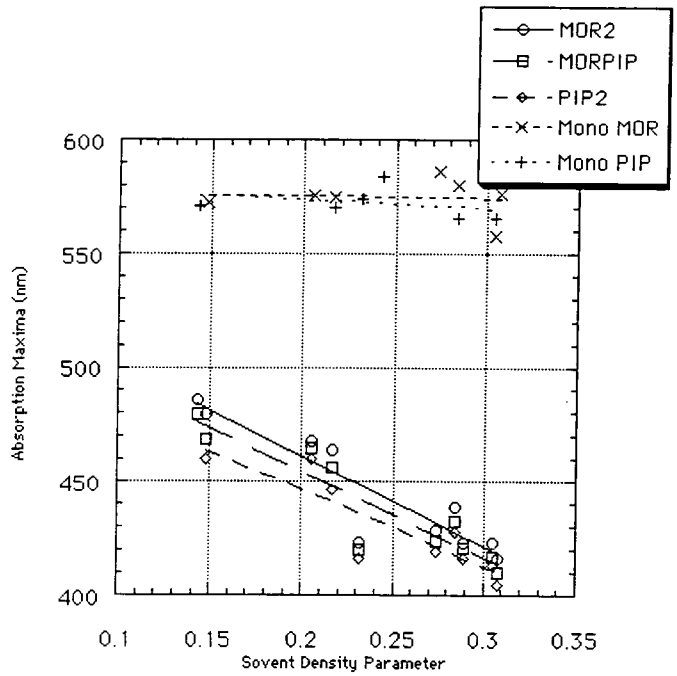


Figure 3.22 Solvatochromic shifts against the solvent density parameter

### 3.3.5 Dipole moments

The calculations of molecular dipole moments for all molecules considered in this section were performed using MOPAC [31]. The AM1 Hamiltonian was used in these MOPAC calculations including the minimization of the molecular geometry for the three compounds, PIP2, MORPIP, and MOR2. The theoretical structure and the theoretical dipole moment of MORPIP were obtained by *ab initio* calculations [32,33]. The dipole moments of MORPIP and PIP2 were obtained experimentally. The dipole moments of these materials are shown in Table 3.3. The experimental value of MORPIP (15 ± 1 Debye) in chloroform is an excellent fit with the theoretical *ab initio* value (15.0 Debye) in the gas phase. The experimental value of PIP2 (16.5 ± 1 Debye) is a reasonable fit with the MOPAC value (15.8 Debye), but MOPAC tends to underestimate the dipole moments. Although the dipole moment measurement of MOR2 was carried out, reasonable values were not obtained due to its low solubility.

Table 3.3. Experimental and theoretical values of dipole moment for MOR2, MORPIP and PIP2

| | MOR2 | MORPIP | PIP2 |
|---|---|---|---|
| Theoretical | 12.4[a] (MOPAC) | 13.5 (MOPAC) | 15.8 (MOPAC) |
| | | 15.0 (*ab initio*) | |
| Experimental[c] | ND[b] | 15.0[a] ± 1 | 16.5 ± 1 |

a: All units are Debye. b: (not determined) c: all experimental values are from chloroform solutions

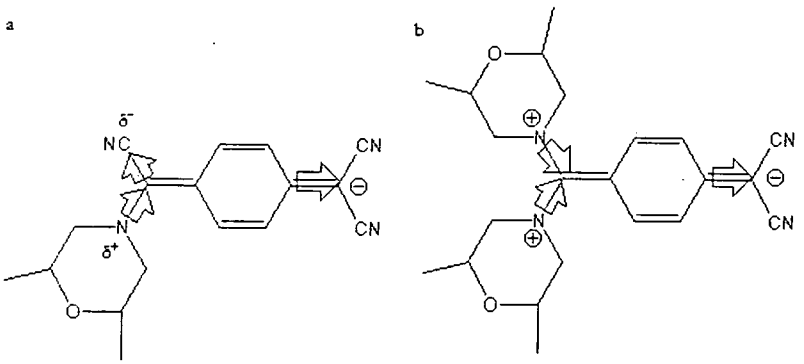


Figure 3.23 Charge separation in mono a) and di substituted b) dicyanoquinomethanes

The MOPAC calculations show that mono amino substituted tricyanoquinomethanes such as Mono MOR (5.8 Debye) have lower dipole moments than di amino substituted dicyanoquinodimethanes due to the different charge transfer systems, as shown in Fig.3.23.a. The amino substituent is an electron donor, so charge can move to the dicyano methylene moiety which is a stronger electron acceptor, but this will be affected by the cyano moiety next to the donor. This disturbs the charge transfer along the molecule from the donors (morpholines) to the strong acceptor (dicyano methylene moiety).

The dipole moment of MORPIP was determined experimentally in three different solvents (chloroform, dichloromethane, and acetone). The BLA model predicts that with the increase of the polarity of the solvent (or the reaction field) the zwitterionic nature increases, so the more polar solutes enhance the dipole moment. Previous studies of DEMI clearly support this theory because the molecular dipole moment of DEMI is measured from 12 Debye (in chloroform) up to 45 Debye with an increase in polarity [21,22,34]. So the enhancement from the reaction field created by the solvent polarity on solutes affects the molecular dipole moment, if the polarity of the solvent is large. With an increase in polarity, the experimental error of the molecular dipole moment measurement becomes large. The results of the dipole moment measurements for MORPIP in various solvents are shown in Table 3.4.

Table 3.4 Experimental values of dipole moments for MORPIP in three solvents.

| | Chloroform | Dichloromethane | Acetone |
|---|---|---|---|
| $\Delta f$ | 0.148 | 0.217 | 0.284 |
| Dipole moment (Debye) | $15.0 \pm 1$ | $12.5 \pm 3$ | $10 \pm 5$ |

The dipole moments were the same (around 15D) as a function of the solvent density parameter ($\Delta f$). The trend of the dipole moment in the three solvents is different from zwitterionic molecules such as DEMI.

### 3.3.6 Comparison between crystal and theoretical structures

Bond length alternation (BLA) can be used to characterise the nature of molecules, i.e. either the benzenoid or the quinoid structure. The backbone of the molecules considered here is shown in Fig.3.23, as a basis for comparison of the bond lengths [19,20]. Each bond length from the donor to the acceptor through the benzene ring is shown in Table 3.4. The ideal form of the TCNQ (quinoidal) and zwitterionic (benzenoid) backbone were obtained and shown in Table 3.5. The average bond deviation ($D^S$) in the backbone of each structure from the ideal TCNQ backbone is defined in eq.3.5 [35].

$$D^S = \frac{\sum_{i=1}^{N_b} \left| b_i^S - b_i^{TCNQ} \right|}{N_b} \tag{3.5}$$

The average bond deviations of each structure and the ideal zwitterionic form ($D^{ZWIT}$) were calculated and are shown in Table 3.5. If the average bond deviation is zero ($D^S$=0), the structure would be 100% quonoidal character, i.e. 0% zwitterionic character. If the average bond deviation is 0.053Å, the structure has 100% zwitterionic character [35]. Therefore the degree of the zwitterionic (benzenoid) character ($\chi_S$) of each molecule can be defined by

$$\chi_S = \left( 1 - \left( \frac{D^{ZWIT} - D^S}{D^{ZWIT}} \right) \right) \times 100 \tag{3.6}$$

The degree of the benzenoid character of each structure was obtained, as shown in Table 3.5.

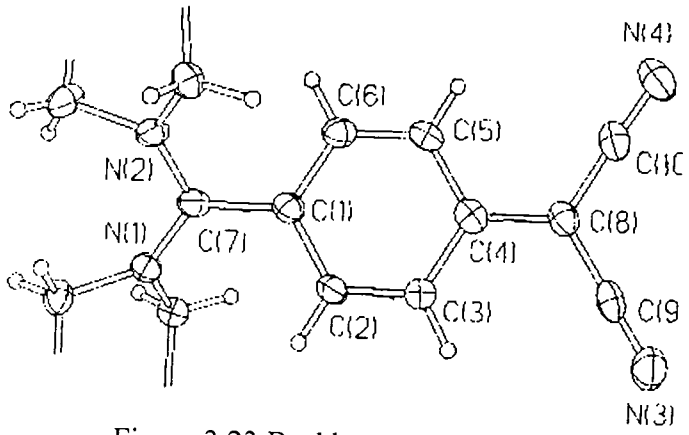


Figure 3.23 Backbone of the molecules

| Bond length | Quinoid | Benzenoid | MOR2 | MORPIP | PIP2 | *ab initio* | Mono PIP |
|---|---|---|---|---|---|---|---|
| N1 - C7 | —— | —— | 1.346 | 1.348 | 1.346 | 1.376 | —— |
| N2 - C7 | —— | —— | 1.350 | 1.339 | 1.346 | 1.382 | 1.321 |
| C7 - C1 | 1.392 | 1.470 | 1.459 | 1.459 | 1.465 | 1.384 | 1.428 |
| C1 - C2 | 1.432 | 1.380 | 1.409 | 1.395 | 1.408 | 1.419 | 1.430 |
| C2 - C3 | 1.352 | 1.380 | 1.375 | 1.372 | 1.378 | 1.348 | 1.363 |
| C3 - C4 | 1.342 | 1.380 | 1.418 | 1.414 | 1.414 | 1.417 | 1.415 |
| C4 - C5 | 1.432 | 1.380 | 1.418 | 1.397 | 1.414 | 1.417 | 1.419 |
| C5 - C6 | 1.352 | 1.380 | 1.377 | 1.374 | 1.378 | 1.346 | 1.361 |
| C6 - C1 | 1.432 | 1.380 | 1.409 | 1.401 | 1.408 | 1.416 | 1.418 |
| C4 - C8 | 1.392 | 1.470 | 1.440 | 1.442 | 1.447 | 1.394 | 1.427 |
| Twist angle | —— | —— | 42.4 | 45.3 | 41.3 | 11.7 | 17.8 |
| D[a] | 0.0 | 0.053 | 0.030 | 0.035 | 0.033 | 0.0099 | 0.017 |
| $\chi_a$(%) | 0 | 100 | 56.5 | 66.7 | 62.9 | 18.8 | 32.7 |

Unit of bond lengths is Å
Unit of twist angle is degree

Table 3.5 Bond lengths and twist angles

The *ab initio* theoretical model of MORPIP has the lowest benzenoid character (18.8%). This is because the model was obtained in the gas phase where there is no

reaction field. The actual molecular model deduced from the crystallographic data under the presence of the crystal field was obtained.

As the induced field increases from the gas phase (zero) to the crystal lattice (crystal field), the benzenoid character increases from 18.8% to 66.7%. The twist angle also increases from 11.2° (the *ab intio* model) to 45.3° (the molecular model deduced by crystallographic data). The top views of both models gives clear picture of the twist angle shown in Fig. 3.25. Dipole moments of MORPIP also increase from 13.5 Debyes to 18.5 Debyes calculated by MOPAC for both models without any further minimisation.

The increase of the dipole moments from the gas phase to the crystal state is because of the increase in benzenoid character, i.e. the more polar structure as shown in Fig.3.4. In the case of 2-methyl-4-nitroaniline (MNA), the crystal field effects enhance the molecular dipole moments from 9 to 20 D [28]. The enhancement of the molecular dipole moments of MORPIP was smaller than in MNA, because the twist in the structure between the $\pi$ conjugation systems prevents movement of charges. However, the estimated dipole moment in the crystal lattice (18.5Debye) is still a large value in the presence of the crystal field.

In the crystal lattice the movement of the twist is very restricted, but in solution the twist can rotate easily. The potential energy and the molecular dipole moment as a function of the twist angle were obtained by *ab initio* calculation. The experimentally obtained dipole moment is compared with the result of *ab initio* calculation in next section.

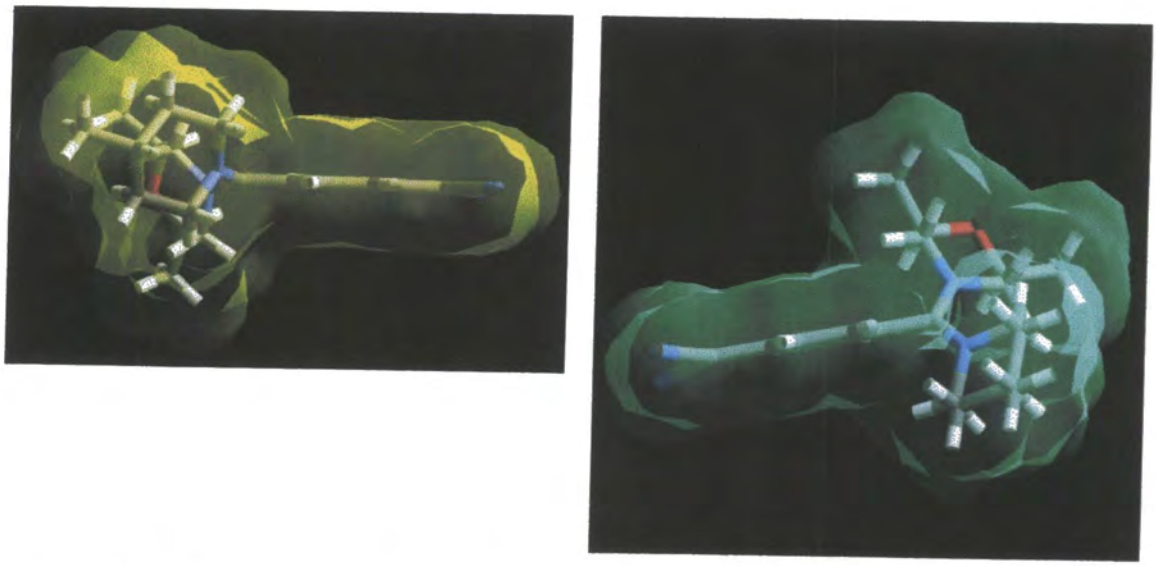

Figure 3.24 Side views of theoretical model (left) and the crystal structure (right) of MORPIP

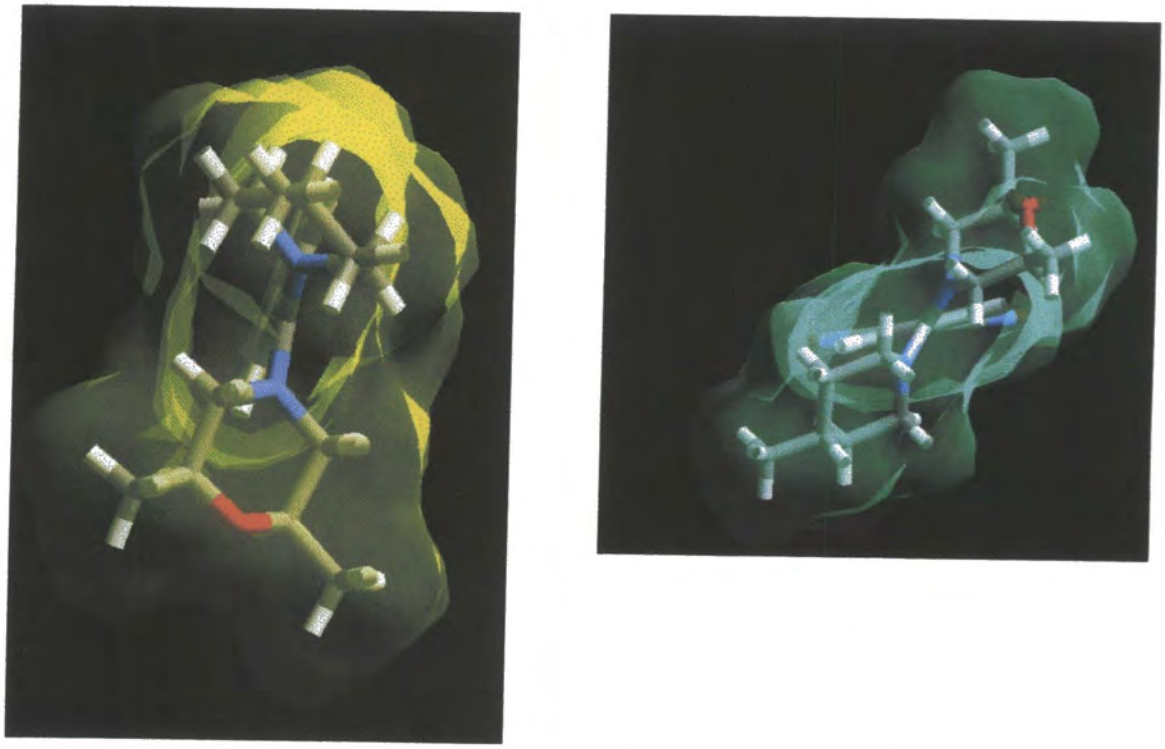

Figure 3.25 Top views of theoretical (left) and the crystal structure (right) of MORPIP

### 3.3.7 Twist angles and dipole moments

The *ab initio* calculation of dipole moment and potential energy for MORPIP was carried out as a function of the twist angles as shown in Fig.3.26.

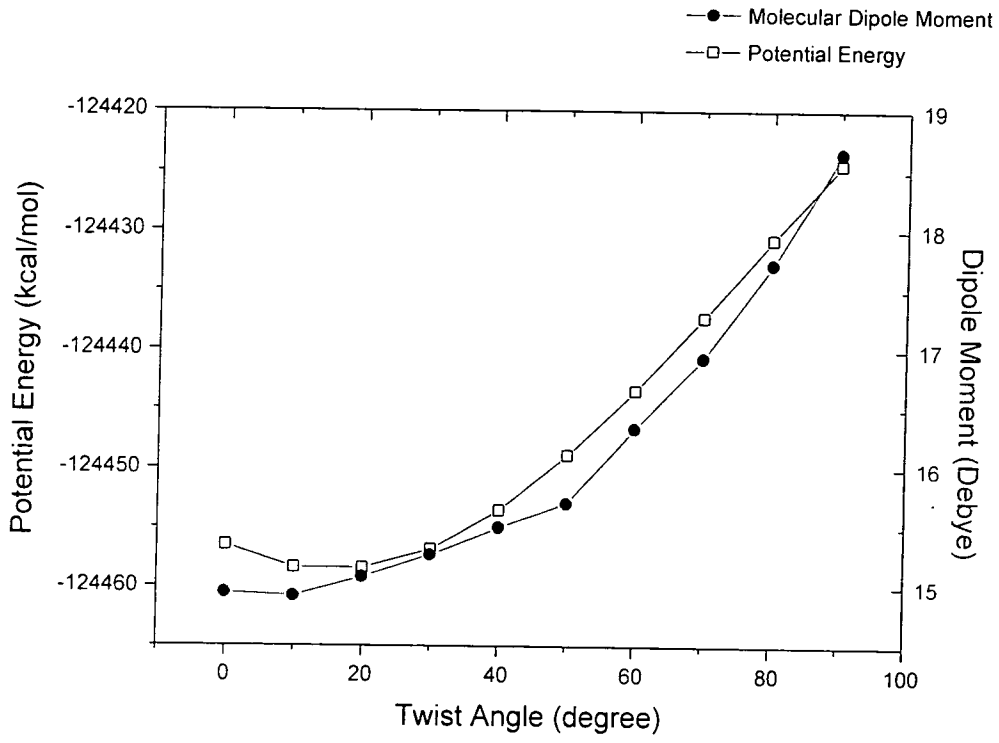


Figure 3.26 The dipole moment and potential energy of MORPIP by *ab intio* calculation

The *ab initio* calculation predicts that an increase of the twist angle will bring an increase in dipole moment and an increase of the potential energy of the molecule. The increase of the molecular dipole moment as a function of the twist angle is similar to the prediction of the MOPAC calculation in 3.3.6, which used the *ab inito* and the deduced molecular structures, although the increase of the dipole moment between 11° and 45° degrees is smaller than MOPAC calculation.

The solvatochromic shift of MORPIP in solution indicates the ground state is highly polar in nature. In general, the reaction field (defined in Chapter 1) enhances the molecule dipole in polar solvents. However, the experimentally obtained dipole moments in solution are of a similar order (15 Debye) as shown in 3.3.5. This indicates that the reaction field forces some alternations of the twist of the molecule, which tends to keep the dipole approximately constant. The molecule can rotate easily up to 50° in solution because the change of the potential energy between 0° and 50° is relatively small (within 5kcal/mol) as shown in Fig.3.26. Hence the experimentally obtained molecular dipole moment in solution is close to the value from the *ab initio* calculation. There is an enhancement to the molecular dipole moment from the crystal field as a result of the close packing in the crystal lattice [28]. The 45° twist of the molecule is stabilised by the crystal field, producing a relatively polar and a reduction in potential energy of the molecule, according to the crystallographic data.

## 3.4 Conclusion

Large dipole moments of MORPIP and PIP were measured in chloroform (15±1D) and (16.5±1D), respectively. Theoretical predictions (15.0 D for MORPIP by *ab inito* and 15.8 D for PIP2 by MOPAC supported these experimental values. Negative solvatochromism for MORPIP, MOR2, and PIP2 was observed, e.g. these experimental results indicated that the three molecules were highly dipolar and strongly zwitterionic in nature. Such molecules tend to form centrosymmetric crystals. The molecular structure deduced from X-ray crystallographic data was obtained for PIP2. The crystal packing of PIP2 was centrosymmetric ($C_2/c$). Despite the incorporation of chiral groups MOR2 was still centrosymmetric ($P2_1/c$), because

of the use of a racemic mixture. A small SHG signal was observed from MOR2 crystals. R and S MOR2 molecules in the crystal cell interact differently with circularly polarized light (optical activity) to give rise to second harmonic light from the centrosymmetric crystals. The introduction of molecular asymmetry enhances the formation of noncentrosymmetric crystals. The crystal packing of MORPIP was noncentrosymmetric ($P2_12_12_1$). The intensity of the second harmonic generation of MORPIP was 25 times that of urea using the Kurtz powder technique. The optimum molecular arrangement for SHG in the orthorhombic crystal system is a tetrahedral arrangement in the unit cell. The molecular arrangement of MORPIP is very close to the optimum, but two of the four molecules in the unit cell are inactive in SHG. We also found that the achiral, asymmetric Mono PIP also had a noncentrosymmetric crystal structure (P*n*). The intensity of second harmonic light from Mono PIP was 13 times that of urea. The angle ($\theta_{mono}$) between the molecular charge transfer axis and the two fold axis for Mono PIP was 22.4°. The optimum angle for the crystal system of Mono PIP is 35.26°. Hence, The angle ($\theta_{mono}$) is relatively close to the optimum angle for SHG. Consequently, the estimated effective nonlinearity from crystallographic data for MORPIP (50%) is lower than that for Mono PIP (85%). The theoretical nonlinearity of the second order including the effect from the crystallographic arrangements for MORPIP is much higher than for Mono PIP (4.7:1), but the ratio of the observed second harmonic generation from MORPIP and Mono PIP is 2:1 (25 U:13U). The observed second harmonic generation from Mono PIP was higher than the theoretically estimated value. There is likely to be some enhancement to the nonlinearity of Mono PIP from the crystal field in the unit cell.

The experimentally obtained molecular dipole moment for MORPIP is of an order of 15 Debye in chloroform, dichloromethane, and acetone. This is approximately the same value from the *ab initio* calculation.

The structure deduced from crystallographic data suggests that the most favourable molecular structure should be the twist angle of 45°. This is because the presence of the crystal field enhances the dipole moments, makes the molecules polar and twisted, and makes the potential energy at 45° favourable.

The calculated $\mu\beta(0)$ of DEMI is $-9450\times10^{-48}$ esu from an EFISH experiment [21,22]. This value is very high, but the absorption maximum is around 700nm so it is not suitable for LAN applications as described in 1.1.1. The estimated $\mu\beta(0)$ of MORPIP using the experimental value for $\mu$ and $\beta(0)$ from the MOPAC calculation is $-930\times10^{-48}$ esu. This value is still higher than normal conventional chromophores such as dimethylaminonitrostilbene (DANS). The value of $\mu\beta(0)$ is $363\times10^{-48}$ esu [36,37]. MORPIP can meet the requirements for the devices to be used in POFs LANs, and the absorption maximum is below 500nm. Therefore the low absorption necessary between 550nm and 700nm is achieved.

## Chapter 3: References

[1] S.K.Kurtz, T.T.Perry, J.Appl.Phys., **39**, 1968, 3798

[2] D.J.Williams, Angew.Chem.Int.Ed.Engl., **23**, 1984, 690

[3] N.Isaacs, Physical Organic Chemistry, Longman Science&Technical, Harlow (1995)

[4] J.Wilson, J.F.B.Hawkes, Optoelectronics, Prentice Hall, London (1989)

[5] M.S.Wong, C.Bosshard, P.Günter, Adv.Mater., **9**, 1997, 837

[6] M.Ravi, S.Cohen, I.Agranat, T.P.Radhakirishnan, Structural Chemitry, 7,1996, 225,

[7] M.Ravi, D.N.Rao, S.Cohen, I.Agranat, T.P.Radhakirishnan, J.Mater., **6**, 1996, 1119

[8] M.Ravi, D.N.Rao, S.Cohen, I.Agranat, T.P.Radhakirishnan, Chem.Mater., **9**, 1997, 830

[9] J.L.Oudar, R.Hierle, J.Appl.Phys., **48**, 1977, 2699

[10] M.Barzoukas, D.Josse, P.Fremaux, J.Zyss, J.F.Nicoud, J.O.Morely, J.Opt.Soc. Am.B, **4**, 1987, 977

[11] J.Zyss, J.F.Nicoud, M.Coquillay, J.Chem.Phys., **81**, 1984, 4160

[12] D.S.Chemla, J.Zyss, Nonlinear Optical Properties of Organic Molecules and Crystals Vol. 1, Academic Press Inc., London (1987)

[13] J.Zyss, D.S.Chemla, J.F.Nicould, J.Chem.Phys., **74**,1981,4800

[14] K.D.Singer, J.E.Sohn, S.J.Lalama, Appl.Phys.Lett., **49**, 1986, 248

[15] K.D.Singer, M.G.Kuzyk, J.E.Sohn, J.Opt.Soc.Am.B., **4**, 1987, 968

[16] P.N.Prasad, D.J.Williams, Introduction to Nonlinear Optical Effects in Molecules and Polymers, John Wiley&Sons, Inc., New York (1991)

[17] C.Reichardt, Solvent and Solvent effects in Organic Chemistry, Weinheim, (1988)

[18] P.Suppan, J.Chem.Soc., (A), 1968, 3125

[19] F.Meyers, S.R.Marder, B.M.Pierce, J.L.Brédas, J.Chem.Soc., **116**, 1994, 10703,

[20] R.Ortiz, S.R.Marder, L.Cheng, B.G.Tiemann, S.Cavagnero, J.W.Ziller, J.Chem.Soc., Chem.Comm., 1994, 2263

[21] M.Szablewski, P.R.Thomas, A.Thornton, D.Bloor, G.H.Cross, J.M.Cole, J.A.K. Howard, M.Malagoli, F.Meyers, J.Brédas, W.Wenseleers, E.Goovaerts, J.Am. Chem. Soc., **119**, 1997, 3144

[22] P.R.Thormas, Ph.D.Thesis submitted to Physics Department, University of Durham (1998)

[23] E.A.Guggenheim, J.Chem.Soc.Fraday Trans., **45**, 1949, 714

[24] W.R.Hertler, H.D.Hartzler, D.S.Acker, R.E.Benson, J.Am.Chem.Soc., **84**, 1962, 3387

[25] M.J.Buerger, Elementary Crystallography, Chapman&Hall Ltd., London (1956)

[26] J.Zyss, J.L.Oudar, Phys.Rev.A.**26**, 1982, 2028

[27] J.C.Cole, J.M.Cole, G.H.Cross, M.Farsari, J.A.K.Howard, M.Szablewski, Acta Cryst., **B53**, 1997, 812

[28] S.T.Howard, M.B.Hursthouse, C.W.Lehmann, P.R.Mallinson, C.S.Frampton, J. Chem.Phys., **97**, 1992, 5616

[29] E.W.Meijer, E.E.Havinga, G.L.A.Rikken, Phys.Rev.Lett., 65, 1990, 37

[30] E.W.Meijer, E.E.Havinga, Synthetic Metals, **55-51**, 1993, 4010

[31] J.J.P.Stewart, J.Computer-Aided Molecular Design, **4**, 1990, 1

[32] S.J.Clark, C.J.Adam, G.J.Ackland, J.White, J.Crain, Liquid Crystal, **22**, 1997, 469

[33] W.G.Richards, D.L.Cooper, *ab initio* molecular orbital calculations for chemists, Clarendon Press, Oxford (1983)

[34] M.Szablewski, J.Org.Chem., **59**, 1994, 954

[35] F.H.Allen, L.Brammer, O.Kennard, A.G.Orpen, R.Taylor, D.G.Watson, J.Chem., Soc.,Perkin. Trans.2,1987,1

[36] S.R.Marder, L.-T.Cheng, B.G.Tiemann, A.C.Friedli, M.Blanchard-Desce, J.W.Perry, J.Skindhoy, Science, **263**, 1994, 511

[37] V.P.Rao, A.K.Y.Jen, K.Y.Wong, K.J.Drost, J.Chem.Com., 1993, 1118

# Chapter 4: Luminescence Properties

## 4.1 Introduction

### 4.1.1 Photophysical processes

Each electron in a molecule has a spin angular momentum with spin quantum numbers ($s=\pm 1/2$). The positive and negative signs of the spin quantum numbers show that an electron possesses spin-up (positive) and spin-down (negative), indicated by the use of arrows, $\uparrow$ or $\downarrow$. Two electrons can have their spins opposed ($\uparrow,\downarrow$) in the same orbital. The spin multiplicity is given by $2S+1$ where S is the sum of the spin quantum numbers. The spin multiplicity gives the number of possible states. The singlet state occurs for two electrons with opposed spins, i.e. the spin multiplicity is 1 ($S=0$). In general the ground state of the majority of organic molecules is a singlet state defined as $S_0$. The singlet excited state ($S_1$) can be created by the photoexcitation [1]. If the excited electron changes its spin from opposed to parallel such as ($\uparrow,\uparrow$), the spin multiplicity becomes 3 as $S=1$. This state is termed a triplet state. The first excited triplet state is called $T_1$. Fluorescence occurs when the emitted radiation coming from the excited state that has the same spin multiplicity as the ground state. Phosphorescence occurs when the emitted radiation coming from a state with different spin multiplicity from the ground state, such as the " forbidden" de-excitation from $T_1$ to $S_0$[1]. IC stands for internal conversion, which is a vibrational relaxation decay (VR). ISC stands for intersystem crossing, which is the first excited triplet state ($T_1$) from an excited singlet state (S) [1]as shown in Fig.4.1.

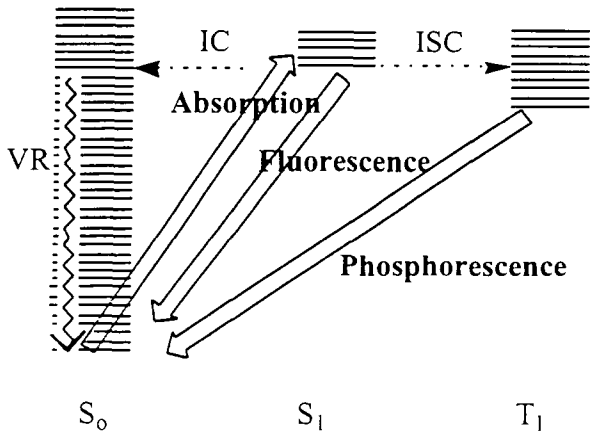


Figure 4.1 Schematic diagram of fluorescence and phosphorescence

## 4.1.2 The kinetics of photophysical processes

### 4.1.2.1 Lifetimes

A concentration of electronically excited molecules, expressed as [M*], is generated by the absorption and radiation of photons greater in energy than the $S_0$-$S_1$ separation. The concentration decays to zero as a function of time as a result of the spontaneous emission of radiation, which can be written as

$$[M^*] \rightarrow M + h\nu \qquad (4.1)$$

where $h\nu$ is a photon of lower or the same energy the photon absorbed by the ground state molecule (M). The spontaneous emission process is a random process that follows first order kinetics [1].

$$-\frac{d}{dt}[M^*] = k_r^o[M^*] \qquad (4.2)$$

The nature and properties of the excited states determine the rate of the spontaneous emission process, i.e. the coefficient of the first order kinetics ($k_r^o$) in e.q.4.2. The integration of e.q.4.2 leads to eq.4.3.

$$[M^*] = [M^*]_o e^{-k_r^o t} \tag{4.3}$$

where $[M^*]_o$ is the initial concentration of the electronically excited molecules (at t=0). The lifetime of a radiative process is defined as the reciprocal of the first order rate coefficient

$$\tau_r^o = \frac{1}{k_r^o} \tag{4.4}$$

Experimentally an intense radiation beam can create a large initial concentration of electronically excited states. The measured rate of emission as a function of time determines the radiative process. This measured rate of the radiative process is not characterized by the lifetime defined by eq.4.4, because other processes such as nonradiative decay may affect the measured decay of the excited molecule concentration. The measured rate coefficient can be defined to include all of the possible pathways by which the excited molecules can decay:

$$-\frac{d}{dt}[M^*] = k^o_f [M^*] + k_{ISC}[M^*] + k_{IC}[M^*] \tag{4.5}$$

where $k^o_f$ is the natural fluorescence rate coefficient (the radiative decay process), $k_{IC}$ is the rate coefficient for internal conversion (non-radiative process), and $k_{isc}$ is the rate coefficient for intersystem crossing to the triplet state. All of the decay processes follow the first order decay kinetics. So the overall decay process is still an exponential decay. The concentration of excited state can be expressed by

$$[M^*] = [M^*]_o e^{-k_f t}, k_f = k_f^o + k_{ISC} + k_{IC} \tag{4.6}$$

The measured lifetime is thus defined by

$$\tau_f = \frac{1}{k_f} = \frac{1}{(k_f^o + k_{ISC} + k_{IC})} \tag{4.7}$$

### 4.1.2.2 Single photon counting technique

One of the techniques which can be used to measure the lifetime ($\tau_f$) is the time-correlated single photon counting technique [1-3]. Time-resolved spectroscopy can give the kinetics of the emission process [4-25]. A typical set up for single photon counting is shown in Fig.4.2.

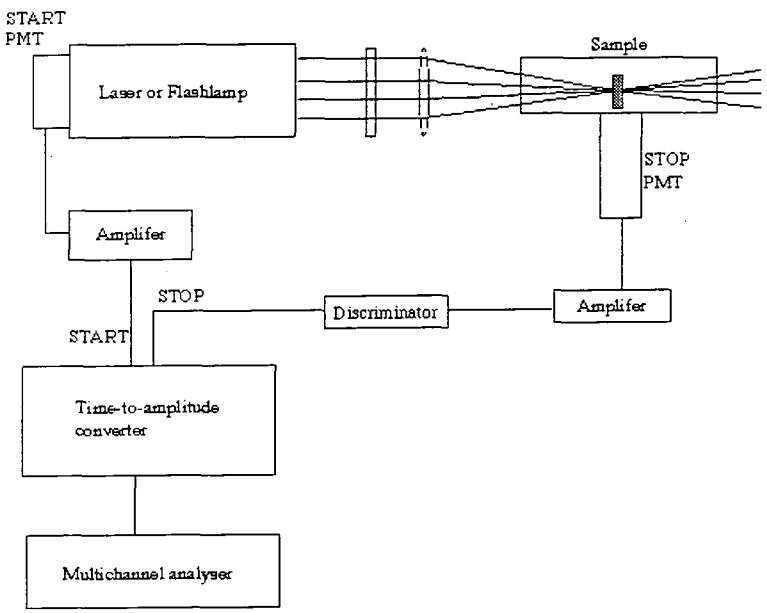


Figure 4.2 A typical single photon counting technique set up

The set up consists of two photomultipliers (PMTs). The first one is called the START photomultiplier, which is attached to the excitation light source such as a laser or a flash lamp. The START photomultiplier sends a signal when it detects a pulse of light from the excitation light source, and triggers a time-to-amplitude converter, which is an electronic device to initiate a voltage ramp that increases steadily from zero. A photon emitted from the sample may be detected by the STOP photomultiplier. If the STOP photomultiplier detects a photon, it sends a signal to the time-to-amplitude converter that stops any further increase. Therefore the time difference between the excitation pulse and the detected emitted photon is converted

into a voltage. The time-to-amplitude converter is connected to a multichannel analyzer that breaks the voltage range into sequence of channels. Each channel keeps count of the number of times that a certain voltage is obtained. The cycle of counting photons is repeated thousands of times per second.

The intensity of emitted light determines the probability of a single photon being emitted at a specific time. The obtained amplitudes stored in the multichannel analyzer are the histogram of the emitted light intensity, which is the emission decay profile.

#### 4.1.2.3 Quantum yield

Quantum yield [5,12,15-17, 26-29] can be defined as:

$$\Phi_f = \frac{\text{Number of molecules fluorescing per unit time per unit volume}}{\text{Number of quanta absorbed per unit time per unit volume}} \quad (4.8)$$

The eq.4.8 can be rewritten because the number of absorbed or emitted photons are related to their intensities:

$$\Phi_f = \frac{I_f}{I_{abs}} \quad (4.9)$$

where $I_f$ is the intensity of fluorescence and $I_{abs}$ is that of absorbed radiation. The eq.4.9 can be expressed by the rates of fluorescence and absorption:

$$\Phi_f = \frac{\frac{d}{dt}[h\nu']}{\frac{d}{dt}[h\nu]} \quad (4.10)$$

where $h\nu'$ is emitted photons, $h\nu$ is absorbed photons where $\nu \geq \nu'$. All of the excitation and emission process follow the first order kinetics as shown in Table 4.1.

Table 4.1 A list of the kinetic schemes

| | | |
|---|---|---|
| $M + hv \rightarrow M^*$ | excitation | $k_{abs}[M][hv]$ |
| $M^* \rightarrow M + hv'$ | fluorescence | $k_f^o[M^*]$ |
| $M^* \rightarrow M$ | other decay processes | $k_{ISC}[M^*] + k_{IC}[M^*]$ |

The absorption process depends on the concentration of the ground state molecules and the concentration of photons. Therefore, the rates of absorption and fluorescence can be rewritten as:

$$-\frac{d}{dt}[hv] = k_{abs}[M][hv] \tag{4.11}$$

$$\frac{d}{dt}[hv'] = k_f^o[M^*] \tag{4.12}$$

Hence, the change of the concentration of excited state is:

$$-\frac{d}{dt}[M^*] = k_f[M^*] - k_{abs}[M][hv] \tag{4.13}$$

This expression in eq.4.13 is not very useful due to the difficulty in measuring the concentration of the excited state. The quantum yield is determined by "steady-state" measurements of the absorbed and emitted radiation intensities as defined in e.q.4.9. The steady state concentration of excited state molecules, M*, does not change, because the rates of production and of decay are equally balanced. Therefore under the steady state conditions the rate of change of the concentration of excited molecules is zero. Hence, the eq.4.13, can be as

$$k_f[M^*] = k_{abs}[hv][M] \tag{4.14}$$

From eq.4.11-13;

$$k_{abs}[hv][M] = \frac{k_f^o[M^*]}{\Phi_f} \quad (4.15)$$

Therefore from both eq.4.14 and e.q.4.15

$$\Phi_f = \frac{k_f^o}{k_f} = \frac{\tau_f}{\tau_f^o} \quad (4.16)$$

## 4.1.3 Stokes Shift and solvent polarity indicator ($E_T(30)$)

### 4.1.3.1 Stokes Shift and Frank-Condon Principle

The electronic transition excited by the electromagnetic radiation occurs rapidly ($10^{-15}$ s) compared to nuclear motion ($10^{-12}$ s). Hence, the motion of the nuclei remains essentially frozen at the equilibrium configuration of the ground state during the transition. The electronically excited state is likely to have a different structure from the ground state [30-32]. Therefore the nuclear configuration will be changed after the electronic transition. The Frank-Condon excited state is the state immediately after the electronic transition, which has not changed its configuration to reach the equilibrium excited state by vibrational relaxation [30-32] as shown in Fig.4.3.

The Stokes shift [1,33-42] can be defined as the energy difference between excitation and emission as shown in Fig.4.3 and eq.4.17. The study of emission and absorption spectra probes the dynamics of electronically excited molecules [1,33-42]. The effects of solvents, i.e., solvent polarity change, can be observed as solvatochromic shifts caused by the change of the internal coordinate (q) in Fig.4.3. The change of the internal coordinate can bring about a molecular dipole moment change. *p*-cyano-dialkyl anilines form TICT excited state [6,7,9,10,25,43-49], which brings about a change of the internal coordinate, as described in 1.7. As a result of it,

the change of the molecular dipole moment between the first equilibrium excited state and the ground state is up to 10 Debye [9,10]. The Stokes shift ($\Delta v$) is influenced by the polarity of the solvent and the change of the dipole moments between the equilibrium excited state, and the Stokes shift ground state can be given by

$$\Delta v = v_{\max}^{abs} - v_{\max}^{ems} = \frac{2(\mu_e - \mu_g)^2}{cha^3}\left(\frac{\varepsilon - 1}{2\varepsilon + 1} - \frac{n^2 - 1}{2n^2 + 1}\right) \qquad (4.17)$$

where ε, $n$ are the dielectric constant and refractive index of the medium, respectively. $\mu_e$ and $\mu_g$ are the excited state and the ground state dipole moment, and $a$ is the Onsager cavity defined in Chapter 1. The polarity (solvent density) parameter ($\Delta f$) in eq.4.17, is $\Delta f = \left(\frac{\varepsilon - 1}{2\varepsilon + 1}\right) - \left(\frac{n^2 - 1}{2n^2 + 1}\right)$ (as defined in 3.3.4)

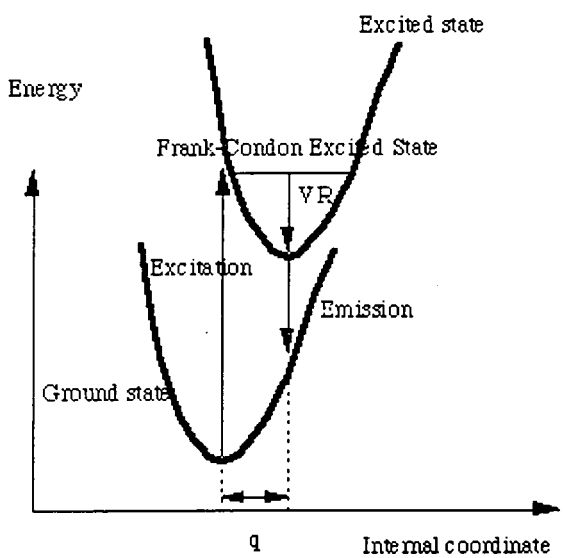


Figure 4.3 Schematic diagram of Stokes shift

#### 4.1.3.2 Solvent polarity indicator ($E_T(30)$)

From the e.q.4.17 the Stokes shift is dependent on the solvent polarity where the function of solvent polarity is the expression in the final bracket. This solvent parameter uses dielectric constants and refractive indices, which are macroscopic parameters for the medium, therefore, the solute and solvent interactions are partially taken into account [30,50]. Most of the materials studied here are highly polar and zwitterionic, and show negative solvatochromism, for which solute and solvent interactions must be considered carefully. $E_T(30)$ has been used and recognized as a useful solvent parameter to describe the solute and solvent interactions of such molecules [11,12,25,30,42,45,50]. The solvent polarity values are based on a pyridinium *N*-phenolate betaine dye that is also zwitterionic and shows negative solvatochromism. The molar electronic transition energies of the dye were measured in different solvents at room temperature, and normal pressure (1bar). $E_T(30)$ parameters were obtained experimentally. As $E_T(30)$ is a microscopic polarity parameter solute/solvent interactions are taken into account [30,50].

## 4.2 Experimental

### 4.2.1 Quantum efficiency measurements in various alcohols

Emission and photoexcitation spectra were recorded on a Perkin Elmer Luminescence Spectrometer LS 50B. Absorption spectra recorded on a Perkin Elmer Lambda 19. Solutions were prepared in methanol, ethanol, 1-propanol, 1-butanol, 1-pentanol, 1-hexanol, ethylene glycol, and glycerol without degassing. After filtration (0.5 μm filters), solutions of the optical density 0.055±0.01 at 375nm were prepared as well as a solution of quinine sulphate dihydrate in 0.5M sulphuric acid with the



same optical density. The quinine sulphate dihydrate sample was placed in the fluorometer. The emission spectrum of quinine sulphate dihydrate was recorded as a reference to estimate the quantum yields of samples. The quantum yield of quinine sulphate dihydrate is 59% and relatively temperature independent. Therefore quinine sulphate dihydrate is useful as a standard quantum yield reference [58]. The area of quinine sulphate dihydrate in the emission spectrum is compared to that of samples for the quantitative analysis. All of the emission spectra were measured with the same slit widths. The emission spectra were compared with the spectrum of quinine sulphate dihydrate.

### 4.2.2 Preparation of spin coated PMMA films and their luminescence properties

Emission, and photoexcitation spectra were recorded on a Perkin Elmer Luminescence Spectrometer LS 50B. Absorption spectra recorded on a Perkin Elmer Lambda 19.

The film sample was placed in the Perkin Elmer fluorimeter. Emission spectra excited at the absorption maxima of samples were recorded. Photoexcitation spectra detected at the emission maxima were recorded. Film samples were prepared as described in the following example.

MORPIP (11mg) and PMMA pellets (1.218g) were dissolved in 3ml of DMF in a sample bottle. The mixture was stirred for several days to ensure complete dissolution. The glass substrates were cleaned with acetone and then a mixture of acetone and isopropanol. Films were prepared by spin coating. As soon as the PMMA solution was dropped to a clean glass substrate, the spinner was switched on to give a clear PMMA film. The speed of spinner was set at 2000rpm for 10-15

seconds. The spin coated PMMA films were kept in an oven at 80 °C typically for several days under vacuum.

### 4.2.3 Luminescence property at low temperature

Emission, and photoexcitation spectra recorded on a Spex Fluoromax fluorimeter. Absorption spectra recorded on a Perkin Elmer Lambda 15.

A sample solution was prepared in a glass forming solvent, either 1-propanol or 2-methyl THF. A typical optical density of absorption maximum was below 0.5. The background scan of the UV/Vis spectra was carried out with the sample in a cryostat. The sample in a special low temperature cuvette was placed inside a cryostat. The absorption, emission and photoexcitation spectra were obtained at room temperature. Liquid nitrogen was poured into the cryostat. The temperature of the cryostat was controlled with an Oxford Instrument temperature controller. Absorption, emission and photoexcitation spectra were obtained in the range of room temperature to 80K.

A MORPIP doped PMMA film was also placed in the cryostat. Absorption, emission and photoexcitation spectra were obtained at room temperature, 200K,125K, and 80K.

### 4.2.4 Time resolved spectroscopy

Excitation provided using a cavity dumped DCM dye laser (Coherent 7210 cavity dumper, and 700 series dye laser), which was synchronously pumped by the second harmonic of a mode-locked Nd:YAG laser (Coherent Antares 76-s). This produced a 3.8 MHz pulse train at wavelengths in the range of 610-680nm. The detection system consists of a 0.22m subtractive dispersion double

monochromator (Spex 1680), microchannel plate PMT (Hamamatsu R3809U), 1-GHz Amplifier and Timing discriminator (EG&G Ortec 9327), time-to-amplitude converter (Tennelec TC864), and a multichannel pulse-to-height analyser (Tennelec PCA II card).

Before the time resolved spectroscopy measurement, steady state measurements were carried out to study emission and absorption spectra in a glass forming solvent as described earlier in order to select the excitation and detection wavelengths. A solution was prepared for the time resolved spectroscopy with an optical density under 0.5. The sample solution in a cuvette was placed inside the cryostat. The temperature of the cryostat was controlled with an Oxford Instrument temperature controller. Time resolved spectroscopy using the single photon counting technique was carried out at room temperature, 200K, 125K and 80K.

## 4.3 Results and Discussion

The luminescence properties of three compounds (MORPIP, Si and AMINO), shown in Fig.4.4, were investigated.

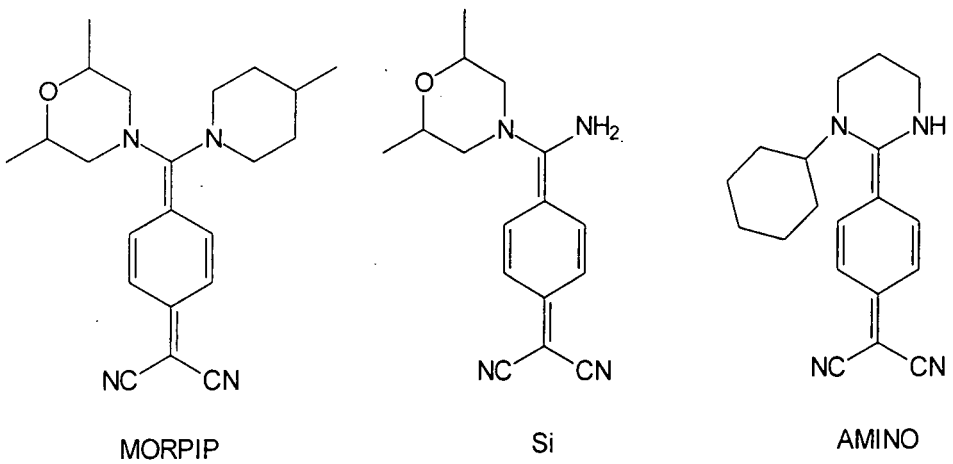


MORPIP Si AMINO

Figure 4.4 The compounds investigated in the luminescence study

### 4.3.1 Fluorescence in solutions

The fluorescence properties in various alcohols as a function of viscosity and polarity were investigated [11-14,24].

**(a) MORPIP**

The MORPIP solutions in normal alcohols (from methanol to hexanol), diethylene glycol and glycerol (8 solutions) were prepared for the measurements of emission spectra. The viscosity of the solvent can be controlled by the increase of a number of hydroxyl groups that leads to the enhancement of the hydrogen bonding network in the medium (diethylene glycol and glycerol) [11-14,24]. The polarity of solvent also can be changed by the extension of the molecular lengths (normal alcohols).

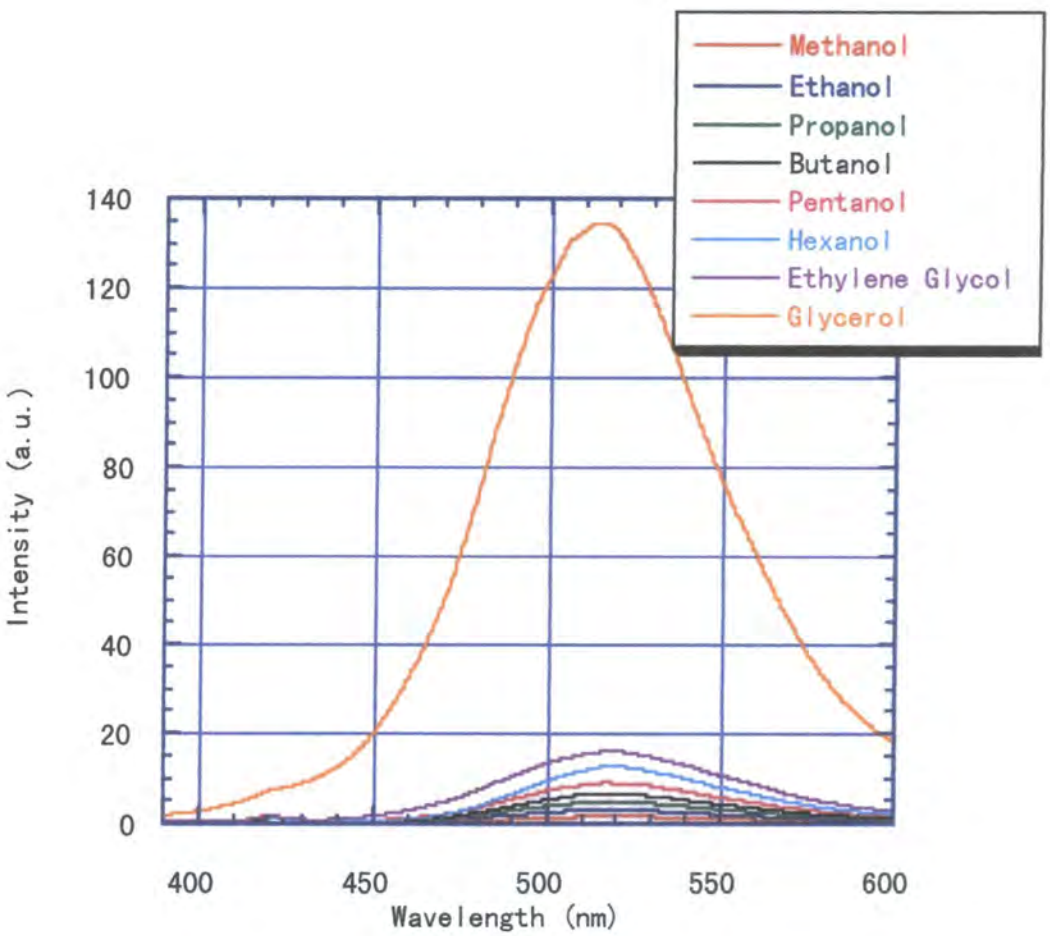


Figure 4.5 Emission spectra of MORPIP in various alcohols

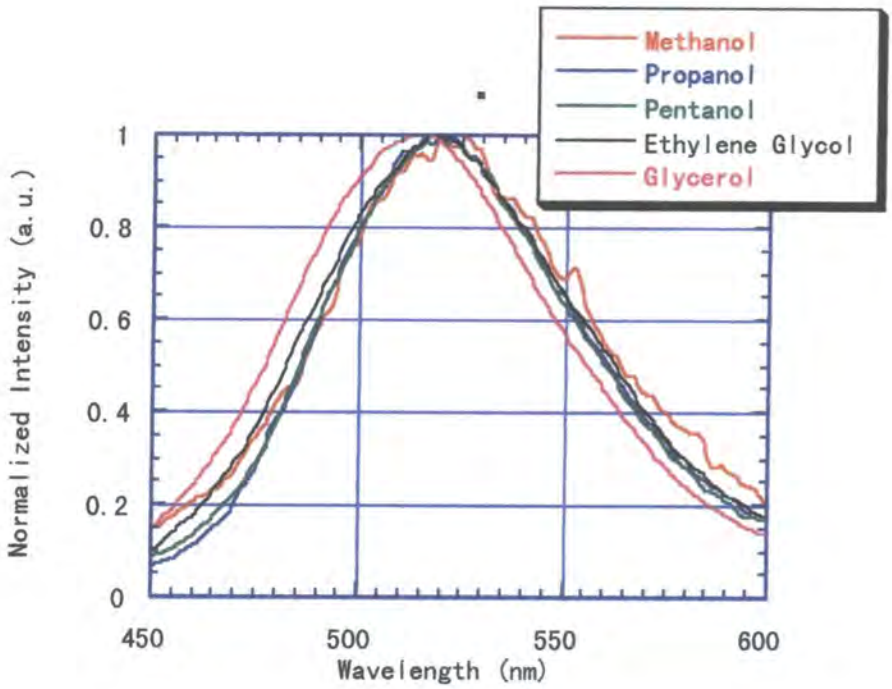


Figure 4.6 Emission spectra against normalized intensity in various alcohols

All of the solutions were excited at 375nm, and the results of emissions are shown in Fig.4.5. The normalized emission spectra are also shown in Fig.4.6. The quantum yields were obtained from the quantitative analysis, and shown in Table 4.2. As shown in Fig.4.5, intensities increased from methanol to glycerol. The intensity of emission from the solution of quinine sulphate dihydrate in 0.5M sulphuric acid was used as a reference comparing with those of emission spectra from MORPIP solutions. The emission from methanol solution was very weak so the spectra became noisy as shown in Fig.4.6.

Stokes shifts and quantum yields of MORPIP are shown in Table 4.2. In eq.4.17, the change of Stokes shift is influenced by the two factors, the solvent polarity and the change between the excited and ground state dipole moments. As shown in Fig.4.7, Stokes shifts in various alcohols was plotted as a function of the polarity parameter, $\Delta f$.

Table 4.2 Stokes shifts and quantum yields of MORPIP in alcohols

| | Stokes shift ($cm^{-1}$) | Quantum yield (%) | $\Delta f$ | Viscosity (nP) |
|---|---|---|---|---|
| Methanol | 5160[a] | 0.13[b] | 0.309[c] | 0.544 |
| Ethanol | 4620 | 0.14 | 0.290 | 1.07 |
| 1-Propanol | 4240 | 0.37 | 0.275 | 1.95 |
| 1-Butanol | 4150 | 0.49 | 0.264 | 2.54 |
| 1-Pentanol | 3970 | 0.71 | 0.254 | 3.62 |
| 1-hexanol | 4010 | 0.97 | 0.243 | 4.58 |
| Diethylene Glycol | 5040 | 1.38 | 0.266 | 30.2 |
| Glycerol | 5400 | 11.84 | 0.265 | 934 |

a: the experimental error of Stokes shift ($\pm 40 cm^{-1}$), b: the experimental error of quantum yield (10%)

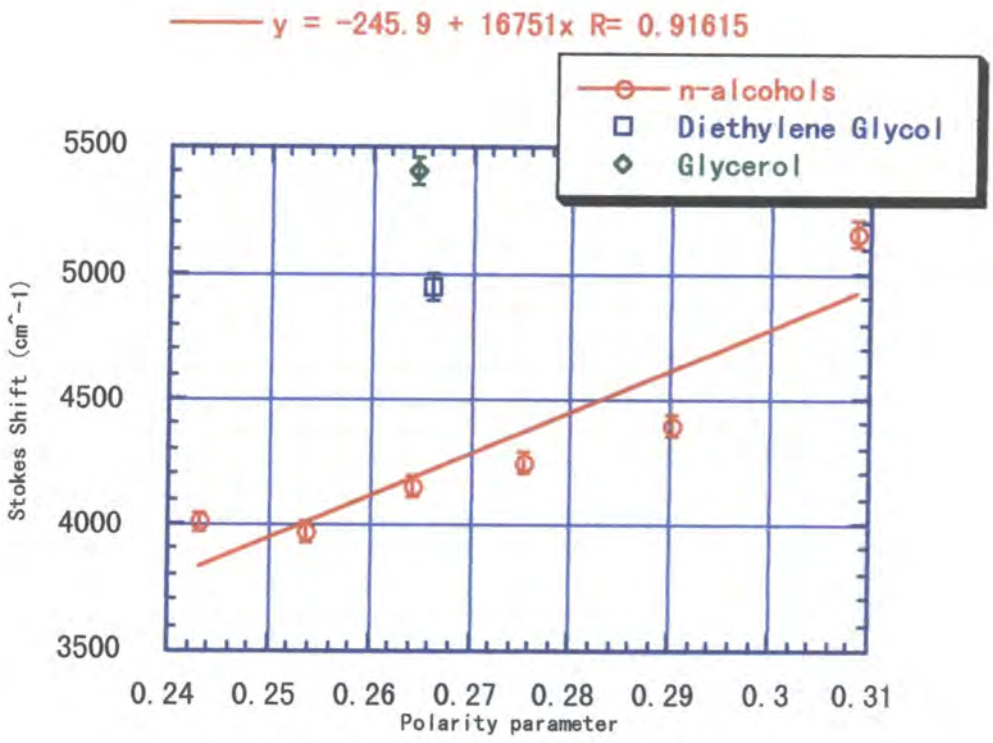


Figure 4.7 Stokes shift for MORPIP against the polarity parameter ($\Delta f$)

Stokes shifts in normal alcohols are proportional to the solvent polarity, $\Delta f$, as shown in Fig.4.7. In 3.3.5, molecular dipole moments (i.e. the ground state dipole moment) in solutions (chloroform, dichloromethane, and acetone) were found to be of a similar order (around 15D) as a function of solvent polarity. Therefore the change of the dipole moments between the excited and the ground states is approximately the same in normal alcohols (low viscosity solvents) because of eq.4.17.

The Stokes shifts in diethylene glycol and glycerol did not fit as a function of the polarity parameter considered here as shown in Fig.4.7. Both of them have two or three dimensional hydrogen bonding networks. These hydrogen bonding networks give rise to the viscosity of the medium. Therefore the diethylene glycol ($\Delta f$=0.266) and glycerol ($\Delta f$=0.265) solutions have almost the same polarity as the butanol solution ($\Delta f$=0.264), but both of them show larger Stokes shift than the butanol solution due to the different viscosity (different hydrogen bonding networks) (30.2nP for Diethylene Glycol and 934nP for Glycerol). However, the $E_T(30)$ parameter provides a good fit for the Stokes shift of MORPIP in all solutions considered here, as shown in Fig.4.8. This is because the $E_T(30)$ parameter is a microscopic polarity parameter taking into account the solute and solvent interactions [50].

Quantum yields in normal alcohols from methanol to hexanol as a function of the solvent polarity parameter ($\Delta f$) have an excellent fit, but the quantum yields of diethylene glycol and glycerol do not fit this parameter as shown in Fig.4.9.

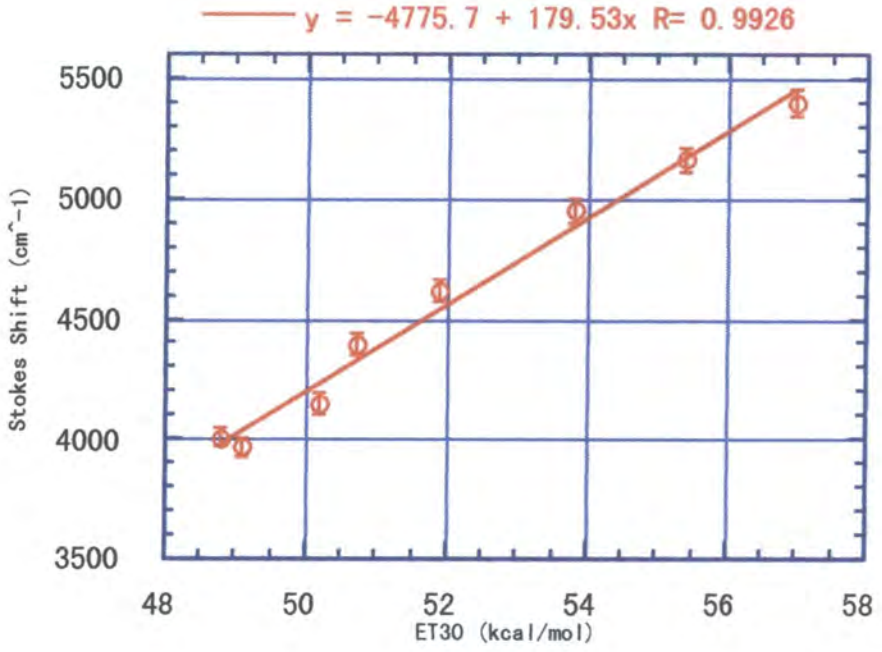


Figure 4.8 Stokes shift for MORPIP against $E_T(30)$ parameter

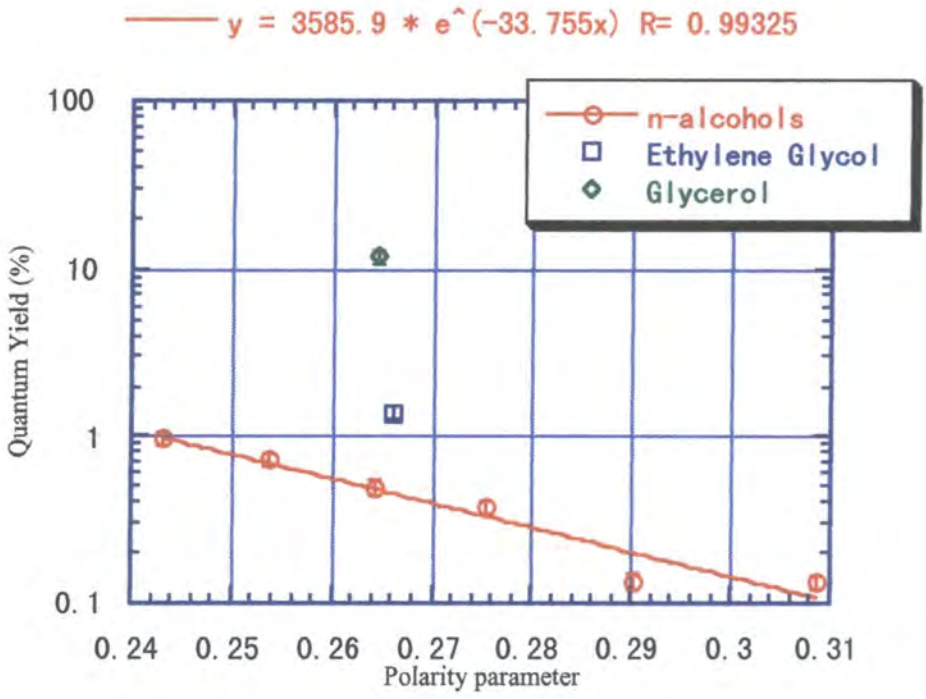


Figure 4.9 Quantum yield of MORPIP against the polarity parameter ($\Delta f$)

For the low viscosity alcohols the quantum yield follows the polarity (solvent density) parameter ($\Delta f$). The solution of diethylene glycol ($\Delta f$=0.266) has almost the same polarity (solvent density) as 1-butanol ($\Delta f$=0.264), but the quantum yield of the diethylene glycol solution is one magnitude larger than that of the butanol solution because of the constraining effect [21,24,29,51,52]. The viscosity of the diethylene glycol solution (30.2nP) is also one magnitude larger than that of the butanol solution (2.54nP). The quantum yield of the glycerol solution (11.8%) is far higher than that of the butanol solution (0.49%), although both of them also have the same solvent density parameter ($\Delta f$=0.264). This is also attributed to the constraining effect of the viscous solution [21,24,29,51,52].

The quantum yield in glycerol was very large (11.8%) whilst quantum yield in methanol was very small (0.13%). For further investigations of the constraining effect on luminescence properties, glass-forming solvents at low temperature were employed.

**(b) Si**

Quantum yield measurements of Si in various solutions were carried out. All emission spectra were obtained the same method as the previous MORPIP measurements. All samples were excited at 375nm. The intensities of emission increased from methanol to glycerol, as the quantum yields increased.
Quantum yields and Stokes shifts of solutions were obtained and shown in Table 4.3.

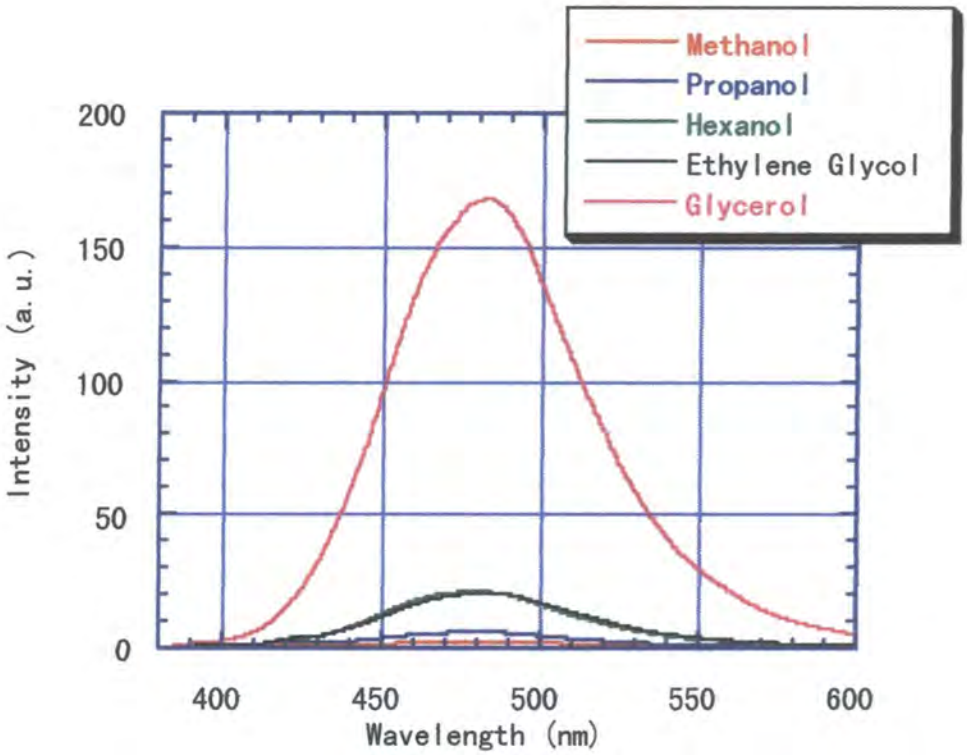


Figure 4.10 Emission spectra of Si in various alcohols

Table 4.3 Quantum yields and Stokes shifts of Si in various alcohols

| | Stokes Shift ($cm^{-1}$) | Quantum yield (%) |
|---|---|---|
| Methanol | 5810[a] | 0.16[b] |
| Ethanol | 5230 | - |
| 1-Propanol | 5050 | 0.4 |
| 1-Butanol | 4680 | - |
| 1-Pentanol | 4660 | 1.4 |
| 1-Hexanol | 4440 | - |
| Diethylene Glycol | 5570 | 1.5 |
| Glycerol | 6060 | 12.4 |

a: the experimental error of Stokes shift (±40 $cm^{-1}$), b: the experimental error of quantum yield (10% of the value)

The Stokes shifts in normal alcohols is proportional to the solvent polarity ($\Delta f$). However the constraining effect was found as shown in Fig.4.11. This trend is very similar to the case of MORPIP. This is not very surprising due to the structural similarity, although emissions of Si were around 480nm (blue emission) and these of MORPIP were around 520nm (green emission).

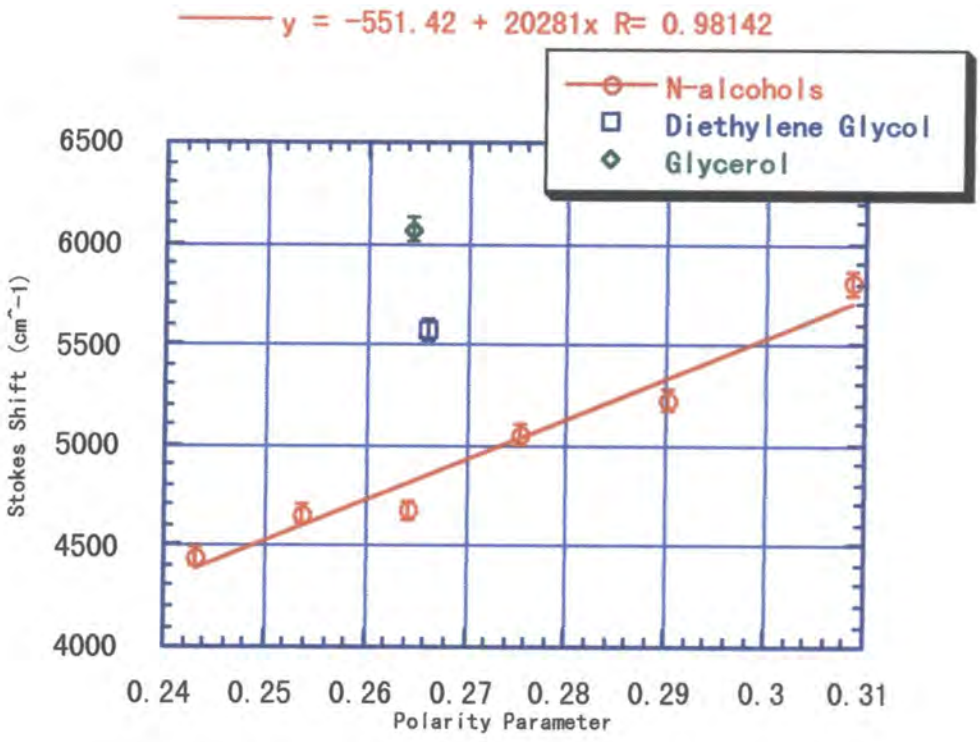


Figure 4.11 Stokes Shift on Si in various alcohols

The $E_T(30)$ parameter provides a good fit for the Stokes shift of Si as shown in Fig.4.12. Quantum yields of Si in normal alcohols from methanol to hexanol as a function of the solvent polarity parameter ($\Delta f$) have an excellent fit, but the quantum yields of diethylene glycol and glycerol do not fit this parameter as shown in Fig.4.13.

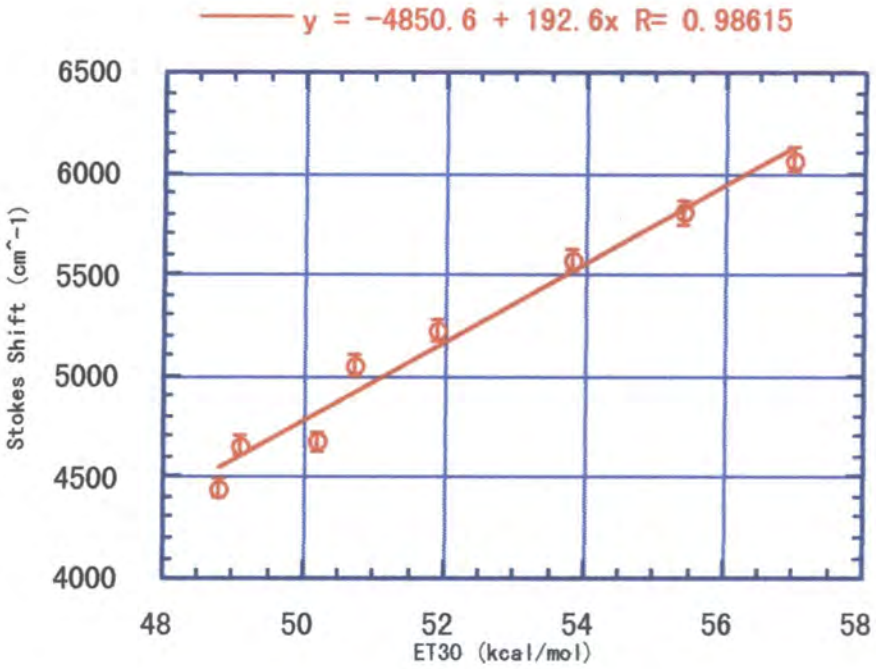


Figure 4.12 Stokes Shift against $E_T(30)$ for Si

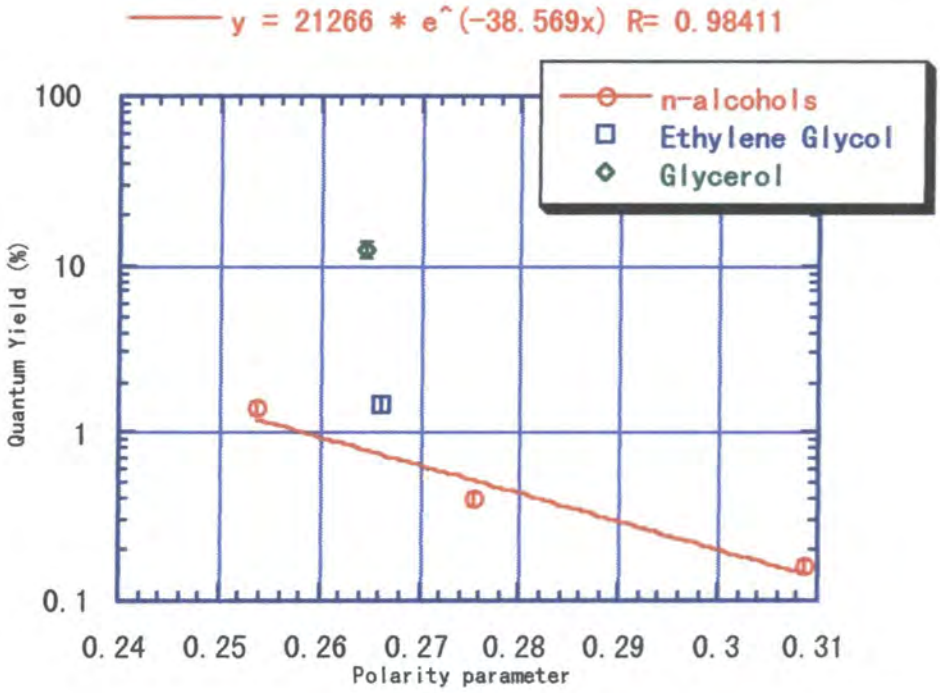


Figure 4.13 Quantum yields of Si against polarity parameter

**(C) AMINO**

Absorption maxima of AMINO were around 350nm, and emission maxima were around 480nm. This compound had the largest Stokes shift among the three compounds studied. Emission spectra of AMINO in various alcohols are shown in Fig.4.14, and the quantum yields and Stokes shifts of solutions of AMINO were obtained and shown in Table 4.4.

Table 4.4 Quantum yield and Stokes shift of AMINO in various alcohols

| | Stokes shift ($cm^{-1}$) | Quantum Yield (%) |
|---|---|---|
| Methanol | 7380[a] | 0.22[b] |
| Ethanol | 6770 | - |
| 1-Propanol | 6500 | 0.53 |
| 1-Butanol | 6160 | - |
| 1-Pentanol | 6010 | 1.3 |
| 1-Hexanol | 5670 | - |
| Diethylene Glycol | 7990 | 2.32 |
| Glycerol | 6630 | 21.76 |

a: the experimental error (±40 $cm^{-1}$), b: the experimetal error (10% of the values)

All three compounds studied here have the same trend in terms of quantum yields against the solvent density. Under the circumstance of low viscosity quantum yields follow the solvent density parameter ($\Delta f$). For the high viscosity solutions such as glycerol there is no correlation between the solvent polarity parameter and quantum yields, as a result of the constraining effect the viscous solvent [21,24,29,51,52]. These experiments show that the radiative decay process (the quantum yield) is

influenced by the solvent polarity and the hydrogen bonding. The Stokes shift for AMINO was slightly different from the others. The Stokes shift in diethylene glycol was higher than in glycerol.

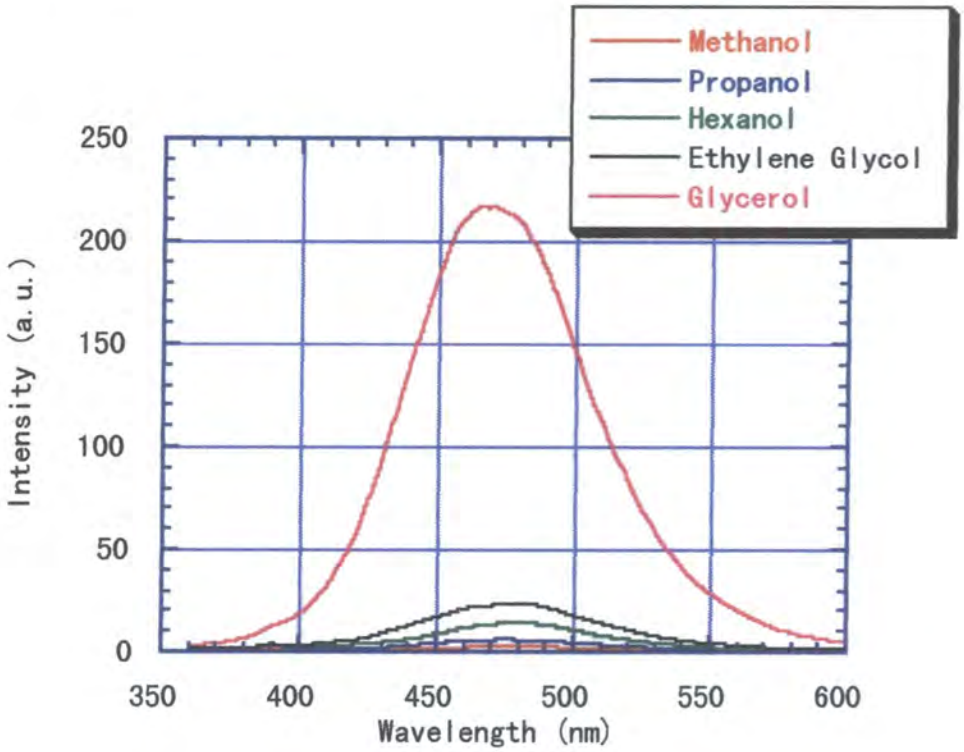


Figure 4.14 Emission spectra of AMINO in various alcohols

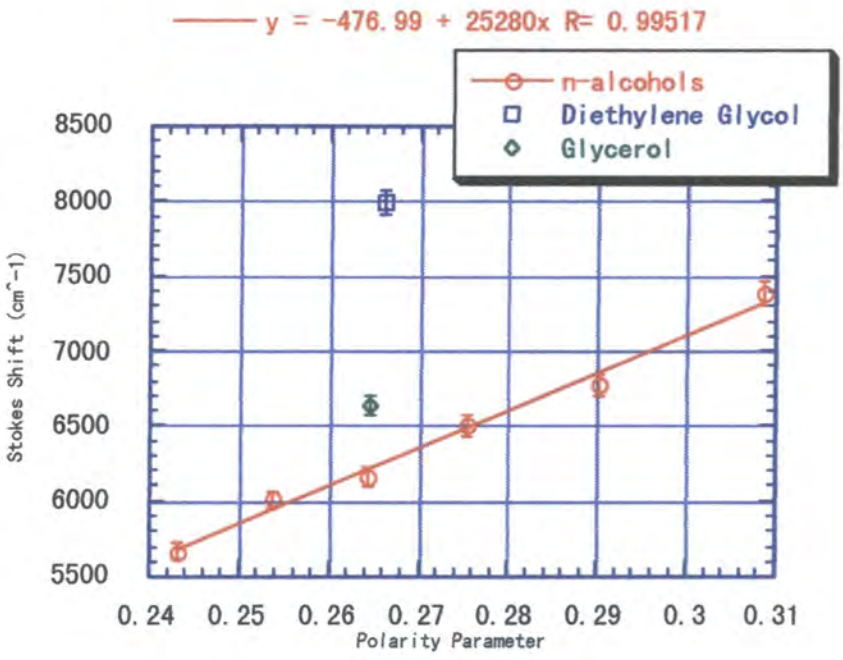


Figure 4.15 Stokes Shift for AMINO for various alcohols

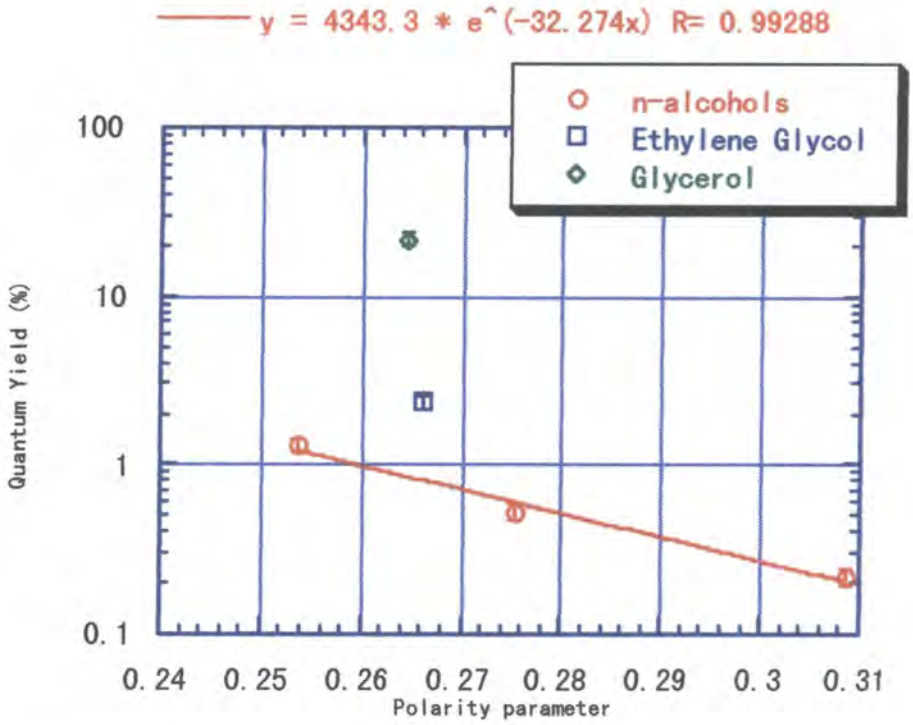


Figure 4.16 Quantum yield of AMINO against polarity parameter

## 4.3.2 Fluorescence in glass-forming solvents

Additional information can be gained by the study of fluorescence in glass at low temperature. Glass-forming solvents give a glassy medium at low temperature such as 80 K [3,4,21-23,51-59]. The constraining effect gives rise to the enhancement of intensity of emission in solution. It can be observed in the glassy medium at low temperature. The comparison of the emission intensities between in glass and in solution can provide more detailed information of the constraining effect.

### 4.3.2.1 MORPIP

**(a) EPA**

The solvent mixture (Ether/Ethanol/Isopentane=2:2:5), EPA, was prepared to give a nice glassy medium [58]. The cryostat was cooled by liquid nitrogen without

temperature control, so all spectra were taken at either room temperature or low temperature. There are large shifts between room temperature and low temperature (the glassy state) of both the emission and absorption spectra. These shifts are carefully compared in terms of energies. The absorption maximum at room temperature was at 22,500 $cm^{-1}$ (445nm). At low temperature it was at 25,100 $cm^{-1}$ (399nm). The emission maximum at room temperature was 19,530 $cm^{-1}$ (512nm). At low temperature it was at 22,520 $cm^{-1}$ (444nm). The shift of the absorption maximum between room temperature and low temperature was 2600 $cm^{-1}$. The shift of the emission maximum was 2990 $cm^{-1}$. Therefore, the shifts of both emission and absorption spectra were almost the same between at low and room temperatures. These shifts can be attributed to a solvatochromic shift, i.e. due to the density change of the medium.

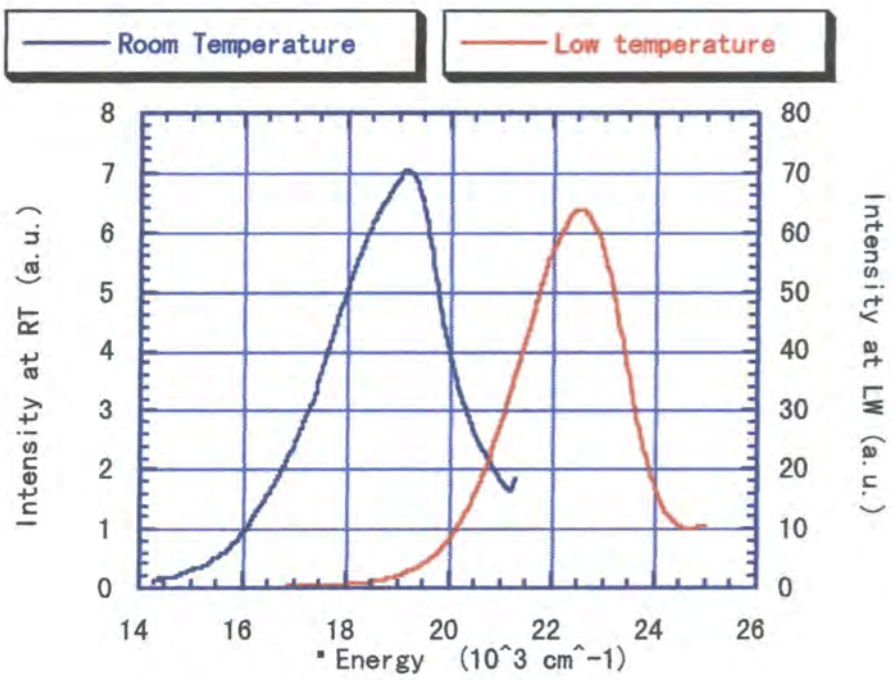


Figure 4.17 Emission spectra of MORPIP in EPA

As shown in Fig.4.17, the values of intensity between low temperature (the glassy state) and room temperature (the liquid state) were significantly different. The maximum value of the intensity at room temperature was around 8, but that of the intensity at low temperature was around 70. The intensity of emission is directly related to the quantum yield in eq.4.19. Therefore, this experimental result implies that the quantum yield in the solid state (the glassy state) is much higher than in the liquid.

**(b) 2-methyl tetrahydrofuran (2-methyl THF)**

2-methyl THF is a glass forming solvent [54,59]. EPA forms a nice glassy medium, but the three solvents, which make it up can evaporate during the course of the experiment changing the ratio (2:2:5) slightly. The use of a single solvent such as 2-methyl THF is a more accurate way to carry out the low temperature study. Absorption spectra of MORPIP in 2-methyl THF are shown in Fig.4.18.

The maximum of the absorption spectrum at 294K and 80K was at 21,400 $cm^{-1}$ (467nm) and at 22,700 $cm^{-1}$ (441nm), respectively. Therefore the shift of absorption maximum between the temperatures was 1300 $cm^{-1}$. The maximum of the emission spectrum at 294K and 80K was at 18,300 $cm^{-1}$ (546nm), and at 19,200 $cm^{-1}$ (520nm), respectively. The shift of emission maximum was 900 $cm^{-1}$. Therefore, the shifts of both emission and absorption spectra are almost the same between 80K and 294K. These shifts can be attributed due to a solvatochromic shift, i.e. due to the density change of the medium

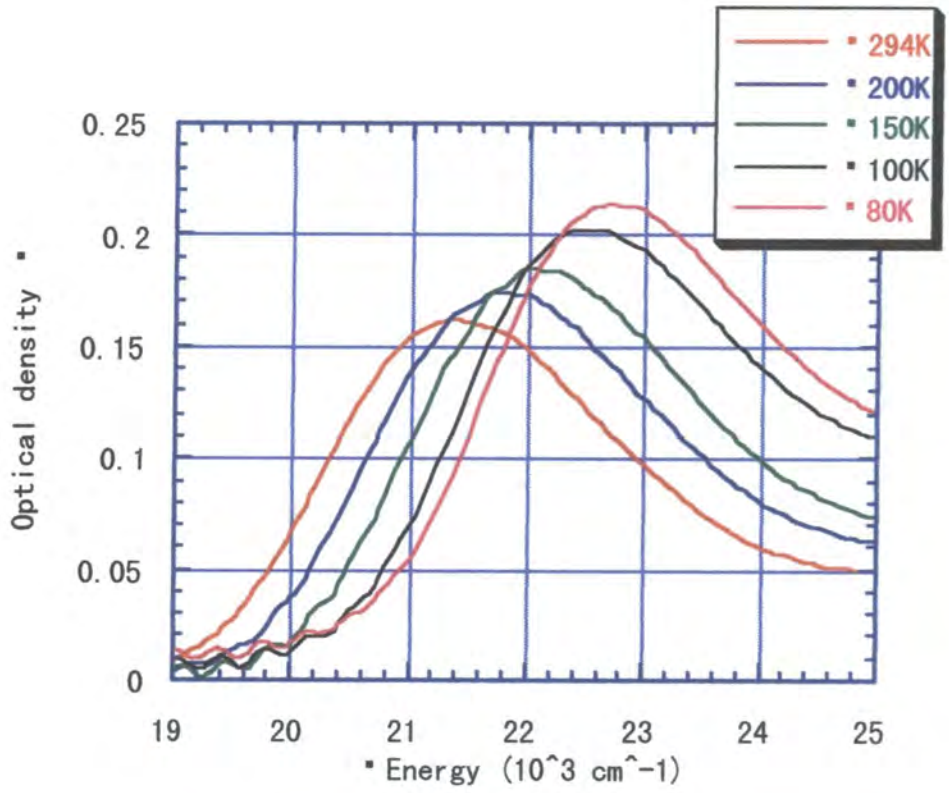


Figure 4.18 Absorption spectra of MORPIP in 2-methyl THF

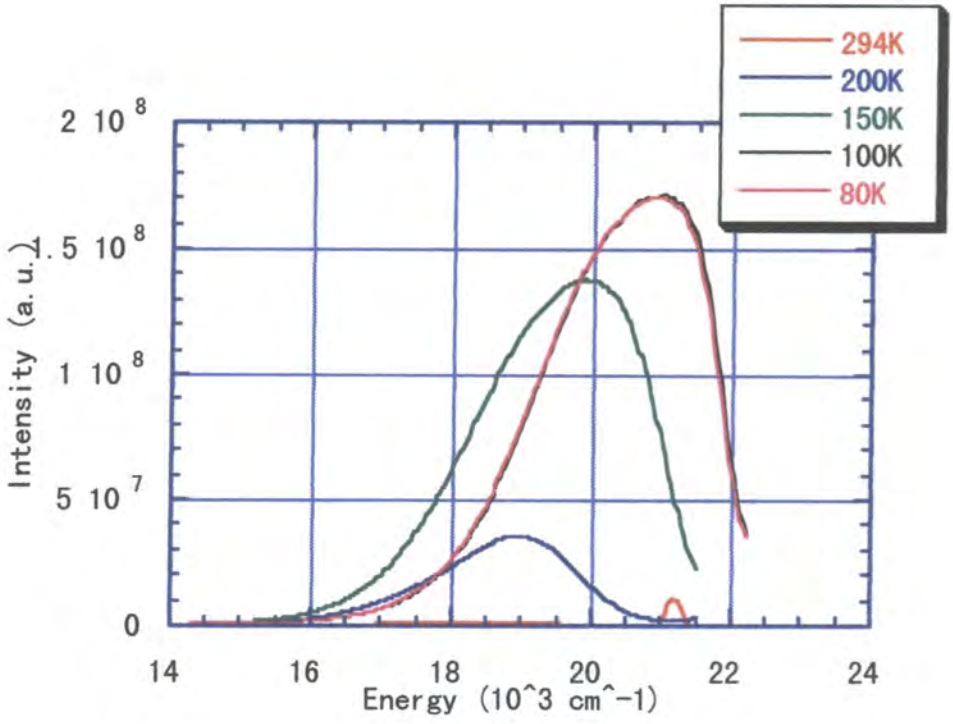


Figure 4.19 Emission spectra of MORPIP in 2-methyl THF

Emission spectra of MORPIP in 2-methyl THF at various temperatures are shown in Fig.4.19. Very weak emission was observed at 294K, but as the temperature decreased, stronger emission was observed. The formation of the glassy medium occurs below 200K, and is completed between 150K and 100K, as reflected in the increase of emission intensity as shown in Fig.4.19. The observed intensity of emission in the solid state (the glassy state) was higher than that of emission in the liquid state.

**c) 1-Propanol**

Some normal alcohols form a glass such as 1-propanol [3,4,17,58]. Absorption and emission spectra of MORPIP in 1-propanol are presented in Fig.4.20, and Fig.4.21., respectively.

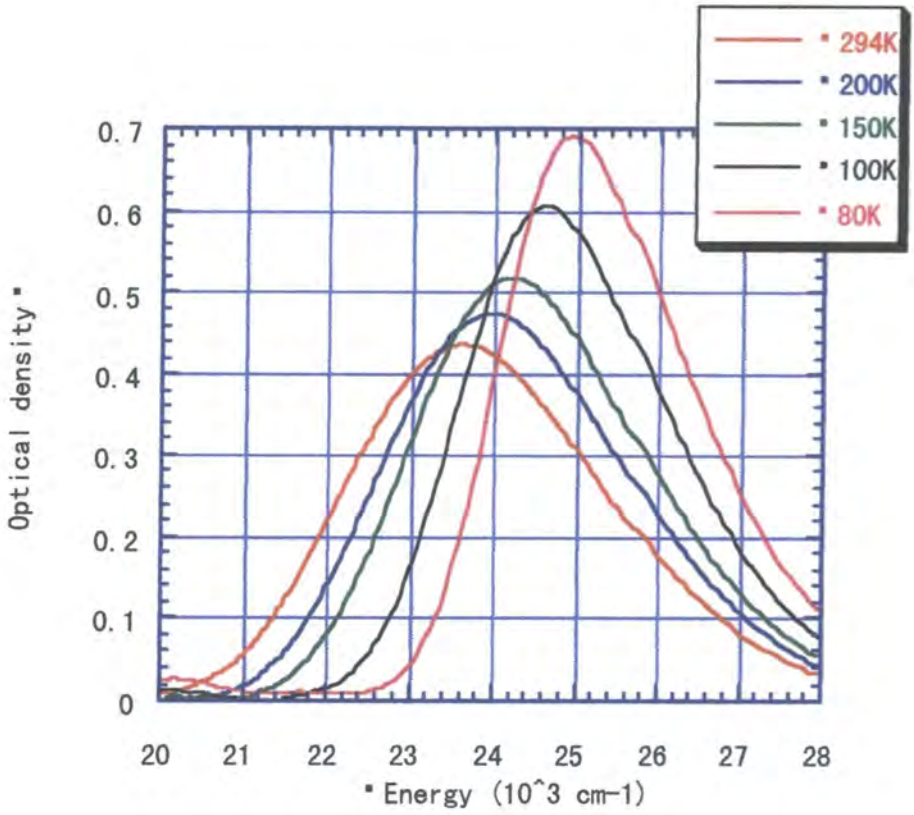


Figure 4.20 Absorption spectra of MORPIP in 1-propanol at various temperatures

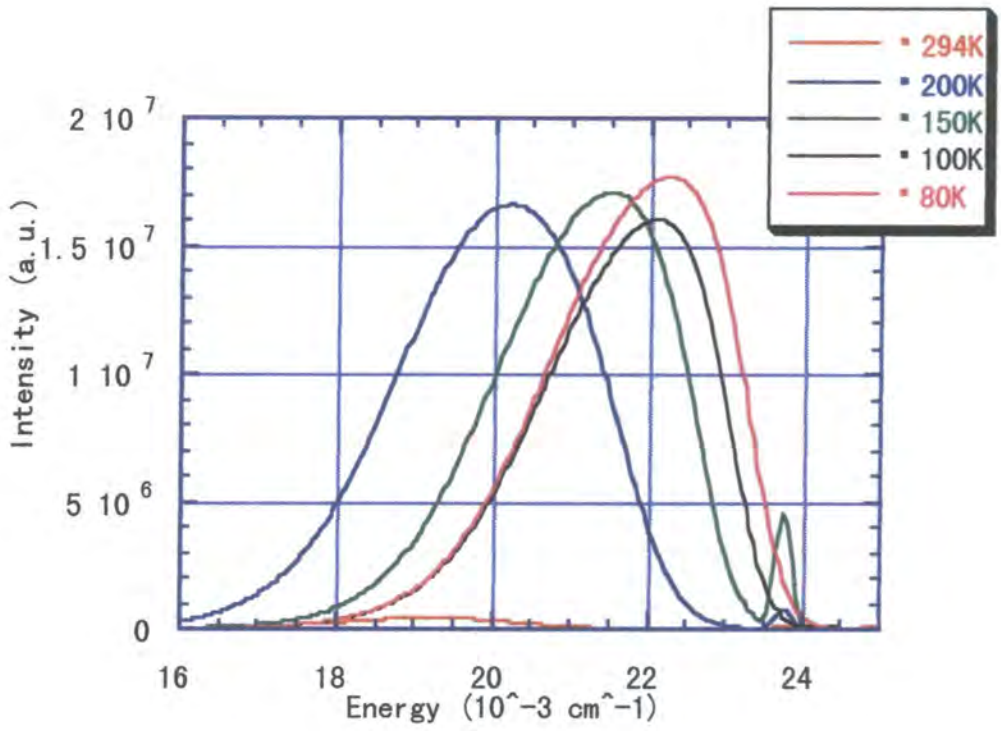


Figure 4.21 Emission spectra of MORPIP in 1-propanol at various temperatures

As shown in Fig.4.20, the absorption spectra became sharper at low temperature. The maxima of the absorption spectra at 294K and 80K were 23,600 $cm^{-1}$ (424nm) and 24,900 $cm^{-1}$ (401nm), respectively. Therefore the shift of absorption maxima between the temperatures was 1300 $cm^{-1}$. The maximum of the emission spectra at 294K and 80K were 19,200 $cm^{-1}$ (520nm), and 22,000 $cm^{-1}$ (450nm), respectively. The shift of the emission maximum was 3000 $cm^{-1}$. There was a large shift of emission compared with that of absorption. Therefore the Stokes shift changed from 4400 $cm^{-1}$ at room temperature to 2715 $cm^{-1}$ at 80K. The change of the Stokes shifts between low and room temperature can be attributed not only to solvatochromic shift, but also the enhancement of the hydrogen bonding network in the solvent as it was cooled down. The estimated quantum yield at 80K is 13% relative to the measured quantum yield at

room temperature. The estimated value is not very precise because the change of the refractive index is not taken into account.

**(d) Summary of data of MORPIP on the low temperature study**

Table 4.5 Summary

| | Absorption Maxima ($cm^{-1}$) | Emission Maxima ($cm^{-1}$) | Absorption Shift($cm^{-1}$) | Emission Shift ($cm^{-1}$) | Stokes Shift ($cm^{-1}$) |
|---|---|---|---|---|---|
| EPA | 22500[a] (RT) | 19530[b] (RT) | | | 3000[e] (RT) |
| | 25100 (LT) | 22570 (LT) | 2600[c] | 2990[d] | 2600 (LT) |
| 2-methyl | 21400[a] (RT)[f] | 18300[a] (RT) | | | 3100 (RT) |
| THF | 22700 (LT)[g] | 19200 (LT) | 1300 | 900 | 3500 (LT) |
| 1 Propanol | 23600[a] (RT)[f] | 19200[a] (RT) | | | 4400 (RT) |
| | 24900 (LT)[g] | 22000 (LT) | 1300 | 3000 | 2900 (LT) |

a: accuracy ±50 $cm^{-1}$, b: accuracy ±20 $cm^{-1}$, c: accuracy ±100 $cm^{-1}$, d: accuracy ±40 $cm^{-1}$, e: accuracy ±70 $cm^{-1}$, f: at 294K, g: at 80K

### 4.3.2.2 Si and AMINO

Since both Si and AMINO had very similar trends, the data for both are presented together in Table 4.6.

All intensities of the glassy state (the solid state) at low temperatures were one magnitude higher than in the liquid state at room temperature due to the constraining effect [21,24,29,51,52].

Table 4.6 Summary of data of Si and AMINO on the low temperature study

| | Absorption maxima ($cm^{-1}$,nm) | Emission maxima ($cm^{-1}$,nm) | Absorption shift ($cm^{-1}$) | Emission shift ($cm^{-1}$) | Stokes shift ($cm^{-1}$) |
|---|---|---|---|---|---|
| Si EPA | 26,600[a] (RT) | 24,130[b] (RT) | | | 2475[e] (RT) |
| | 27,000 (LT) | 23,640 (LT) | 400[d] | 484[d] | 3313 (LT) |
| Si | 25,900[a](RT)[f] | 21,000[a] (RT) | | | 4898[c] (RT) |
| 1-Propanol | 26,200 (LT) | 23100 (LT)[g] | 300[c] | 2113[c] | 3125 (LT) |
| Amino EPA | 27,030[a] (RT) | 24,070 (RT) | | | 2960[e] (RT) |
| | 28,250 (LT) | 24,420 (LT) | 1222[d] | 350[d] | 3829 (RT) |

a: accuracy ±50 $cm^{-1}$, b: accuracy ±20 $cm^{-1}$, c: accuracy ±100 $cm^{-1}$, d: accuracy ±40 $cm^{-1}$, e: accuracy ±70 $cm^{-1}$, f: at 294K, g: at 80K

## 4.3.3 Fluorescence in solid media

### 4.3.3.1 Polymeric films prepared from different solvents

**(a) MORPIP**

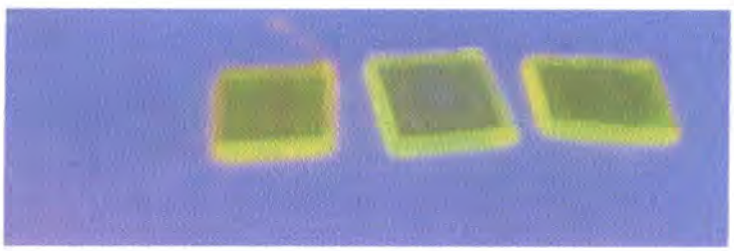

Glass DMF Cyclohexanone TMU

Figure 4.22 MORPIP doped PMMA films from different spin coating solvents under UV light

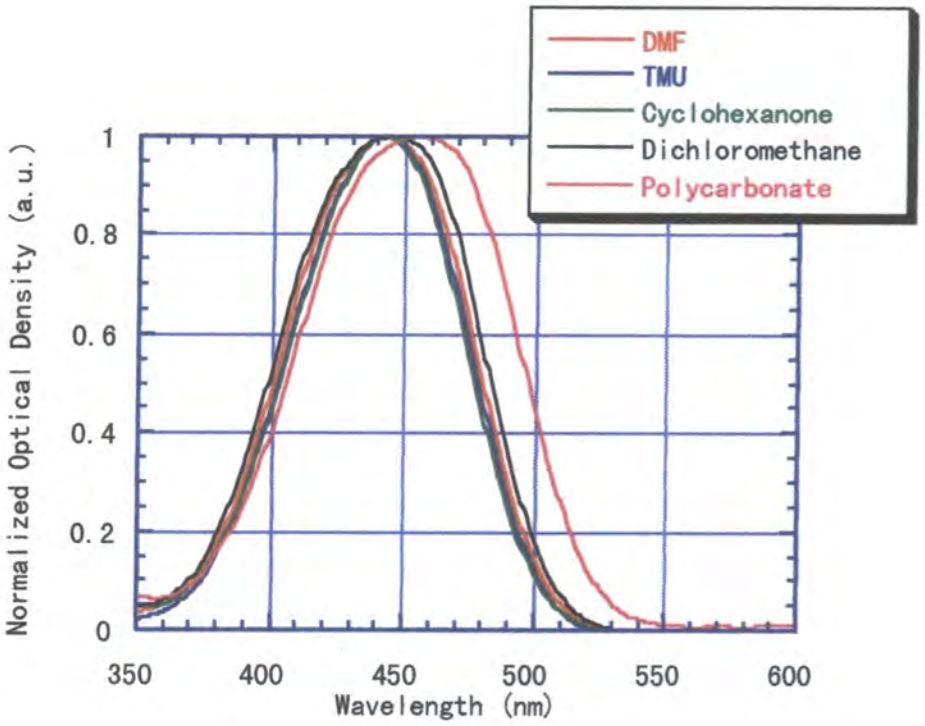


Figure 4.23 Absorption spectra of the polymeric films (MORPIP) from different solvents

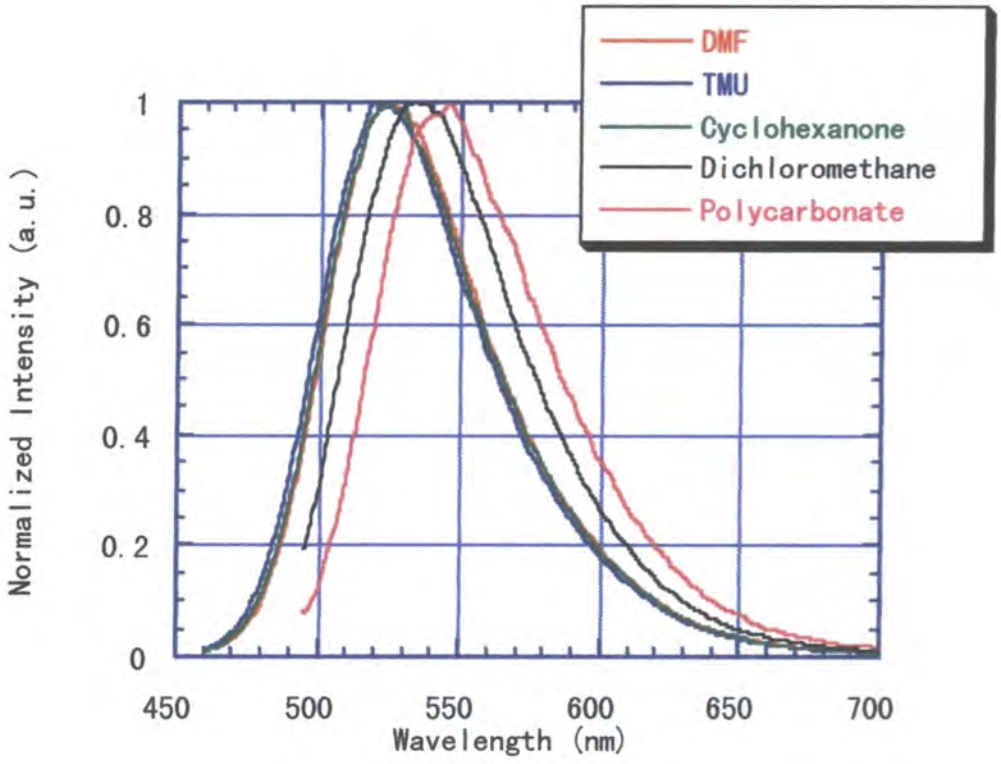


Figure 4.24 Emission spectra of polymeric films (MORPIP) from different solvents

Table 4.7 Quantum yield and Stokes shift on MORPIP doped polymeric films

| Casting Solvent | Absorption Maxima ($cm^{-1}$,nm) | Emission Maxima ($cm^{-1}$,nm) | Stokes shift ($cm^{-1}$) | Quantum Yield (%) |
|---|---|---|---|---|
| DMF | 22,620[d] (442.0)[e] | 19,100[d] (523.5)[e] | 3520[f] | 38[g] |
| TMU | 22,570 (443.1) | 19,250 (519.5) | 3320 | 32 |
| Cyclohexanone | 22,520 (443.9) | 19,100 (523.5) | 3420 | 28 |
| Cyclohexanone[a] | 22,570 (442.8) | 18,640 (536.5) | 3930 | 27 |
| Cyclohexanone[b] | 22,570 (443.0) | 18,740 (533.5) | 3830 | 22 |
| Dichloromethane | 22,420 (446.0) | 18,760 (533.5) | 3660 | 25 |
| Dichloromethane[c] | 21,930 (455.6) | 18,330 (545.5) | 3600 | 15 |

a: calix[6]arene (2% wt/wt) was added to a cyclohexanone solution. b: calix[6]arene (7% wt/wt) was added to a cyclohexanone solution. c:polycarbonate was dissolved into a dichloromethane solution. d: accuracy (±20 $cm^{-1}$), e: (nm) accuracy (±1nm), f: accuracy (±40nm), g: experimental error, ±3%.

Chromophores can be incorporated into polymeric media by either dip coating or spin coating [60-62]. The solvents used for both coating methods were an important factor, because the intensities of the films were different as observed by eye, as shown in Fig.4.22. The quantum yield of each film was obtained in an integrating sphere [27].

The four casting solvents, DMF, TMU, cyclohexanone, dichloromethane, were used to prepare MORPIP doped PMMA films, and dichloromethane was used to prepare MORPIP doped poylcarbonate. Doping levels of MORPIP in the polymer

matrix were chosen to be under 1% (around 0.8%) in order to reduce the possibility of aggregation. The absorption and emission spectra of the doped polycarbonate film were different from similarly doped PMMA films as shown in Fig.4.23, and 4.24. This is because MORPIP exists in the different environments. The quantum yield of the PMMA films is higher than that of the polycarbonate films. This may be due to the different "free volume" in the PMMA and the polycarbonate matrices [60]. The free volume of the PMMA films is smaller than that of the polycarbonate films, because the side chains of PMMA fill up the free volume in the PMMA matrix around the main chains. Therefore the molecular mobility of MORPIP in the PMMA matrix is more constrained than in the polycarbonate matrix [60]. Consequently, the quantum yield in the PMMA films is higher than in polycarbonate films due to the constraining effect from the smaller free volume in the PMMA medium.

There were only small shifts in absorption and emission spectra for the PMMA films prepared from TMU, DMF, and cyclohexanone solutions. However, the Stokes shift for the PMMA films prepared from the dichloromethane solution was larger than that of the PMMA films prepared from TMU, DMF, and cyclohexanone, and a red shift of the emission spectrum for the PMMA films prepared from dichloromethane solution was found (~10nm). Hence the PMMA films prepared from dichloromethane provide different local environments from other PMMA films. This is also confirmed by the result of the quantum yield measurements. The quantum yield of the PMMA films prepared from DMF solution (38%) was much higher than that of the PMMA films prepared from dichloromethane solution (25%). Hence different casting solvents can create different environments in the PMMA matrices. Quantum yields of the PMMA films prepared from different casting solvents are plotted against the polarity of casting solvents as shown in Fig.4.25.

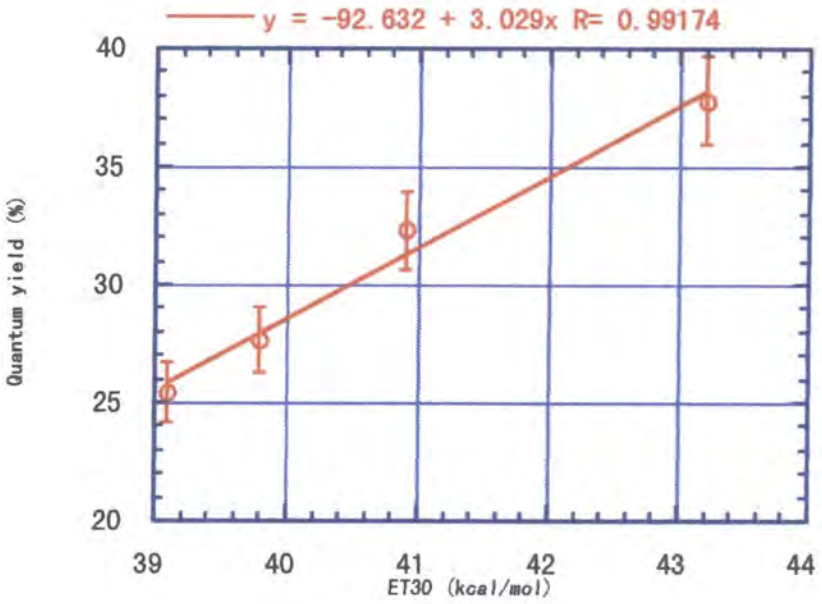


Figure 4.25 Quantum yields of MORPIP films prepared from different casting solvents against the polarity of the casting solvents

The possible reasons for the different local environments in the different films is the association among the doped molecules (MORPIP), differences in the polymer matrix, and solvent molecules remaining in the medium. The inclusion of solvent molecules changes the density of the medium, which leads to the change of the free volume of the medium, as the casting solutions have different polarity, dielectric constants, and refractive indices, i.e. different density. Calix[6]arene is known as a large and non-polar molecule [63]. The PMMA films were prepared from cyclohexanone solutions at two different doping levels of calix[6]arene. As the doping level of calix[6]arene was increased, the decrease of the quantum yields of the films was observed (doping level-QY: 0% - 28%, 2% -27%, 7% - 22%). This experimental observation supports the hypothesis that the changes in quantum yield for polymer matrices is due to the presence of the residual solvent in the film.

Lastly, laser desorption mass spectroscopy on these MORPIP doped PMMA films was carried out to confirm the inclusion of solvent molecules, but the molecular weights of used solvents such as DMF (73) or MORPIP (364) were too small to detect, because this spectroscopy was designed for the determination of molecular weight of polymers (at least more than 1000), not for those small solvent and dye molecules. Hence conclusive results in support of the presence of solvent in the films were not obtained from the laser desorption mass spectroscopy.

**(b) Si and AMINO**

AMINO and Si were also doped into a PMMA matrix. Quantum yields of the doped PMMA films were obtained, and are summarized below. A similar trend on the change of quantum yields of those compounds as MORPIP was found.

Table 5.8 Quantum yields of Si and AMINO doped films

| | Absorption Maxima | Emission Maxima | Stokes Shift ($cm^{-1}$) | Quantum Yield (%) |
|---|---|---|---|---|
| Si DMF | 25,480[a] (392.5)[b] | 20,550[a] (486.5)[b] | 4930[c] | 32[d] |
| Si TMU | 25,720 (388.8) | 21,050 (475.0) | 4670 | 23 |
| AMINO DMF | 26,950 (371.1) | 21,210 (471.5) | 5740 | 19 |
| AMINO TMU | 26,980 (370.7) | 21,340 (469.5) | 5640 | 7.2 |

a: ($cm^{-1}$) accuracy (±20 $cm^{-1}$), b: (nm) accuracy (±1 nm), c: accuracy (±40 $cm^{-1}$), d: 3% of the values.

#### 4.3.3.2 Emissions from the crystalline state

Very strong emissions were observed by eye from MORPIP powders crystallized above the acetonitrile solution as shown in Fig.4.26.

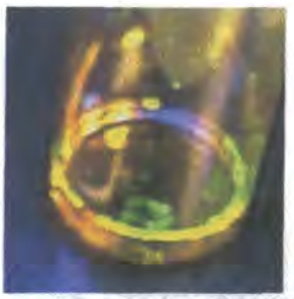

Figure 4.26 Emissions from the powder of MORPIP under UV light

Table 4.9 Quantum yields of powders

| MORPIP | Si | AMINO |
|---|---|---|
| 23% | 15% | 8% |

Quantum yields of powders were estimated by the same method used for the polymeric films, and are summarized in Table 4.9. Due to the difficulty in growing crystals the molecular structures deduced from X-ray crystallographic data for AMINO and Si could not be obtained.

The molecular structure deduced from crystallographic data of MORPIP, the twist angle and molecular dipole moments were discussed in Chaper 3. The twist between the amino moieties (donors) and the benzene ring ($\pi$-conjugation unit) is 45.4° and the estimated dipole moment of the MORPIP molecule in the crystal cell is 18.5 Debye. A high molecular dipole moment in the crystal is reasonable in response to the existence of the crystal field [64]. The twist in the structure is constrained by the crystal lattice. Hence the strong emissions from the crystalline state were observed.

the crystal lattice. Hence the strong emissions from the crystalline state were observed.

**4.2.3.3 Low temperature study on chromophores doped into a PMMA matrix.**

The behaviour of the PMMA films at low temperature was investigated. The increase of the intensity at low temperature was carefully studied. At low temperature non-radiative decay will be cut off [17]. The shifts of absorption and emission maxima are shown in Table.410. As noted in 4.3.3.1, the absorption maxima of the films from DMF and TMU solutions, as well as the change of the absorption maxima over the range of temperatures, were found to be similar. However, the Stokes shifts of the films from DMF and TMU solutions were not identical, so the local environment of the films from the DMF solution is different that of the films from the TMU solutions.

Table 4.10. Emission and Absorption Maxima of PMMA films on low temperature sutdy

| Films | Temperature (K) | Absorption Maxima | Emission Maxima | Stokes Shift |
|---|---|---|---|---|
| MORPIP | 294 | 22400[a] (447)[b] | 18200[a] (549)[b] | 4200[c] |
| DMF | 200 | 22400 (447) | 18500 (540) | 3900 |
| | 80 | 22700 (441) | 18700 (534) | 4000 |
| MORPIP | 294 | 22400 (447) | 18900 (529) | 3500 |
| TMU | 200 | 22400 (446) | 19000 (526) | 3400 |
| | 80 | 22600 (442) | 19200 (522) | 3500 |

a: ($cm^{-1}$) accuracy ±100 $cm^{-1}$, b: (nm) accuracy ±1 nm, c: ($cm^{-1}$) accuracy ±200 $cm^{-1}$

The emission intensity increases for both films between at 294K and 80K. The intensity at 80K ($6\times10^7$) was about three times as large as the intensity at 279K ($2.15\times10^7$) for the DMF films as shown in Fig.4.23. The increase of the intensity was only about twice for the TMU films from 294K ($1.7\times10^7$) to 80K ($3.5\times10^7$) as shown in Fig.4.23. The increase of the intensity for both films at low temperature was influenced by two factors. Firstly, a decrease of the free volume in the media occurs due to the decrease of temperature [64], i.e. constraining effect in the medium (although it is much smaller than in a glass forming solvent). Secondly the non-radiative decay is cut off [17].

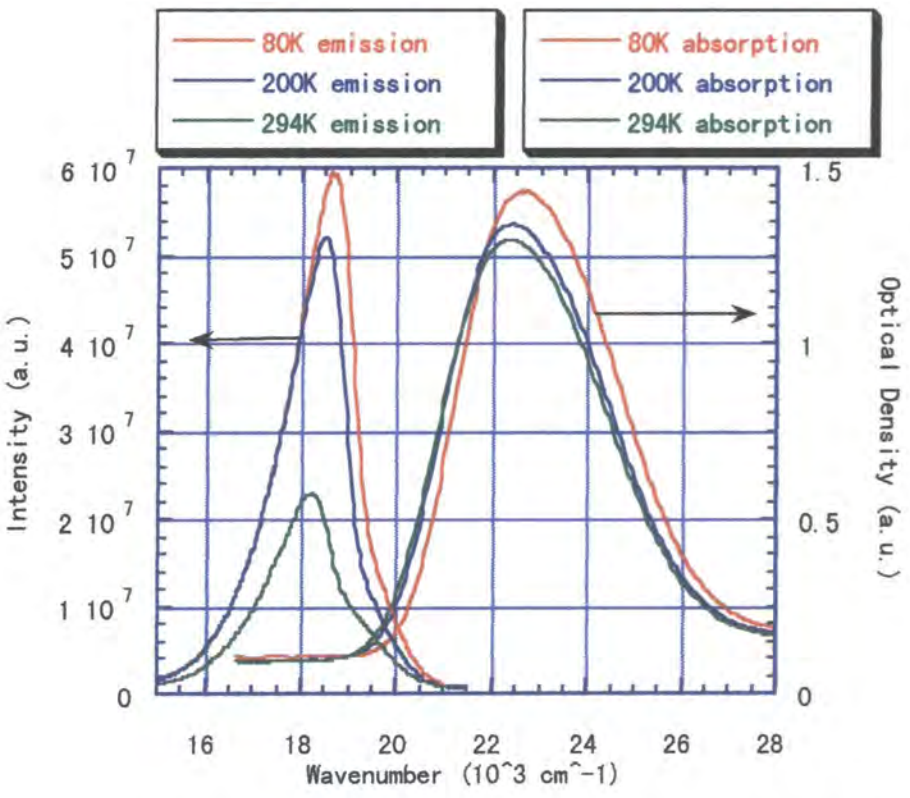


Figure 4.23 Absorption and emission spectra of the PMMA films (DMF) at various temperatures

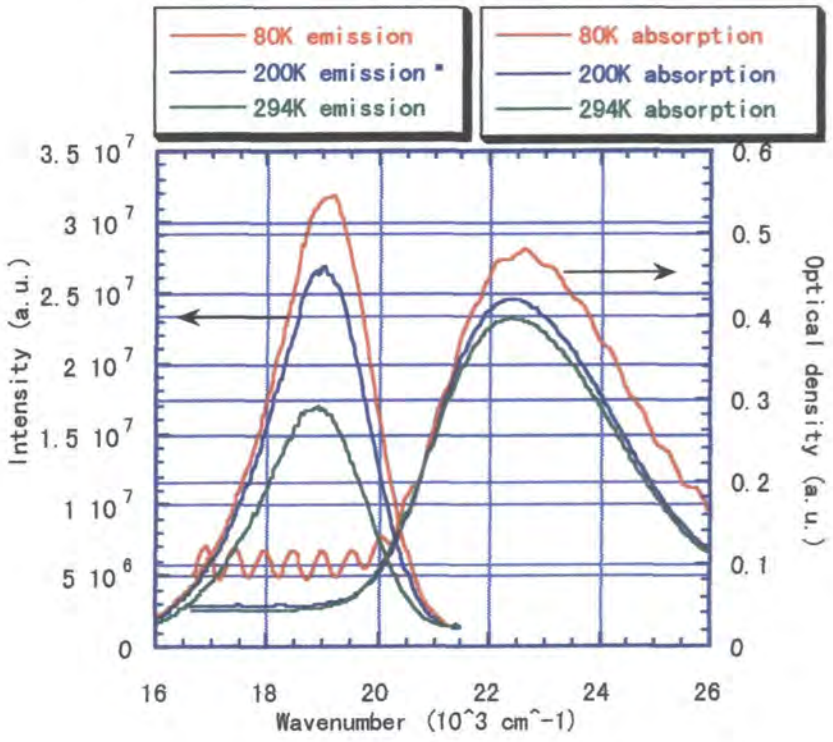


Figure 4.24 Absorption and emission spectra of PMMA films (TMU) at various temperatures

### 4.3.4 Time resolved spectroscopy

The lifetime of an emitting molecule gives information on the kinetics of the emitting process, i.e. the mechanism of the emitting process [1-25]. The single photon counting technique was used to determine the lifetime of MORPIP and Si in 1-propanol at low temperature. The wavelength of optical excitation that was used was at 340nm. The emissions of MORPIP at 294K and 80K were detected at 520nm and at 450nm, respectively. The emissions of Si at 294K and at 80K were detected at 480nm and at 430nm, respectively. As shown in Fig.4.25, time resolved spectroscopy for MORPIP in 1-propanol was obtained. At room temperature the lifetime was too

short to detect, as the signal at room temperature was identical to the instrument response.

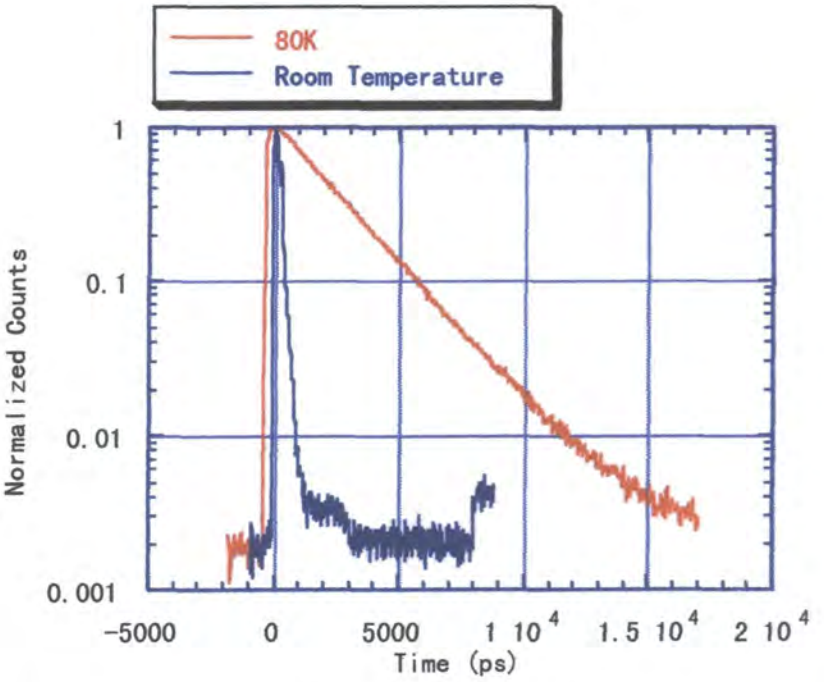


Figure 4.25 Time resolved spectroscopy for MORPIP in 1-Propanol

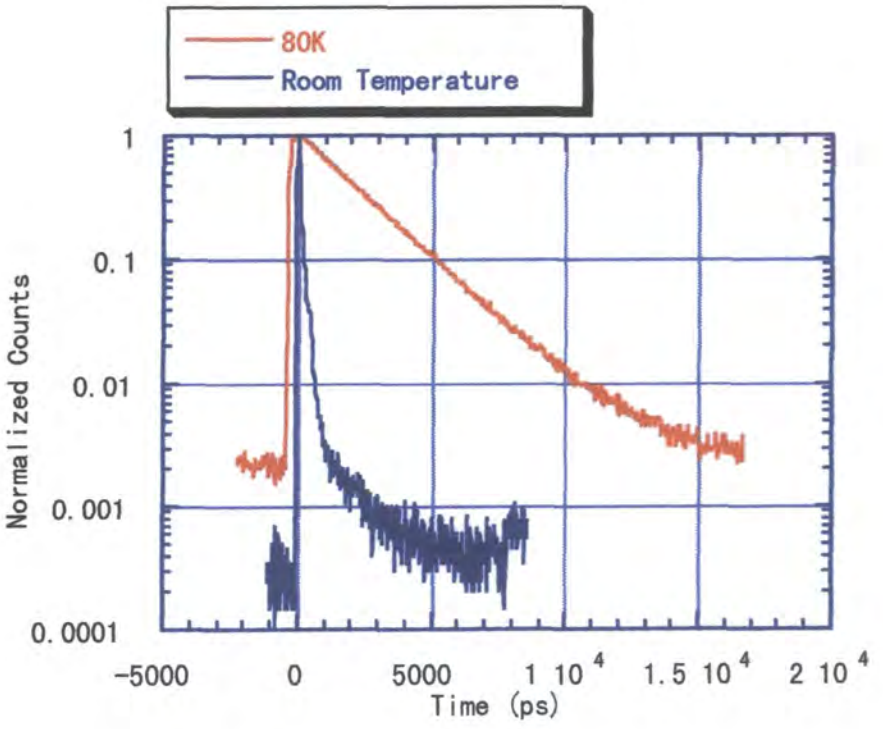


Figure 4.26. Time resolved spectroscopy for Si in 1-Propanol

As previously discussed steady state measurements in 1-propanol, the intensity of emission in the glass at 80K was much larger than that of the emission at 294K. Based upon this observation it would be expected that lifetimes at 80K would be greater. A single exponential decay was obtained at 80K to give the lifetime for MORPIP in a glass forming solvent. A similar result was obtained at 80 K for Si as shown in Fig.4.26.

Table 4.12 The lifetime of MORPIP in 1-propanol and fitting parameters

| | Lifetime (ns) | Qui2[a] |
|---|---|---|
| MORPIP at 80K | 2.5±0.2 | 1.9 |
| SI at 80K | 2.3±0.2 | 1.9 |

a:fitting parameter (the best fit=1)

The determination of the lifetime from the single exponential decay was carried out by standard time-correlated single photon counting methods using the software package, glife4. The fitted graph, extracted lifetime, and all fitting parameters are shown in Figs;4.27, 4.28 and Table 4.12. The terms, Qui2 in Table 4.12 give an indication of how the exponential decay matches the fitting graph. If the values of Qui 2 is 1±0.1, the exponential decay matches the fitted graph well [2]. Both single exponental decays for MORPIP and Si match reasonably well with a small residue as shown in Fig.4.27, and 4.28.

A typical lifetime of TICT molecules is a range of between nano seconds and tens of nano seconds, because the emitting process has to form the emitting TICT state that includes the structural change [6,7,9,10,25]. Since the lifetimes of Si and

MORPIP were 2.3±0.2 and 2.5±0.2 ns, respectively, this implies that structural change occurred during the emitting process for these molecules.

Low temperature studies in glass forming solvents (1-propanol and 2-methyl THF) were carried out as described in 4.3.2. As shown in Fig.4.20, in propanol the line width of the absorption spectrum at 294K was about 4000cm$^{-1}$ and that of the absorption spectrum at 80K was about 3000cm$^{-1}$. However, for 2-methyl THF the line widths of the absorption spectra at 294K and 80K ,as shown in Fig.4.18, are identical (3000cm$^{-1}$). As the lifetime of MORPIP in 1-propanol was obtained, the homogeneous line width can be calculated from the lifetime using the uncertainty principle [65], which is given as

$$\Delta E \Delta t \geq \frac{\hbar}{2} \qquad (4.18)$$

The calculated homogeneous line width for MORPIP in 1-propanol is $1.1\times10^{-3}$ cm$^{-1}$. The observed line widths at 294K and at 80K for both glasses are much larger than the calculated homogeneous line width ($1.1\times10^{-3}$ cm$^{-1}$) in 1-propanol. This implies that the observed line widths are due to inhomogeneous broadening [59]. The same line width at 294K and at 80K in 2-methyl THF implies that disorder in liquid and in a glass is unchanged. This is a unique observation, because normally the line width becomes narrower at low temperature in solvents such as 1-propanol [59]. The glassy state perhaps could not form well due to the existence of impurities in 2-methyl THF.

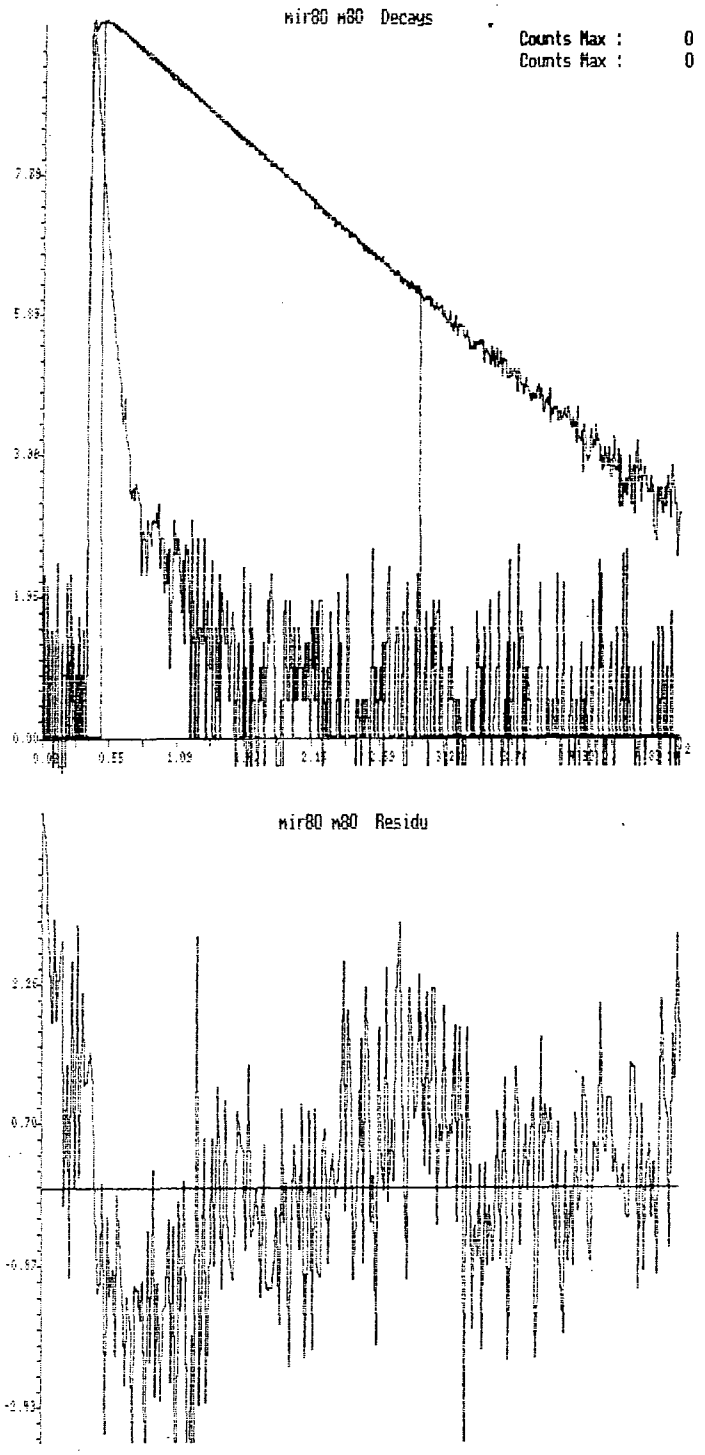


Figure 4.27 Fitted graph and residue of the decay of MORPIP at 80K

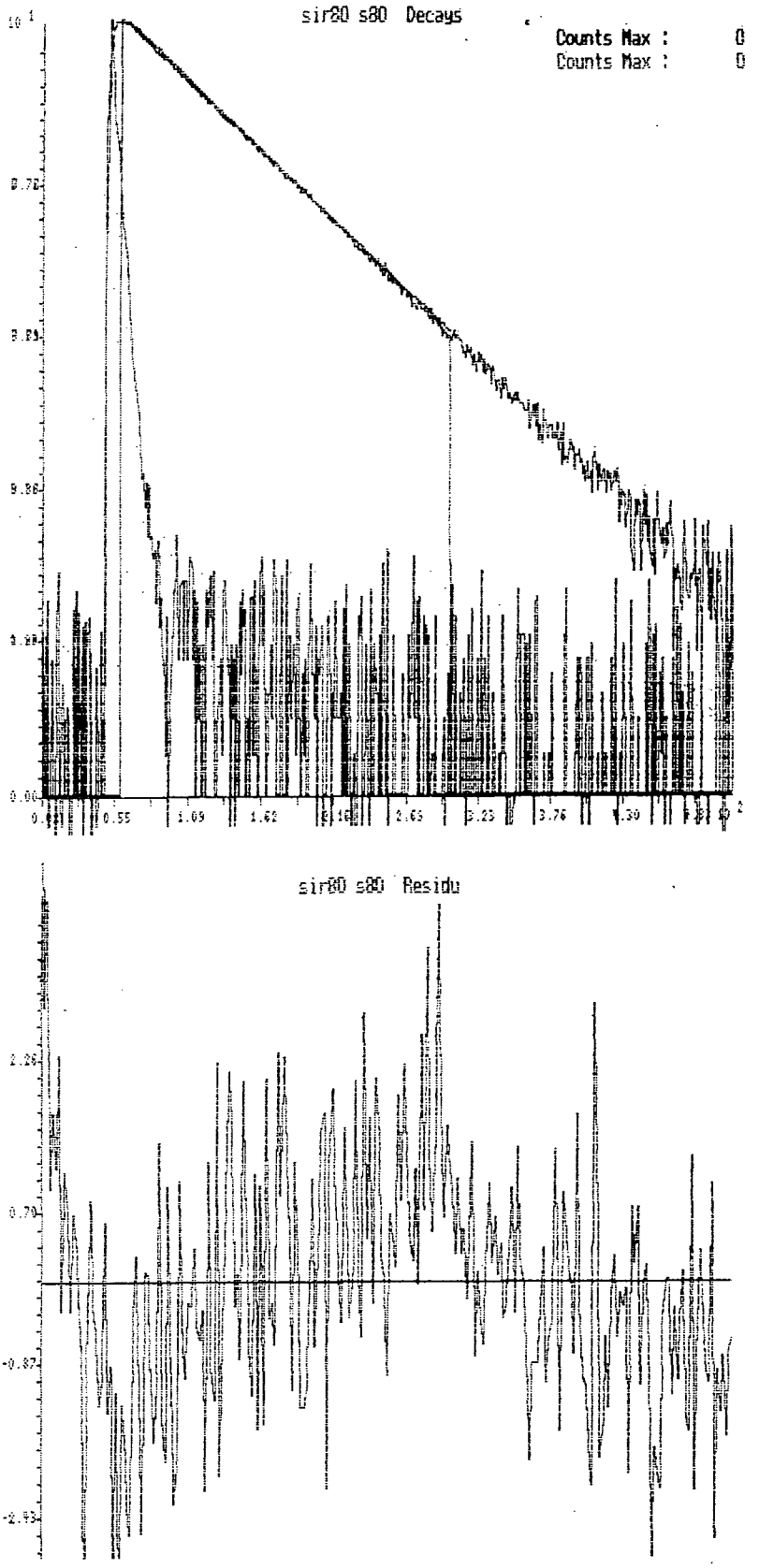


Figure 4.28 Fitted graph and residue of the decay of Si at 80K

### 4.3.5 Mechanism of the emitting process

The quantum yield of MORPIP in methanol is 0.1%, but in glycerol the quantum yield increases up to 11.8% due to the constraining effect of the matrix as noted in 4.3.1.a. This effect can be seen in different molecules such as tetraphenyl ethylene (TPE) [21,24,29,51,52]. The lifetime of TPE is 6ps in low viscosity solvents at room temperature, but the lifetime increases to 60ps in ethylene glycol and 600ps in glycerol [21]. The increase of the lifetime of TPE has been attributed to torsionally induced non-radiative decay, which decreases as the viscosity increases, i.e. the molecule becomes more constrained by the matrix. Since the torsional motion of TPE in the excited state is responsible to non-radiative decay, it is possible that non-radiative decay of MORPIP is also determined by the torsional motion of the

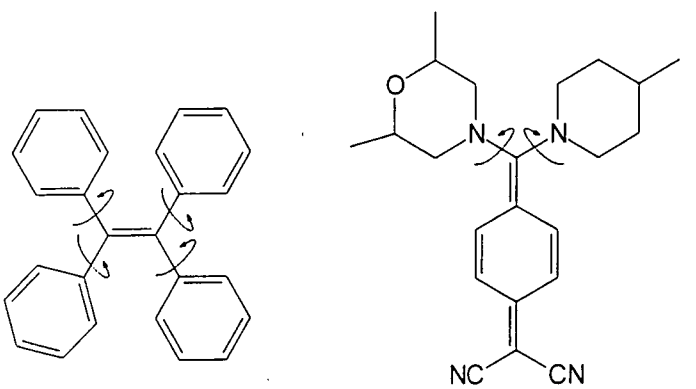


TPE MORPIP

molecule as shown in Fig.4.29.

Figure 4.29 Non radiative decay mechanism

TPE has bulky biphenyl groups between the ethylenic bond as shown in Fig.4.29, so the torsional motion of the ethylenic bond with the bulky biphenyl groups is hindered, when TPE is in a highly networked hydrogen bonding medium [21,25]. MORPIP also has relatively bulky piperidine and morpholine rings in the donor

moiety, so the torsional motion of the relatively bulky groups will also be hindered when MORPIP is in a highly networked hydrogen bonding medium.

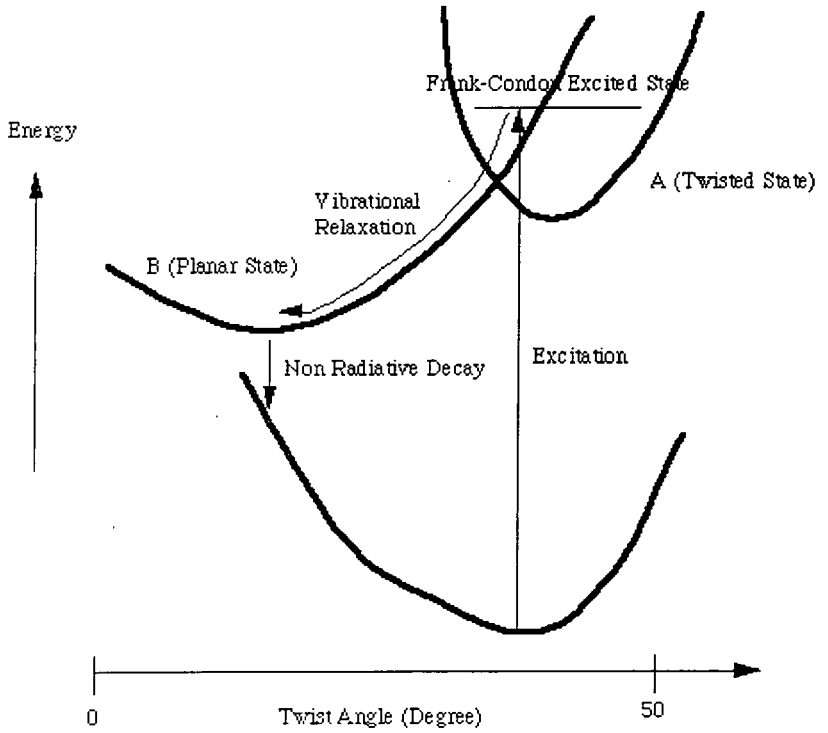


Figure4.30 Emission mechanism in a non-viscous medium

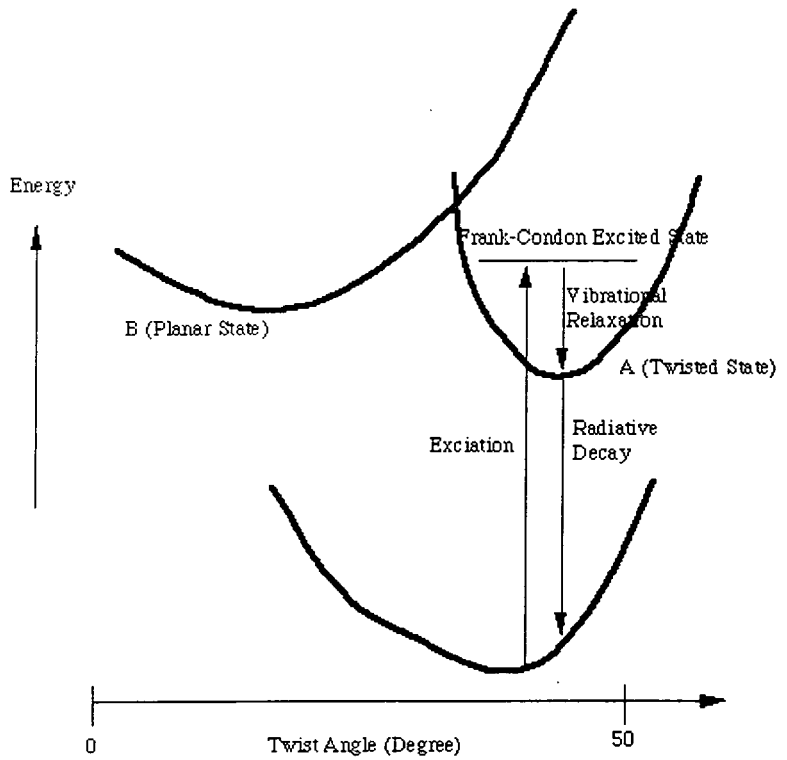


Figure 4.31 Emission mechanism in a viscous medium

The possible emission mechanism in a non-viscous medium is shown in Fig.4.30. The MORPIP molecule can be excited to a Frank-Condon state, which decays rapidly to the equilibrium more planar excited state (B state) via vibrational relaxation as the molecule can twist freely. The potential energy of the ground state of MORPIP in the gas phase as a function of the twist angle was predicted by *ab initio* calculation, as discussed in 3.3.7. The molecule decays from the planar state to the ground state via non-radiative decay process [21,24,25].

The possible emission mechanism in a viscous medium or in a solid is after excitation decays rapidly to a twisted excited state (A state) by vibrational relaxation [21,25,29,51,52,66]. This is because the planar excited state will be somewhat higher in energy relative to the twisted excited state in the viscous or solid media, where the molecule can not twist easily. As a consequence of this the non-radiative decay of MORPIP will be hindered. All absorption and emission spectra of MORPIP showed a blue shift, i.e., negative solvatochromism, on the formation of the glassy state at low temperatures [51]. This experimental observation supports the view that a twisted excited state is favoured in rigid local environments, and the energy gap between the twisted excited state and the ground state is smaller in the glassy state.

## 4.4 Conclusion

Three newly synthesized compounds, MORPIP, AMINO, and Si, were investigated for their luminescence properties. MORPIP was the most extensively studied of the three compounds. The Stokes shifts and quantum yields in non-viscous solvents is a linear function of the solvent density ($\Delta f$). This suggests that the change of the dipole moments between the excited state and the ground state is approximately constant.

However, the quantum yields and Stokes shifts in high viscosity solvents do not follow the function of $\Delta f$. Large quantum yields in high viscosity solvents were measured, up to 11.4% for MORPIP in glycerol. A high quantum yield was also measured in the crystalline form of MORPIP (23%). This is a unique observation, the quantum yield of the powder of MORPIP is much higher than that of MORPIP in methanol (0.1%).

The molecular structure deduced by the crystallographic data (MORPIP) and theoretical modeling suggests that it is highly polar and twisted structure. The emission mechanisms in a viscous medium and a non-viscous medium were proposed using the crystallographic molecular structure and *ab inito* calculation. The twisted excited state (radiative decay) becomes favourable, when the molecule is constrained by a viscous medium such as a highly networked hydrogen bonding medium [21,25,29,51,52,66].

The constraining effect of the matrix was confirmed by studies in the glass forming solvents such as EPA. A large increase of emission intensity was found in glassy states at low temperatures. The quantum yields of a doped film prepared from polymeric matrices using different casting solvents were measured. Quantum yields in polymeric matrices prepared from different coating solvents were measured up to 37% as a result of the different "free volume" in polymer matrices. The fluorescence properties of the PMMA films prepared from the different spin coating solvents (DMF and TMU) were investigated at low temperatures. The Stokes shifts and the increase in emission intensity between room temperature and low temperature measurements of the PMMA films prepared from DMF and TMU solutions were not identical, this suggests that the MORPIP in the both PMMA films is in a different local

environment. Experimental observations indicate the retention of solvent in the polymer matrices and effect on "free volume" as a result of it.

## Chapter4: References

[1] A.Gilbert, J.Baggott, P.J.Wanger, Essential of Molecular Photochemistry, Blackwell Science (1995)

[2] J.R.Lakowicz, Topics in Fluorescence Spectroscopy Vol.1 Techniques, Plenum Press, New York (1991)

[3] J.Y.Ye, T.Hattori, H.Nakatsuka, Y.Maruyama, M.Ishikawa, Phys.Rev.B., **56**, 1997, 5286

[4] J.Y.Ye, T.Hattori, H.Inouye, H.Ueta, H.Nakatsuka, Y.Maruyama, M.Ishikawa, Phys.Rev.B., **53**, 1996, 8349

[5] J.Seixas de Melo,R.S.Becker,F.Elisei,A.L.Macanita,J.Chem.Phys.,**107**,1997,6062

[6] G.Saielli, A.Polimeno, P.L.Nordio, P.Bartolini, M.Ricci, R.Righini, Chem.Phys., **223**,1997,51

[7] D.Braun, P.L.Nordio, A.Polimeno, G.Saielli, Chem.Phys., **208**, 1996, 127

[8] G.J.Dixon, Laser Focus World, October, 1997, 115

[9] Y.Wang, M.McAuliffe, F.Novak, K.B.Eisenthal, J.Phys.Chem., **85**,1981,3736

[10] Y.Wang, K.B.Eisenthal, J.Chem.Phys., **77**, 1982, 6076

[11] K.M.Keery, G.R.Fleming, Chem.Phys.Lett., **93**, 1982, 322

[12] K.G.Casey, E.L.Quitevis, J.Phys.Chem., **92**, 1988, 6590

[13] C.J.Tredwell, A.D.Osborne, J.C.S.Fraday II, **76**, 1980, 1627

[14] A.D.Osborne, J.C.S.Fraday II, **76**, 1980, 1638

[15] A.Sarkar, S.Chakravoriti, J.Lumesecence, **78**, 1998, 205

[16] A.Costela, I.Garcia-Moreno, J.Barroso, R.Sastre, J.Appl.Phys., **83**, 1998, 650

[17] E.Laitinen, K.Salonen, T.Harju, J.Chem.Phys., **105**, 1996, 9771

[18] J.B.Birk, G.N.R.Tripathi, M.D.Lumb, Chem.Phys., **33**, 1978, 185

[19] J.R.Andrews, B.S.Hudson, J.Chem.Phys., **68**, 1978, 4587

[20] S.P.Velsko, G.R.Fleming, J.Chem.Phys., **76**, 1982, 3553

[21] P.F.Barbra, S.D.Rand, P.M.Rentzepis, J.Am.Chem.Soc., **103**, 1981, 2156

[22] P.F.Barbara, L.E.Brus, P.M.Rentzepis, Chem.Phys.Lett., **69**, 1980, 447

[23] P.F.Barbara, P.M.Rentzepis, L.E.Brus, J.Am.Chem.Soc., **102**, 1980, 2786

[24] D.Ben-Amotz, C.B.Harris, Chem.Phys.Lett., **119**, 1985, 305

[25] J.Hicks, M.Vndersall, Z.Babarogic, K.B.Eisenthal, Chem.Phys.Lett., **116**, 1985, 18

[26] I.L.Arbeloa, K.KRohatgi-Mukherjee, Chem.Phys.Lett., **128**, 1986, 474

[27] N.C.Greenham, I.D.W.Samuel, G.R.Hayes, R.T.Phillips, Y.A.R.R.Kessenser, S.C.Moratti, A.B.Holmes, R.H.Friend, Chem.Phys.Lett., **241**, 1995, 89

[28] E.D.Cehelnik, R.B.Cundall, J.R.Lockwood, T.F.Palmer, J.Phys.Chem., **79**, 1975, 1369

[29] S.Sharafy, K.A.Muszkat, J.Am.Chem.Soc., **93**, 1971, 4119

[30] C.Reichardt, Solvents and Solvent Effects in Organic Chemistry, 2nd ed., Weinheim, Cambridge (1991)

[31] J.Frank, J.Chem.Soc.Trans.Fraday, **21**, 1926, 536

[32] C.U.Condon, Phys.Rev., **32**, 1928, 858

[33] J.Herbich, A.Kapturkiewicz, J.Am.Chem.Soc., **120**, 1998, 1014

[34] H.Lami, N.Glasser, J.Chem.Phys., **84**, 1986, 597

[35] P.Suppan, J.Chem.Soc., (A), 1968, 3125

[36] J-J.Aaron, M.Maafi, C.Kerebet, C.Párkányi, M.S.Antonious, N.Motohashi, J. Photochem.Photobiol.A:Chem., **101**, 1996, 127

[37] A.K.Dutta, K.Kamada, K.Ohta, J.Photochem.Photobiol.A:Chem., **93**, 1996, 57

[38] G.Liu, L.Heisler, L.Li, M.G.Steinmetz, J.Am.Chem.Soc., **118**, 1996, 11412

[39] B.Bagchi, D.W.Oxtoby, G.R.Fleming, Chem.Phys., **86**, 1984, 254

[40] I.L.Arbeloa, K.KRohatgi-Mukherjee, Chem.Phys.Lett., **128**, 1986, 474

[41] L.Reynolds, J.A.Gardecki, S.J.V.Frankland, M.L.Horng, M.Maroncelli, **100**, 1996,10337

[42] C.F.Zhao, R.Gvishi, U.Narang, G.Ruland, P.N.Prasad, J.Phys.Chem., **100**, 1996, 4526

[43] W.Retting, J.Luminescence, **26**, 1980, 21,

[44] K.A.Zachariasse, M.Grobyes, Th.von der Haar, A.Hebecker, Yu.V.Il'ichev, Y-B.Jiang, O.Morawski, W.Kühnle, J.Photochem.Photobiol. A:Chem., **102**, 1996, 59

[45] O.Morawski, W.Kühnle, J.Photochem.Photobiol. A:Chem., **102**, 1996, 59

[46] Z.R.Grabowski, J.Dokowski, Pure&Appl.Chem., **55**, 1983, 245

[47] A.Kawski, G.Piszczek, Z.Naturforsch., **52a**, 1997, 409,

[48] A.L.Sobolewski, W.Domcke, Chem.Phys.Lett., **250**, 1996, 428

[49] W.Retting, Angew.Chem.Int.Ed.Engl., **25**, 1986, 971

[50] C.Reichart, Chem.Rev., **94**, 1994, 2319

[51] M.A.El-Byoumi, F.M.A.Halim, J.Chem.Phys., **48**, 1968, 2536

[52] J.Kordas, M.A.El-Bayoumi, J.Am.Chem.Soc., **96**, 1974, 3043

[53] H.T.Oh, Y.Kanematsu, A.Kurita, T.Kushida, J.Luminescence, **66&67**, 1996, 310

[54] R.Reichart, F.Stickel, R.S.Fee, M.Maroncelli, Chem.Phys.Lett., **229**, 1994, 302

[55] J.Yu, P.Ervolino, M.Berg, J.Chem.Phys., **96**, 1992, 8750

[56] E.Laitinen, K.Salonen, T.Harju, J.Chem.Phys., **105**, 1996, 9771

[57] G.Fischer, G.Seger, K.A.Muszkat, E.Fischer, J.Chem.Soc.Perkin II, 1975, 1569

# Chapter 5: Photodegradation

## 5.1 Introduction

The intensity of transmitted light through nonlinear optical polymer waveguides changes significantly during continuous transmission of laser radiation. The chemical change of the active dopants in the medium that originate the photodegradation occurs during the course of radiation [1-11]. A possible mechanism of the photodegradation is that the presence of oxygen in the polymeric medium causes the photosensitized oxidation reaction of olefinically unsaturated bonds in the nonlinear optical chromophores [1-3]. The photo-oxidation reaction occurs through the formation of singlet oxygen by an energy transfer from the excited state of the chromophores [1-3].

The optical damage of DEMI doped PMMA matrix was investigated by Y.Ren et al [12]. For example, a DEMI doped PMMA matrix was spin coated on glass substrates to form waveguides. Intense light at 633 nm was coupled into the waveguide. The absorption maximum of DEMI was around 700nm, so DEMI absorbs the input light at 633 nm. At the beginning of the experiment, the transmitted light level was normalized to zero. As the photodegradation process occurred, the transmitted light increased due to the reduction in absorption. The two experimental conditions, in air and under vacuum, were used with the results, as shown in Fig.5.1 and Fig.5.2, respectively.

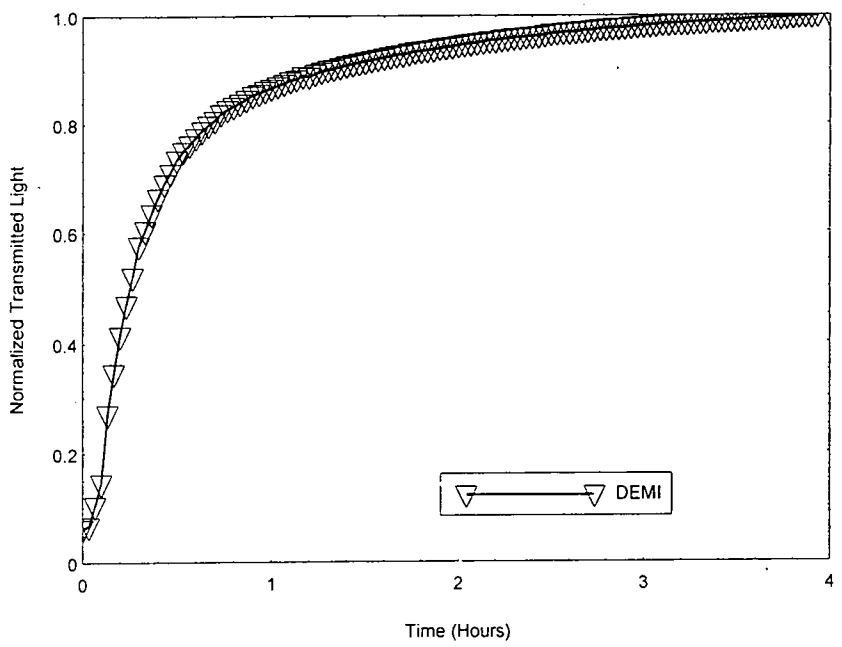


Figure 5.1 Photodegradation of DEMI waveguide at 633nm in air

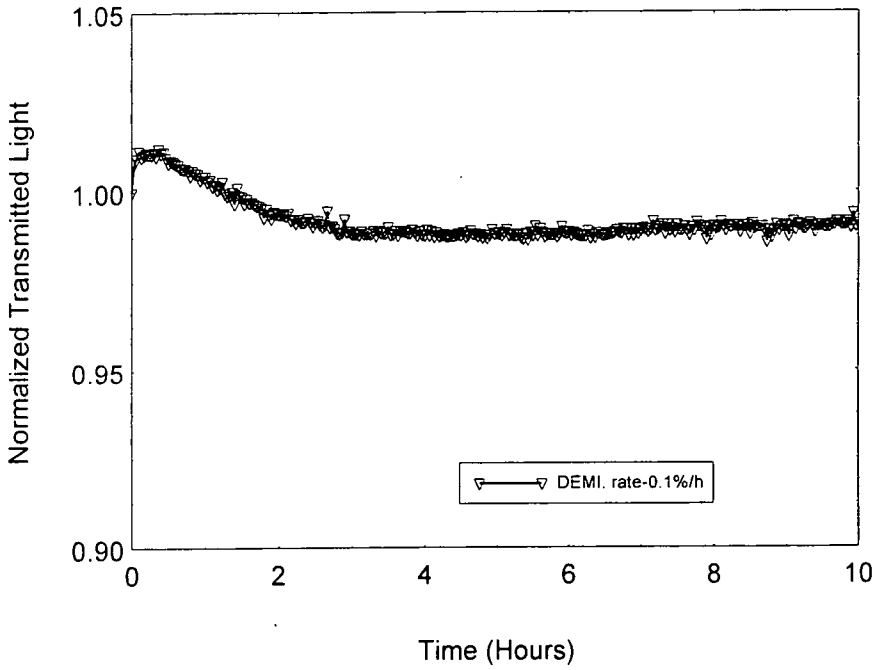


Figure 5.2 Photodegradation of DEMI waveguide under vaccum

As shown in Fig.5.1, the photodegradation process was completed within four hours. However, under vacuum the photodegradation process did not occur. This shows that the photo-degradation is due to photo-oxidation. Singlet oxygen is important for the mechanism of the photo-oxidation process [1-3,13], as shown in Fig.5.3.

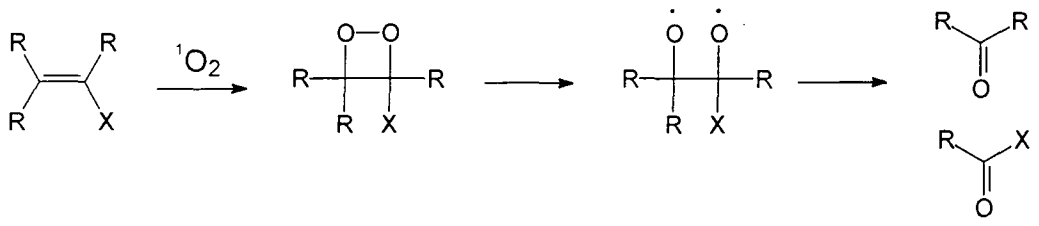


R=Alkyl groups, X=N,S,orO

Figure 5.3 A mechanism of the cleavage of the carbon double bond

This cleavage mechanism can occur photochemically via singlet oxygen generated by light [8]. The formation of singlet oxygen suggests that the formation of triplet states in the polymeric medium containing DEMI. DEMI has olefinically unsaturated bonds that are easily oxidized in this manner. Therefore, in order to improve the photostability against singlet oxygen the olefinically unsaturated bonds in the charge transfer system of the molecule should be removed. A new strategy was applied to the synthesis for the removal of the olefinically unsaturated bonds in TCNQ adducts [14,15] as shown in Fig.5.4.

Adducts prepared by the reaction of primary or secondary amines with TCNQ give polar molecules without the olefinically unsaturated bonds as described in Chapter 2. So experiments were conducted on the degradation of MORPIP, and related compounds, (AMINO, and Si).

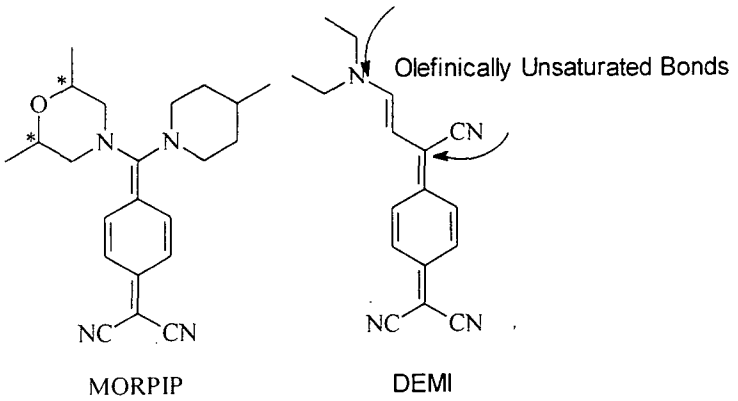


MORPIP DEMI

Figure 5.4 Structure of DEMI and MORPIP

## 5.2 Experimental

### 5.2.1 Photodegdation measurements

An Oriel Quartz Tungsten Halogen lamp (model 66180) was used for photodegration measurements. Solutions were exposed under the white light source radiation. Typically, MORPIP (3mg) was dissolved in acetonitrile of 25 ml. The absorption spectrum of the solution in a 1mm path length cuvette was obtained. The cuvette was placed in front of the lamp. A flask containing copper sulphate was used to remove infra-red light to cut down on heating the sample. The power of the lamp was set at 210 W. The absorption spectrum of the sample was taken as a function of time, for instance every 15 min. The radiation time was determined from the rate of degradation during the first hour of illumination.

## 5.3 Results and Discussion

### 5.3.1 Photodegradation by radiation of a white light source

Stability under normal atmosphere is likely to be important in the production and the operation of low cost devices incorporating the chromophores. Studies of the

photodegradation of MORPIP, Si, and AMINO under normal atmosphere were carried out in various solvents under exposure to a white light source. The use of the white light source for the photodegradation study in liquid states was easy to set up, so it was suitable for the initial study of the photostability of the newly synthesized compounds. Four solvents, acetonitrile, acetone, ethanol, and chloroform were used for this study. Acetonitrile and ethanol are very polar solvents, and chloroform is non-polar. Therefore the effect of solvent and polarity on photodegradation could be investigated.

Photodegradation of three compounds (MORPIP, Si and AMINO) in acetonitrile and acetone is shown in Fig.5.5. The speeds of the decays were found to be slightly different due to the structural difference and the different absorption profile, for example, MORPIP (417nm), Si (394nm), and AMINO (367nm) (all in acetonitrile). Allowing for these factors suggests that the decay mechanism is the same in all cases.

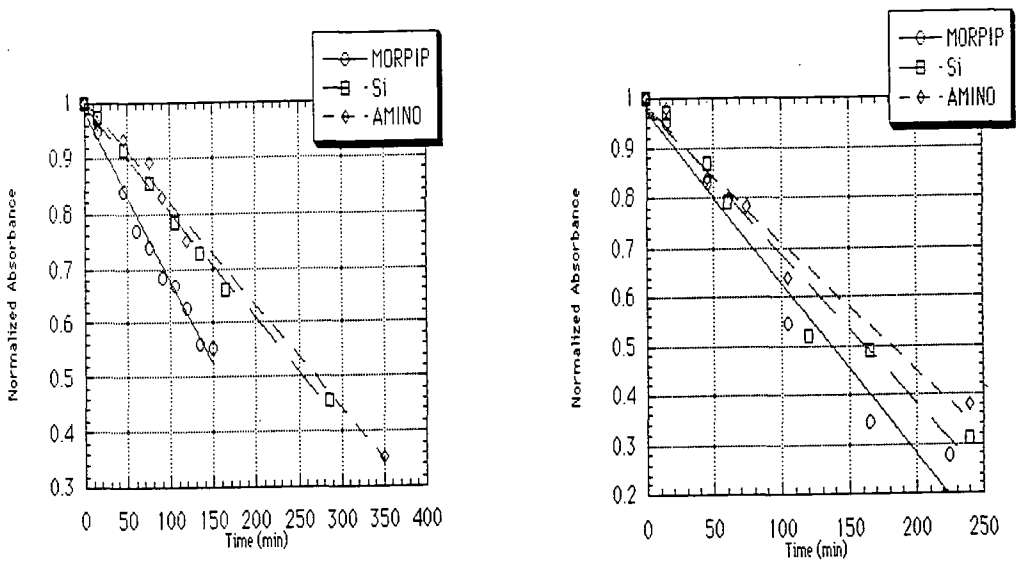


Figure 5.5 Photodegradation for three compounds in acetonitrle (left) and acetone (right)

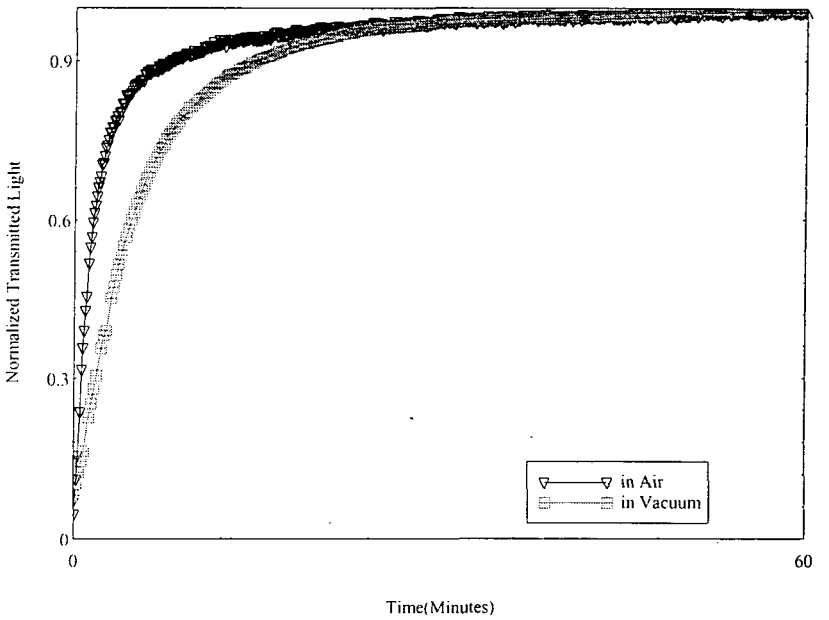


Figure 5.6 Photodegradation of MORPIP in PMMA matrix degraded at 458 nm

The study of the photodegradation of MOR2 doped PMMA films was carried out by Y.Ren [12] et al, and is shown in Fig.5.6. The films were degraded under vacuum and in air within ten minutes. The film in air (~5 min) was degraded more quickly than under vacuum (~10 min). This suggests that two photodegradations are present, photo-oxidation and another photodegradation process, because the photodegradation was observed even under vacuum. Although two different excitation wavelengths were used for photodegradation experiments of DEMI (633nm) and MORPIP (458nm), photodegradation of MORPIP in air as shown in Fig.5.6 was completed relatively more quickly than that of DEMI as shown in Fig.5.1, as a result of two different photodegradation processes. The other photodegradation process occurs under vacuum, so could be via free radicals. Free radicals can be created in the absence of oxygen [16]. Generally, it is very easy to form free radials in halogen containing solvents such as chloroform and difficult to form them in alcohols such as ethanol [17]. So the photodegradation of MORPIP in ethanol (left) and in

chloroform (right) was studied as shown in Fig.5.7. Photostability in chloroform was very low and photostability in ethanol was relatively high. These experimental observations in both solutions support the possible photodegradation via free radicals.

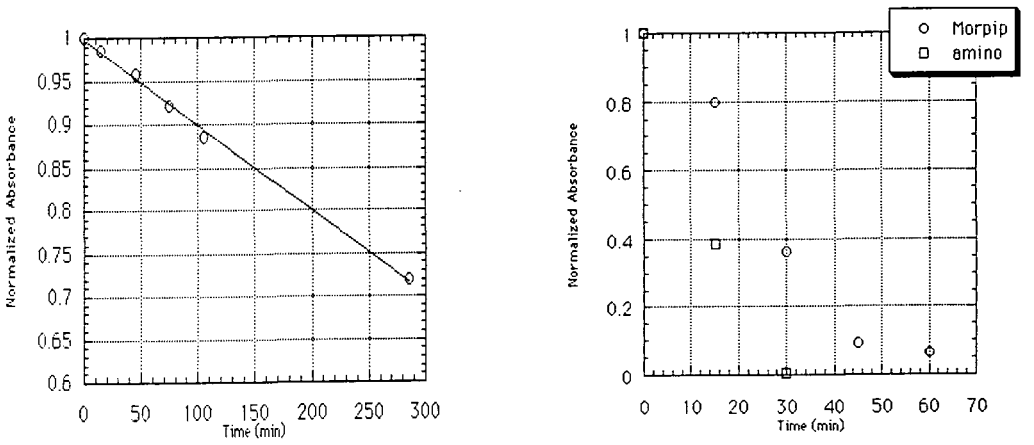


Figure 5.7 Photodegradation for MORPIP in ethanol (left) and in chloroform (right)

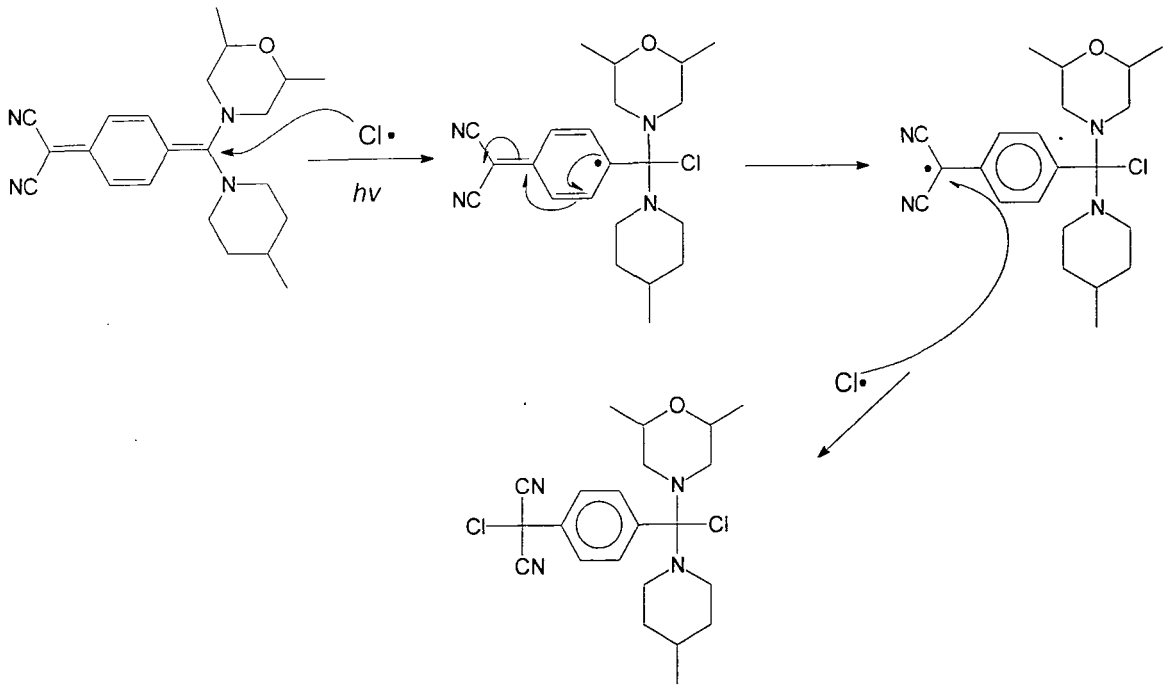


Figure 5.8 A possible photodegradation mechanism of MORPIP in chloroform

A possible photodegradation mechanism of MORPIP is shown in Fig.5.8. A free radical molecule of Cl• is used as an example to illustrate the possible mechanism in Fig.5.8, but there can be several free radical molecules in chloroform (•CCl, H•, and •$CHCl_2$). Therefore, there will be a number of the degradation products formed via free radical reactions.

The free radial reactions between acetonitrile [18] or acetone [19] and TCNQ have been reported. The reported reaction mechanisms and products are similar to the proposed mechanism shown in Fig.5.8. The same degradation mechanism shown in Fig.5.8 seems likely to occur in polymer matrices such as PMMA. In the PMMA matrix free radicals (•$OCH_2$-, •$COCH_2$-) can be created by a Norrish reaction as shown Fig.5.9 [9-11].

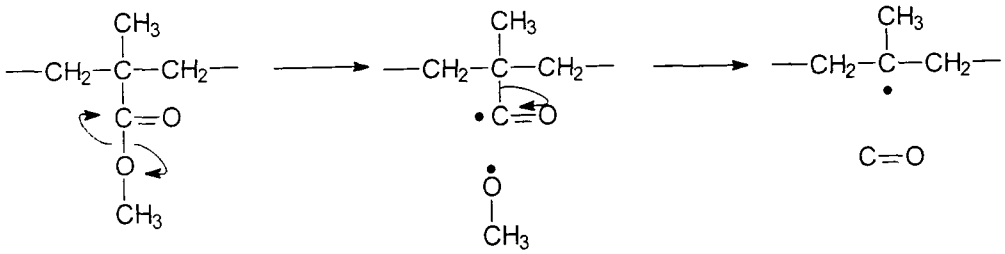

Figure 5.9 Possible degradation mechanism of PMMA

The part of the polymer chain with free radicals can react with the chromophores such as MORPIP to give the cross linked polymer between the chromophores (MORPIP) and the polymer matrix (PMMA) [9,11].

The study of NMR spectra before and after the photodegradation supports the mechanism of the photodegradation. MOR2 was used for the NMR study as it has a similar structure relative to MORPIP. MOR2 was dissolved into $CD_2Cl_2$ in an NMR

tube. Before the exposure to the white light source, the NMR spectrum of the prepared sample was recorded, and the part of the spectrum is shown in Fig.5.10 (left). This one single peak related to the benzene protons (4H) at 7.1ppm was observed. The single peak suggests that the four protons of the benzene ring should have the same environment in terms of the electronic distribution of the benzene protons.

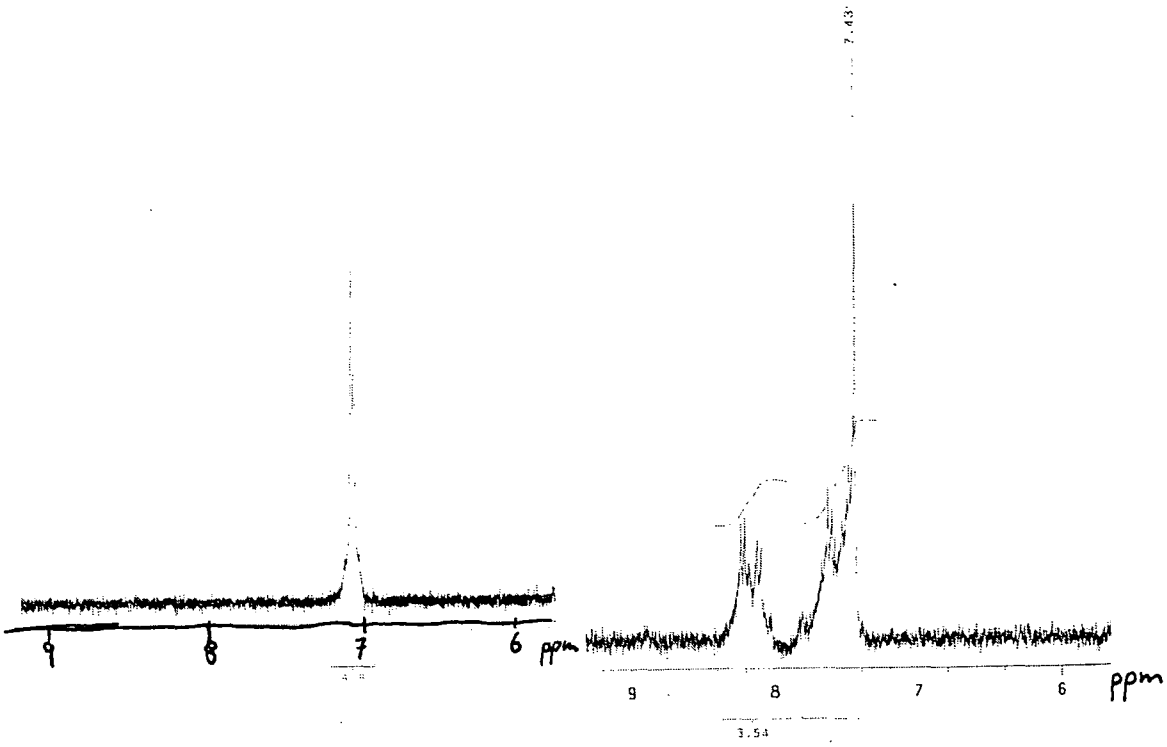


Figure 5.10 NMR spectra of MOR2 (left) and the degraded product (right)

After the completion of the exposure of the white light source, the yellow solution changed to the colourless solution. The NMR spectrum of the colourless solution was recorded and is shown in Fig.5.10 (right). A number of the multiplets between 7 and 8ppm were observed. The NMR spectra indicate that there is more than one product present as a result of photodegradation, e.g. as shown in Fig.5.8 where the complex substitution would lead to two sets of multiplets in the degraded NMR spectrum.

## 5.3 Conclusion

In order to prevent the photo-oxidation process for TCNQ adducts such as DEMI, newly synthesized TCNQ adducts not containing the olefinically unsaturated bonds were prepared. However the expected photostability was not observed due to other photodegradation mechanisms.

# Chapter 5: References

[1] K.Hong, M.Mortazavi, H.Yoons, ACS Synposium Series, American Chemical Society (1995), 333

[2] J.R.Sheats, J.Phys.Chem., **94**,1990, 7194

[3] R.D.Scurlock, B.Wang, P.R.Ogilby, J.R.Sheats, R.L.Clough, J.Am.Chem.Soc., **177**, 1995, 10194

[4] K.K.Okudaira, S.Hasegawa, P.T.Sprunger, E.Morikawa, U.Saile, K.Seki, Y.Harada, N.Ueno, J.Appl.Phys., **83**, 1998, 4292

[5] S.Popov, Pure Appl.Opt., 1998, 1379

[6] M.Yan, L.J.Rothberg, F.Papadimitrakopoulos, M.E.Galvin, T.M.Miller, Phys.Rev. Lett., **73**, 1994, 744

[7] N.A.Weir, J.Arct, A.Ceccarelli, Eur.Polym.J., **32**, 1992, 805

[8] S.Panlasem, J.Kuczynski, J.K.Thomas, Macromolecules, **27**, 1994, 3773

[9] H.Zweifel, Chemia, **47**, 1993, 390

[10] R.Gooden, M.Y.Hellman, R.S.Hutton, F.H.Winslow, Macromolecules, **17**, 1984, 2830

[11] J.R.MacCallum, in The Encyclopedia of Advanced Materials,Pergamon Vol 3 1979, Edited by D.Bloor,R.J.Brook,M.C.Flemings,S.Mahajan (1994)

[12] Y.T.Ren, G.H.Cross, Private communications (1995-1998)

[13] A.R.Frimer, Chem.Rev., **79**, 1979, 359,

[14] W.R.Hertler, H.D.Hartzler, D.S.Acker, R.E.Benson, J.Am.Chem.Soc., **84**, 1962, 3387

[15] B.P.Bespalov, V.V.Titov, Russian.Chem.Rev., **44**, 1975, 1091

[16] N.Isaacs, Physical Organic Chemistry, 2nd Ed, Longman Scientific&Technical, 1995, (Harlow)

[17] I.U.P.A.C. Free Radical In Solution, Butterworth, London (1966)

[18] M.Farcasiu, C.S.Russell, J.Org.Chem., **41**, 1976, 571

[19] K.Tsujimoto, T.Fujimori, M.Ohashi, J.Chem.Soc., Chem.Com., 1986, 304

# Chapter 6: Closing Remarks

## 6.1 Conclusions

### 6.1.1 Synthesis

New TCNQ derivatives were synthesised by the substitution of primary and secondary amines onto TCNQ. A new reaction mechanism was discovered. A mono substituted amino tricyanoquinodimethane was reacted with 1,3-bis(3,3,3-trifluoropropyl) tetramethyl disilazane. In the course of the reaction it is thought that a positive charge is delocalised over adjacent silicon and nitrogen atoms. This leads to the cleavage of bonds between the silicon and the nitrogen. Few papers in the literature report studies of TCNQ derivatives with primary and secondary amines for nonlinear optics, and there has been no report to date of the luminescence properties of any TCNQ derivatives such as those described in this thesis.

### 6.1.2 Nonlinear optical properties and related properties

The dipole moments of the newly synthesised compounds such as MORPIP were approximately 15 Debye in a range of solvents. The measured dipole moments were consistent with the theoretical dipole moments calculated using *ab initio* and MOPAC calculations. Large second harmonic generation (25 times urea) was observed from MORPIP using the Kurtz powder technique. The estimated $\mu\beta(0)$ of the molecular structure of MOPPIP deduced from crystallographic data using MOPAC calculation was calculated to be $-930\times10^{-48}$ esu. This value is a relatively high value compared to most other nlo organic chromophores. More importantly, the absorption maxima of the newly synthesised compounds occur at wavelengths below

500nm. Hence they are transparent between 550nm and 700nm where LAN networks will operate.

### 6.1.3 Luminescence properties

The behaviour of the molecules on optical excitation is affected by the local environment, principally by the constraint imposed on the changes in molecular geometry. In liquids this is determined by the viscosity of the medium. The solvent molecules in low viscosity solvents move rapidly to accommodate the change in shape of the fluorescing molecule. In high viscosity solvents the motion of the solvent molecules is slow and the fluorescing molecule is constrained. The latter is also true in the glass forming solvents above their glass transition temperature.

In solid phases (crystals, glass, polymer films) the concept of viscosity is no longer valid. However, each situation has a distinct "free volume" in the region of the fluorescing molecule. It is this 'free volume' and its variation from sample to sample (e.g. in the PMMA films) that allows the changes in molecular geometry that occurs during excitation and fluorescence.

Very weak fluorescence was measured in non-viscous solvents and strong fluorescence was measured in high viscosity solvents such as glycerol due to the constraining effect of the medium. Unusual emission was observed from the crystalline state of MORPIP and high quantum yields of the PMMA films were measured. The unique observation of quantum yields, which vary with coating solvent, is evaluated. Possible emission mechanisms in non-viscous media and viscous media are presented.

### 6.1.4 Photodegradation

Photo-oxidation is the main cause of the photodegradation process of chromophores such as DEMI. This is because olefinically unsaturated bonds can be oxidised in air. Photostability in air is an important condition for the low cost fabrication of devices using such chromophores. The newly synthesised compounds were hoped to be more stable in air due to the absence of olefinically unsaturated bonds. However, photodegradation via formations of free radicals occurred. The possible degradation via free radicals is discussed. Hence, on improvement in photostability was not observed.

## 6.2 Future work

Physical properties (dipole moments) of AMINO and Si need to be studied for the evaluation of the nature of molecules. Single crystals of AMINO and Si suitable for X-ray crystallographic studies will determine the molecular structure. Such studies will allow studies the twist angles in the crystal lattice. Theoretical models using either MOPAC or *ab inito* calculations need to be obtained. Theoretical models, molecular structure and the twist angles between donor moieties and the benzene ring deduced from X-ray crystallographic data, and physical properties such as molecular dipole moment can be used to evaluate possible emission mechanisms for AMINO and Si.

Time resolved spectroscopy on MORPIP doped PMMA and polycarbonate films should be carried out to evaluate the kinetics of the emission process depending on coating solvents and polymer matrices. The kinetics of the emission process of different PMMA films can support the change of quantum yields depending on the coating solvents and the polymer matrices.

The dependence on the twist angle of the colour of emission and quantum yields should be studied using the known similar TCNQ derivatives.

The luminescence properties of the two compounds described in Chapter 2 need to be studied in further detail. FPHPIP has a very rigid conformation and hence strong emission in the crystalline state was observed under an UV lamp. MORPROL shows strong yellow emission in the crystalline state under an UV lamp.

Improvement of photostability has to be considered. The effects of the inclusion of radical inhibitors on photodegradation should be studied.

In order to improve photostability for chromophores, a new approach was attempted. The immobilisation of a TCNQ derivative inside the cavity of a calixarene would be likely to improve the photostability of the TCNQ derivative due to shielding singlet oxygen and radical provided by the cavity. Several amines were employed in an attempt to attach a bridge across the cavity of a calix[6]arene. 2,6,Dimethyl pyridine was bridged across the lower rim of the calix[6]arene cavity [1]. However, the product did not react with any methylation reagents to give a pyridium salt inside the cavity. Hydrogenation of the pyridine ring inside the cavity was attempted, but the target product was not obtained. Failures of any reactions with the bridged calix[6]arene is probably a consequence of the constraints of the cavity size. Recently, chromophores using calixarenes for nonlinear optics were reported [2]. This work suggests that studies of the use of calixarenes should be worth pursuing.

## Chapter 6: References

[1] H.Ross,U.Lüning,Angew.Chem.Int.Ed.Engl., **34**, 1995, 2555

[2] O.Pietraskiewicz, M.Kozkial, M.Pietraziewcz, Adv.Mater.Opt.Electro., **8**, 1998, 277

# Appendix I: Crystallographic data

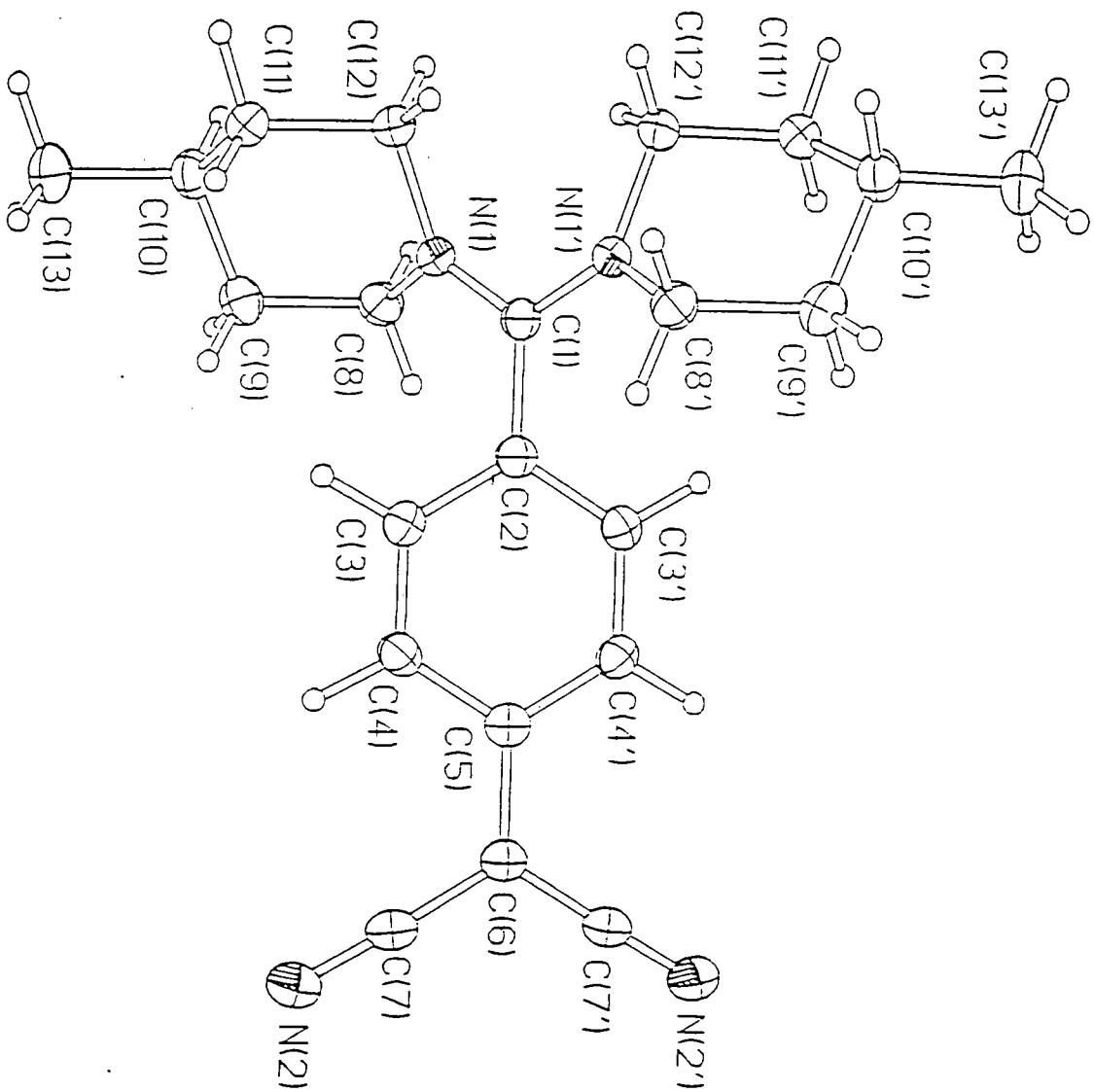


**PIP2**

Table 1. Crystal data and structure refinement for 1.

| | |
|---|---|
| Identification code | 98asb001 |
| Empirical formula | C22 H28 N4 |
| Formula weight | 348.48 |
| Temperature | 150(2) K |
| Wavelength | 0.71073 A |
| Crystal system | Monoclinic |
| Space group | C2/c |
| Unit cell dimensions | a = 16.768(1) A alpha = 90 deg.<br>b = 12.281(1) A beta = 107.26(1) deg.<br>c = 10.010(1) A gamma = 90 deg. |
| Volume | 1968.5(3) A^3 |
| Z | 4 |
| Density (calculated) | 1.176 g/cm^3 |
| Absorption coefficient | 0.071 mm^-1 |
| F(000) | 752 |
| Crystal size | 0.35 x 0.25 x 0.07 mm |
| Theta range for data collection | 2.09 to 26.00 deg. |
| Index ranges | -21<=h<=21, -15<=k<=15, -12<=l<=10 |
| Reflections collected | 8379 |
| Independent reflections | 1939 [R(int) = 0.0534] |
| Observed reflections, I>2sigma(I) | 1538 |
| Refinement method | Full-matrix least-squares on F^2 |
| Data / restraints / parameters | 1901 / 0 / 176 |
| Goodness-of-fit on F^2 | 1.110 |
| Final R indices [I>2sigma(I)] | R1 = 0.0422, wR2 = 0.0973 |
| R indices (all data) | R1 = 0.0612, wR2 = 0.1209 |
| Largest diff. peak and hole | 0.196 and -0.223 e.A^-3 |

Table 2. Atomic coordinates ( x 10^4) and equivalent isotropic displacement parameters (A^2 x 10^3) for 1. U(eq) is defined as one third of the trace of the orthogonalized Uij tensor.

| | x | y | z | U(eq) |
|---|---|---|---|---|
| N(1) | 4294(1) | 8349(1) | 2447(1) | 22(1) |
| N(2) | 4324(1) | 2061(1) | 4105(2) | 36(1) |
| C(1) | 5000 | 7806(2) | 2500 | 22(1) |
| C(2) | 5000 | 6613(2) | 2500 | 23(1) |
| C(3) | 4583(1) | 6021(1) | 3295(2) | 24(1) |
| C(4) | 4576(1) | 4899(1) | 3287(2) | 24(1) |
| C(5) | 5000 | 4299(2) | 2500 | 24(1) |
| C(6) | 5000 | 3121(2) | 2500 | 25(1) |
| C(7) | 4628(1) | 2526(1) | 3371(2) | 26(1) |
| C(8) | 3452(1) | 7934(1) | 1690(2) | 26(1) |
| C(9) | 2871(1) | 7933(2) | 2612(2) | 29(1) |
| C(10) | 2834(1) | 9049(1) | 3271(2) | 27(1) |
| C(11) | 3726(1) | 9418(1) | 4025(2) | 26(1) |
| C(12) | 4290(1) | 9438(1) | 3076(2) | 25(1) |
| C(13) | 2305(1) | 9031(2) | 4280(2) | 37(1) |

Table 3. Bond lengths [A] and angles [deg] for 1.

| | | | |
|---|---|---|---|
| N(1)-C(1) | 1.346(2) | N(1)-C(12) | 1.479(2) |
| N(1)-C(8) | 1.481(2) | N(2)-C(7) | 1.162(2) |
| C(1)-N(1') | 1.346(2) | C(1)-C(2) | 1.465(3) |
| C(2)-C(3) | 1.408(2) | C(2)-C(3') | 1.408(2) |
| C(3)-C(4) | 1.378(2) | C(3)-H(3) | 0.99(2) |
| C(4)-C(5) | 1.414(2) | C(4)-H(4) | 1.00(2) |
| C(5)-C(4') | 1.414(2) | C(5)-C(6) | 1.447(3) |
| C(6)-C(7) | 1.415(2) | C(6)-C(7') | 1.416(2) |
| C(8)-C(9) | 1.527(2) | C(8)-H(81) | 0.99(2) |
| C(8)-H(82) | 0.99(2) | C(9)-C(10) | 1.531(2) |
| C(9)-H(91) | 1.00(2) | C(9)-H(92) | 1.00(2) |
| C(10)-C(13) | 1.529(2) | C(10)-C(11) | 1.530(2) |
| C(10)-H(10) | 1.03(2) | C(11)-C(12) | 1.527(2) |
| C(11)-H(111) | 1.00(2) | C(11)-H(112) | 1.00(2) |
| C(12)-H(121) | 1.02(2) | C(12)-H(122) | 0.97(2) |
| C(13)-H(131) | 0.97(2) | C(13)-H(132) | 1.02(2) |
| C(13)-H(133) | 1.02(2) | | |
| | | | |
| C(1)-N(1)-C(12) | 123.1(1) | C(1)-N(1)-C(8) | 122.9(1) |
| C(12)-N(1)-C(8) | 113.9(1) | N(1)-C(1)-N(1') | 120.5(2) |
| N(1)-C(1)-C(2) | 119.7(1) | C(3)-C(2)-C(3') | 117.8(2) |
| C(3)-C(2)-C(1) | 121.1(1) | C(4)-C(3)-C(2) | 121.2(2) |
| C(4)-C(3)-H(3) | 119.5(10) | C(2)-C(3)-H(3) | 119(1) |
| C(3)-C(4)-C(5) | 121.3(2) | C(3)-C(4)-H(4) | 119.1(10) |
| C(5)-C(4)-H(4) | 119.6(10) | C(4)-C(5)-C(4') | 117.2(2) |
| C(4)-C(5)-C(6) | 121.38(10) | C(7)-C(6)-C(7') | 117.9(2) |
| C(7)-C(6)-C(5) | 121.07(10) | N(2)-C(7)-C(6) | 178.3(2) |
| N(1)-C(8)-C(9) | 111.93(13) | N(1)-C(8)-H(81) | 106.3(10) |
| C(9)-C(8)-H(81) | 109.0(10) | N(1)-C(8)-H(82) | 108.5(10) |
| C(9)-C(8)-H(82) | 111.9(10) | H(81)-C(8)-H(82) | 109.0(14) |
| C(8)-C(9)-C(10) | 111.96(14) | C(8)-C(9)-H(91) | 109.2(10) |
| C(10)-C(9)-H(91) | 109.1(10) | C(8)-C(9)-H(92) | 108.8(11) |
| C(10)-C(9)-H(92) | 111.1(11) | H(91)-C(9)-H(92) | 107(2) |
| C(13)-C(10)-C(11) | 110.6(2) | C(13)-C(10)-C(9) | 112.2(2) |
| C(11)-C(10)-C(9) | 108.62(13) | C(13)-C(10)-H(10) | 108.6(10) |
| C(11)-C(10)-H(10) | 108.5(10) | C(9)-C(10)-H(10) | 108.2(10) |
| C(12)-C(11)-C(10) | 113.16(14) | C(12)-C(11)-H(111) | 109.1(9) |
| C(10)-C(11)-H(111) | 108.8(9) | C(12)-C(11)-H(112) | 107.5(10) |
| C(10)-C(11)-H(112) | 110.0(10) | H(111)-C(11)-H(112) | 108.1(14) |
| N(1)-C(12)-C(11) | 109.43(13) | N(1)-C(12)-H(121) | 108.9(10) |
| C(11)-C(12)-H(121) | 110.1(9) | N(1)-C(12)-H(122) | 108.3(10) |
| C(11)-C(12)-H(122) | 109.5(10) | H(121)-C(12)-H(122) | 110.5(14) |
| C(10)-C(13)-H(131) | 112.8(12) | C(10)-C(13)-H(132) | 109.3(11) |
| H(131)-C(13)-H(132) | 107(2) | C(10)-C(13)-H(133) | 110(1) |
| H(131)-C(13)-H(133) | 109(2) | H(132)-C(13)-H(133) | 108(2) |

Symmetry transformations used to generate equivalent atoms (primed): -x+1,y,-z+1/2

Table 4. Anisotropic displacement parameters (A^2 x 10^3) for 1. The anisotropic displacement factor exponent takes the form: -2 pi^2 [ h^2 a*^2 U11 + ... + 2 h k a* b* U12 ]

| | U11 | U22 | U33 | U23 | U13 | U12 |
|---|---|---|---|---|---|---|
| N(1) | 23(1) | 19(1) | 25(1) | -2(1) | 11(1) | -1(1) |
| N(2) | 46(1) | 24(1) | 43(1) | 2(1) | 20(1) | -2(1) |
| C(1) | 26(1) | 21(1) | 19(1) | 0 | 9(1) | 0 |
| C(2) | 26(1) | 21(1) | 23(1) | 0 | 9(1) | 0 |
| C(3) | 28(1) | 23(1) | 24(1) | -1(1) | 11(1) | 1(1) |
| C(4) | 28(1) | 22(1) | 24(1) | 2(1) | 10(1) | -2(1) |
| C(5) | 24(1) | 22(1) | 23(1) | 0 | 4(1) | 0 |
| C(6) | 28(1) | 20(1) | 28(1) | 0 | 8(1) | 0 |
| C(7) | 30(1) | 19(1) | 29(1) | -1(1) | 7(1) | 1(1) |
| C(8) | 24(1) | 25(1) | 28(1) | -2(1) | 7(1) | -3(1) |
| C(9) | 24(1) | 33(1) | 32(1) | 1(1) | 10(1) | -5(1) |
| C(10) | 24(1) | 30(1) | 31(1) | 4(1) | 12(1) | 3(1) |
| C(11) | 28(1) | 22(1) | 31(1) | -2(1) | 14(1) | 0(1) |
| C(12) | 27(1) | 19(1) | 32(1) | -2(1) | 14(1) | -1(1) |
| C(13) | 30(1) | 44(1) | 43(1) | 0(1) | 19(1) | -1(1) |

Table 5. Hydrogen coordinates ( x 10^4) and isotropic displacement parameters (A^2 x 10^3) for 1.

| | x | y | z | U(eq) |
|---|---|---|---|---|
| H(3) | 4306(10) | 6419(14) | 3897(17) | 25(4) |
| H(4) | 4279(10) | 4503(15) | 3876(18) | 28(4) |
| H(81) | 3223(11) | 8435(15) | 888(19) | 30(5) |
| H(82) | 3511(10) | 7198(15) | 1326(18) | 29(5) |
| H(91) | 3073(11) | 7380(15) | 3373(19) | 28(5) |
| H(92) | 2301(12) | 7689(15) | 2036(20) | 38(5) |
| H(10) | 2574(11) | 9591(15) | 2482(20) | 34(5) |
| H(111) | 3971(10) | 8915(14) | 4828(17) | 21(4) |
| H(112) | 3720(11) | 10169(16) | 4406(19) | 36(5) |
| H(121) | 4076(10) | 9993(15) | 2297(19) | 29(5) |
| H(122) | 4859(11) | 9613(14) | 3628(18) | 24(4) |
| H(131) | 1760(13) | 8697(16) | 3875(21) | 45(6) |
| H(132) | 2605(12) | 8586(17) | 5141(23) | 44(6) |
| H(133) | 2227(13) | 9800(19) | 4600(23) | 55(6) |

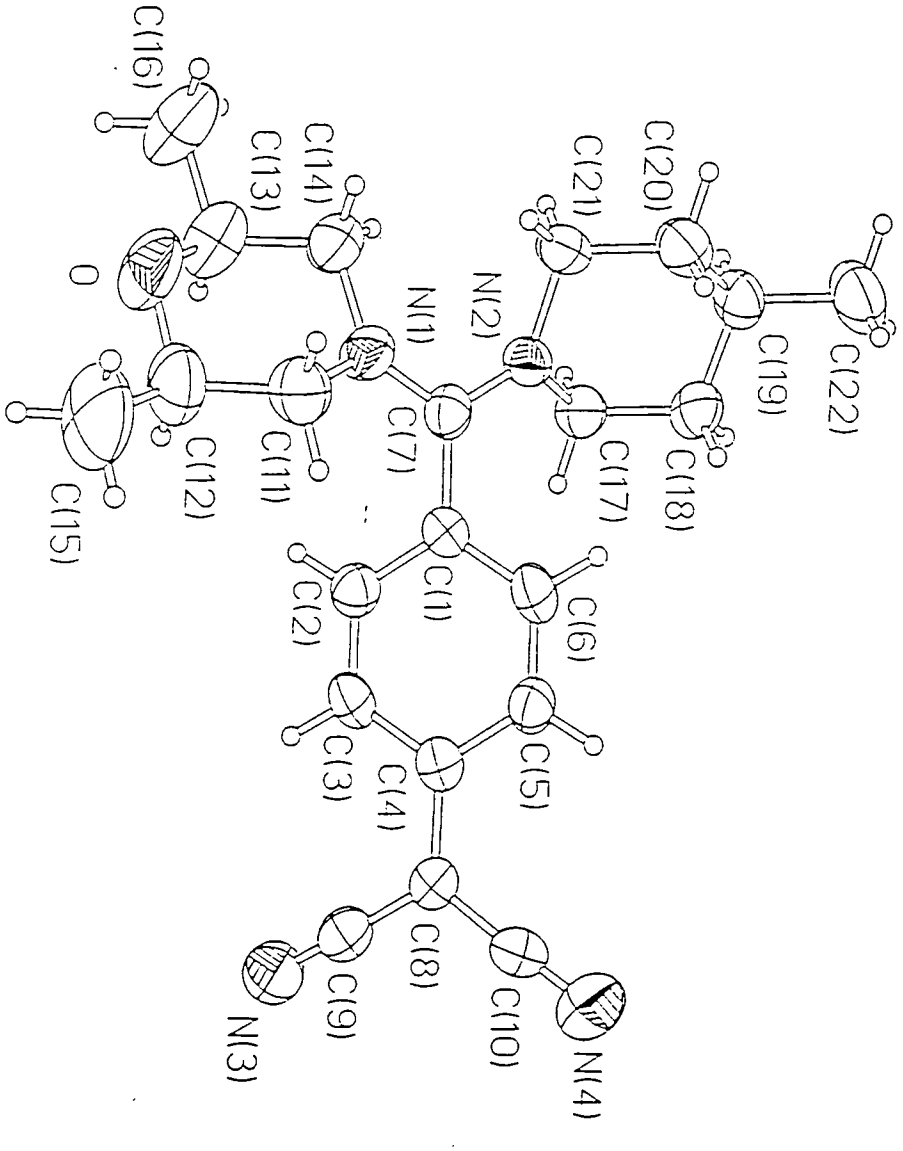
C(16)
C(13)
C(14)
C(21)
C(20)
O
N(1)
N(2)
C(19)
C(22)
C(15)
C(12)
C(11)
C(7)
C(17)
C(18)
C(2)
C(1)
C(6)
C(3)
C(4)
C(5)
C(8)
C(9)
C(10)
N(3)
N(4)

**MORPIP**

Table 1. Crystal data and structure refinement for 1.

| | |
|---|---|
| Identification code | MORPIP |
| Empirical formula | C22 H28 N4 O |
| Formula weight | 364.48 |
| Temperature | 295(2) K |
| Wavelength | 0.71073 A |
| Crystal system | Orthorhombic |
| Space group | P2(1)2(1)2(1) |
| Unit cell dimensions | a = 8.5185(8) A alpha = 90 deg.<br>b = 13.0243(10) A beta = 90 deg.<br>c = 19.2632(14) A gamma = 90 deg. |
| Volume | 2137.2(3) A^3 |
| Z | 4 |
| Density (calculated) | 1.133 g/cm^3 |
| Absorption coefficient | 0.071 mm^-1 |
| F(000) | 784 |
| Crystal size | 0.40 x 0.36 x 0.03 mm |
| Theta range for data collection | 1.89 to 25.35 deg. |
| Index ranges | -10<=h<=10, -15<=k<=14, -23<=l<=20 |
| Reflections collected | 13167 |
| Independent reflections | 3909 [R(int) = 0.0980] |
| Observed reflections, I>2sigma(I) | 2257 |
| Absorption correction | None |
| Refinement method | Full-matrix least-squares on F^2 |
| Data / restraints / parameters | 3873 / 0 / 250 |
| Goodness-of-fit on F^2 | 1.262 |
| Final R indices [I>2sigma(I)] | R1 = 0.0759, wR2 = 0.1211 |
| R indices (all data) | R1 = 0.1625, wR2 = 0.1688 |
| Absolute structure parameter | 0(4) |
| Largest shift/e.s.d. ratio | 0.000 |
| Largest diff. peak and hole | 0.214 and -0.188 e.A^-3 |

Table 2. Atomic coordinates ( x 10^4) and equivalent isotropic displacement parameters (A^2 x 10^3) for 1. U(eq) is defined as one third of the trace of the orthogonalized Uij tensor.

| | x | y | z | U(eq) |
|---|---|---|---|---|
| O | 6904(5) | 8670(3) | 5782(2) | 86(1) |
| N(1) | 5292(4) | 8203(3) | 7026(2) | 53(1) |
| N(2) | 5046(4) | 7766(3) | 8198(2) | 44(1) |
| N(3) | -596(6) | 3919(4) | 5896(2) | 82(2) |
| N(4) | -3470(6) | 5471(4) | 7492(3) | 86(2) |
| C(1) | 3166(5) | 7082(3) | 7374(2) | 42(1) |
| C(2) | 3173(5) | 6419(3) | 6805(2) | 46(1) |
| C(3) | 1876(5) | 5845(3) | 6639(2) | 44(1) |
| C(4) | 486(5) | 5892(3) | 7038(2) | 40(1) |
| C(5) | 493(5) | 6553(4) | 7609(2) | 48(1) |
| C(6) | 1791(6) | 7132(4) | 7772(2) | 49(1) |
| C(7) | 4544(5) | 7700(3) | 7541(2) | 44(1) |
| C(8) | -852(6) | 5270(4) | 6855(2) | 47(1) |
| C(9) | -725(6) | 4526(4) | 6325(3) | 54(1) |
| C(10) | -2295(7) | 5361(4) | 7205(3) | 54(1) |
| C(11) | 4477(6) | 8589(4) | 6400(2) | 65(2) |
| C(12) | 5307(8) | 8288(5) | 5754(2) | 80(2) |
| C(13) | 7738(7) | 8234(5) | 6354(3) | 78(2) |
| C(14) | 6957(6) | 8517(4) | 7029(2) | 65(2) |
| C(15) | 4526(9) | 8770(7) | 5120(3) | 124(3) |
| C(16) | 9415(8) | 8663(6) | 6338(3) | 104(2) |
| C(17) | 4852(6) | 6913(3) | 8695(2) | 48(1) |
| C(18) | 4084(6) | 7270(4) | 9369(2) | 53(1) |
| C(19) | 4965(6) | 8167(4) | 9688(2) | 55(1) |
| C(20) | 5121(6) | 9022(4) | 9152(2) | 60(1) |
| C(21) | 5902(6) | 8661(4) | 8482(2) | 57(1) |
| C(22) | 4178(7) | 8557(5) | 10345(2) | 82(2) |

Table 3. Bond lengths [A] and angles [deg] for 1.

| | | | |
|---|---|---|---|
| N(1)-C(1) | 1.346(2) | N(1)-C(12) | 1.479(2) |
| N(1)-C(8) | 1.481(2) | N(2)-C(7) | 1.162(2) |
| C(1)-N(1') | 1.346(2) | C(1)-C(2) | 1.465(3) |
| C(2)-C(3) | 1.408(2) | C(2)-C(3') | 1.408(2) |
| C(3)-C(4) | 1.378(2) | C(3)-H(3) | 0.99(2) |
| C(4)-C(5) | 1.414(2) | C(4)-H(4) | 1.00(2) |
| C(5)-C(4') | 1.414(2) | C(5)-C(6) | 1.447(3) |
| C(6)-C(7) | 1.415(2) | C(6)-C(7') | 1.416(2) |
| C(8)-C(9) | 1.527(2) | C(8)-H(81) | 0.99(2) |
| C(8)-H(82) | 0.99(2) | C(9)-C(10) | 1.531(2) |
| C(9)-H(91) | 1.00(2) | C(9)-H(92) | 1.00(2) |
| C(10)-C(13) | 1.529(2) | C(10)-C(11) | 1.530(2) |
| C(10)-H(10) | 1.03(2) | C(11)-C(12) | 1.527(2) |
| C(11)-H(111) | 1.00(2) | C(11)-H(112) | 1.00(2) |
| C(12)-H(121) | 1.02(2) | C(12)-H(122) | 0.97(2) |
| C(13)-H(131) | 0.97(2) | C(13)-H(132) | 1.02(2) |
| C(13)-H(133) | 1.02(2) | | |
| | | | |
| C(1)-N(1)-C(12) | 123.1(1) | C(1)-N(1)-C(8) | 122.9(1) |
| C(12)-N(1)-C(8) | 113.9(1) | N(1)-C(1)-N(1') | 120.5(2) |
| N(1)-C(1)-C(2) | 119.7(1) | C(3)-C(2)-C(3') | 117.8(2) |
| C(3)-C(2)-C(1) | 121.1(1) | C(4)-C(3)-C(2) | 121.2(2) |
| C(4)-C(3)-H(3) | 119.5(10) | C(2)-C(3)-H(3) | 119(1) |
| C(3)-C(4)-C(5) | 121.3(2) | C(3)-C(4)-H(4) | 119.1(10) |
| C(5)-C(4)-H(4) | 119.6(10) | C(4)-C(5)-C(4') | 117.2(2) |
| C(4)-C(5)-C(6) | 121.38(10) | C(7)-C(6)-C(7') | 117.9(2) |
| C(7)-C(6)-C(5) | 121.07(10) | N(2)-C(7)-C(6) | 178.3(2) |
| N(1)-C(8)-C(9) | 111.93(13) | N(1)-C(8)-H(81) | 106.3(10) |
| C(9)-C(8)-H(81) | 109.0(10) | N(1)-C(8)-H(82) | 108.5(10) |
| C(9)-C(8)-H(82) | 111.9(10) | H(81)-C(8)-H(82) | 109.0(14) |
| C(8)-C(9)-C(10) | 111.96(14) | C(8)-C(9)-H(91) | 109.2(10) |
| C(10)-C(9)-H(91) | 109.1(10) | C(8)-C(9)-H(92) | 108.8(11) |
| C(10)-C(9)-H(92) | 111.1(11) | H(91)-C(9)-H(92) | 107(2) |
| C(13)-C(10)-C(11) | 110.6(2) | C(13)-C(10)-C(9) | 112.2(2) |
| C(11)-C(10)-C(9) | 108.62(13) | C(13)-C(10)-H(10) | 108.6(10) |
| C(11)-C(10)-H(10) | 108.5(10) | C(9)-C(10)-H(10) | 108.2(10) |
| C(12)-C(11)-C(10) | 113.16(14) | C(12)-C(11)-H(111) | 109.1(9) |
| C(10)-C(11)-H(111) | 108.8(9) | C(12)-C(11)-H(112) | 107.5(10) |
| C(10)-C(11)-H(112) | 110.0(10) | H(111)-C(11)-H(112) | 108.1(14) |
| N(1)-C(12)-C(11) | 109.43(13) | N(1)-C(12)-H(121) | 108.9(10) |
| C(11)-C(12)-H(121) | 110.1(9) | N(1)-C(12)-H(122) | 108.3(10) |
| C(11)-C(12)-H(122) | 109.5(10) | H(121)-C(12)-H(122) | 110.5(14) |
| C(10)-C(13)-H(131) | 112.8(12) | C(10)-C(13)-H(132) | 109.3(11) |
| H(131)-C(13)-H(132) | 107(2) | C(10)-C(13)-H(133) | 110(1) |
| H(131)-C(13)-H(133) | 109(2) | H(132)-C(13)-H(133) | 108(2) |

Symmetry transformations used to generate equivalent atoms (primed): -x+1,y,-z+1/2

Table 4. Anisotropic displacement parameters (A^2 x 10^3) for 1. The anisotropic displacement factor exponent takes the form: -2 pi^2 [ h^2 a*^2 U11 + ... + 2 h k a* b* U12 ]

| | U11 | U22 | U33 | U23 | U13 | U12 |
|---|---|---|---|---|---|---|
| O | 93(3) | 101(3) | 62(2) | 29(2) | 17(2) | -8(3) |
| N(1) | 50(2) | 64(3) | 45(2) | 10(2) | -2(2) | -11(2) |
| N(2) | 52(3) | 45(2) | 36(2) | 3(2) | -4(2) | -8(2) |
| N(3) | 90(4) | 78(4) | 79(3) | -28(3) | 20(3) | -28(3) |
| N(4) | 60(3) | 103(4) | 96(4) | -15(3) | 14(3) | -7(3) |
| C(1) | 44(3) | 44(3) | 37(2) | -4(2) | -2(2) | -2(3) |
| C(2) | 44(3) | 50(3) | 44(3) | 0(2) | 0(2) | 2(3) |
| C(3) | 49(3) | 46(3) | 38(2) | -10(2) | -4(2) | 8(2) |
| C(4) | 42(3) | 41(3) | 38(2) | 0(2) | -3(2) | 7(2) |
| C(5) | 39(3) | 64(3) | 40(2) | -5(2) | 3(2) | 3(3) |
| C(6) | 56(3) | 51(3) | 40(3) | -12(2) | 1(2) | 7(3) |
| C(7) | 46(3) | 43(3) | 42(3) | -2(2) | 5(2) | 2(2) |
| C(8) | 44(3) | 52(3) | 45(3) | -4(2) | 5(2) | -6(2) |
| C(9) | 55(3) | 54(3) | 54(3) | 4(3) | 6(3) | -11(3) |
| C(10) | 52(3) | 56(3) | 54(3) | -7(3) | -6(3) | -11(3) |
| C(11) | 74(4) | 72(4) | 49(3) | 12(3) | -10(3) | -6(3) |
| C(12) | 99(5) | 95(5) | 47(3) | 10(3) | 6(3) | -2(4) |
| C(13) | 76(4) | 84(4) | 73(4) | 18(4) | 20(3) | 2(4) |
| C(14) | 61(4) | 81(4) | 52(3) | 6(3) | 4(3) | -17(3) |
| C(15) | 142(7) | 177(8) | 54(4) | 42(4) | -5(4) | -7(7) |
| C(16) | 81(5) | 128(6) | 102(5) | 31(4) | 30(4) | -12(5) |
| C(17) | 50(3) | 48(3) | 45(3) | 6(2) | -3(2) | -2(3) |
| C(18) | 56(3) | 61(3) | 43(3) | 11(3) | 1(2) | -4(3) |
| C(19) | 54(3) | 72(4) | 38(2) | -2(3) | -8(2) | 2(3) |
| C(20) | 69(4) | 61(3) | 49(3) | -6(3) | -3(3) | -8(3) |
| C(21) | 62(3) | 62(3) | 46(3) | -4(3) | -6(3) | -21(3) |
| C(22) | 109(5) | 89(5) | 49(3) | -15(3) | 2(3) | -6(4) |

Table 5. Hydrogen coordinates ( x 10^4) and isotropic displacement parameters (A^2 x 10^3) for 1.

| | x | y | z | U(eq) |
|---|---|---|---|---|
| H(2) | 4073(5) | 6364(3) | 6535(2) | 55 |
| H(3) | 1912(5) | 5415(3) | 6253(2) | 53 |
| H(5) | -399(5) | 6602(4) | 7885(2) | 57 |
| H(6) | 1754(6) | 7567(4) | 8154(2) | 59 |
| H(11A) | 3417(6) | 8318(4) | 6390(2) | 84 |
| H(11B) | 4408(6) | 9332(4) | 6423(2) | 84 |
| H(12) | 5313(8) | 7539(5) | 5708(2) | 104 |
| H(13) | 7765(7) | 7485(5) | 6306(3) | 101 |
| H(14A) | 7026(6) | 9253(4) | 7098(2) | 84 |
| H(14B) | 7497(6) | 8183(4) | 7410(2) | 84 |
| H(15A) | 5075(35) | 8564(30) | 4707(3) | 152(17) |
| H(15B) | 3454(18) | 8545(29) | 5093(14) | 152(17) |
| H(15C) | 4555(49) | 9505(7) | 5161(12) | 152(17) |
| H(16A) | 10017(17) | 8357(28) | 6705(16) | 172(19) |
| H(16B) | 9891(21) | 8504(31) | 5899(10) | 172(19) |
| H(16C) | 9388(8) | 9394(8) | 6400(24) | 172(19) |
| H(17A) | 4209(6) | 6382(3) | 8486(2) | 62 |
| H(17B) | 5871(6) | 6617(3) | 8798(2) | 62 |
| H(18A) | 4062(6) | 6705(4) | 9697(2) | 69 |
| H(18B) | 3009(6) | 7474(4) | 9277(2) | 69 |
| H(19) | 6023(6) | 7932(4) | 9811(2) | 71 |
| H(20A) | 4086(6) | 9289(4) | 9045(2) | 78 |
| H(20B) | 5735(6) | 9578(4) | 9349(2) | 78 |
| H(21A) | 6984(6) | 8474(4) | 8574(2) | 74 |
| H(21B) | 5898(6) | 9214(4) | 8145(2) | 74 |
| H(22A) | 4792(23) | 9103(18) | 10541(10) | 103(12) |
| H(22B) | 3148(18) | 8807(25) | 10235(4) | 103(12) |
| H(22C) | 4097(37) | 8006(8) | 10675(7) | 103(12) |

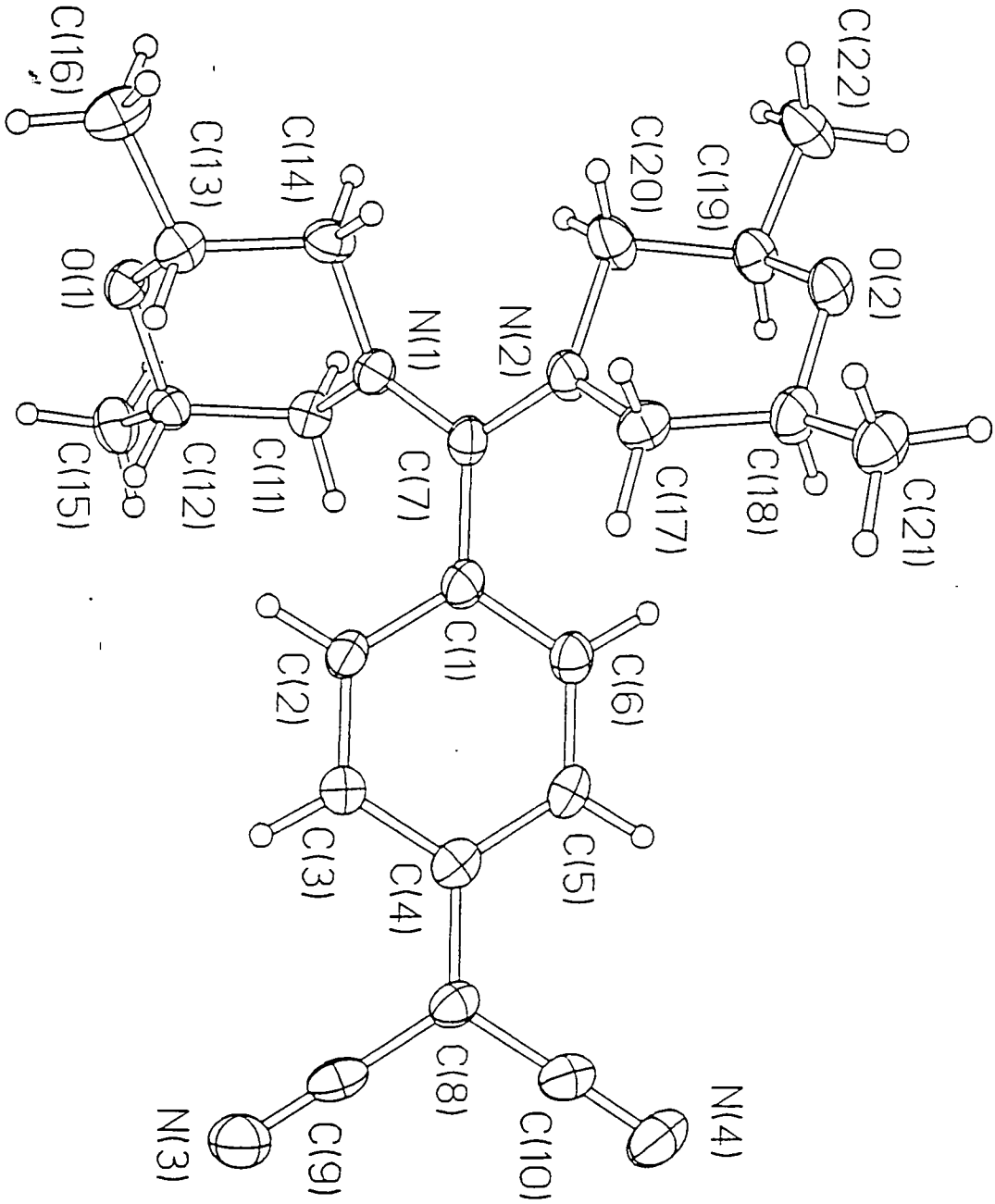
C(16)
C(13)
C(14)
O(1)
N(1)
N(2)
C(20)
C(19)
C(22)
O(2)
C(15)
C(12)
C(11)
C(7)
C(17)
C(18)
C(21)
C(2)
C(1)
C(6)
C(3)
C(4)
C(5)
C(8)
C(9)
C(10)
N(3)
N(4)

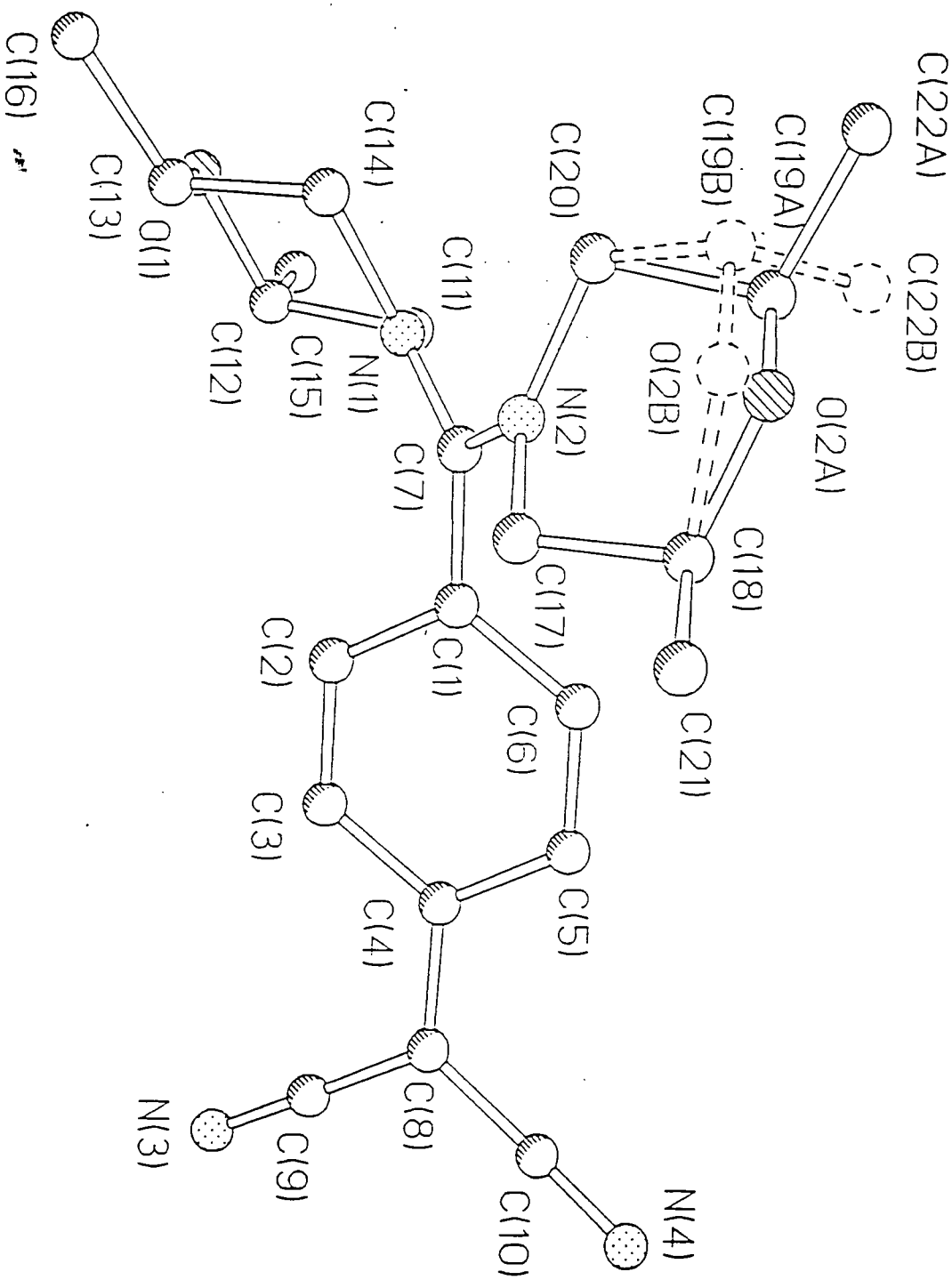
C(22A)
C(22B)
C(19A)
C(19B)
C(20)
C(14)
C(16)
C(13)
O(1)
C(11)
O(2A)
O(2B)
C(12)
C(15)
N(1)
N(2)
C(7)
C(18)
C(17)
C(1)
C(2)
C(6)
C(21)
C(3)
C(5)
C(4)
C(8)
N(3)
C(9)
C(10)
N(4)

**MOR2**

Table 1. Crystal data and structure refinement for 1.

| | |
|---|---|
| Identification code | 98asb002 |
| Empirical formula | C22 H28 N4 O2 |
| Formula weight | 380.48 |
| Temperature | 150(2) K |
| Wavelength | 0.71073 A |
| Crystal system | Monoclinic |
| Space group | P2(1)/c |
| Unit cell dimensions | a = 10.075(1) A alpha = 90 deg.<br>b = 13.981(1) A beta = 107.94(1) deg<br>c = 15.656(1) A gamma = 90 deg. |
| Volume, Z | 2098.1(3) A^3, 4 |
| Density (calculated) | 1.205 g/cm^3 |
| Absorption coefficient | 0.079 mm^-1 |
| F(000) | 816 |
| Crystal size | 0.25 x 0.15 x 0.12 mm |
| Theta range for data collection | 2.00 to 25.00 deg. |
| Limiting indices | -13<=h<=12, -18<=k<=18, -16<=l<=20 |
| Reflections collected | 12321 |
| Independent reflections | 3689 [R(int) = 0.0670] |
| Observed reflections, I>2sigma | 2587 |
| Refinement method | Full-matrix least-squares on F^2 |
| Data / restraints / parameters | 3569 / 4 / 273 |
| Goodness-of-fit on F^2 | 1.137 |
| Final R indices [I>2sigma(I)] | R1 = 0.0602, wR2 = 0.1115 |
| R indices (all data) | R1 = 0.1024, wR2 = 0.1445 |
| Largest diff. peak and hole | 0.202 and -0.245 e.A^-3 |

Table 2. Atomic coordinates ( x 10^4) and equivalent isotropic displacement parameters (A^2 x 10^3) for 1. U(eq) is defined as one third of the trace of the orthogonalized Uij tensor.

| | x | y | z | U(eq) |
|---|---|---|---|---|
| O(1) | 5958(2) | 5047(1) | 1411(1) | 24(1) |
| O(2A) | 1188(3) | 4336(3) | 4306(2) | 26(1) |
| O(2B) | 1221(15) | 4731(11) | 4350(10) | 27(5) |
| N(1) | 3779(2) | 4352(2) | 2034(1) | 23(1) |
| N(2) | 2111(2) | 4459(2) | 2780(1) | 26(1) |
| N(3) | -2084(3) | 3092(2) | -2558(2) | 39(1) |
| N(4) | -3762(3) | 1526(2) | -712(2) | 41(1) |
| C(1) | 1443(3) | 3729(2) | 1300(2) | 25(1) |
| C(2) | 1321(3) | 3998(2) | 411(2) | 25(1) |
| C(3) | 290(3) | 3627(2) | -306(2) | 26(1) |
| C(4) | -697(3) | 2963(2) | -181(2) | 25(1) |
| C(5) | -530(3) | 2660(2) | 711(2) | 26(1) |
| C(6) | 501(3) | 3040(2) | 1426(2) | 26(1) |
| C(7) | 2474(3) | 4186(2) | 2055(2) | 23(1) |
| C(8) | -1834(3) | 2622(2) | -925(2) | 26(1) |
| C(9) | -1973(3) | 2883(2) | -1822(2) | 28(1) |
| C(10) | -2887(3) | 2013(2) | -802(2) | 29(1) |
| C(11) | 4533(3) | 3705(2) | 1602(2) | 24(1) |
| C(12) | 5165(3) | 4231(2) | 971(2) | 23(1) |
| C(13) | 5134(3) | 5688(2) | 1754(2) | 26(1) |
| C(14) | 4630(3) | 5183(2) | 2463(2) | 26(1) |
| C(15) | 6163(3) | 3586(2) | 688(2) | 32(1) |
| C(16) | 6028(3) | 6557(2) | 2125(2) | 37(1) |
| C(17) | 694(3) | 4793(2) | 2736(2) | 27(1) |
| C(18) | 180(3) | 4318(2) | 3450(2) | 31(1) |
| C(19A) | 2482(3) | 3922(3) | 4303(2) | 26(1) |
| C(19B) | 2619(18) | 4392(14) | 4468(12) | 32(5) |
| C(20) | 3106(3) | 4530(3) | 3693(2) | 36(1) |
| C(21) | -1133(3) | 4811(2) | 3510(2) | 35(1) |
| C(22A) | 3434(4) | 3934(3) | 5261(2) | 37(1) |
| C(22B) | 2733(18) | 3288(13) | 4518(12) | 35(5) |

Table 3. Bond lengths [A] and angles [deg] for 1.

| | | | |
|---|---|---|---|
| O(1)-C(13) | 1.434(3) | O(1)-C(12) | 1.440(3) |
| O(2A)-C(18) | 1.410(4) | O(2A)-C(19A) | 1.428(4) |
| O(2B)-C(19B) | 1.44(2) | O(2B)-C(18) | 1.585(14) |
| N(1)-C(7) | 1.346(3) | N(1)-C(11) | 1.473(3) |
| N(1)-C(14) | 1.477(3) | N(2)-C(7) | 1.350(3) |
| N(2)-C(20) | 1.475(3) | N(2)-C(17) | 1.483(3) |
| N(3)-C(9) | 1.160(4) | N(4)-C(10) | 1.156(4) |
| C(1)-C(6) | 1.409(4) | C(1)-C(2) | 1.409(4) |
| C(1)-C(7) | 1.459(4) | C(2)-C(3) | 1.375(4) |
| C(3)-C(4) | 1.418(4) | C(4)-C(5) | 1.418(4) |
| C(4)-C(8) | 1.440(4) | C(5)-C(6) | 1.377(4) |
| C(8)-C(9) | 1.416(4) | C(8)-C(10) | 1.419(4) |
| C(11)-C(12) | 1.519(3) | C(12)-C(15) | 1.515(4) |
| C(13)-C(16) | 1.517(4) | C(13)-C(14) | 1.529(4) |
| C(17)-C(18) | 1.522(4) | C(18)-C(21) | 1.520(4) |
| C(19A)-C(22A) | 1.510(5) | C(19A)-C(20) | 1.550(5) |
| C(19B)-C(20) | 1.46(2) | C(19B)-C(22B) | 1.55(2) |
| | | | |
| C(13)-O(1)-C(12) | 112.0(2) | C(18)-O(2A)-C(19A) | 112.4(3) |
| C(19B)-O(2B)-C(18) | 110(1) | C(7)-N(1)-C(11) | 123.4(2) |
| C(7)-N(1)-C(14) | 124.0(2) | C(11)-N(1)-C(14) | 112.5(2) |
| C(7)-N(2)-C(20) | 123.7(2) | C(7)-N(2)-C(17) | 123.8(2) |
| C(20)-N(2)-C(17) | 112.4(2) | C(6)-C(1)-C(2) | 117.6(2) |
| C(6)-C(1)-C(7) | 121.9(2) | C(2)-C(1)-C(7) | 120.5(2) |
| C(3)-C(2)-C(1) | 121.3(3) | C(2)-C(3)-C(4) | 121.3(3) |
| C(3)-C(4)-C(5) | 117.2(2) | C(3)-C(4)-C(8) | 121.4(3) |
| C(5)-C(4)-C(8) | 121.4(2) | C(6)-C(5)-C(4) | 121.1(2) |
| C(5)-C(6)-C(1) | 121.5(3) | N(1)-C(7)-N(2) | 119.5(2) |
| N(1)-C(7)-C(1) | 120.8(2) | N(2)-C(7)-C(1) | 119.7(2) |
| C(9)-C(8)-C(10) | 116.1(2) | C(9)-C(8)-C(4) | 121.9(2) |
| C(10)-C(8)-C(4) | 122.1(3) | N(3)-C(9)-C(8) | 179.6(3) |
| N(4)-C(10)-C(8) | 178.9(3) | N(1)-C(11)-C(12) | 112.3(2) |
| O(1)-C(12)-C(15) | 106.9(2) | O(1)-C(12)-C(11) | 110.8(2) |
| C(15)-C(12)-C(11) | 110.6(2) | O(1)-C(13)-C(16) | 107.5(2) |
| O(1)-C(13)-C(14) | 110.0(2) | C(16)-C(13)-C(14) | 112.5(2) |
| N(1)-C(14)-C(13) | 108.0(2) | N(2)-C(17)-C(18) | 111.7(2) |
| O(2A)-C(18)-C(21) | 108.6(2) | O(2A)-C(18)-C(17) | 112.5(2) |
| C(21)-C(18)-C(17) | 110.3(2) | C(21)-C(18)-O(2B) | 97.4(6) |
| C(17)-C(18)-O(2B) | 102.3(6) | O(2A)-C(19A)-C(22A) | 107.1(3) |
| O(2A)-C(19A)-C(20) | 108.9(3) | C(22A)-C(19A)-C(20) | 110.6(3) |
| O(2B)-C(19B)-C(20) | 115(1) | O(2B)-C(19B)-C(22B) | 113(2) |
| C(20)-C(19B)-C(22B) | 98(1) | C(19B)-C(20)-N(2) | 119.7(8) |
| N(2)-C(20)-C(19A) | 106.1(2) | | |

Table 4. Anisotropic displacement parameters (A^2 x 10^3) for 1. The anisotropic displacement factor exponent takes the form: -2 pi^2 [ h^2 a*^2 U11 + ... + 2 h k a* b* U12 ]

| | U11 | U22 | U33 | U23 | U13 | U12 |
|---|---|---|---|---|---|---|
| O(1) | 22(1) | 24(1) | 30(1) | -1(1) | 12(1) | 0(1) |
| O(2A) | 21(1) | 34(2) | 26(2) | 2(1) | 11(1) | 8(1) |
| N(1) | 18(1) | 27(1) | 24(1) | -1(1) | 8(1) | -1(1) |
| N(2) | 18(1) | 40(2) | 20(1) | 5(1) | 6(1) | 2(1) |
| N(3) | 40(2) | 38(2) | 34(2) | -2(1) | 4(1) | -6(1) |
| N(4) | 29(1) | 43(2) | 53(2) | -13(1) | 15(1) | -10(1) |
| C(1) | 19(1) | 30(2) | 26(2) | 1(1) | 9(1) | 0(1) |
| C(2) | 22(1) | 26(2) | 27(2) | 3(1) | 9(1) | -5(1) |
| C(3) | 27(2) | 28(2) | 24(2) | 1(1) | 8(1) | -3(1) |
| C(4) | 22(1) | 21(2) | 32(2) | -2(1) | 10(1) | 3(1) |
| C(5) | 25(2) | 22(2) | 34(2) | 2(1) | 13(1) | -3(1) |
| C(6) | 24(1) | 30(2) | 27(2) | 4(1) | 10(1) | 3(1) |
| C(7) | 22(1) | 26(2) | 23(2) | 6(1) | 8(1) | 1(1) |
| C(8) | 21(1) | 26(2) | 30(2) | -5(1) | 8(1) | -1(1) |
| C(9) | 21(2) | 22(2) | 37(2) | -9(1) | 4(1) | -2(1) |
| C(10) | 23(2) | 29(2) | 34(2) | -10(1) | 7(1) | 1(1) |
| C(11) | 24(1) | 21(2) | 26(2) | 1(1) | 9(1) | 2(1) |
| C(12) | 27(1) | 21(2) | 21(1) | 0(1) | 7(1) | 1(1) |
| C(13) | 23(1) | 26(2) | 30(2) | -1(1) | 9(1) | 2(1) |
| C(14) | 22(1) | 31(2) | 25(2) | -8(1) | 7(1) | 0(1) |
| C(15) | 39(2) | 30(2) | 32(2) | 1(1) | 19(1) | 5(1) |
| C(16) | 34(2) | 28(2) | 46(2) | -6(2) | 9(2) | -4(1) |
| C(17) | 15(1) | 35(2) | 29(2) | 2(1) | 4(1) | 3(1) |
| C(18) | 21(1) | 41(2) | 32(2) | 2(1) | 12(1) | 2(1) |
| C(19A) | 26(2) | 30(3) | 25(2) | 2(2) | 10(2) | 7(2) |
| C(20) | 18(1) | 69(2) | 19(2) | 4(2) | 3(1) | 5(2) |
| C(21) | 23(2) | 44(2) | 40(2) | 1(2) | 12(1) | 3(1) |
| C(22A) | 36(2) | 52(3) | 21(2) | 1(2) | 7(2) | 12(2) |

Table 5. Hydrogen coordinates ( x 10^4) and isotropic displacement parameters (A^2 x 10^3) for 1.

| | x | y | z | U(eq) |
|---|---|---|---|---|
| H(2) | 1962(3) | 4447(2) | 307(2) | 30 |
| H(3) | 239(3) | 3819(2) | -898(2) | 31 |
| H(5) | -1141(3) | 2189(2) | 816(2) | 31 |
| H(6) | 581(3) | 2831(2) | 2017(2) | 32 |
| H(111) | 3882(3) | 3210(2) | 1259(2) | 31 |
| H(112) | 5284(3) | 3377(2) | 2071(2) | 31 |
| H(12) | 4404(3) | 4448(2) | 429(2) | 30 |
| H(13) | 4303(3) | 5894(2) | 1249(2) | 34 |
| H(141) | 5440(3) | 4967(2) | 2966(2) | 34 |
| H(142) | 4067(3) | 5626(2) | 2704(2) | 34 |
| H(151) | 5642(4) | 3056(7) | 327(10) | 42(5) |
| H(152) | 6865(11) | 3331(10) | 1221(2) | 42(5) |
| H(153) | 6626(14) | 3956(4) | 329(10) | 42(5) |
| H(161) | 6825(12) | 6366(3) | 2637(8) | 59(6) |
| H(162) | 5470(6) | 7034(6) | 2322(12) | 59(6) |
| H(163) | 6367(17) | 6834(8) | 1656(4) | 59(6) |
| H(171) | 41(3) | 4643(2) | 2135(2) | 35 |
| H(172) | 705(3) | 5495(2) | 2815(2) | 35 |
| H(18) | -31(3) | 3629(2) | 3292(2) | 40 |
| H(19A) | 2308(3) | 3250(3) | 4075(2) | 34 |
| H(201) | 3225(3) | 5207(3) | 3888(2) | 47 |
| H(202) | 4027(3) | 4272(3) | 3705(2) | 47 |
| H(211) | -1887(6) | 4724(11) | 2945(5) | 43(5) |
| H(212) | -948(6) | 5496(3) | 3621(12) | 43(5) |
| H(213) | -1408(11) | 4532(9) | 4004(8) | 43(5) |
| H(22A) | 4322(10) | 3631(15) | 5284(3) | 55 |
| H(23A) | 2991(11) | 3572(14) | 5635(3) | 55 |
| H(24A) | 3606(19) | 4592(3) | 5484(6) | 55 |

# Appendix II: Luminescence data

| Stokes Shift | Absorption | Emission | Wavelength | Stokes Shift | Quantum Yield | Density Param | Viscosity | Refractive Ind |
|---|---|---|---|---|---|---|---|---|
| morpip Alcoholes | | | | | | | | |
| MeOH | 410 | 520 | 110 | 5159.474672 | 0.132 | 0.30856 | 0.544 | 1.329 |
| EtOH | 419 | 519.5 | 100.5 | 4617.070297 | 0.136 | 0.29013 | 1.07 | 1.36 |
| PrOH | 423 | 515.5 | 92.5 | 4242.019843 | 0.37 | 0.27529 | 1.95 | 1.384 |
| BuOH | 425 | 516 | 91 | 4149.566803 | 0.492 | 0.26423 | 2.54 | 1.3993 |
| PenOH | 429 | 517 | 88 | 3967.663542 | 0.717 | 0.25379 | 3.62 | 1.409 |
| HexOH | 431 | 521 | 90 | 4007.998183 | 0.966 | 0.24329 | 4.58 | 1.418 |
| Ethlene Glycol | 412 | 520 | 108 | 5041.075429 | 1.38 | 0.26627 | 30.2 | 1.446 |
| Glycerol | 402 | 513.5 | 111.5 | 5401.425201 | 11.84 | 0.26467 | 934 | 1.474 |
| | | | | | | | | |
| Morpip films | | | | | | | | |
| DMF | 442 | 523.5 | 81.5 | 3522.237637 | 37.75 | | | |
| TMU | 443 | 519.5 | 76.5 | 3324.085279 | 32.34 | | | |
| Cyc | 444 | 523.5 | 79.5 | 3420.32577 | 27.7 | | | |
| Calix20 | 443 | 536.5 | 93.5 | 3934.034447 | 26.99 | | | |
| Calix70 | 443 | 533.5 | 90.5 | 3829.220976 | 21.79 | | | |
| DCM | 446 | 533 | 87 | 3659.798585 | 25.44 | | | |
| Polycarbonate | 456 | 545.5 | 89.5 | 3598.018879 | 15.07 | | | |
| | | | | | | | | |
| Si Alcoholes | | | | | | | | |
| MeOH | 376 | 481 | 105 | 5805.723891 | 0.16 | | | |
| EtOH | 385 | 482 | 97 | 5227.138007 | | | | |
| PrOH | 387 | 481 | 94 | 5049.772492 | 0.4 | | | |
| BuPH | 392 | 480 | 88 | 4676.870748 | | | | |
| PenOH | 394 | 482.5 | 88.5 | 4655.322059 | 1.4 | | | |
| HexOH | 397 | 482 | 85 | 4442.02891 | | | | |
| Ethylene Glyco | 380 | 482 | 102 | 5568.901507 | 1.47 | | | |
| Glycerol | 373 | 482 | 109 | 6062.763508 | 12.38 | | | |
| | | | | | | | | |
| Si Films | | | | | | | | |
| DMF | 393 | 486.5 | 93.5 | 4890.308037 | 32 | | | |
| TMU | 389 | 475 | 86 | 4654.309295 | 23 | | | |
| | | | | | | | | |
| Amino Alcoholes | | | | | | | | |
| MeOH | 352.5 | 476.5 | 124 | 7382.43546 | 0.216 | | | |
| EtOH | 360 | 476 | 116 | 6769.374416 | | | | |
| PrOH | 365 | 478.5 | 113.5 | 6498.618686 | 0.53 | | | |
| BuPH | 369 | 477.5 | 108.5 | 6157.862626 | | | | |
| PenOH | 372 | 479 | 107 | 6004.893708 | 1.3 | | | |
| HexOH | 378 | 481 | 103 | 5665.005665 | | | | |
| Ethylene Glyco | 347 | 480 | 133 | 7985.110471 | 2.32 | | | |
| Glycerol | 358 | 469.5 | 111.5 | 6633.706368 | 21.76 | | | |
| | | | | | | | | |
| Amino Films | | | | | | | | |
| DMF | 371 | 471.5 | 100.5 | 5745.270156 | 19 | | | |
| TMU | 371 | 468.5 | 97.5 | 5609.460715 | 7.2 | | | |
| | | | | | | | | |
| Low temperature | | | | | | | | |
| ESP | | | | | | | | |
| Morpip | | | | | | | | |
| RT | 445 | 512 | 67 | 2940.660112 | | | | |
| 80K | 399 | 444 | 45 | 2540.134119 | | | | |

# Appendix II: Luminescence data

| Stokes Shift | Ab | Em | Wavelength | Wavenumber | Quantum Yiel | Density Paran |
|---|---|---|---|---|---|---|
| morpip Alcohols | | | | | | |
| MeOH | 410 | 520 | 110 | 5159.474672 | 0.132 | 0.30856 |
| EtOH | 419 | 519.5 | 100.5 | 4617.070297 | 0.136 | 0.29013 |
| PrOH | 423 | 515.5 | 92.5 | 4242.019843 | 0.37 | 0.27529 |
| BuOH | 425 | 516 | 91 | 4149.566803 | 0.492 | 0.26423 |
| PenOH | 429 | 517 | 88 | 3967.663542 | 0.717 | 0.25379 |
| HexOH | 431 | 521 | 90 | 4007.998183 | 0.966 | 0.24329 |
| Ethlene Glyco | 412 | 520 | 108 | 5041.075429 | 1.38 | 0.26627 |
| Glycerol | 402 | 513.5 | 111.5 | 5401.425201 | 11.84 | 0.26467 |
| | | | | | | |
| Morpip films | | | | | | |
| DMF | 442 | 523.5 | 81.5 | 3522.237637 | 37.75 | |
| TMU | 443 | 519.5 | 76.5 | 3324.085279 | 32.34 | |
| Cyc | 444 | 523.5 | 79.5 | 3420.32577 | 27.7 | |
| Calix20 | 443 | 536.5 | 93.5 | 3934.034447 | 26.99 | |
| Calix70 | 443 | 533.5 | 90.5 | 3829.220976 | 21.79 | |
| DCM | 446 | 533 | 87 | 3659.798585 | 25.44 | |
| Polycarbonate | 456 | 545.5 | 89.5 | 3598.018879 | 15.07 | |
| | | | | | | |
| Si Alcohols | | | | | | |
| MeOH | 376 | 481 | 105 | 5805.723891 | 0.16 | |
| EtOH | 385 | 482 | 97 | 5227.138007 | | |
| PrOH | 387 | 481 | 94 | 5049.772492 | 0.4 | |
| BuPH | 392 | 480 | 88 | 4676.870748 | | |
| PenOH | 394 | 482.5 | 88.5 | 4655.322059 | 1.4 | |
| HexOH | 397 | 482 | 85 | 4442.02891 | | |
| Ethylene Glyc | 380 | 482 | 102 | 5568.901507 | 1.47 | |
| Glycerol | 373 | 482 | 109 | 6062.763508 | 12.38 | |
| | | | | | | |
| Si Films | | | | | | |
| DMF | 393 | 486.5 | 93.5 | 4890.308037 | 32 | |
| TMU | 389 | 475 | 86 | 4654.309295 | 23 | |
| | | | | | | |
| Amino Alcohols | | | | | | |
| MeOH | 352.5 | 476.5 | 124 | 7382.43546 | 0.216 | |
| EtOH | 360 | 476 | 116 | 6769.374416 | | |
| PrOH | 365 | 478.5 | 113.5 | 6498.618686 | 0.53 | |
| BuPH | 369 | 477.5 | 108.5 | 6157.862626 | | |
| PenOH | 372 | 479 | 107 | 6004.893708 | 1.3 | |
| HexOH | 378 | 481 | 103 | 5665.005665 | | |
| Ethylene Glyc | 347 | 480 | 133 | 7985.110471 | 2.32 | |
| Glycerol | 358 | 469.5 | 111.5 | 6633.706368 | 21.76 | |
| | | | | | | |
| Amino Films | | | | | | |
| DMF | 371 | 471.5 | 100.5 | 5745.270156 | 19 | |
| TMU | 371 | 468.5 | 97.5 | 5609.460715 | 7.2 | |
| | | | | | | |
| Low temperature | | | | | | |
| ESP | | | | | | |
| Morpip | | | | | | |
| RT | 445 | 512 | 67 | 2940.660112 | | |
| 80K | 399 | 444 | 45 | 2540.134119 | | |
| | | | | | | |
| Si | | | | | | |
| RT | 376 | 414.5 | 38.5 | 2470.292329 | | |

| | | | | |
|---|---|---|---|---|
| Si | | | | |
| RT | 376 | 414.5 | 38.5 | 2470.292329 |
| 80K | 371 | 423.5 | 52.5 | 3341.427012 |
| | | | | |
| Amino | | | | |
| RT | 370 | 415.5 | 45.5 | 2959.638339 |
| 80K | 354 | 409.5 | 55.5 | 3828.563151 |
| | | | | |
| 2MeTHF | | | | |
| Morpip | | | | |
| RT | 467 | 546 | 79 | 3098.257916 |
| 80K | 441 | 520 | 79 | 3444.967731 |
| | | | | |
| PR | | | | |
| Morpip | | | | |
| RT | 424 | 520 | 96 | 4354.13643 |
| 80K | 401 | 450 | 49 | 2715.433638 |
| | | | | |
| Si | | | | |
| RT | 386 | 476 | 90 | 4898.33239 |
| 80K | 381 | 432.5 | 51.5 | 3125.331877 |
| | | | | |
| Low temperature flims | | | | |
| MORPIP DMF | | | | |
| RT | 447 | 549 | 102 | 4156.428406 |
| 200K | 447 | 540 | 93 | 3852.846135 |
| 80K | 441 | 534 | 93 | 3949.145201 |
| | | | | |
| MORPIP TMU | | | | |
| RT | 447 | 529 | 82 | 3467.772971 |
| 200K | 446 | 526 | 80 | 3410.11782 |
| 80K | 442 | 522 | 80 | 3467.346267 |

# Appendix III: Solvatochromic data

| | DMSO | MeCN | DMF | Methanol | Ethanol | Acetone | THF | DCM | CHCl3 |
|---|---|---|---|---|---|---|---|---|---|
| MOR2 | 423 | 424 | 428 | 416 | 423 | 439 | 468 | 464 | 479 |
| MORPIP | 420 | 417 | 424 | 410 | 421 | 432 | 465 | 456 | 469 |
| PIP2 | 416 | 413 | 419 | 405 | 416 | 428 | 460 | 446 | 460 |
| THIO2 | 431 | 434 | 435 | 424 | ND | 448 | 476 | 492 | ND |
| FPHPIP2 | 419 | 426 | 426 | ND | ND | 438 | ND | 465 | ND |
| Si | 387 | 394 | 393 | 376 | 388 | 404 | 427 | ND | ND |
| AMINO | 364 | 367 | 369 | 364 | 361 | 378 | 403 | 395 | 384 |
| Cyclo | 409 | 414 | 414 | 409 | 407 | 423 | 441 | ND | ND |
| Refractive Index | 46.7 | 37.5 | 36.7 | 32.7 | 24.6 | 20.7 | 7.6 | 8.9 | 4.8 |
| Dielectric Constant | 1.589 | 1.344 | 1.4305 | 1.3288 | 1.3611 | 1.3588 | 1.42 | 1.4242 | 1.4459 |
| Density Parameter | 0.232 | 0.30545 | 0.27438 | 0.30843 | 0.28889 | 0.256629 | 0.205452 | 0.216685 | 0.147996 |

ND=Not Determined